

AFFDL-TR-69-28

DEVELOPMENT AND EXPERIMENTAL VERIFICATION OF A COMPUTER PROGRAM FOR  
PREDICTING TEMPERATURE DISTRIBUTION AND HEAT TRANSFER THROUGH  
COATED AND UNCOATED, SINGLE OR MULTI-GLAZE WINDOW SYSTEMS

Gary M. Korb  
Ronald D. Dayton  
Duncan Sommerville  
Midwest Research Institute

\*\*\* Export controls have been removed \*\*\*

This document is subject to special export controls and each transmittal to foreign governments or foreign nationals may be made only with prior approval of the Air Force Flight Dynamics Laboratory (FDIS), Wright-Patterson Air Force Base, Ohio 45433.

## FOREWORD

This research was performed to develop and experimentally verify a computer program for predicting the temperatures of and heat transfer through windows of advanced Air Force aerospace vehicles. In addition to supplying data for validation of the computer program, the heat transfer test results provide experimental data on realistic window components. The work was performed from June 1966 to February 1969 by Gary M. Korb, Ronald D. Dayton, and Duncan Sommerville of Midwest Research Institute, 425 Volker Boulevard, Kansas City, Missouri 64110. The work was sponsored by the Air Force Flight Dynamics Laboratory, Air Force Systems Command, Wright-Patterson Air Force Base, under Contract No. AF 33(615)-5164, Project No. 1368, "Structural Design Concepts," Task No. 136802, "Window System Concepts."

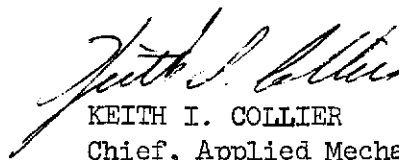
Lt. Joseph S. Pharmer and Lt. David B. Reuber, USAF, of the Air Force Flight Dynamics Laboratory, were project engineers for the periods of June 1966 - March 1967 and March 1967 - February 1969, respectively.

Acknowledgement is hereby given to the following individuals for their counsel and assistance: Dr. Frank Kreith, Consultant and Professor of Mechanical Engineering, University of Colorado; Mr. Robert Gardon, Consultant, Farmington, Michigan; Mrs. Leilah G. Fay of the ASNCD Open Shop Computer Facility, Wright-Patterson Air Force Base; and Dr. Florence Metz, Mr. Harold Finch, Mr. Eugene Moeller, Mr. Michael Noland, and Mr. Hermann Fasel of Midwest Research Institute.

Publication of this report does not constitute Air Force approval of the report's findings or conclusions. It is published only for the exchange and stimulation of ideas.

This report was submitted by the authors in February 1969.

This technical report has been reviewed and is approved.



KEITH I. COLLIER  
Chief, Applied Mechanics Branch  
Structures Division  
Air Force Flight Dynamics Laboratory

## ABSTRACT

The severe thermal environment of future hypervelocity aerospace vehicles will place rigorous demands on direct vision window systems. At the high temperatures encountered, heat will be transferred within window materials by both conduction and radiation. This report describes the development and experimental verification of a computer program for predicting the temperature distribution and heat transfer through coated and uncoated, single or multiple glaze window systems. The heat balance equations in the computer program account for emission, attenuation, and absorption of radiant energy within the glaze. Reflection and transmission of glaze surfaces having multilayer, thin-film coatings are computed. Window temperatures and heat flux can be predicted for transient conditions of individual and/or combined convective and radiative heating. The computer program was experimentally verified with heat transfer tests in which specimens of various glaze materials and thicknesses were used. Typical aerospace reflection and antireflection coatings were employed on one and/or both surfaces of the test specimens. The work was performed in three phases. In the first phase the research was applicable to single uncoated glazes. In the second phase the scope was expanded to include coated single glazes, and in the third phase coated and uncoated multiple glazes were investigated. Good agreement between the analytical and experimental results was obtained. The computer program is written in FORTRAN IV language and for the IBM 7094 digital computer. A program user's manual is available as a separate publication.

(This document is subject to special export controls and each transmittal to foreign governments or foreign nationals may be made only with prior approval of the Air Force Flight Dynamics Laboratory (FFDL), Wright-Patterson Air Force Base, Ohio 45433.)

# *Contrails*

# Contracts

## CONTENTS

SECTION	PAGE
I. INTRODUCTION . . . . .	1
II. COMPUTER PROGRAM . . . . .	3
A. DESCRIPTION AND CAPABILITIES . . . . .	3
B. ANALYTICAL MODEL . . . . .	4
C. RADIATION WITHIN THE GLAZE . . . . .	6
D. HEAT BALANCE EQUATIONS . . . . .	6
E. BOUNDARY CONDITIONS . . . . .	7
F. GLAZE THERMOPHYSICAL AND OPTICAL PROPERTIES . . . . .	9
G. FLIGHT CONVECTIVE AND RADIATIVE HEATING . . . . .	11
H. NUMERICAL SOLUTION . . . . .	12
III. EXPERIMENTAL PROGRAM . . . . .	13
A. TEST APPARATUS . . . . .	13
B. WINDOW TEST SPECIMENS . . . . .	25
C. THIN-FILM COATINGS . . . . .	25
D. COATING TEMPERATURE LIMITS . . . . .	25
E. TEMPERATURE SENSORS . . . . .	29
F. SUPERPOSITION TESTS . . . . .	32
G. HEAT TRANSFER TESTS . . . . .	32
H. COATING AND GLAZE DAMAGE . . . . .	35
IV. ANALYTICAL AND EXPERIMENTAL RESULTS . . . . .	38
A. COMPUTER PROGRAM VERIFICATION . . . . .	38
B. ADDITIONAL EXPERIMENTAL RESULTS . . . . .	53
C. ADDITIONAL ANALYTICAL RESULTS . . . . .	53
V. CONCLUSIONS . . . . .	67
APPENDIX A - EQUATIONS FOR COMPUTING RADIATION WITHIN WINDOW GLAZES .	69
APPENDIX B - EQUATIONS USED TO COMPUTE TRANSMITTANCE AND REFLECTANCE OF COATED AND UNCOATED GLAZE SURFACES . . . . .	99
APPENDIX C - THERMOPHYSICAL AND OPTICAL PROPERTIES OF GLAZE MATERIALS . . . . .	111
APPENDIX D - CORRELATIONS USED TO PREDICT IN-FLIGHT HEATING . . . . .	119

# Contrails

## CONTENTS (CONTINUED)

	PAGE
APPENDIX E - SUPERPOSITION TESTS . . . . .	127
APPENDIX F - EXPERIMENTAL RESULTS . . . . .	137
REFERENCES . . . . .	188

# Contrails

## LIST OF FIGURES

FIGURE	TITLE	PAGE
1	WINDOW PANE CROSS SECTION . . . . .	4
2	PRIMARY AND MULTIPLE REFLECTED RADIANT ENERGY . . . . .	5
3	ABSORPTION COEFFICIENT FOR VYCOR (96% FUSED SILICA) . . . . .	10
4	RADIATIVE AND CONVECTIVE TRANSPARENT BOUNDARY APPARATUS . . . . .	14
5	MODIFIED VERSION OF TBA NO. 2 FOR VACUUM TESTING. . . . .	15
6	HIGH TEMPERATURE RADIANT HEATER . . . . .	16
7	SCHEMATIC OF WINDOW AND HEATER CONFIGURATION. . . . .	18
8	CONFIGURATION FACTORS FOR TWO PARALLEL DISKS. . . . .	19
9	RADIATION IN VACUUM WITH $h = 9/16$ IN. . . . .	21
10	CONVECTIVE TRANSPARENT BOUNDARY APPARATUS . . . . .	22
11	TEST SPECIMEN SUPPORT . . . . .	24
12	SCHEMATIC OF APPARATUS COMPONENTS, INSTRUMENTS, AND CONTROLS. . . . .	26
13	WINDOW TEST SPECIMEN . . . . .	27
14	CALIBRATION FIXTURE - OPEN. . . . .	30
15	CALIBRATION FIXTURE - CLOSED . . . . .	31
16	PARALLEL OUTER-INNER GLAZINGS OF THE MULTIPLE GLAZE TESTS . . . . .	34
17	1/4-IN. FUSED SILICA WINDOW HEATED BY RADIATION, STEADY- STATE CONDITIONS. . . . .	39
18	1/4-IN. FUSED SILICA WINDOW HEATED BY CONVECTION, STEADY- STATE CONDITIONS. . . . .	40
19	EFFECTIVE EMISSIVITY OF 1/4-IN. FUSED SILICA PLATE. . . . .	41

FIGURES (CONTINUED)

FIGURE	TITLE	PAGE
20	MEASURED AND COMPUTED TRANSIENT TEMPERATURES. . . . .	42
21	MEASURED AND COMPUTED TRANSIENT TEMPERATURES AND HEAT FLUX.	43
22	1/4-IN. FUSED SILICA, 1/8-IN VYCOR DOUBLE WINDOW HEATED BY RADIATION IN AIR, STEADY-STATE CONDITIONS . . . . .	47
23	1/4-IN. FUSED SILICA, 1/8-IN. VYCOR DOUBLE PANE WINDOW HEATED BY CONVECTION IN AIR, STEADY-STATE CONDITIONS . . . . .	48
24	1/4-IN. FUSED SILICA, 1/8-IN. VYCOR DOUBLE PANE WINDOW HEATED BY RADIATION AND CONVECTION IN AIR, STEADY-STATE CONDITIONS. . . . .	49
25	1/4-IN. FUSED SILICA, 1/8-IN. VYCOR DOUBLE PANE WINDOW HEATED BY RADIATION IN A VACUUM, STEADY-STATE CONDITIONS.	50
26	COMPUTED TEMPERATURE DISTRIBUTION IN 1/4-IN. FUSED SILICA, OPAQUE AND SEMITRANSSPARENT ANALYSIS . . . . .	54
27	COMPUTED TEMPERATURE DISTRIBUTION IN 1/4-IN. FUSED SILICA, HEATED BY RADIATION AND CONVECTION . . . . .	55
28	COMPARISON OF TEMPERATURES AND CABIN HEAT FLUX OF WINDOW SYSTEM HEATED BY RADIATION IN AIR AND IN A VACUUM . . . . .	57
29	THERMAL PERFORMANCE OF A DOUBLE PANE WINDOW DURING A HYPERSONIC SKIP-GLIDE RE-ENTRY. . . . .	59
30	PORTION OF HYPERSONIC SKIP-GLIDE RE-ENTRY TRAJECTORY. . . . .	60
31	THERMAL PERFORMANCE OF A DOUBLE PANE WINDOW DURING A MACH 3 SUPERSONIC FLIGHT . . . . .	61
32	MACH 3 SUPERSONIC TRANSPORT FLIGHT PATH . . . . .	62
33	THERMAL PERFORMANCE OF A DOUBLE PANE WINDOW IN 200 NM CIRCULAR ORBIT . . . . .	64



# Contrails

## FIGURES (CONCLUDED)

FIGURE	TITLE	PAGE
34	STAGNATION POINT HEAT TRANSFER RATE . . . . .	65
35	THERMAL PERFORMANCE OF A DOUBLE PANE WINDOW ASSUMING WINDOW HEATING TO BE 0.02 TIMES $q_{st}$ OF FIGURE 33 . . . . .	66
A-1	MULTIPLE-GLAZE WINDOW SYSTEM. . . . .	82
E-1	SELECTED BOUNDARY CONDITIONS. . . . .	129
E-2	BOUNDARY CONDITIONS THAT CAN BE ELIMINATED BY APPLICATION OF SUPERPOSITION PRINCIPLE. . . . .	129
E-3	SUPERPOSITION TEST IN VACUUM WITH $h = 9/16$ IN. . . . .	131
E-4	SUPERPOSITION TEST IN VACUUM WITH $h = 8.0$ IN. . . . .	132
E-5	SCHEMATIC OF HEAT FLOW BETWEEN TWO PARALLEL PLATES FOR RAYLEIGH NUMBER $\ll 1700$ . . . . .	133
E-6	SUPERPOSITION TESTS . . . . .	134
E-7	PHASE III TEST SETUP. . . . .	136

# Contracts

## LIST OF TABLES

TABLE	TITLE	PAGE
I	VARIATION OF GLAZE TEMPERATURES AND HEAT FLUX WITH THICKNESS FOR FUSED SILICA HEATED BY RADIATION AND CONVECTION . . . . .	45
II	VARIATION OF GLAZE TEMPERATURES AND HEAT FLUX WITH TYPICAL GLAZE MATERIALS FOR 1/4-IN. WINDOW HEATED BY RADIATION AND CONVECTION . . . . .	45
III	EFFECT OF TYPICAL WINDOW COATINGS ON TEMPERATURES AND HEAT FLUX OF 1/4-IN. FUSED SILICA SPECIMEN HEATED BY RADIATION AND CONVECTION . . . . .	45
IV	TEMPERATURES AND HEAT FLUXES FOR VARIOUS GLAZE CONFIGURATIONS AND A CONSTANT RADIATIVE INPUT . . . . .	51
V	TEMPERATURES AND HEAT FLUXES FOR VARIOUS GLAZE CONFIGURATIONS AND A CONSTANT CONVECTIVE INPUT . . . . .	51
VI	TEMPERATURES AND HEAT FLUXES FOR VARIOUS COATING CONFIGURATIONS ON A 1/4-IN. FUSED SILICA AND 1/8 IN. VYCOR WINDOW SYSTEM IN AN AIR ENVIRONMENT . . . . .	52
VII	TEMPERATURES AND HEAT FLUXES FOR VARIOUS COATING CONFIGURATIONS ON A 1/4-IN. FUSED SILICA AND 1/8-IN. VYCOR WINDOW SYSTEM IN A VACUUM ENVIRONMENT . . . . .	52
VIII	EFFECT OF NUMBER OF GLAZES IN A WINDOW SYSTEM ON TEMPERATURES AND HEAT FLUX . . . . .	58
B-I	TRANSMITTANCE OF UV-IR COATING ON VYCOR GLAZE . . . . .	106
B-II	TRANSMITTANCE OF UV-IR COATING ON FUSED SILICA GLAZE . . . . .	106
B-III	TRANSMITTANCE OF UV-IR COATING ON ALUMINOSILICATE GLAZE. . . . .	107
B-IV	TRANSMITTANCE OF HEA COATING ON VYCOR GLAZE . . . . .	107
B-V	TRANSMITTANCE OF HEA COATING ON FUSED SILICA GLAZE . . . . .	107
B-VI	TRANSMITTANCE OF HEA COATING ON ALUMINOSILICATE GLAZE . . . . .	108

# Contrails

## TABLES (CONCLUDED)

TABLE	TITLE	PAGE
B-VII	TRANSMITTANCE OF GOLD COATING ON VYCOR GLAZE . . . . .	108
B-VIII	TRANSMITTANCE OF GOLD COATING ON FUSED SILICA GLAZE . . .	108
B-IX	TRANSMITTANCE OF GOLD COATING ON ALUMINOSILICATE GLAZE . .	109
C-I	MATERIAL - FUSED SILICA . . . . .	113
C-II	MATERIAL - VYCOR (96 PERCENT SILICA) . . . . .	114
C-III	MATERIAL - ALUMINOSILICATE . . . . .	115
C-IV	MATERIAL - BOROSILICATE . . . . .	116
C-V	MATERIAL - SODA LIME . . . . .	117
D-I	COEFFICIENT FOR THE LEAST-SQUARES FIT, LOW TEMPERATURE: 1000 ≤ T ≤ 8000°K . . . . .	122
D-II	COEFFICIENTS FOR THE LEAST-SQUARES FIT, HIGH TEMPERATURE: 8000 ≤ T ≤ 18000°K . . . . .	123

# *Contrails*

# Contrails

## SECTION I

### INTRODUCTION

Previously, pilot visibility has been treated as a relatively minor problem in the design of aircraft. The aircraft designer simply modified his design to provide the pilot with the most advantageous view of the outside surroundings from within the confines of the cockpit using ordinary, highly transparent window materials. However, the severe thermal environment of future hypersonic (Mach 5+) and hypervelocity (Mach 10+) aerospace vehicles will place much more rigorous demands on direct vision window systems than were ever contemplated in our current window designs. Steady-state temperatures approaching 2000°F will be experienced, not for a few brief minutes, but for prolonged periods of time during hypersonic cruise and lifting re-entry flight.

If direct vision systems continue to play a major role in mission performance, design engineers must undertake new design approaches rather than continue the preferred method of modification and improvement of an existing, proven design. The limited amount of operational experience of high-temperature windows has underscored the severity of this problem. The designer of advanced high-temperature window systems will require realistic approaches to aid him in evaluating thermal shock, thermal gradients, and heat soak conditions of transparent materials. Toward this end, Midwest Research Institute under contract to the Air Force has completed the development of a computer program to predict the heat flux and temperature distributions through high-temperature transparent materials, both coated and uncoated. The glazes,\* the coatings, and the test conditions have been selected to simulate the requirements and the thermal environment of hypersonic flight. This approach yields empirical data on realistic window components in addition to supplying input data for validation of the computer program.

The work was performed in three phases. In the first phase, the research was applicable to single uncoated glazes. In the second phase, the scope was expanded to include coated single glazes, and in the third phase, coated and uncoated multiple glazes were investigated.

During Phase I, 27 single glaze experimental tests were conducted involving three window glaze materials, three glaze thicknesses, and three

---

\* The term glaze as used in this discussion refers to window materials such as fused silica, plastic, etc.

# Contrails

modes of heat transfer. The three specimen materials tested were fused silica, aluminosilicate, and 96% fused silica having thicknesses of 1/8, 1/4, and 3/8 in. Each of the nine specimens was subjected to convective, radiative, and combined radiative and convective heating. Modifications of the single glaze computer program (Ref. 1) were completed, resulting in a good correlation between the computer and experimental glaze temperatures and heat flux.

Eighty-five single glaze tests were conducted in Phase II of the research program. These tests were similar to those conducted in Phase I with the exception of the test specimens. The glaze specimens were of the same materials and thicknesses as those of Phase I, but employed thin-film coatings on one or both surfaces. A subroutine was added to the computer program which calculated the transmittance and reflectance of glaze surfaces having thin-film, multiple-layer coatings. In addition, a routine was included in the program so that the coating transmission and reflection can be read as input data, rather than being computed, if these data are available. The temperatures of and heat fluxes through coated single glazes were computed and compared with those measured experimentally. Good correlation was obtained between the computed and measured values.

During Phase III, 112 double glaze experimental heat transfer tests were conducted in both air and vacuum environments using coated and uncoated glazes of various materials and thicknesses. The computer program was modified and expanded to include the thermal analysis of coated and uncoated, multi-glaze window systems. Computed temperatures of, and heat flux through, double glaze window configurations were in good agreement with the Phase III experimental results.

A discussion of the theory, heat balance equations, and the capabilities of the computer program is presented in Section II of this report. Section III describes the equipment, glaze test specimens, and instrumentation employed in the experimental effort. A comparison and discussion of the experimental and analytical results are presented in Section IV and the conclusions are given in Section V.



## SECTION II

### COMPUTER PROGRAM

A major objective of the effort described in this report was to generate a method of predicting temperature distributions and heat fluxes through coated and uncoated single and multiple-glaze aerospace windows subjected to individual and combined convective and radiative heating. This objective was accomplished by modifying and expanding a computer program previously developed (Ref. 1) for single-glaze windows.

#### A. Description and Capabilities

The computer program is designed for the thermal analysis of window systems containing as many as five window panes of different materials and thicknesses with thin-film coatings on any or all of the glaze surfaces. The spaces between the window panes can contain a moving gas, a stationary gas, or a vacuum. Transient window temperatures and heat flux to the cabin can be computed for time-dependent radiative and/or convective heating conditions. The computer program contains subroutines for computing the heat flux to the window using accepted aerodynamic heating correlations. As an alternative option, heat transfer rates to the window can be included in the input data. Reflection and transmission of the glaze surfaces may be computed for coated and uncoated window panes or be input if these data are available. The basic assumptions made in the analysis are:

1. The heat transfer is one-dimensional and normal to the glaze.
2. The window panes are composed of plane parallel, optically smooth, homogeneous, and isotropic glaze material.
3. The materials are considered to be nondispersive.
4. Any external radiant source is considered perfectly diffuse and initially unpolarized.
5. Radiation emitted within the glaze is considered to be perfectly diffuse and initially unpolarized.
6. Attenuation of radiation within the glaze material is described by the Bouguer-Lambert law.
7. Radiative emission within the glaze is described by Gardon's derived volumetric emissive power.

## B. Analytical Model

Assuming one-dimensional heat transfer to be the case, an analytical model was established by treating each window pane as being composed of 11 finite slices or elements (Figure 1).

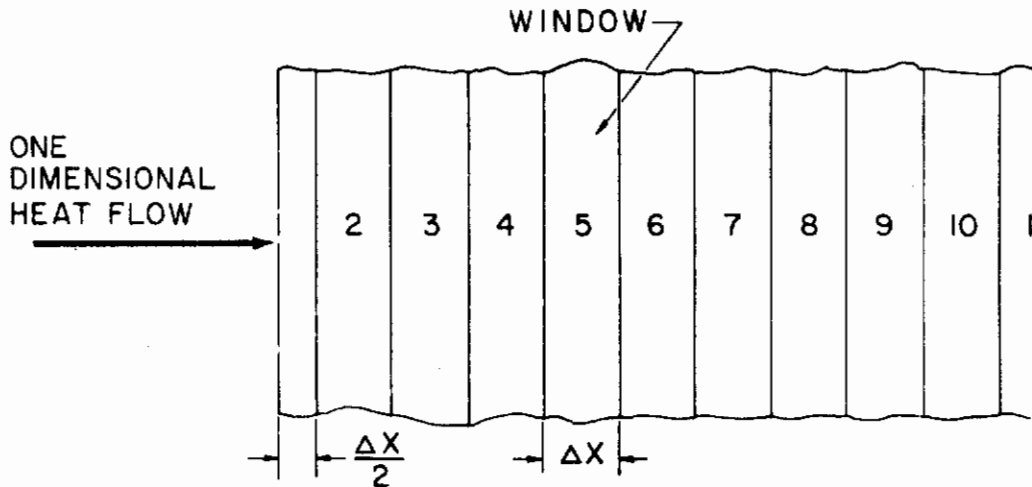


Figure 1 - Window Pane Cross Section

Unlike opaque bodies, absorption by diathermanous materials takes place in depth, and unlike perfectly transparent materials, semitransparent materials partially absorb impinging radiation. Thus, the energy absorbed by each element within the window is that received by both conduction and radiation since the glaze is considered transparent or semitransparent to radiation emitted within given spectral bands. Each slice receives radiant energy from each of the remaining ten elements as well as from external radiant sources. Radiation from an external source is partially reflected and partially refracted at the glass surface. A portion of the refracted energy is absorbed as it traverses the window and is then partially reflected back into the glass at the second surface. This internally reflected radiation is treated as multiple reflected beams which are partially reflected each time they reach the surfaces and are partially absorbed each time they traverse the window. Radiation energy emitted from each elemental slice is also absorbed and multiply reflected within the glass. Thus, each element absorbs energy emitted directly from the external and internal sources as well as from the multiple reflections of the radiation from these sources (Figure 2).



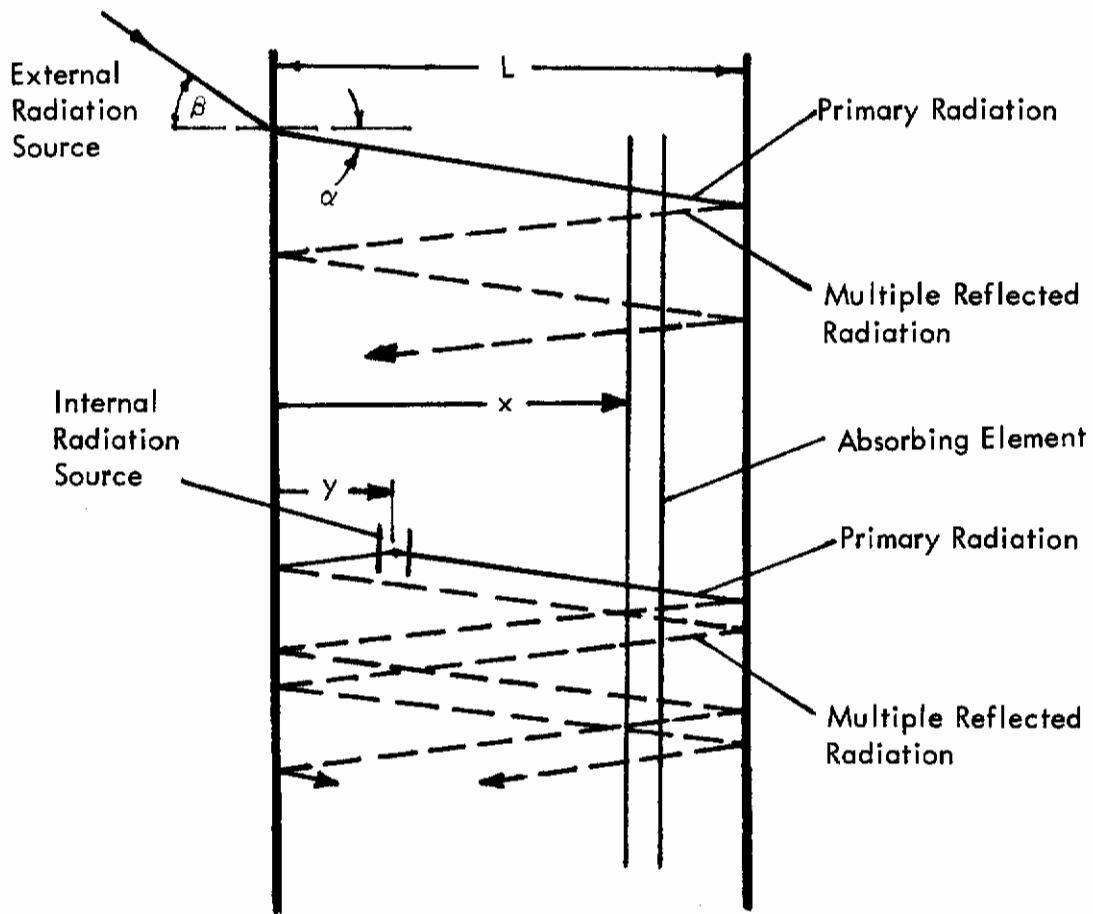


Figure 2 - Primary and Multiple Reflected Radiant Energy

## C. Radiation Within the Glaze

The theory employed in the analysis is that developed by Gardon (Refs. 2 and 3) and used by Lis, Barile, and Engholm (Ref. 1) in the initial development phases of the subject computer program. This theory has as its basis the well-known Bouguer-Lambert law and a volumetric emissive power derived by Gardon (Ref. 4) to compute the radiant energy absorbed and emitted, respectively, by the elements within the glaze. The Bouguer-Lambert law,

$$I_x = I_0 e^{-\gamma_\lambda x \sec \alpha}$$

relates the attenuation and absorption of radiation to an absorption coefficient,  $\gamma$ , and to the distance,  $x \sec \alpha$ , traveled by the radiation. Volumetric emissive power,

$$j_\lambda = \gamma_\lambda n^2 W_{B\lambda} / \pi$$

relates the radiant intensity emitted per unit volume to the glaze absorption coefficient, the glaze index of refraction,  $n$ , and the hemispherical emissive power of a blackbody radiator,  $W_{B\lambda}$ .

The radiant energy that is absorbed by a given element is based on the reduction in intensity of the radiation as the beams pass through the element.

## D. Heat Balance Equations

The general heat balance equation for each element is written in its finite difference form as:

$$\rho c \frac{\Delta T_i}{\Delta t} = \sum_{\lambda} \left[ Q_{A\lambda}(i) - Q_{E\lambda}(i) \right] + K \left[ \frac{T_{i-1} - 2T_i + T_{i+1}}{\Delta x^2} \right]$$

Net heat transfer to and from the glaze element by conduction is defined by the last term in the equation. The term  $Q_{A\lambda}(i)$  represents the radiant energy absorbed by the element at position  $x$ . Sources of this radiation consist of the other elements and surface coatings within the window system and the shock heated air flowing over the window's outer surface. Energy

emitted by the element at position  $x$  is represented by the term  $Q_{E\lambda}(i)$ . Since the absorption and emission of radiation by the elements are spectrally dependent, these values are computed for and summed over finite wavelength bands within the spectral region for which the glaze is considered to be semitransparent. The spectrally dependent glaze properties are considered constant within a given finite wavelength band. The percent of energy emitted within a given finite wavelength band by the external source, the surface coatings, and the glaze elements is based on a table of Planck's blackbody radiation functions. The equations for the radiant energy absorbed and emitted in the glaze, i.e., for  $Q_{A\lambda}(i)$  and  $Q_{E\lambda}(i)$  are developed and presented in Appendix A.

## E. Boundary Conditions

In addition to conduction and radiation within the glaze material, the heat balance equations for the surface elements include terms which account for heat transfer to and from the window by convection and by radiation at wavelengths to which the glaze is considered opaque. For Element 1, the energy balance equation is written as:

$$\begin{aligned} \frac{\Delta x \rho c}{2} \frac{\Delta T_1}{\Delta t} = & \Delta x \sum_{\lambda} \left[ Q_{A\lambda}(1) - Q_{E\lambda}(1) \right] + \frac{k}{\Delta x} \left[ T_1 - T_2 \right] \\ & + \left[ (1 - \rho_L) P_L + (1 - \rho_R) P_R \right] \epsilon \sigma T_H^4 - \left[ (1 - \rho_L) P_L + (1 - \rho_R)(1 - \rho_R) \right] \sigma T_1^4 \\ & + h_a \left[ T_a - T_1 \right] + q_s \end{aligned}$$

In this equation the convective heating or cooling can be input as a heat flux,  $q_s$ , or can be defined using a heat transfer coefficient,  $h$ , times the difference between the air temperature,  $T_a$ , and the element temperature,  $T_1$ . Radiation of wavelengths to which the glaze is considered to be opaque is absorbed and emitted at the surface, and is computed by the terms containing  $T_H^4$  and  $T_1^4$ , respectively. Temperature,  $T_H$ , is that of the shock heated air if the glaze under consideration is the outermost pane in the window system. For the remaining window panes,  $T_H$  is taken as the temperature of the lower surface of the preceding glaze. The symbols  $P_L$  and  $P_R$  represent the percent of energy emitted at wavelengths from zero to the left cutoff point and from zero to the right cutoff point, respectively, of the spectral region in which the glaze is considered to be transparent or semitransparent. For example, fused silica is considered to be transparent

# Contrails

and/or semitransparent over the wavelength region from  $\lambda = 0.4 \mu$  to  $\lambda = 4.8 \mu$ . Thus, the left and right cutoff points for fused silica are at  $0.4$  and  $4.8 \mu$ , respectively. Symbols  $\rho_L$  and  $\rho_R$  are the mean reflectivities of the glaze to radiation in the spectral regions to the left and to the right of the transparent region's cutoff points.

For Element 11 the heat balance equation is written as:

$$\begin{aligned} \frac{\Delta x \rho c}{2} \frac{\Delta T_{11}}{\Delta t} &= \Delta x \sum_{\lambda} \left[ Q_{A\lambda}(11) + Q_{E\lambda}(11) \right] + \frac{k}{\Delta x} \left[ T_{10} - T_{11} \right] \\ &- \left[ (1-\rho_L)P_L + (1-\rho_R)(1-P_R) \right] \sigma T_{11}^4 + \left[ (1-\rho_L)P_L + (1-\rho_R)(1-P_R) \right] \epsilon \sigma T_c^4 \\ &- h_c \left[ T_{11} - T_c \right] \end{aligned}$$

The temperature,  $T_c$ , represents the aircraft or spacecraft cabin temperature if the glaze under consideration is the innermost pane in the window system. For the remaining window panes,  $T_c$  is taken as the temperature of the upper surface of the succeeding glaze.

When predicting the temperatures for uncoated glazes, the reflectivities of the surfaces are computed with Fresnel's equations (see Appendix B, p. 101). The transmittance of the glaze surfaces is computed as  $1-\rho$ .

In many instances the windows of aerospace vehicles employ thin-film coatings designed to provide certain desirable optical features. For example, various coatings have been developed to reflect ultraviolet radiation, to reflect infrared radiation, and to reduce glaze surface reflection in the visual region of the spectrum. For coated glazes, the computer program incorporates a subroutine to compute the reflectance and transmittance of glaze surfaces having single or multiple-layer, dielectric and/or metallic thin-film coatings. The technique employed in the computation is that developed by Berning (Ref. 5) in which the reflectance is determined as the final step in a recursion process which calculates the admittance of each layer of the thin-film coating beginning with the innermost layer and ending with the incident media (see Appendix B). The absorptance of the coating is evaluated as  $1-\rho-\tau$ .

# Contrails

A read-in subroutine is also included in the computer program so that the transmission and reflection of a given thin-film coating can be included in the input data rather than be computed by the thin-film subroutine if these data are available. When the transmission and reflection data for coated surfaces are input, the absorptance of the coating is computed as  $1-\tau-\rho$ .

## F. Glaze Thermophysical and Optical Properties

The glaze properties employed in the analysis, which are considered to be temperature-dependent, are: the glaze index of refraction, thermal conductivity, heat capacitance (density times specific heat) and absorption coefficient. Properties for which the spectral dependence is taken into account include the glaze absorption coefficient and the reflectance, transmittance, and absorptance of the coated glaze surfaces.

The values of index of refraction, thermal conductivity, and heat capacitance were obtained from Ref. 6 for the glaze materials used in the calculations. Spectral values of absorption coefficient were determined by Finch (Appendix A of Ref. 7) based on transmittance of glaze specimens of known thicknesses and taking into account the reflectance of the specimen surfaces. Typical values of absorption coefficient are presented in Figure 3. The dashed line represents the average value of the absorption coefficient used in each of the five finite wavelength bands employed in the numerical integration over the spectral region in which the glaze is considered to be transparent or semitransparent.

The reflectance of uncoated window surfaces is computed from Fresnel's equation as a function of beam incident angle and glaze index of refraction. For coated glaze surfaces the reflectance and transmittance are computed using Berning's analysis as a function of incident angle and the wavelength of the incident beam. Data required for this calculation include the thickness, extinction coefficient, and index of refraction of each layer in the multiple layer coating. Average values of these properties are input for each of the five finite wavelength bands considered in the numerical integration over wavelength.

When the reflectance and transmittance of a coated surface are included in the input data, values must be input as an array versus incident angle for each of the five wavelength bands considered in the analysis.

The thermophysical and optical properties of five typical glaze materials are given in Appendix C. These properties are stored as block data in the computer program. Thus, calculation of the temperatures and the heat flux through window systems constructed from these five materials can be accomplished without inputting glaze property data.

# Contrails

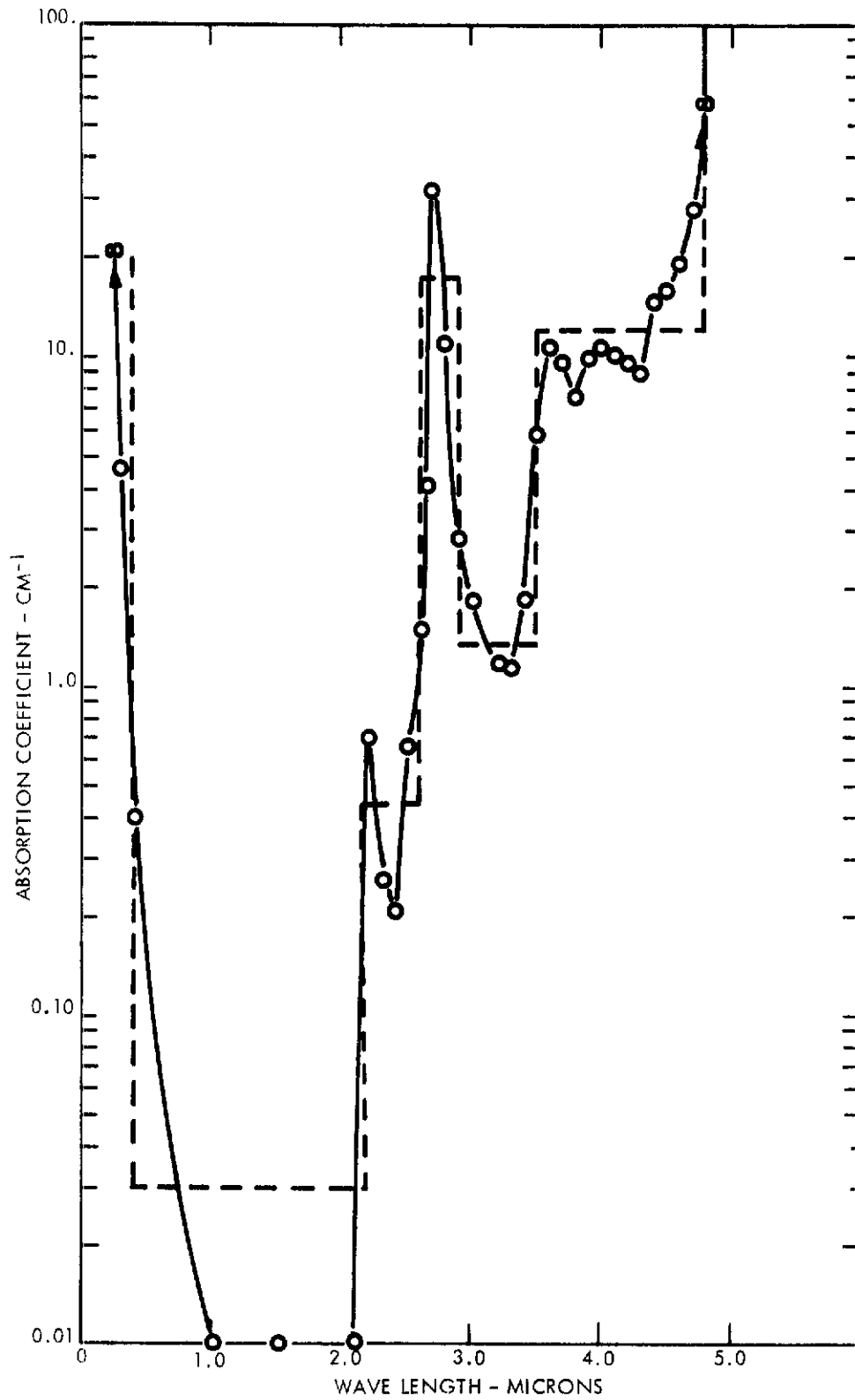


Figure 3 - Absorption Coefficient for Vycor (96% Fused Silica)



## G. Flight Convective and Radiative Heating

Various methods of computing the heat input to the window are used by the program, depending on the mission under consideration, i.e., hypersonic flight, re-entry, supersonic flight, or orbital flight.

For hypersonic flight and re-entry, the convective input to the window is expressed as a percentage of the stagnation point heat transfer rate. The stagnation point convective heating is computed using the correlation of Kemp and Riddell (Ref. 8). The percentage or ratio of convective heat transfer rate at the window to that at the stagnation point is generally determined by heat flux data obtained during wind tunnel tests using a model of the actual vehicle being designed. Radiative heating of the window during hypersonic flight and re-entry is from the hot air in the shock layer. Emissivities of the shock heated air are determined by curve fits of the data of Kivel and Bailey (Ref. 9) which present the emissivity of heated air as a function of its temperature and density. The temperature and density of the air behind the shock wave is determined from the free stream conditions and normal shock relationships.

For supersonic flight, the convective input is computed from a flat plate heating correlation (Ref. 10) based on free stream conditions. No radiative input is considered for the supersonic case because the gaseous radiation is negligible. Since the emissivity of air is relatively low, gaseous radiation does not become significant until extreme air temperatures are reached such as those in the shock layer of hypersonic flight and re-entry.

For orbit and above an input critical altitude in the hypersonic and supersonic flight cases, the convective heating is computed from a free molecular heat transfer correlation (Ref. 8). The radiative heating from the sun is approximated by using a solar temperature of 6000°K and an appropriate form factor. Since the solar radiation is collimated and the computer program analysis assumes the external radiation to be perfectly diffuse, solar heating of the window is only approximated.

The input data required for using the flight heating subroutines are dependent on the type of flight being considered. These data include flight time, altitude, free stream conditions (velocity, temperature, pressure, density, viscosity and Mach number), and shock layer conditions (temperature, pressure, and density). Appendix D contains a discussion and outline of the equations and correlations used by the program to compute inflight heating of aerospace windows.

A convective heating rate versus time can also be included in the input data. This allows the convective heat flux computed by any desirable method to be used in the program. A constant radiative heating rate can be described by input data if so desired by inputting a heat source temperature and emittance, and an appropriate configuration factor. This option was used when computing glaze temperatures for comparison to those measured in the experimental heat transfer tests.

## H. Numerical Solution

The heat balance equations for each glaze element in the window system can be written in either the explicit or implicit form, i.e., the heat transfer between elements and to the surrounding environment can be related to the element temperatures at time  $t$  or time  $t + \Delta t$ . In order not to violate the second law of thermodynamics, an explicit or forward difference equation is subject to a stability criterion which limits the time step used in the numerical solution (Refs. 11 and 12). No stability criteria are required for the implicit or backward difference equation. The heat balance equations employed in the computer solution are of mixed form and written as follows:

$$\rho c \frac{T'_i - T_i}{\Delta t} = \sum_{\lambda} [Q_{A\lambda}(i) - Q_{E\lambda}(i)] + k \left[ \frac{T'_{i-1} - 2T'_i + T'_{i+1}}{\Delta x^2} \right]$$

where the primed temperatures refer to values at time  $t + \Delta t$ . Conductive heat transfer between the elements, described by the last term in the above equation, is based on the element temperatures at time  $t + \Delta t$ . The radiant energy absorbed,  $Q_{A\lambda}(i)$ , and that emitted,  $Q_{E\lambda}(i)$ , by an element at location  $x$  are computed from the glaze element temperatures at the beginning of the time step.

Since the finite difference equations used in the numerical solution are approximations of integral-differential equations, both the implicit and explicit forms are subject to truncation error. To minimize truncation error and insure computational stability, a technique developed by Lis (Ref. 1) is employed in the program. Glaze temperatures at time  $t + \Delta t$  are computed using a given time step,  $\Delta t$ . Next, the glaze temperatures at time,  $t + \Delta t$ , are computed using two  $\Delta t/2$  time steps. This temperature field is compared to that computed using a single time step,  $\Delta t$ , and if the comparison agrees within a prescribed accuracy the computed temperatures are accepted. If the temperature fields do not agree, the given time step is halved and the procedure is repeated until agreement is obtained.



## III.

### EXPERIMENTAL PROGRAM

The experimental effort included heat transfer testing of coated and uncoated glazes subjected to radiative, convective, and combined radiative and convective heating. The test apparatus (Figures 4 and 5) was designed such that the test specimen(s) have a transparent boundary allowing the tests to be carried out under conditions similar to those encountered in flight of aerospace vehicles. This approach yields empirical data on realistic window components in addition to supplying input data on which to validate the computer program.

#### A. Test Apparatus

The test apparatus, Transparent-Boundary Apparatus (TBA) No. 1 (used for radiation and radiation plus convection testing), TBA No. 2 (used for convection only testing), and a modified version of TBA No. 2 (used for vacuum testing), were designed after that used for the work done under Contract No. AF 33(657)-9138 (Ref. 7), with the major differences being in the method of measuring heat flux through the window glaze system and in the manner of attaching potential and current leads to the gold temperature sensors on the glaze specimen. These differences will be described later in this report.

1. Heat sources: The sources of heat for the test apparatus were high velocity convective burners and/or an electric element, radiant heater.

a. Radiant heater: The radiant heater (Figure 6) has a spiral resistance element  $3/8$  in. wide and  $1/16$  in. thick with a resistance of approximately 0.1 ohm; maximum voltage was 20 v. It was made of Hastelloy X alloy, which has an adherent oxide coating at temperatures exceeding  $2000^{\circ}\text{F}$  and has sufficient strength at these temperatures to maintain its shape without sagging. To assure no distortion of the long spiral element, Hastelloy X rods ( $3/32$  in. diameter) were butt welded to the flat spiral strip to provide support. These rods and the terminal rods passed through a refractory insulating block,  $2-1/2$  in. thick, and were held on the back of the block by clips. Thus the refractory block supported the heater element and thermally insulated the rear side of it. Two chromel-alumel thermocouples were employed for measuring the heater temperature.

The heat flow through aerospace windows in actual flight and in simulated flights on the subject computer program is essentially one-dimensional. Therefore, in the experimental program it was important that the impinging radiation be uniformly distributed over the window surface.

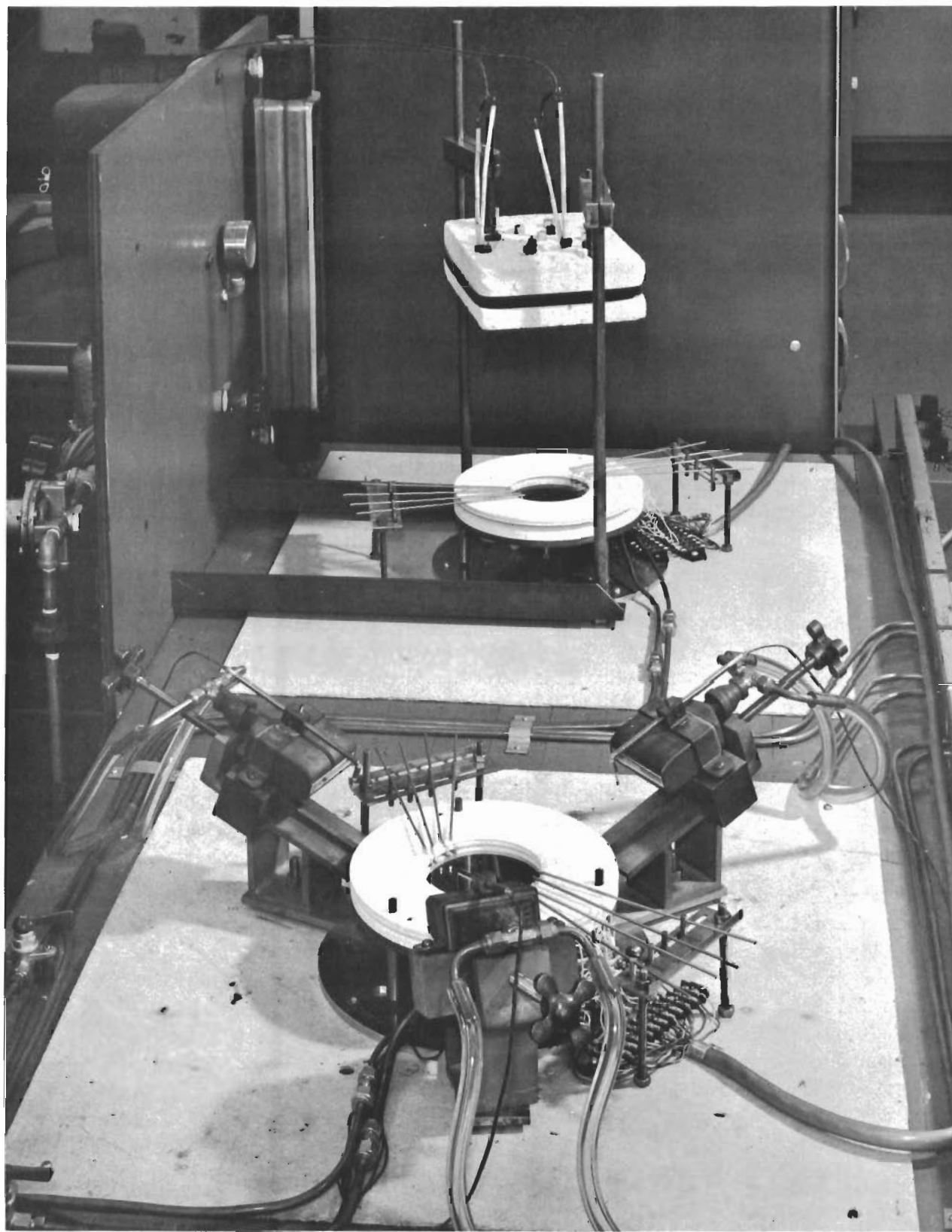


Figure 4 - Radiative and Convective Transparent Boundary Apparatus

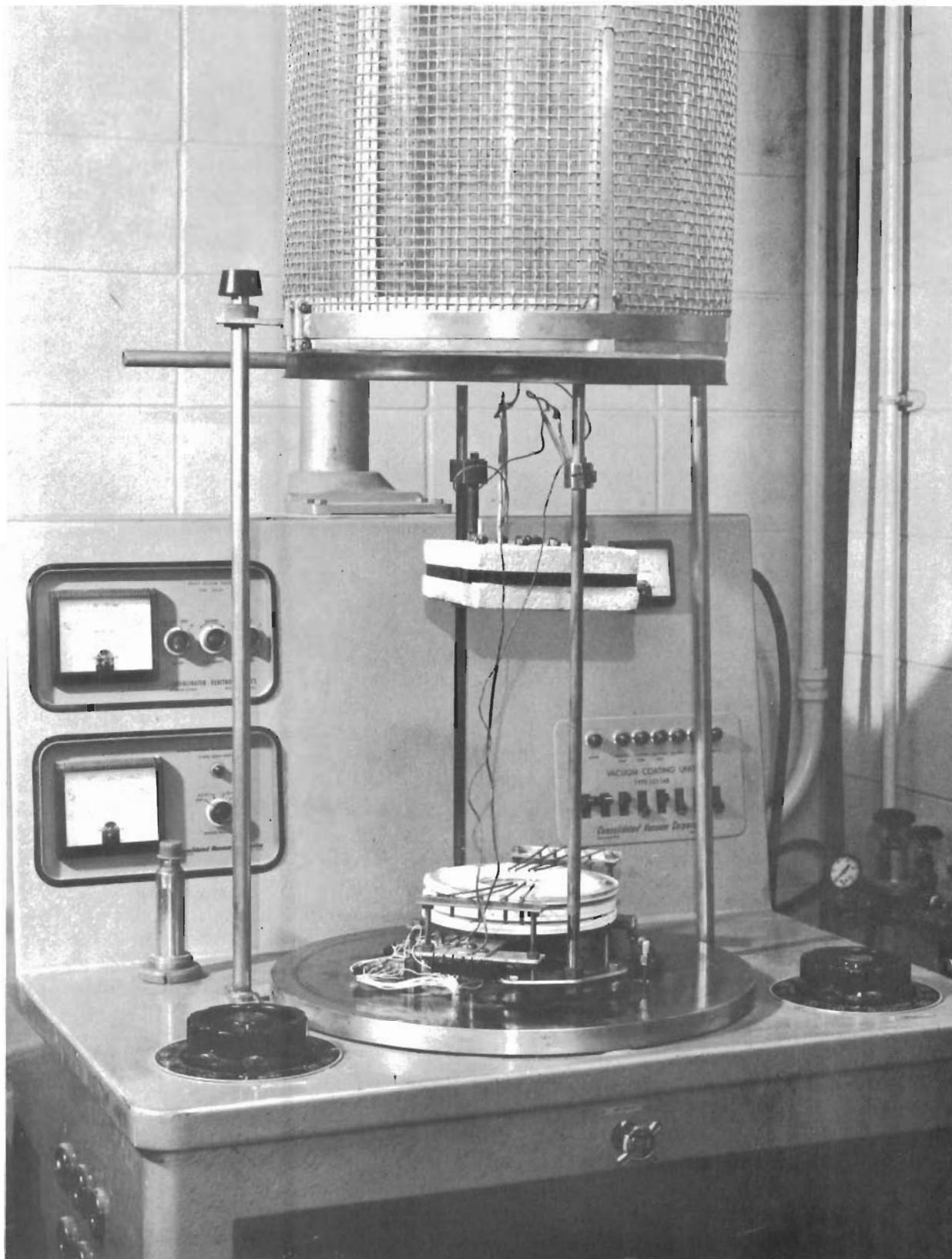


Figure 5 - Modified Version of TBA No. 2 for Vacuum Testing





Figure 6 - High Temperature Radiant Heater

# Contrails

This can be accomplished with a disk-shaped heater provided that its surface temperature,  $T_H$ , is uniform and the relative size and the spacing of the heater and window are carefully analyzed.

The temperature distribution of the heater was determined with an Ircon model 300 optical pyrometer. At  $T_H \approx 1150^\circ\text{F}$  the absolute temperature varied by  $\pm 1\%$ , and at  $T_H \approx 1650^\circ\text{F}$  the absolute temperature varied by  $\pm 2\%$ . These differences result in maximum variations of emissive power of approximately 4 and 8%, respectively.

If the heat is emitted uniformly it will impinge the window uniformly provided either of the following conditions exists:

1. The heater is designed and positioned in such a way that every element on the window surface "sees" nothing but the heater; or
2. The heater is positioned such that it is "seen" equally well by each element of the window surface.

The first criterion is satisfied if  $r_H/r_W \rightarrow \infty$  or  $h \rightarrow 0$ ; the second requires that  $h \rightarrow \infty$ . The variables  $r_H$ ,  $r_W$  and  $h$  are illustrated in Figure 7. These ideal conditions are not practical in the laboratory; therefore, reasonable compromises based on further analysis were made.

The local heat flux impinging the window surface is characterized by

$$q = \sigma F_A \epsilon T_H^4$$

where  $F_A$  is the local configuration factor which allows for the average angle through which the heater is "seen." The shape factor frequently reported and used for two parallel, finite disks is an average value and does not account for local variations. Since it is these variations that must be minimized in the experimental program, the apparatus design was not based solely on the average configuration factor.

By employing shape factor algebra--that is, by subdividing the disks into rings, a study was made by Finch (Ref. 7) to determine the relationship between the local configuration factor and the variables  $h$  and  $r_W$  for  $R_H = 3$ . The results are plotted in Figure 8. For comparison, the average values of  $F_A$  were obtained from configuration charts developed by Hamilton and Morgan (Ref. 13) and are plotted as dashed lines for  $h = 2.0$  in. and  $h = 4.0$  in.

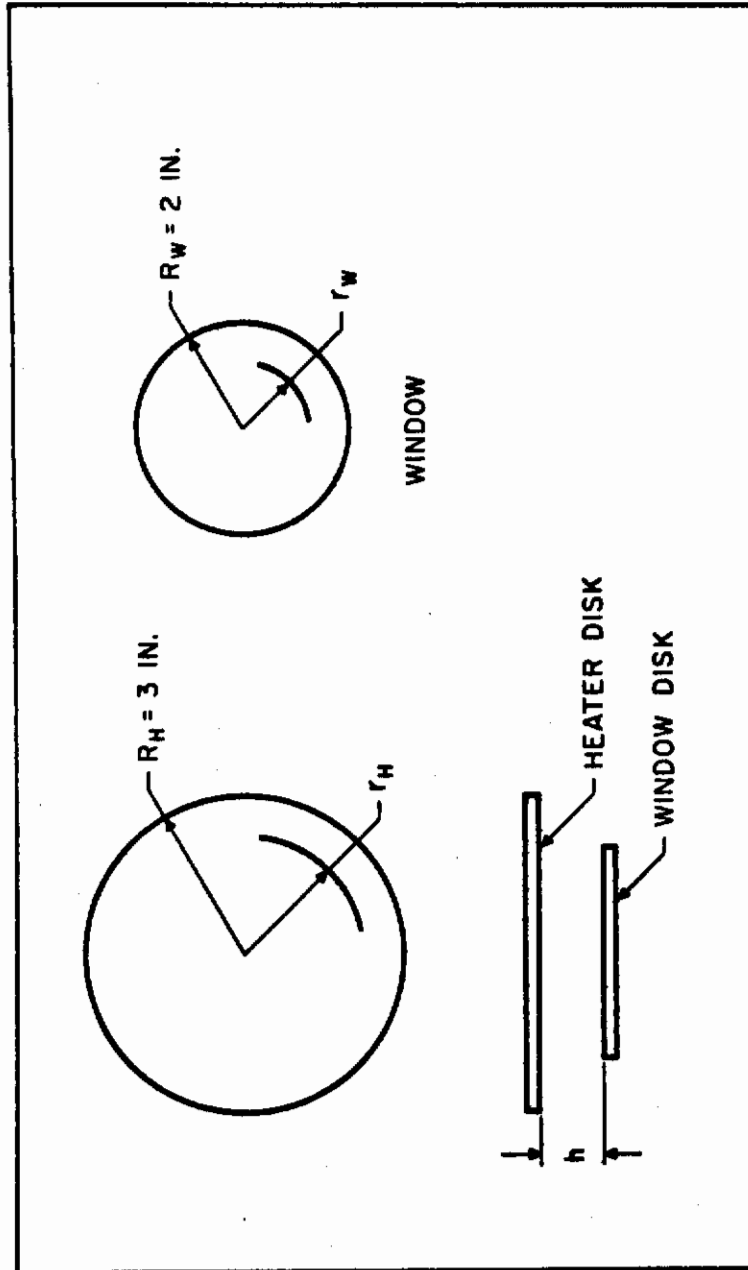


Figure 7 - Schematic of Window and Heater Configuration

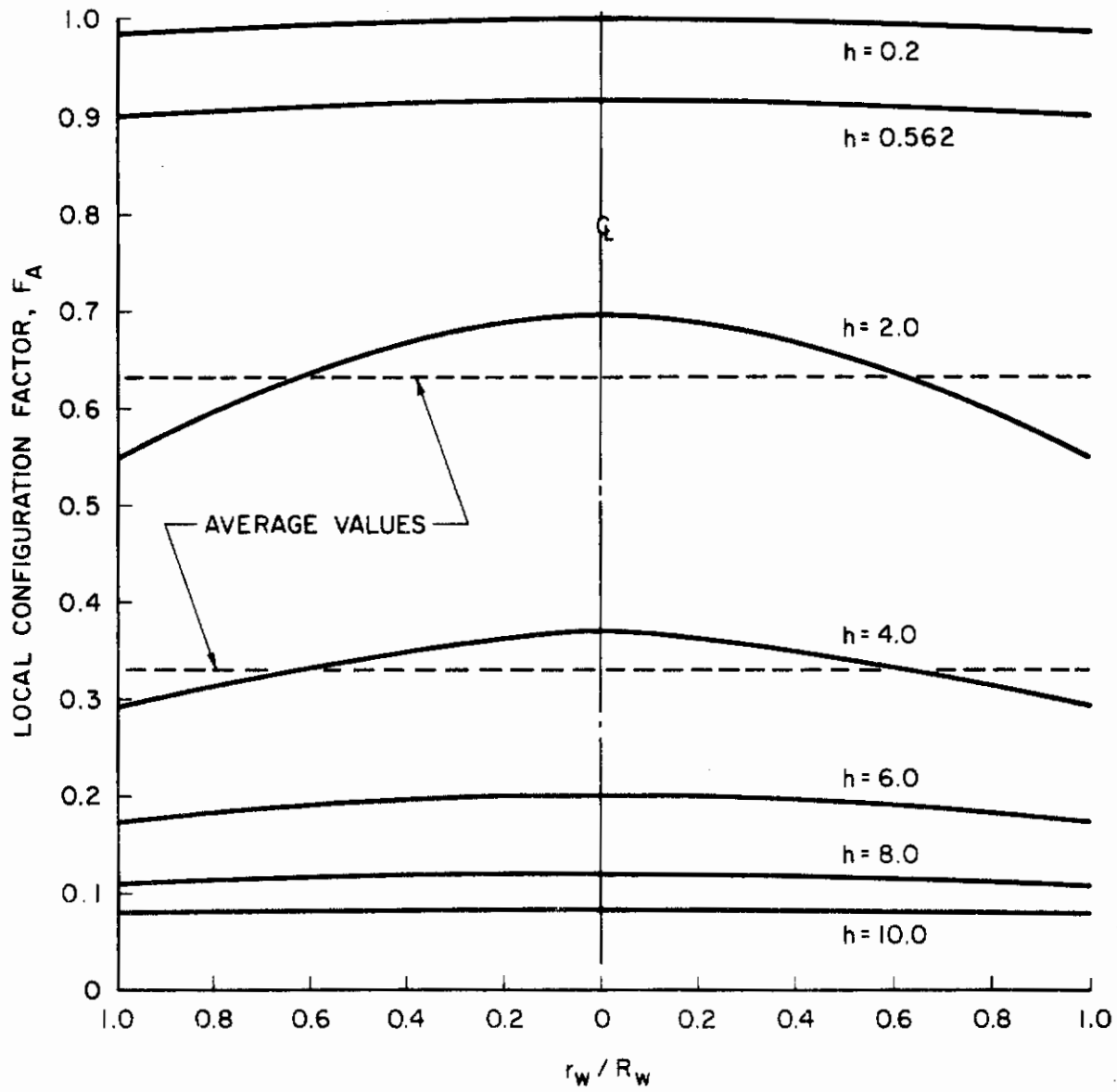


Figure 8 - Configuration Factors for Two Parallel Disks

# Contrails

The configuration factor curves indicate that the percent deviation of the local value of  $F_A$  from the average is greatest when the heater is positioned about 3 in. from the window. At  $h = 2.0$  and  $h = 4.0$  the variation from average is approximately  $\pm 15$  and  $\pm 10\%$ , respectively. As expected,  $F_A$  approaches a constant as  $h \rightarrow 0$  or when  $h \gg 1$ . At  $h = 0.562$  in.,  $F_A$  deviates from the average by less than 2%; at  $h = 8.0$  in., the variation is approximately 4%. Primarily as a result of this analysis, the following heater positions were selected for the experimental program:

$$h = 9/16 \text{ in. and } h = 8 \text{ in.}$$

For the case where radiation was the primary source of heat transfer to the window, the heater was positioned 9/16 in. above the glass, and for the case where radiation and convection were simultaneously used, the heater was placed 8 in. above the window.

To determine the emittance of the radiant heater the heat flux from the heater was measured in a vacuum environment with the heater positioned 9/16 in. above the calorimeter mounted in the heat sink of the test apparatus (Figure 9). Using these data and a configuration factor from Figure 8, a value of 0.93 was computed for the heater emittance from the expression:

$$\epsilon = \frac{q}{\sigma F (T_H^4 - T_C^4)}$$

Temperatures of 2200°F were reached by the radiant heater resulting in a heat flux of 73,000 Btu/hr-ft<sup>2</sup> at the incident surface of the test specimen. At this temperature approximately 81% of the energy is emitted at wavelengths for which the glaze is considered to be transparent or semitransparent to radiation.

b. Convection burners: The convective source consisted of three burners mounted so that they could each be adjusted in three directions (Figure 10). These are SH-3 Selas superheat burners with a rectangular blast opening 2-1/8 in. long by 1/8 in. wide and a flared tongue. The burners were supplied with natural gas and compressed air. Combustion occurs inside the burner and the products of combustion are forced out the blast opening at a high velocity. Various combinations of burner positions were experimentally evaluated to determine the optimum arrangement with respect to uniform heating. These tests were run on a 1/32 in. stainless



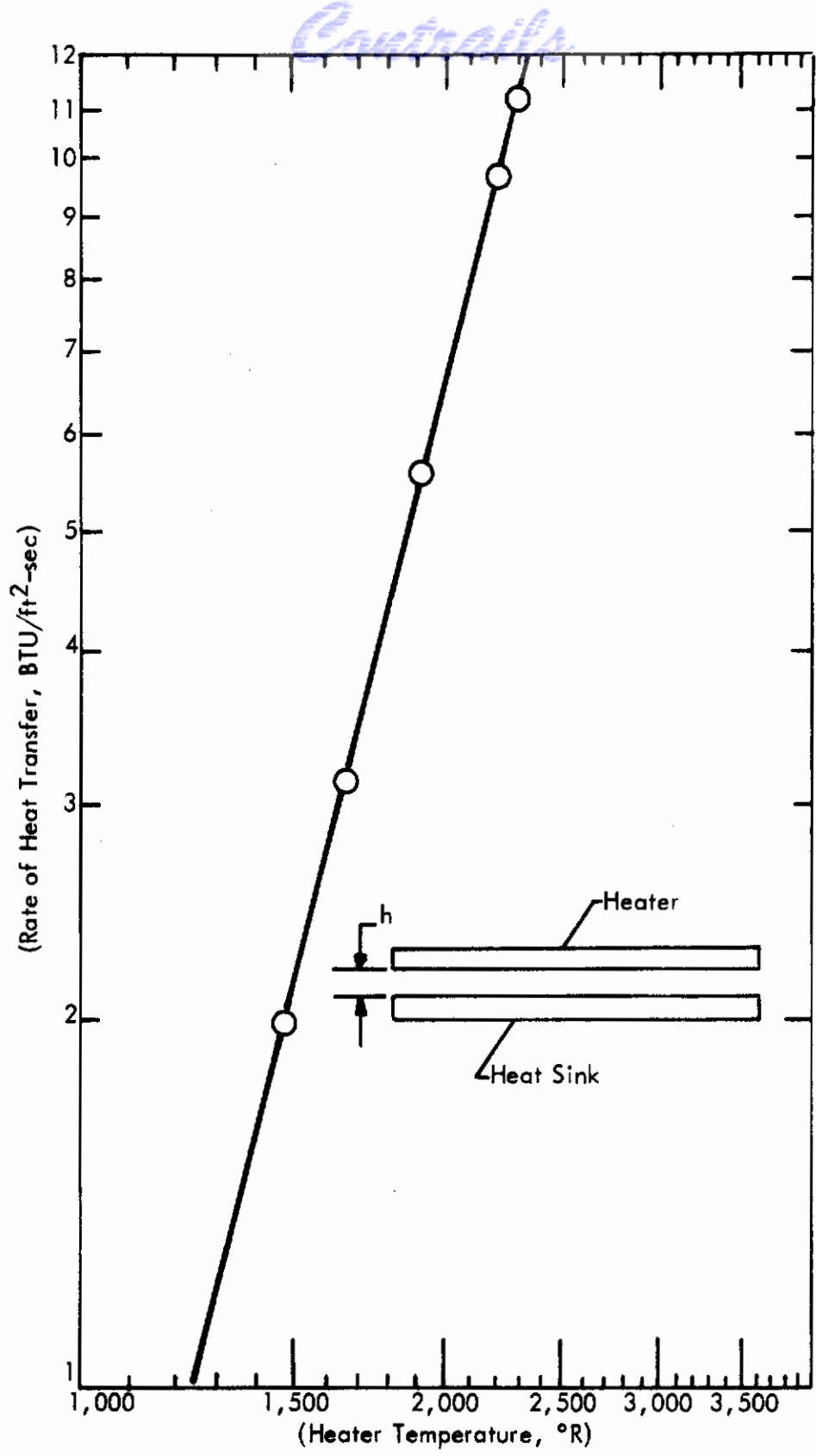


Figure 9 - Radiation in Vacuum With  $h = 9/16$  In.

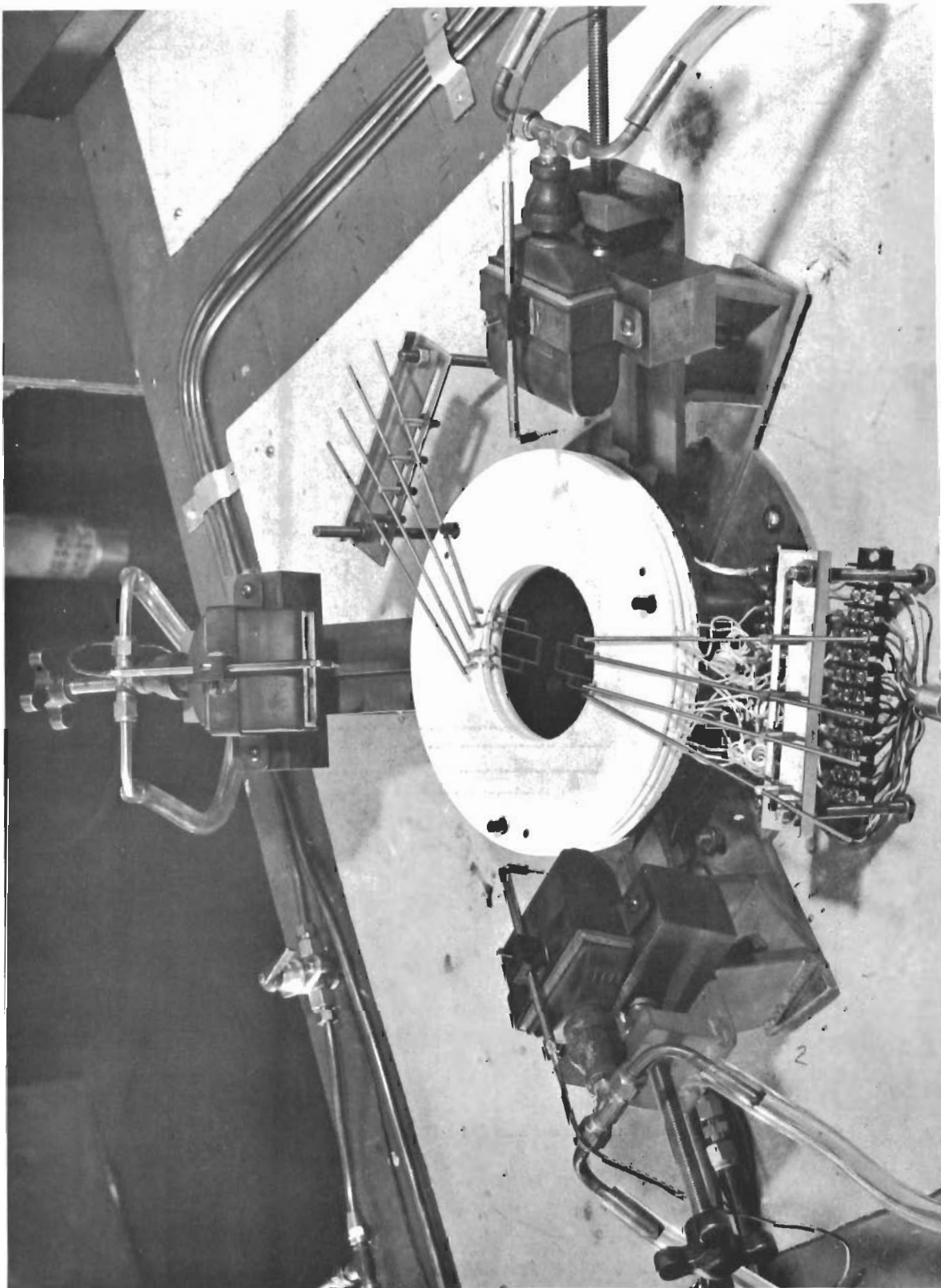


Figure 10 - Convective Transparent Boundary Apparatus

steel disk (in the glaze specimen position); the temperature distribution was determined by thermocouples welded to the backside at 12 different positions. Thermocouples positioned in front of the burners were used to indicate exhaust temperatures. The gas flow rate for each burner was adjusted manually to obtain equal indicated exhaust temperatures. The hot transparent gases were at a static temperature of approximately 3000°F and supplied convective heating rates to 20,000 Btu/hr-ft<sup>2</sup>. This heating rate is typical of that experienced by hypersonic aircraft, for example, flying at Mach 6 at 60,000 ft. or Mach 10 at 120,000 ft.

2. Specimen mounts: Foamed, fused-silica disks were employed to support the test specimens and associated instrumentation circuitry. Contact between the circuitry and the specimen's temperature sensors was made through small leaves of gold foil welded to the ends of the wiring in the disks. Spring rods were employed to insure electrical continuity between the upper glaze temperature sensors and the instrumentation circuitry. These rods applied pressure to small ceramic sticks which held the gold foil against the temperature sensors at the edge of the specimen (Figure 11). In a similar manner, steel leaf springs mounted in the heat sink insured continuity between the circuitry and the lower glaze temperature sensors. This unique and simplified approach provided electrical contact without mechanically bonding the circuitry to the test specimen, as was done for the work done under Contract No. AF 33(657)-9L38 (Ref. 7), and allowed specimen changes in the test apparatus to be easily accomplished. For the multiglaze (two glazes) apparatus, an extra set of foamed, fused-silica disks was needed to support the outer specimen and to provide instrumentation circuitry for the connection between the temperature sensors of the outer specimen and the temperature sensors of the inner specimen. Contact between the circuitry of the extra disks and temperature sensors was achieved by using the pressure applied by the spring rods as explained above and by placing stainless steel wool under each leaf of gold foil so that when pressure was applied through the rods, the steel wool, in effect, acted as a spring and insured good electrical contact between the gold foil connectors and the temperature sensors.

3. Heat sink: The heat sink for the apparatus is a water-cooled copper plate. The surface of the heat sink was coated with a black paint having an emissivity of approximately 0.89. Two commercial heat flux gauges were purchased from Hy-Cal Engineering (Parts Nos. C-7027-A-05-072 and C-1118-C-12-010) and were installed in the heat sink to measure the net heat flux passing through and from the test specimen. Two heat flux gauges were used so that if one failed or underwent a change in calibration, a back-up would be available. A copper-constantan thermocouple along with a thermal switch which activated a buzzer were mounted in the heat sink to prevent overheating of the heat flux gauges.



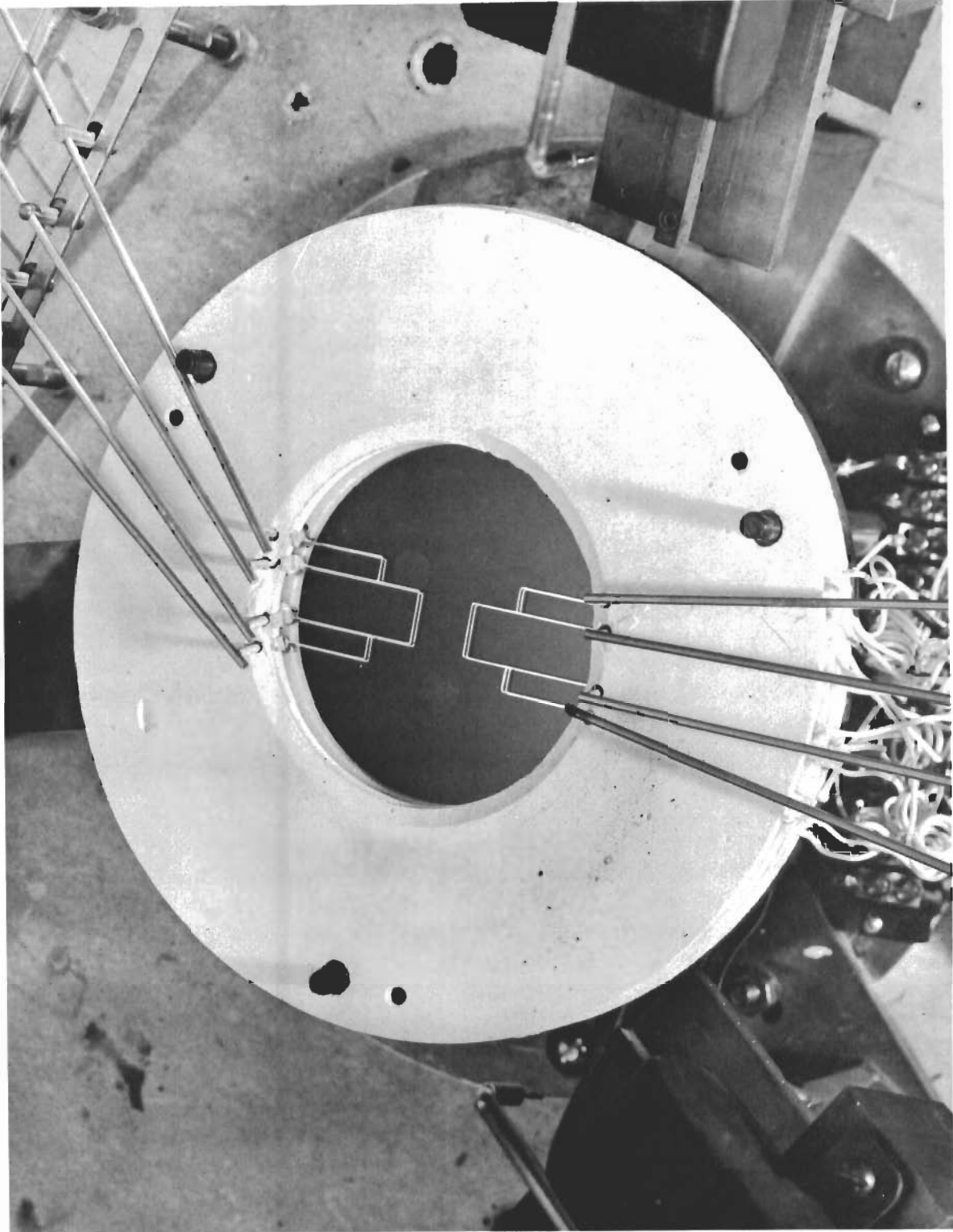


Figure 11 - Test Specimen Support

4. Instrumentation and controls: The instrumentation and controls used with the test apparatus are shown schematically in Figure 12. Signals from the temperature sensors, heat flux gauges, radiant heater thermocouples, burner thermocouples, and heat sink thermocouple were measured with a L&N Model No. 8686, millivolt potentiometer.

The controlling system for the radiant heater consisted of a manually operated DC power supply driving a saturable core reactor. The power supply used was a Trygon Model HR60-2.5A constant voltage source. This system maintained the radiant heater temperature to within  $\pm 0.6\%$ .

## B. Window Test Specimens

The test specimens included combinations of three glaze materials and three thicknesses. The 4-in. diameter specimens (Figure 13) were fabricated from fused silica, 96% fused silica (Vycor), and aluminosilicate. For each material, glaze thicknesses of 1/8 in., 1/4 in., and 3/8 in. were used.

## C. Thin-Film Coatings

Four thin-film coatings were employed on the test specimens for the purpose of reducing heat transmission through the glaze in the infrared region of the spectrum and to increase the transmission in the visual range of the spectrum. These coatings included: (1) a high efficiency anti-reflection coating, (2) an ultraviolet-near infrared reflecting coating, (3) a multi-layer coating containing layers of gold and dielectric materials, and (4) a single layer gold film. The first three of these coatings were developed and applied to the specimens by the Optical Coating Laboratory, Inc. (OCLI), while the single layer gold film was developed and applied to test specimens by Midwest Research Institute.

## D. Coating Temperature Limits

Temperature limits for these coatings were determined when it was revealed that the design temperatures of the coatings were below the temperature specified in the contract to which the specimens were to be heated. The coating supplier (OCLI) suggested that these coatings might function as specified above the design temperatures; however, the supplier did not know at what temperature the coating transmission would be adversely affected. It was decided to determine the limiting temperature for each coating and conduct the coated-specimen heat transfer tests within this temperature limit to preclude deterioration of the coatings.

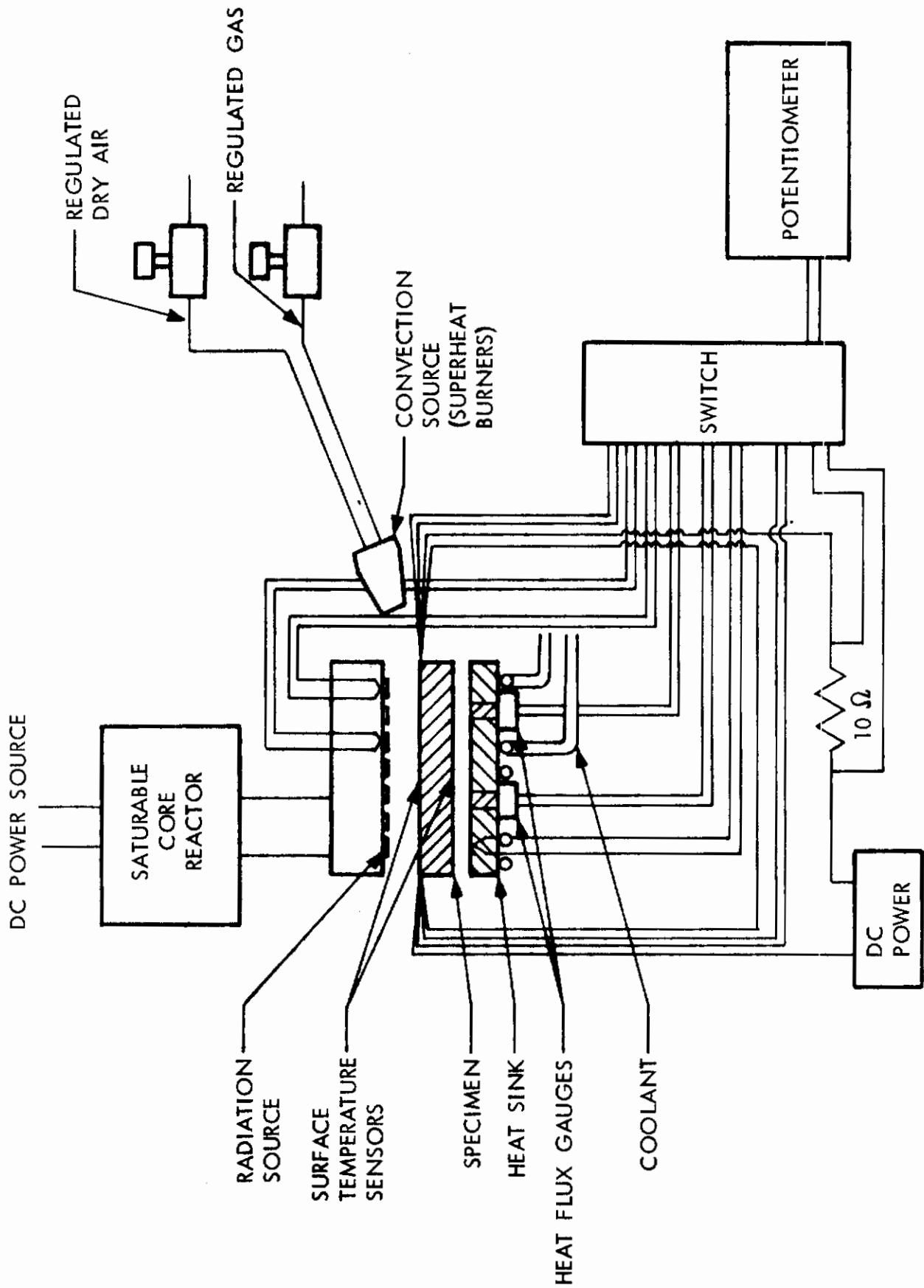


Figure 12 - Schematic of Apparatus Components, Instruments, and Controls

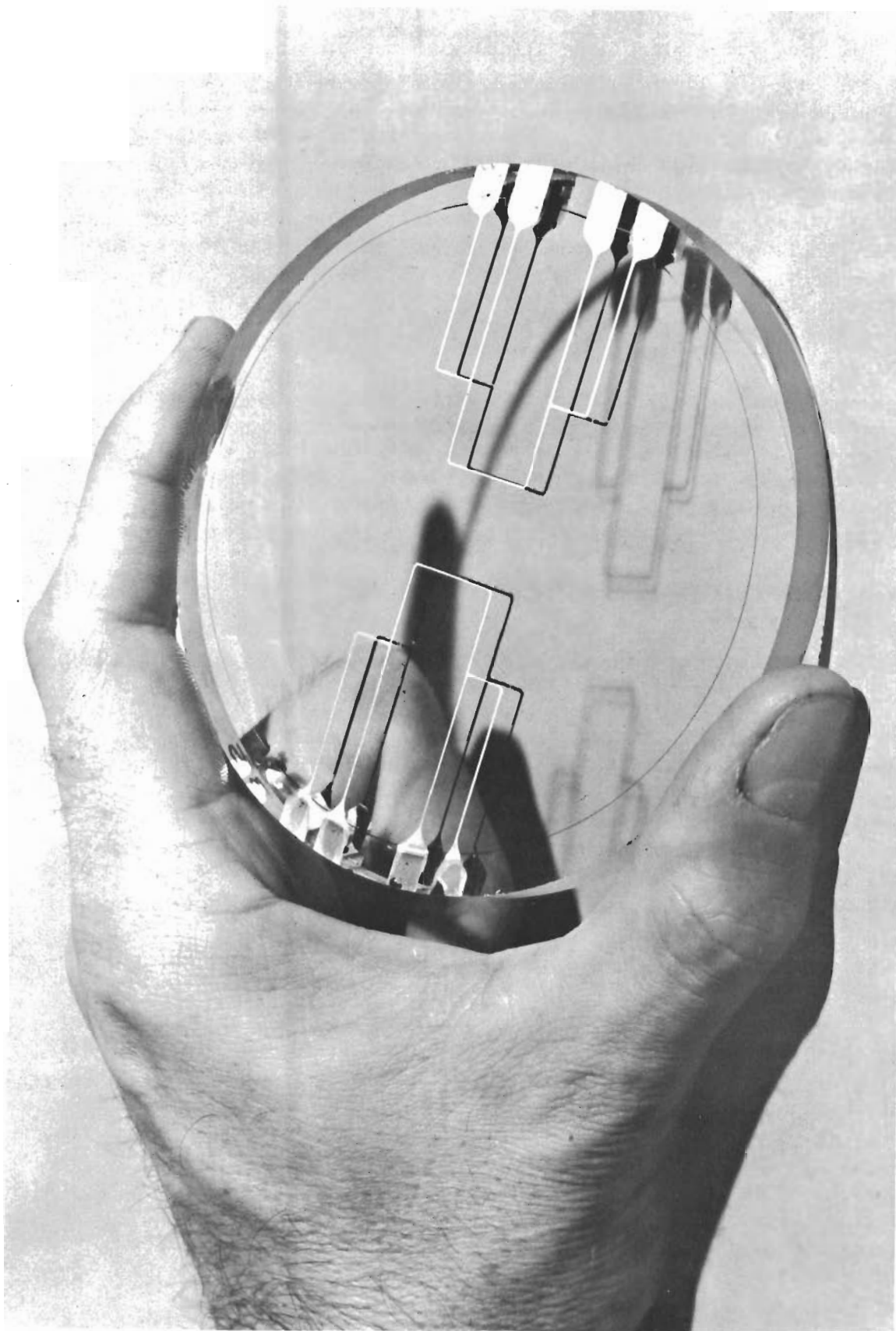


Figure 13 - Window Test Specimen



# Contrails

To this end, Vycor microscope slides with the specified thin-film coatings were used to determine the temperature at which the design transmission of the coatings is adversely affected. This was accomplished by heating the slides to successively higher and higher temperatures and measuring the transmission after each heating cycle.

Two slides with the high efficiency antireflection (HEA) coating were heated for 24 hr. at each 100° interval through 1200°F without apparent damage. Transmission data were taken with some slight transmission changes noted after each heating. During the 1300°F heating the HEA coating was damaged to the extent that deterioration of the coating could be detected visually.

To evaluate the effect of changes in coating transmission on the radiant energy transfer through the coating and into the glaze, the emissive power as well as the change in transmission must be considered at each wavelength. Thus, the change in energy,  $W$ , transferred through the coating and into the glaze can be obtained by evaluating the integral

$$\Delta W = \int_{\lambda_1}^{\lambda_2} (\Delta T)(E) d\lambda$$

where the change in transmission,  $\Delta T$ , and the emissive power,  $E$ , are functions of wavelength,  $\lambda$ . The limits of integration define the wavelength range for which the test specimens (glazes) are considered to be semitransparent to radiant energy. Evaluation of the above integral indicates that the change in transmission of the coating after being heated to 1200°F will result in a change of less than 1% in the radiant energy transferred through the coating. Thus, the upper temperature limit of 1200°F was set for the HEA-coated specimens during the Phase II heat transfer tests.

Two slides coated with the ultraviolet-infrared (UV-IR) coating were heated for 24 hr. at each 200° interval to 1200°F. Transmission data were taken after each heating through 1000°F. The 1200°F heating resulted in severe damage (crazing) of the UV-IR coatings. Changes in the transmission of the coating after being heated to 1000°F will result in a change of approximately 3% in the energy transferred through the coating and into the glaze. Since 3% is within the accuracy of experimental measurement of heating rates, the decision was made to heat the UV-IR coated glazes to 1000°F during the Phase II heat transfer tests.



The transmission of the gold coatings applied by MRI exhibited significant changes after each heating even at relatively low temperature (600°F). It was noted that if the gold coatings were cured at 1000°F for 24 hr., subsequent heatings to 1000°F did not additionally affect the transmission. The initial cure, however, significantly increased the transmission of the gold coating, reducing its effectiveness as an infrared (heat) reflector. The cure was necessary, since without it, changes in the gold coating transmission would occur at some undetermined rate during the heat transfer tests. Without the correct transmission data, the computer program could not be expected to predict the glaze temperatures for these tests. Since the transmission of the gold coatings was already significantly increased by the 1000°F cure, it was decided not to exceed this temperature on the gold coated specimens during the heat transfer tests.

## E. Temperature Sensors

The sensors developed (Ref. 14) for measuring the surface temperatures of the specimens were a gold resistance thermoelement. Gold was adopted because the metal has a high thermal coefficient of resistivity. Two gold grids were vacuum deposited on each side of the specimen as shown in Figure 13. The inner legs of the four grids are connected electrically in a series and act as current conductors. The outer legs of each grid are used as potential taps to measure the voltage drop across the active ("U" shape section) portion of the temperature sensor.

Calibration of the temperature sensors was accomplished by determining their resistance while at various temperature levels in a Hoskins Type FH2040 electric furnace. The specimens were mounted in a special fixture (Figures 14 and 15) constructed of stainless steel and foamed fused silica. External leaf springs of Hastelloy-X applied pressure on small ceramic sticks passing through the case of the fixture. These ceramic sticks, like those employed in the test apparatus, held the instrumentation circuitry of the calibration fixture against the temperature sensors of the test specimens. The specimen temperature was measured with two chromel-alumel thermocouples inserted into the fixture. The reference junction for the thermocouples was maintained at 32°F by means of an ice bath.

The power source for the sensor circuit was a Trygon Model HR20-1.5 constant voltage DC power supply. Instrumentation circuitry similar to that used in the test apparatus was employed in the calibration fixture. The temperature sensors were connected in series. The current was determined by measuring the voltage drop across a precision 10-ohm resistor connected in series with the temperature sensors and a 10 K-ohm resistor. The sensor voltage junctions were connected to a multiple channel switch which, in turn, was connected to a L&N Model 8686 millivolt potentiometer. The output from the two thermocouples was also connected to the switch.

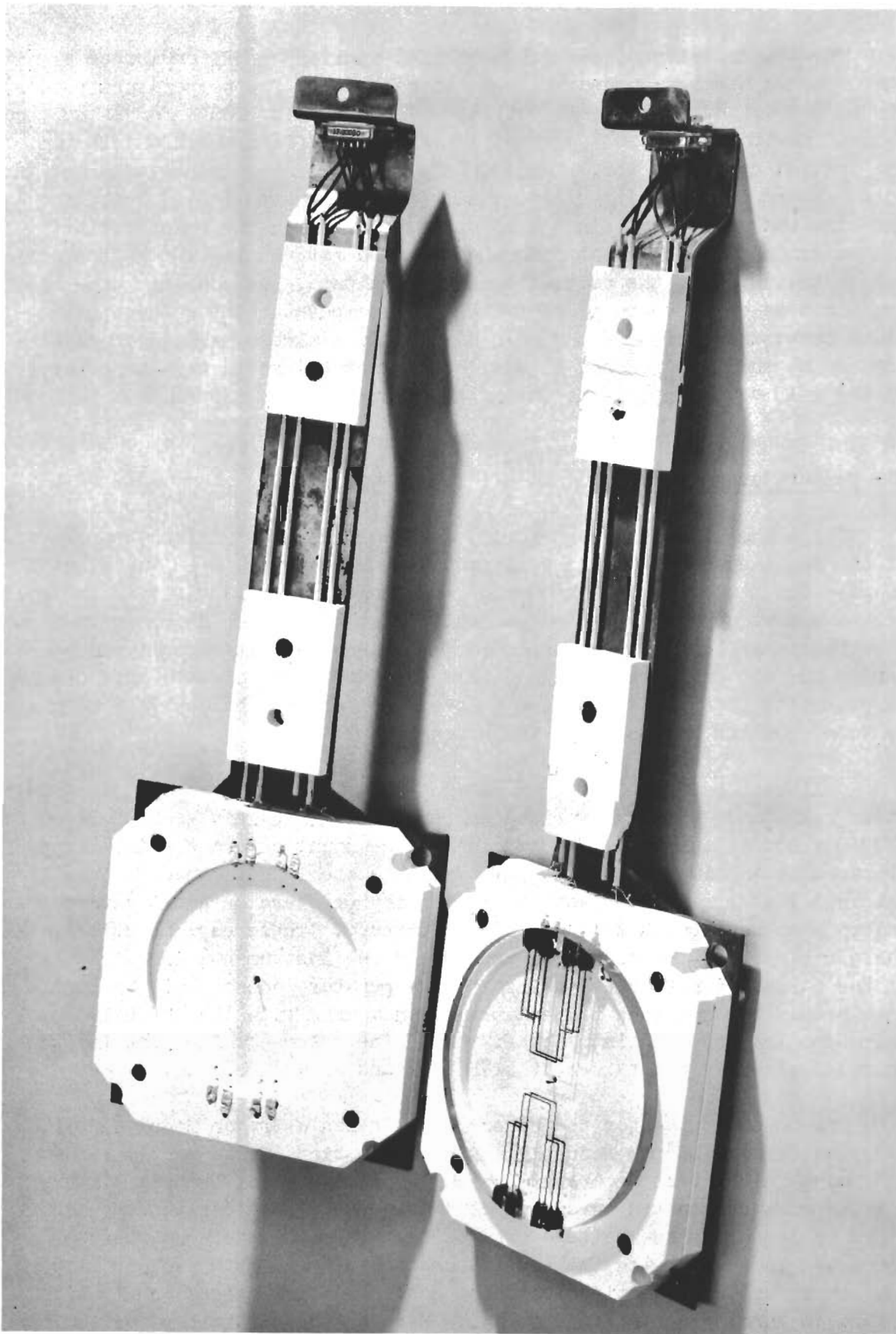


Figure 14 - Calibration Fixture - Open

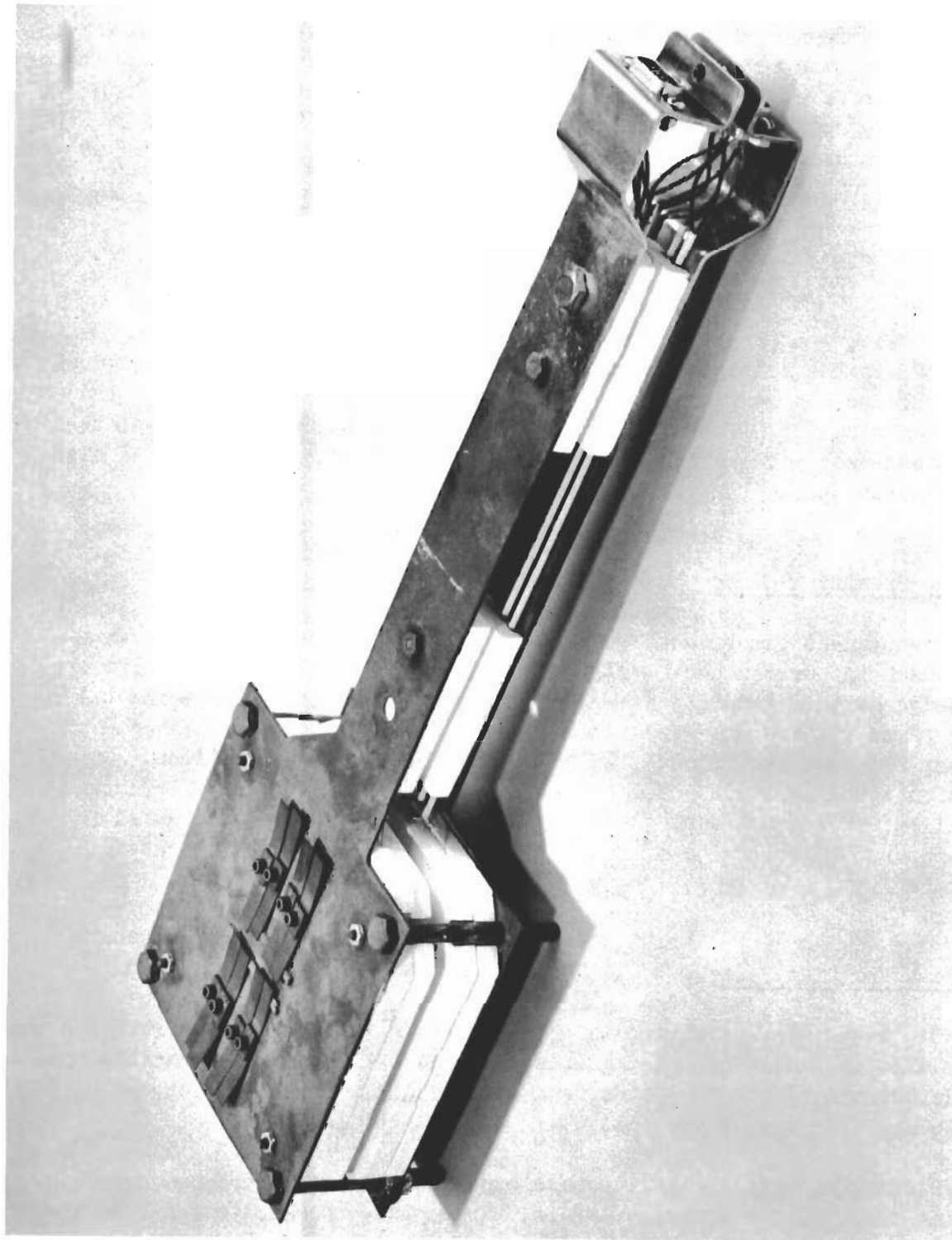


Figure 15 - Calibration Fixture - Closed

# Contrails

After installation in the calibration fixture, the glaze specimen was placed in the furnace and calibration measurements were then made at approximately 300°F intervals from room temperature to the maximum temperature the specimen would undergo during testing. The system was allowed to stabilize at each temperature level before making measurements of the voltage drop across each of the four temperature sensors, the voltage drop across the precision resistor, and the emf output of the thermocouples. At each temperature, as determined by the thermocouples, the resistance of each sensor was then computed from

$$R = \frac{V}{V_o} (R_o)$$

where V is the voltage drop across the sensor, V<sub>o</sub>, is the voltage drop across the precision resistor and R<sub>o</sub> = 10 ohms is the resistance of the precision resistor. The value of R versus temperature was then plotted for each sensor. These calibration plots were used to determine the glaze temperatures during the heat transfer tests.

## F. Superposition Tests

The planned experimental tests used to verify the computer program were based in part on the so-called superposition technique. The primary advantage of this "additive" approach was that it required experimental tests to be run for only two sets of boundary conditions, all-air and all-vacuum, eliminating the need for other possible test combinations. Superposition tests were conducted to demonstrate the validity of all-vacuum and all-air tests as required in the contract for the work discussed in this report. The results of these superposition tests are presented in Appendix E.

## G. Heat Transfer Tests

The tests were performed in three phases. In Phase I, the research was applicable to single uncoated glazes. In Phase II, the scope was expanded to include coated single glazes, and in Phase III, coated and uncoated multiple glazes were investigated.

During Phase I, 27 single-glaze experimental tests were conducted involving three window glaze materials, three glaze thicknesses, and three modes of heat transfer. The three specimen materials tested were fused silica, aluminosilicate, and 96% fused silica having thicknesses of 1/8, 1/4, and 3/8 in. Each of the nine specimens were subjected to convective, radiative, and combined radiative and convective heating.



# Contrails

Eighty-five single glaze tests were conducted in Phase II of the research program. These tests were similar to those conducted in Phase I with the exception of the test specimens. The glaze specimens were of the same materials and thicknesses as those of Phase I, but had thin-film coatings on one or both surfaces. Specimen material and thickness combinations employed in the Phase II tests included:

1. Fused silica, 1/4 in. thick;
2. Fused silica, 3/8 in. thick;
3. Vycor, 1/4 in. thick;
4. Vycor, 1/8 in. thick; and
5. Aluminosilicate, 1/4 in. thick.

Seven each of the specimen types listed above were coated as follows:

1. Gold film, upper surface  
No coating, lower surface
2. No coating, upper surface  
Gold coating, lower surface
3. Gold film, both surfaces
4. High efficiency anti-reflection (HEA), upper surface  
No coating, lower surface
5. HEA, both surfaces
6. Gold film, upper surface  
HEA, lower surface
7. No coating, upper surface  
Ultraviolet-infrared (UV-IR) reflecting coating, lower surface

Modes of specimen heating included radiation, convection, and combined radiation and convection.

During Phase III, 112 double glaze experimental heat transfer tests were conducted in both air and vacuum environments using coated and uncoated glazes of various materials and thicknesses. The combinations of specimen materials, thicknesses, and coatings and the environment and modes of heating are outlined below. Figure 16 is a schematic representing the double glaze window configuration.

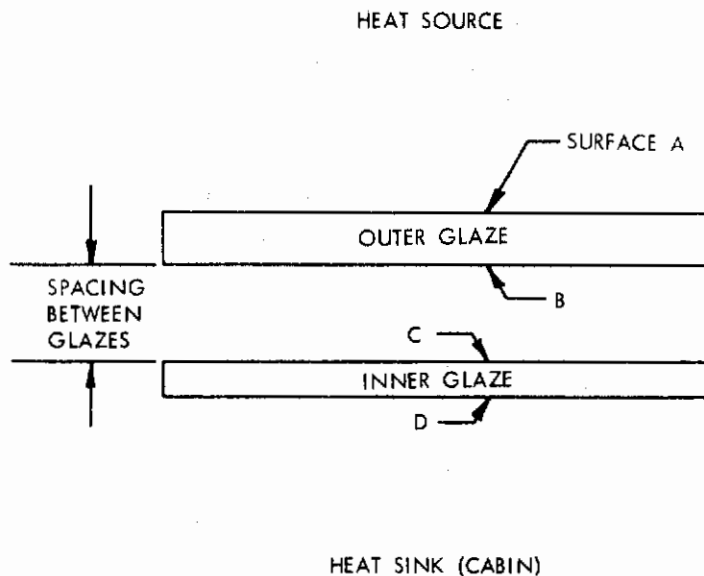


Figure 16 - Parallel Outer-Inner Glazings of the Multiple Glaze Tests

Specimen material and thickness combinations used in the Phase III tests included:

1. 1/4 in. Fused Silica - Outer  
1/8 in. Vycor - Inner
2. 3/8 in. Fused Silica - Outer  
1/8 in. Vycor - Inner
3. 1/4 in. Fused Silica - Outer  
3/8 in. Fused Silica - Inner
4. 1/4 in. Aluminosilicate - Outer  
1/4 in. Aluminosilicate - Inner
5. 1/4 in. Fused Silica - Outer  
1/4 in. Aluminosilicate - Inner
6. 3/8 in. Aluminosilicate - Outer  
1/4 in. Aluminosilicate - Inner



# Contrails

7. 1/4 in. Aluminosilicate - Outer  
3/8 in. Aluminosilicate - Inner
8. 3/8 in. Fused Silica - Outer  
1/4 in. Aluminosilicate - Inner
9. 1/4 in. Fused Silica - Outer  
3/8 in. Aluminosilicate - Inner

Heat transfer tests were conducted on each of the above double glaze window configurations having no surface coatings. Experimental tests were also conducted using each double glaze configuration 1 through 5 with the following surface coating combinations:

1. No Coating - Surface A  
UV-IR Coating - Surface B  
No Coating - Surface C  
No Coating - Surface D
2. No Coating - Surface A  
UV-IR Coating - Surface B  
HEA Coating - Surface C  
HEA Coating - Surface D
3. HEA Coating - Surface A  
HEA Coating - Surface B  
HEA Coating - Surface C  
HEA Coating - Surface D
4. No Coating - Surface A  
UV-IR Coating - Surface B  
Gold Coating - Surface C  
HEA Coating - Surface D

Both the coated and uncoated double glaze configurations, 1 through 5, were used in tests conducted in air and vacuum environments. The uncoated window configurations 6 through 9, were used only in tests conducted in air. Window heating was accomplished by radiation, convection, and combined radiation and convection in the air tests and by radiation in the vacuum tests.

## H. Coating and Glaze Damage

After all Phase III experimental heat transfer tests were completed, several brief tests were conducted in the presence of the Air Force Project Engineer to demonstrate the temperature-time effect on the different coatings

# Contrails

and glaze materials used in this work. These different tests are enumerated and explained below.

In the first test a 3/8 in. thick, fused silica glaze (uncoated) was subjected to a temperature of approximately 1400°F by means of convective heat. With the glaze at this temperature, there was no visual change in the transmission characteristics of the glaze. The glaze did not appear to glow and neither was there any other visual physical change at this temperature. As a measure of fused silica's ability to withstand thermal shock and stress, the convective input to the glaze was cut-off sharply at the 1400°F level and the glaze allowed to cool. The glaze, when subjected to this thermal shock, suffered no apparent damage. Although no Vycor (96% fused silica) glazes were tested in this manner, it is anticipated that had they been, the results would have been identical since the physical properties of the two materials are very similar.

The second test involved a 3/8 in. thick, uncoated, aluminosilicate glaze which was heated by convection to approximately 1200°F. At this temperature, the glaze broke into several pieces. The elapsed time from initial heating to point of failure was approximately 10 min. The probable cause of the breakage was an excessive increase in heating rate which set up a large temperature gradient through the specimen and resulted in severe thermal shock and stresses. Before failure, the transparency of the glaze did not seem to be affected in any way. These results bear out those obtained during the experimental heat transfer tests in which several aluminosilicate glazes broke for no apparent reason other than an increase in heating rate.

Test No. 3 involved a 1/4 in. fused silica glaze which was coated on one surface with a high efficiency anti-reflection (HEA) coating and on the other surface with a multi-layer gold (OCLI) coating. For this test, the glaze was heated by convection to approximately 1400°F with the HEA coated surface being the surface to which the heat was applied. After about 2 hr. at 1400°F, the HEA coating started clouding. A short time later, the coating started blistering at what seemed to be a hot spot on the surface. The rest of the coating changed from the violet to a deep red color. These results agree with those reported earlier in this report in which an HEA coating was damaged to the extent that deterioration of the coating could be detected visually when heated to 1300°F. With this damage, it was obvious that the coating was no longer fulfilling the purpose for which it was intended.

Test No. 4 was conducted using the same coated glaze used for Test No. 3. In this test, the gold coated surface was used as the incident surface; and like the previous test, the glaze was heated by convection to approximately 1400°F. With the glaze and coating at this temperature, there

# Contrails

was no apparent damage to the coating or any visual change in its transmission characteristics.

No test was conducted using the ultraviolet-infrared (UV-IR) coating; but based on results obtained by heating UV-IR coated slides and by examining UV-IR coated glazes after repeated use during the experimental heat transfer tests, it is apparent that subjecting the coating to repeated use and to temperatures of 1000°F and above results in severe damage (crazing) of the coating so that it is no longer performing as intended.

## SECTION IV

### ANALYTICAL AND EXPERIMENTAL RESULTS

#### A. Computer Program Verification

Since a major objective of the experimental heat transfer tests was to verify the validity of the computer program, measured values of window surface temperatures and heat flux to the cabin were compared to those computed. The "heat flux to the cabin" as used in this discussion refers to the flux from the cold side of the window. This includes the heat transfer from the cold surface by convection and radiation, and the radiation through and from the interior of the glazes.

Comparisons of computed and measured glaze surface temperatures and heat flux to the cabin for a single-pane window are presented graphically in Figures 17, 18, 20 and 21, and in Tables I, II and III. All single-pane window tests were conducted in an air environment. Figure 17 presents a comparison of the analytical and experimental results for a 1/4-in. fused silica window heated by radiation. In the experimental tests employing the radiant heater, the heater was placed 9/16 in. above the glaze. In this position, heater temperatures from 1000° to 2200°F resulted in incident radiant flux ranging from 6,700 to 73,000 Btu/hr-ft<sup>2</sup>.

Figure 18 compares measured and computed values of glaze temperatures and the heat flux to the cabin for a 1/4-in. fused silica window that is convectively heated. Different levels of convective heating in the experimental tests were obtained by adjusting the burners to various positions on burner mounts (Figure 10). The convective input to the glaze at steady-state conditions for each burner position was determined by performing a heat balance calculation on the glaze as follows:

$$Q_{in} = \epsilon f(\epsilon) \sigma (T_1^4 - T_{room}^4) + \epsilon f(\epsilon) \epsilon_c \sigma (T_{11}^4 - T_c^4) + \frac{k_{air}}{d} (T_{11} - T_c)$$

The effective emissivity,  $\epsilon f(\epsilon)$ , was determined using the emissivity,  $\epsilon_{\lambda x}$ , of glass plates presented by Gardon (Figure 5 of Ref. 4) as a function of the absorption coefficient times the plate thickness. Since the absorption coefficient and in turn  $\epsilon f(\epsilon)$  are wavelength-dependent, the total effective emissivity of the glass plate was determined for a given temperature from the expression

$$\epsilon f(\epsilon) = \sum_{\lambda} \epsilon_{\lambda x} \Delta P_{\lambda}$$

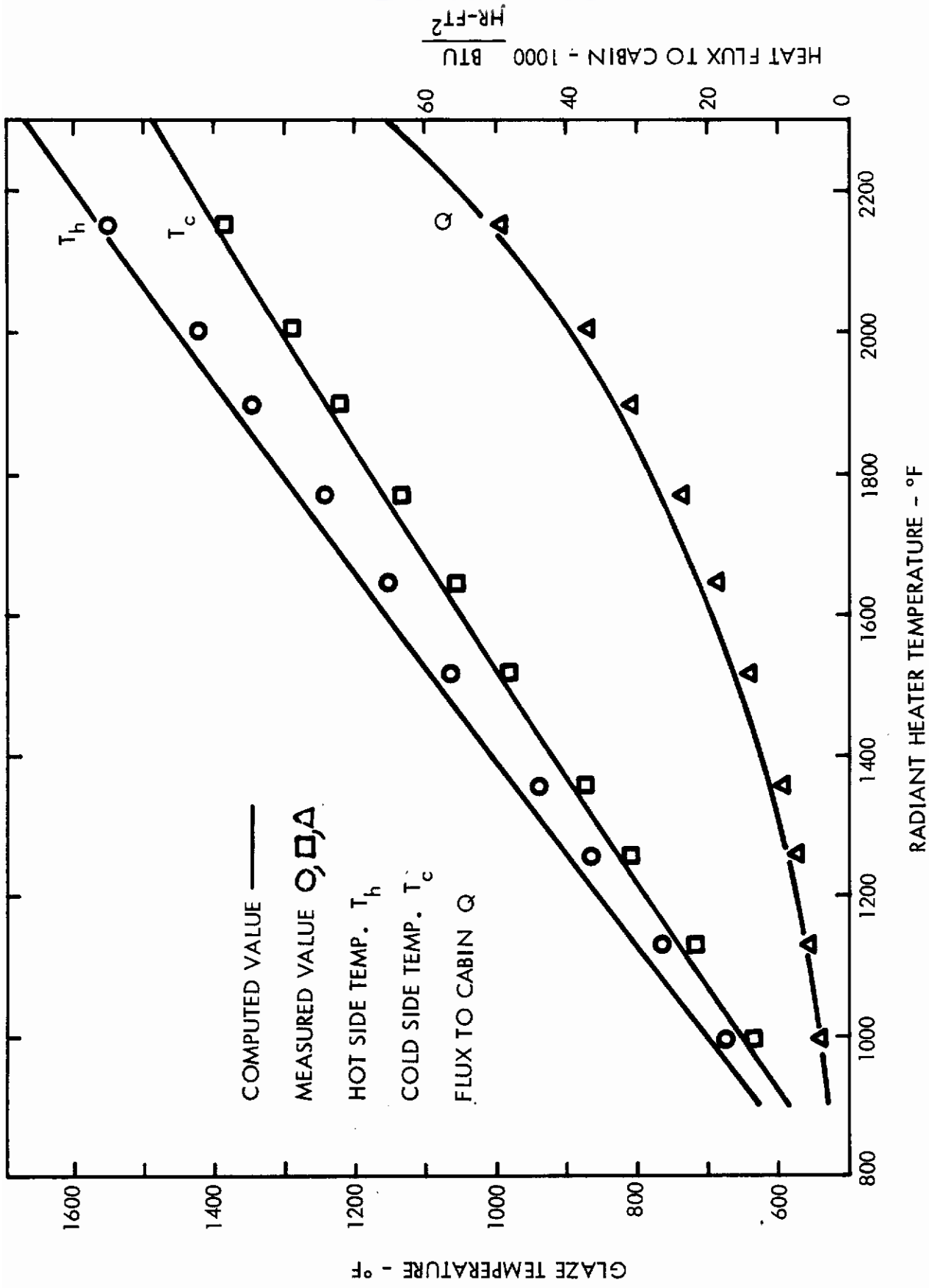


Figure 17 - 1/4-In. Fused Silica Window Heated by Radiation, Steady-State Conditions



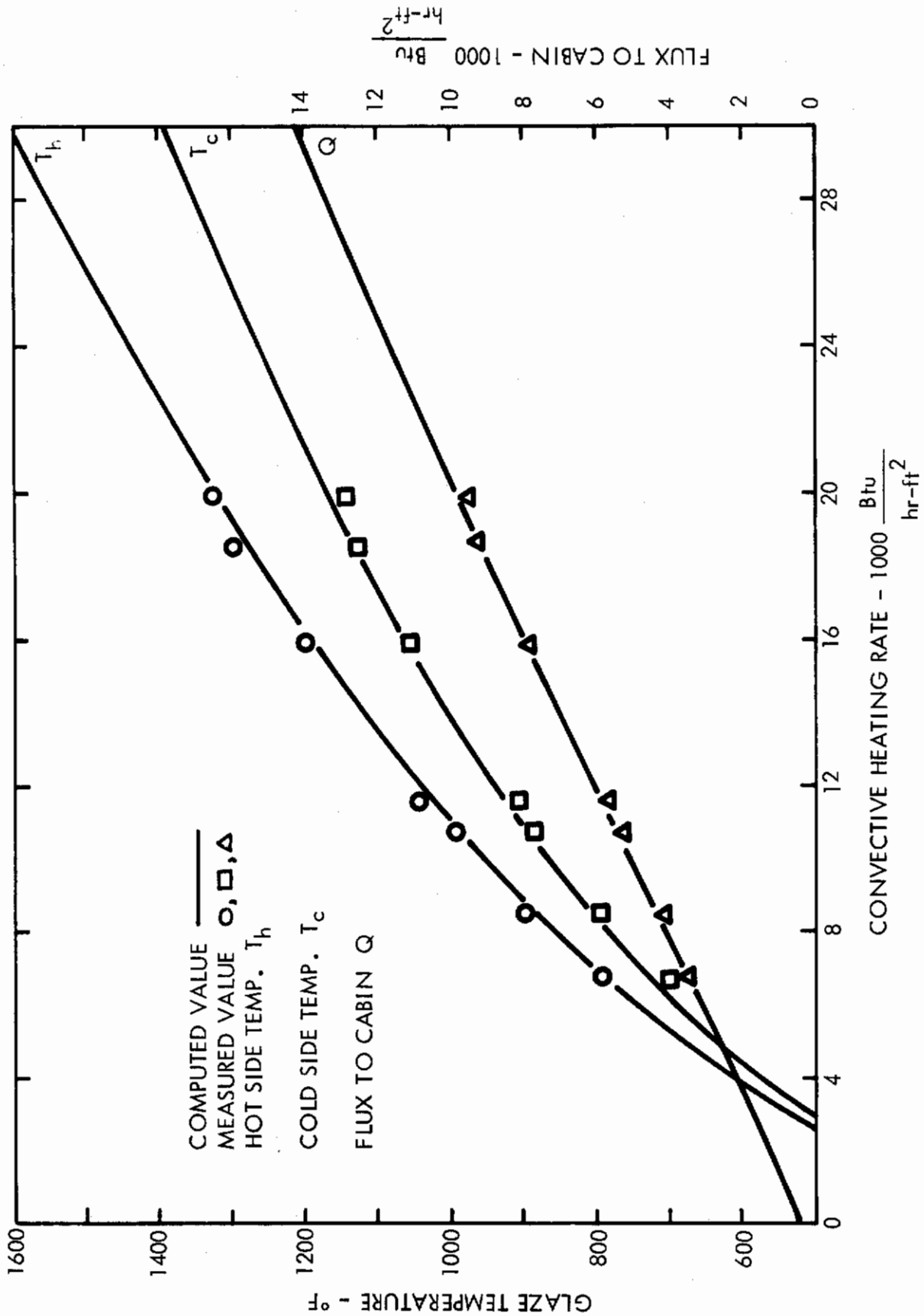


Figure 18 - 1/4-In. Fused Silica Window Heated by Convection, Steady-State Conditions

in which  $\epsilon_{\lambda x}$  and  $\Delta P_{\lambda}$  are evaluated for each finite wavelength band considered in the summation. Values of total effective emissivity vs. temperature computed for a 1/4-in. fused silica plate are plotted in Figure 19. Using these values in the above heat balance equation, the convective heating rates at the glaze surface were determined for each test point. As seen in Figure 18, the experimental convective heating rates ranged from 6,800 to 20,000 Btu/hr-ft<sup>2</sup>.

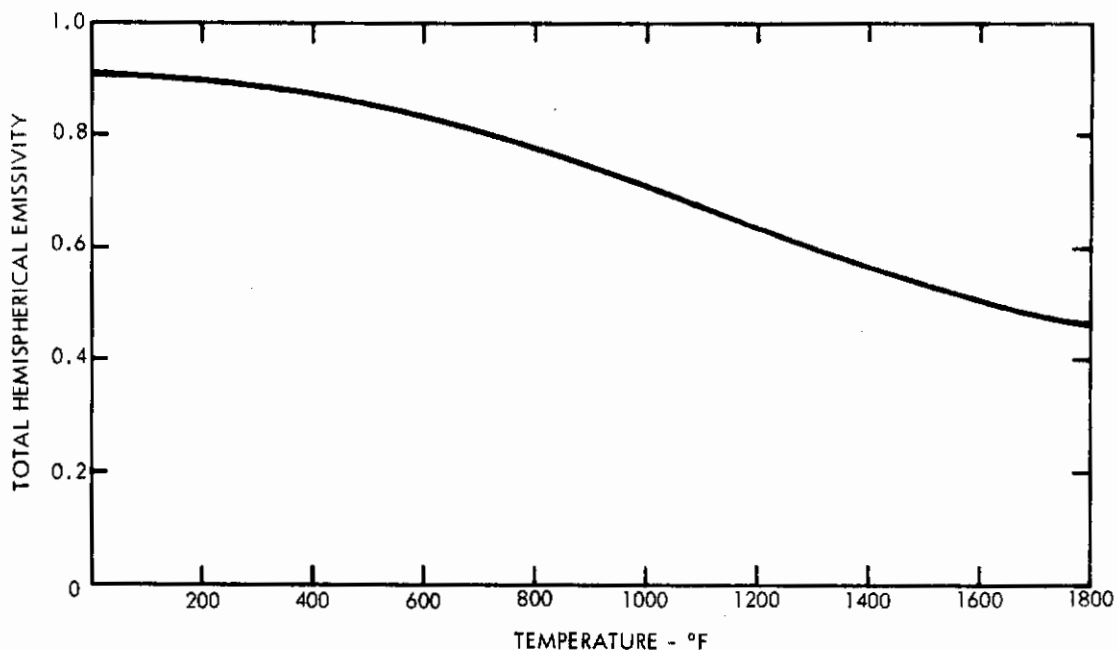


Figure 19 - Effective Emissivity of 1/4 In. Fused Silica Plate

In order to evaluate the capability of the subject computer program to accurately compute transient temperatures, computed values were compared to the glaze cooling and heating experimental test data of Refs. 7 and 15. The glaze cool-down data of Ref. 7 (obtained from a specimen allowed to cool from 900°F to room temperature) are compared to the computed glaze cool-down temperature in Figure 20. Figure 21 compares calculated glaze temperatures and the heat flux to the cabin to the experimental values presented in Figure 9 of Ref. 15. These transient heating data were obtained by instantaneously positioning the specimen under a radiant heat source. The predicted heat flux to the cabin is greater than that measured due to non-one-dimensional radiant flux incident on the glaze and to an instrumentation problem in the test radiometer as explained in Ref. 15.

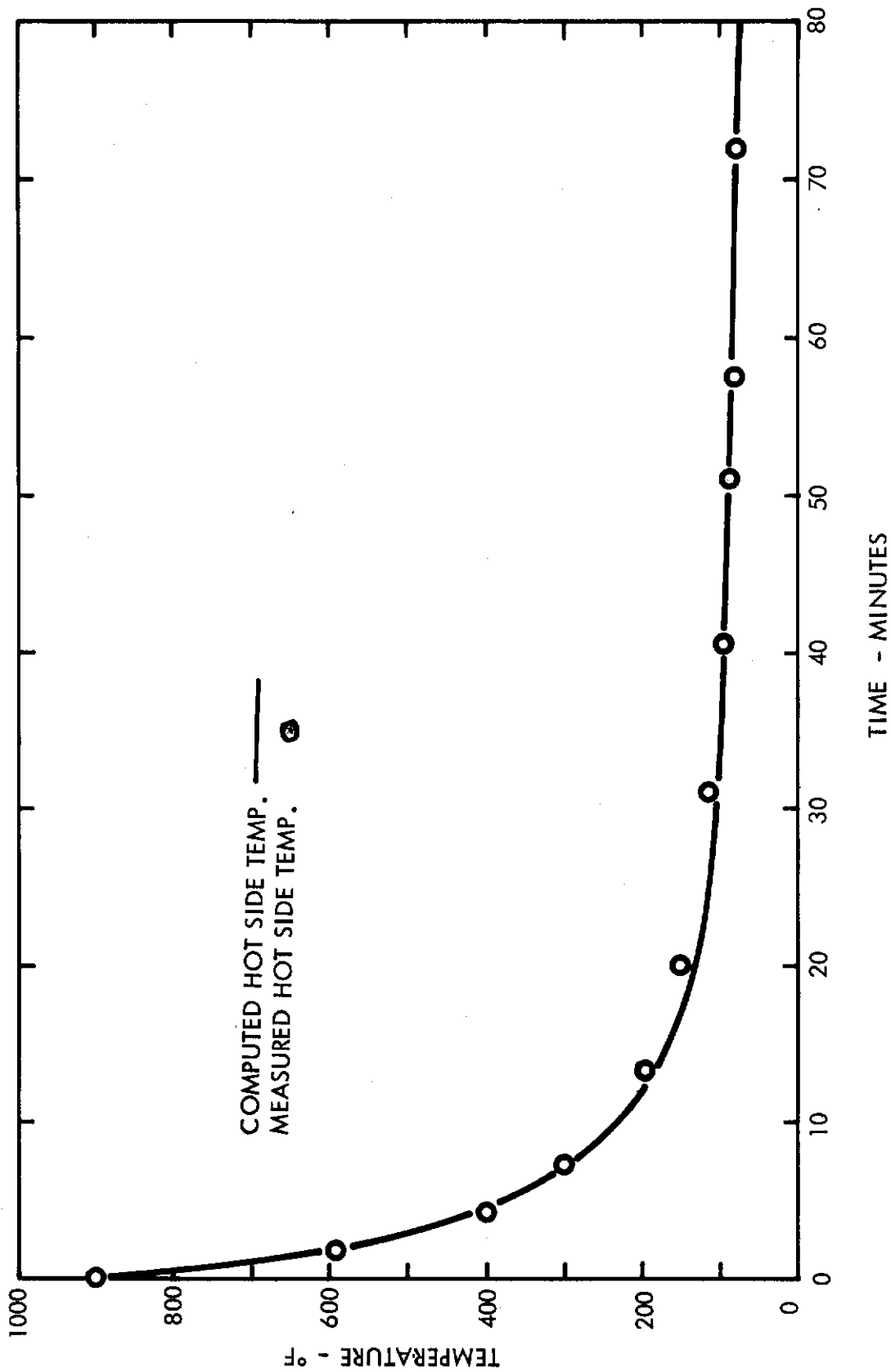


Figure 20 - Measured and Computed Transient Temperatures

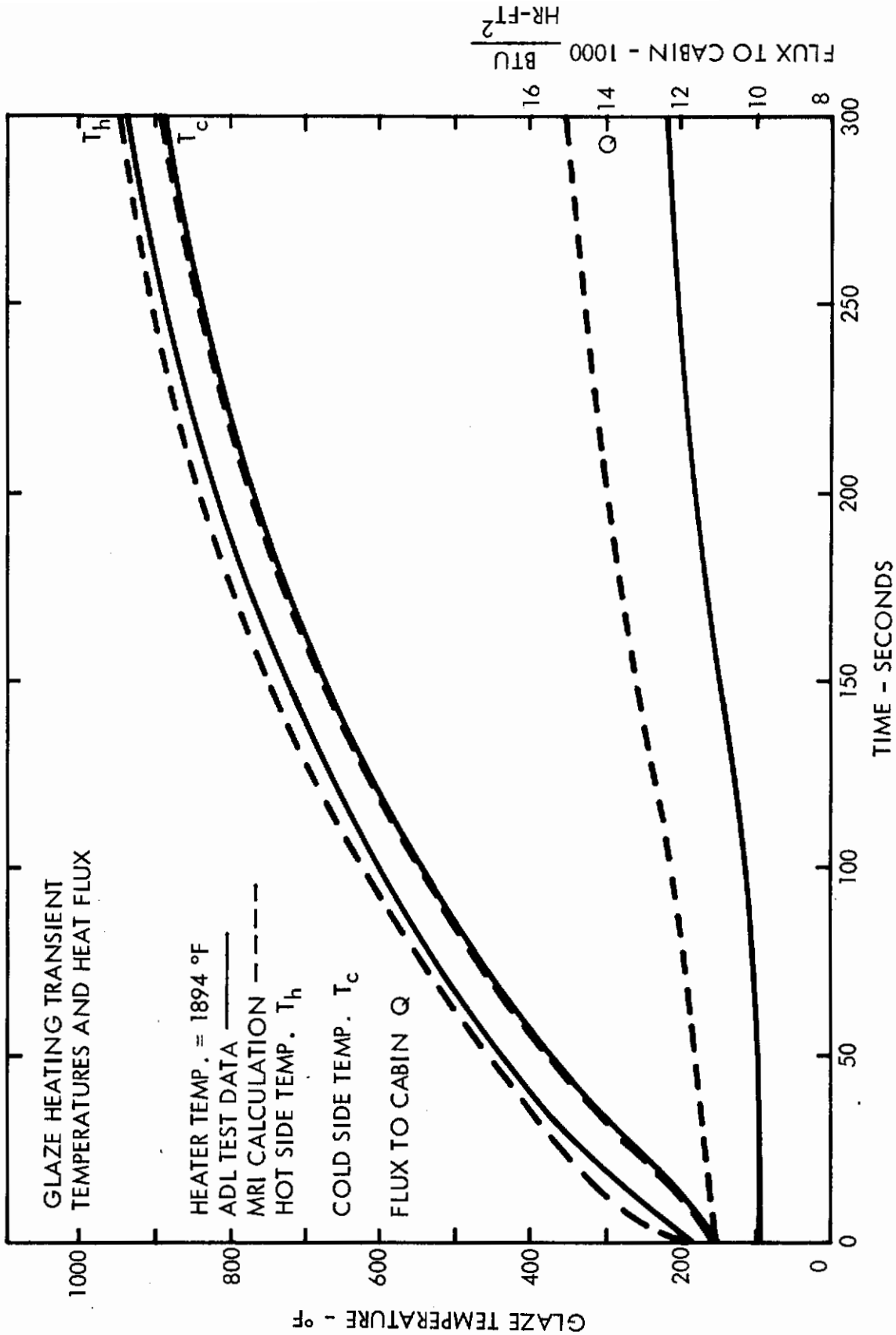


Figure 21 - Measured and Computed Transient Temperatures and Heat Flux

# Contrails

A comparison of computed and measured glaze steady-state temperatures and heat flux is presented in Table I for fused silica test specimens of various thicknesses subjected to radiative and convective heating. As suspected, when the glaze thickness is increased, the hot side temperature is higher, the cold side temperature is lower, and there is a decrease in the heat flux to the cabin.

Table II presents a comparison of analytical and experimental results for 1/4-in. test specimens under thermal equilibrium conditions for the same radiative and convective heating rates. The difference in temperatures of these glaze materials is attributed to their different spectral absorption coefficients.

Computed and measured heat fluxes are compared in Table III for 1/4-in. fused silica specimens having various thin-film coatings on one and/or both surfaces. The coatings, which were deposited on the test specimens by Optical Coating Laboratory, Inc., included an ultraviolet-near infrared reflecting coating (UV-IR), a high-efficiency antireflection coating (HEA) and a gold coating for infrared reflection. Temperatures of the glazes coated with only UV-IR and HEA coatings were close to the temperatures of the noncoated specimen. These two coatings were designed for their optical characteristics at or near the visual region of the spectrum; and their transmission is relatively high for the longer wavelengths at which the major portion of radiant energy is emitted in the cases of Table III. The temperatures and heat flux of the gold coated specimen, however, were significantly lower than those of the uncoated specimen. This is due to the very high reflectance of the gold coating at the longer wavelengths.

The gold coatings referred to in Table III are the multiple layer coatings of OCLI containing layers of gold and dielectric materials. Temperatures of the glazes with the single layer gold coating applied at MRI were not significantly different than temperatures of the uncoated specimens. This was due to a microscopic migration of the gold when heated, resulting in a coating transmission close to that of the uncoated glaze. Since the single layer gold coatings did not operate as an efficient infrared reflector, only the gold-dielectric coating applied by OCLI was employed in the Phase III heat transfer tests.

Comparisons of computed and measured glaze surface temperatures and heat flux to the cabin for double-pane windows are presented graphically in Figures 22 through 25 and in Tables IV through VII. All of these computed and measured data are for steady-state heat transfer conditions.



VARIATION OF GLAZE TEMPERATURES AND HEAT FLUX WITH THICKNESS  
FOR FUSED SILICA HEATED BY RADIATION AND CONVECTION

Window Thickness (in.)	Heat Source	Hot Side Temperature (°F)		Cold Side Temperature (°F)		Flux to Cabin (Btu/hr-ft <sup>2</sup> )	
		Computed	Measured	Computed	Measured	Computed	Measured
1/8	$T_h = 2150^\circ\text{F}$ ↓	1494	1465	1413	1400	52,200	51,100
1/4		1561	1535	1396	1385	50,400	49,400
3/8		1615	1581	1377	1359	49,000	44,000
1/8	$Q_c = 16,000 \frac{\text{Btu}}{\text{hr-ft}^2}$ ↓	1182	1180	1112	1094	8,410	--
1/4		1195	1205	1064	1060	7,960	--
3/8		1215	1190	1032	999	7,550	--

TABLE II

VARIATION OF GLAZE TEMPERATURES AND HEAT FLUX WITH TYPICAL GLAZE MATERIALS  
FOR 1/4-IN. WINDOW HEATED BY RADIATION AND CONVECTION

Window Material	Heat Source	Hot Side Temperature (°F)		Cold Side Temperature (°F)		Flux to Cabin (Btu/hr-ft <sup>2</sup> )	
		Computed	Measured	Computed	Measured	Computed	Measured
Fused Silica	$T_h = 1340^\circ\text{F}$ ↓	958	928	881	855	10,010	9,300
Vycor		998	960	905	875	9,040	8,600
Aluminosilicate		1018	990	903	902	8,410	8,000
Fused Silica	$Q_c = 14,000 \frac{\text{Btu}}{\text{hr-ft}^2}$ ↓	1122	1151	1005	1019	7,020	--
Vycor		1081	1113	955	930	6,840	--
Aluminosilicate		1074	1042	925	913	6,620	--

TABLE III

EFFECT OF TYPICAL WINDOW COATINGS ON TEMPERATURES AND HEAT FLUX OF  
1/4-IN. FUSED SILICA SPECIMEN HEATED BY RADIATION AND CONVECTION

Coatings		Heat Source	Hot Side Temperature (°F)		Cold Side Temperature (°F)		Flux to Cabin (Btu/hr-ft <sup>2</sup> )	
Hot Side	Cold Side		Computed	Measured	Computed	Measured	Computed	Measured
None	None	$T_h = 1450^\circ\text{F}$ ↓	1042	1016	957	940	10,800	10,450
None	UV-IR		1051	1015	966	943	10,440	10,800
HEA	None		1036	1018	949	930	12,300	10,900
HEA	HEA		1037	995	951	910	12,100	10,100
Gold	HEA		810	820	749	755	5,000	4,000
None	None	$Q_c = 13,300 \frac{\text{Btu}}{\text{hr-ft}^2}$ ↓	1095		980		6,650	
None	UV-IR		1105	1072	994	981	6,550	--
HEA	None		1102	1125	989	984	6,730	--
HEA	HEA		1103	1150	991	1013	6,700	--
Gold	HEA		1190	1212	1067	1068	8,130	--

# Contrails

As was done in comparing the analytical and experimental results of the single-pane windows, double-pane window temperatures and heat flux to the cabin were computed and compared to selected experimental data to evaluate the various capabilities of the computer program. The capabilities verified were to compute the temperatures of and heat flux through multiple glaze windows for:

1. A wide range of radiative, convective, and combined radiative and convective heating conditions in air and vacuum environments;
2. Various combinations of glaze materials and thicknesses; and
3. Various combinations of reflective and antireflective coatings on the window glazes.

Figures 22, 23, and 24 present comparisons of analytical and experimental results for a selected double glaze window heated over a wide temperature range by radiation, convection, and combined convection and radiation in an air environment. The glazes employed in the window for which this comparison was made consisted of uncoated 1/4-in. fused silica for the outer pane and uncoated 1/8-in. Vycor for the inner pane. For the radiant heating tests, the heater was positioned 9/16 in. above the upper glaze. The distance between the glaze specimens was 3/8 in. and the inner specimen was 3/16 in. above the apparatus cold plate. Figure 25 presents a comparison of the computed and measured glaze temperatures and heat flux to the cabin for this window system when heated radiantly in a vacuum environment.

Tables IV and V present a comparison of computed and measured temperatures and cabin heat flux for the various combinations of glaze materials and thicknesses employed in the double-pane window configurations heated by radiation and by convection in an air environment. A comparison of the analytical and experimental results is given in Table VI for the various coating combinations employed on a double-pane window system heated in air by radiation and by convection. The computed and measured values compared in Table VII are for the coated double glaze combinations heated by radiation in a vacuum environment.

Based on the good agreement obtained in the comparison of the analytical and experimental results presented in Figures 17 through 25 and Tables I through VII, it is concluded that the developed computer program accurately computes the temperature distribution and heat flux through coated and uncoated, single- and multiple-pane window systems.

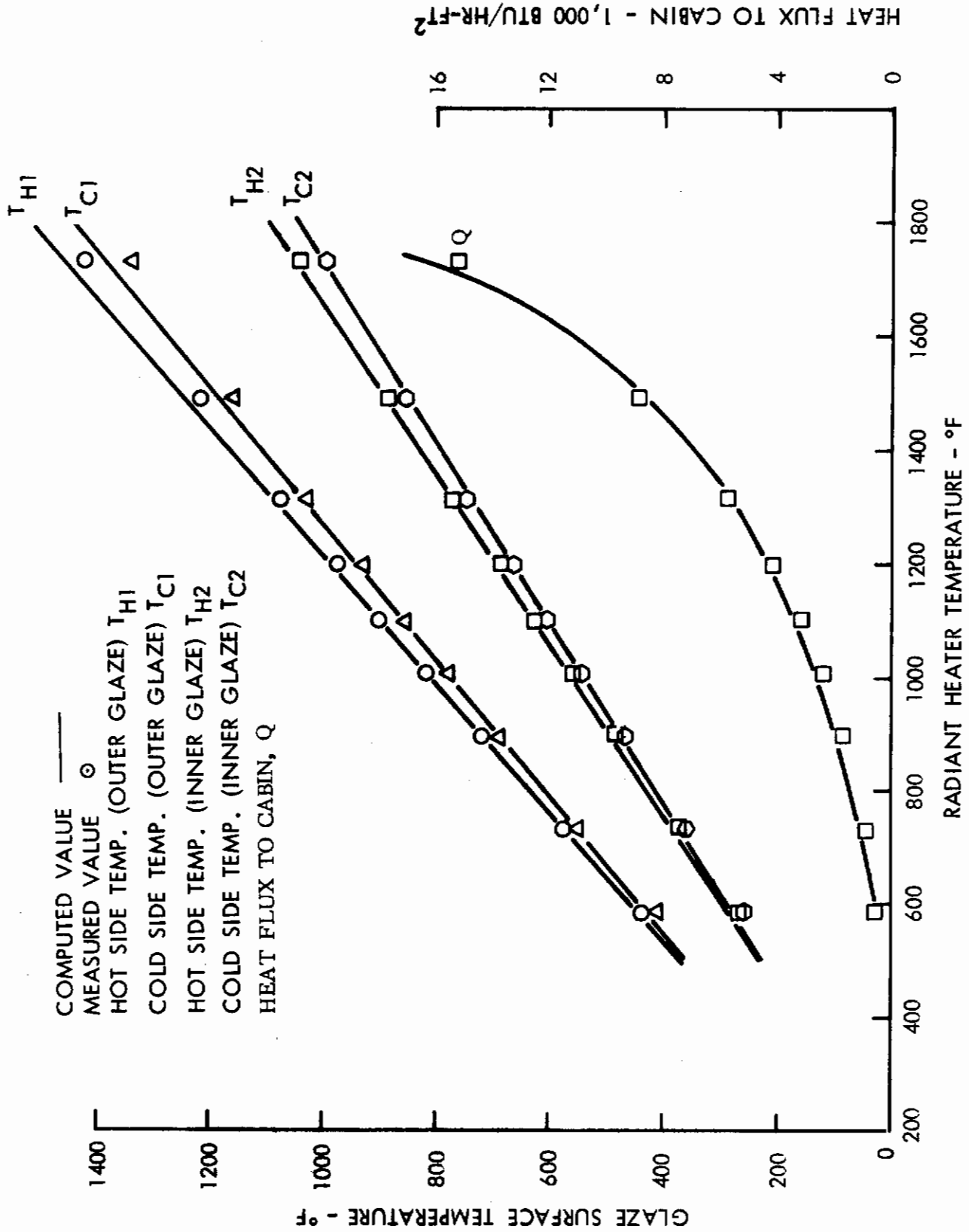


Figure 22 - 1/4-In. Fused Silica, 1/8-In. Vycor Double Window Heated by Radiation in Air, Steady-State Conditions

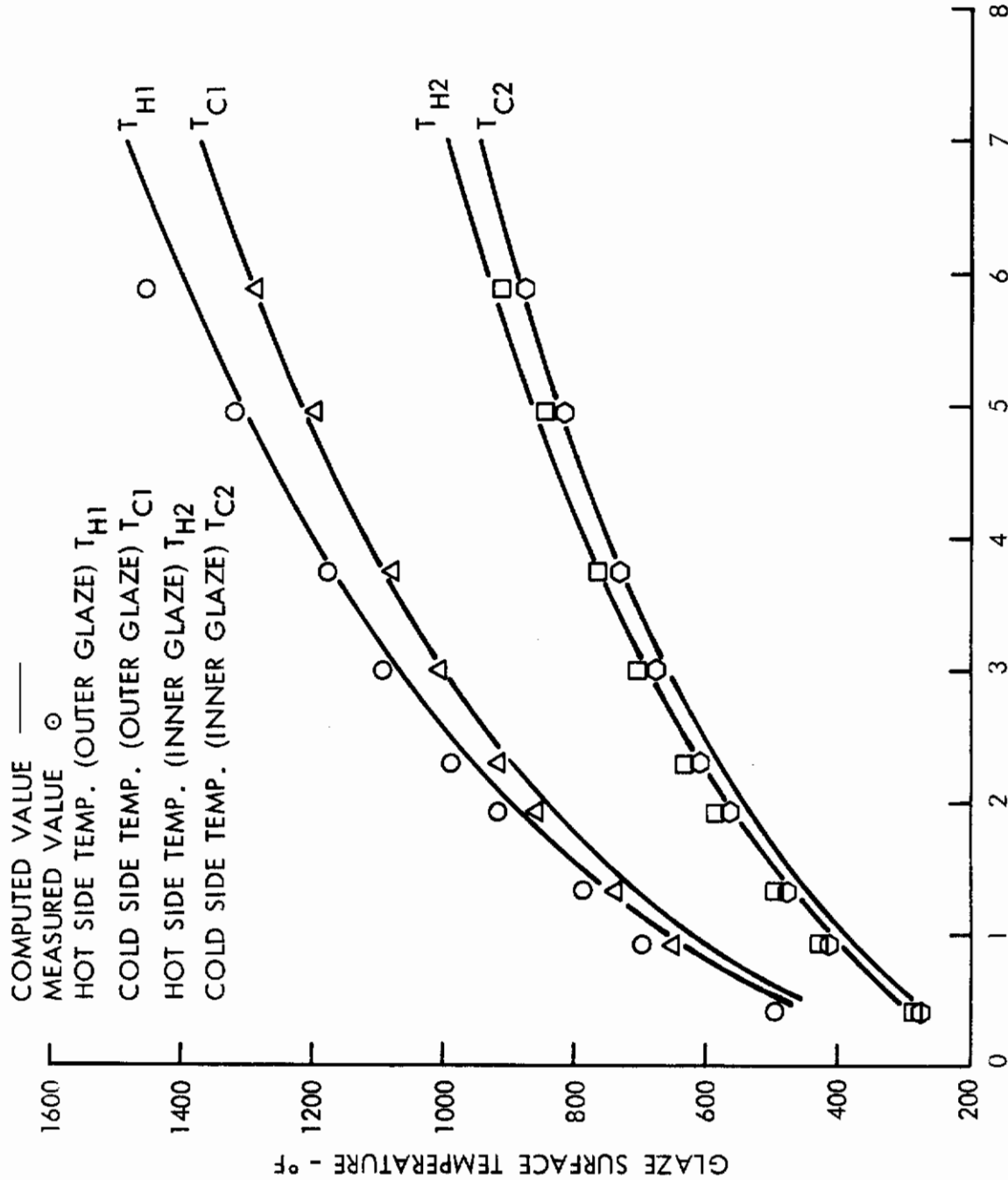


Figure 23 - 1/4-In. Fused Silica, 1/8-In. Vycor Double Pane Window Heated by Convection in Air, Steady-State Conditions  
 HEAT FLUX TO CABIN - 1,000 BTU/HR-FT<sup>2</sup>

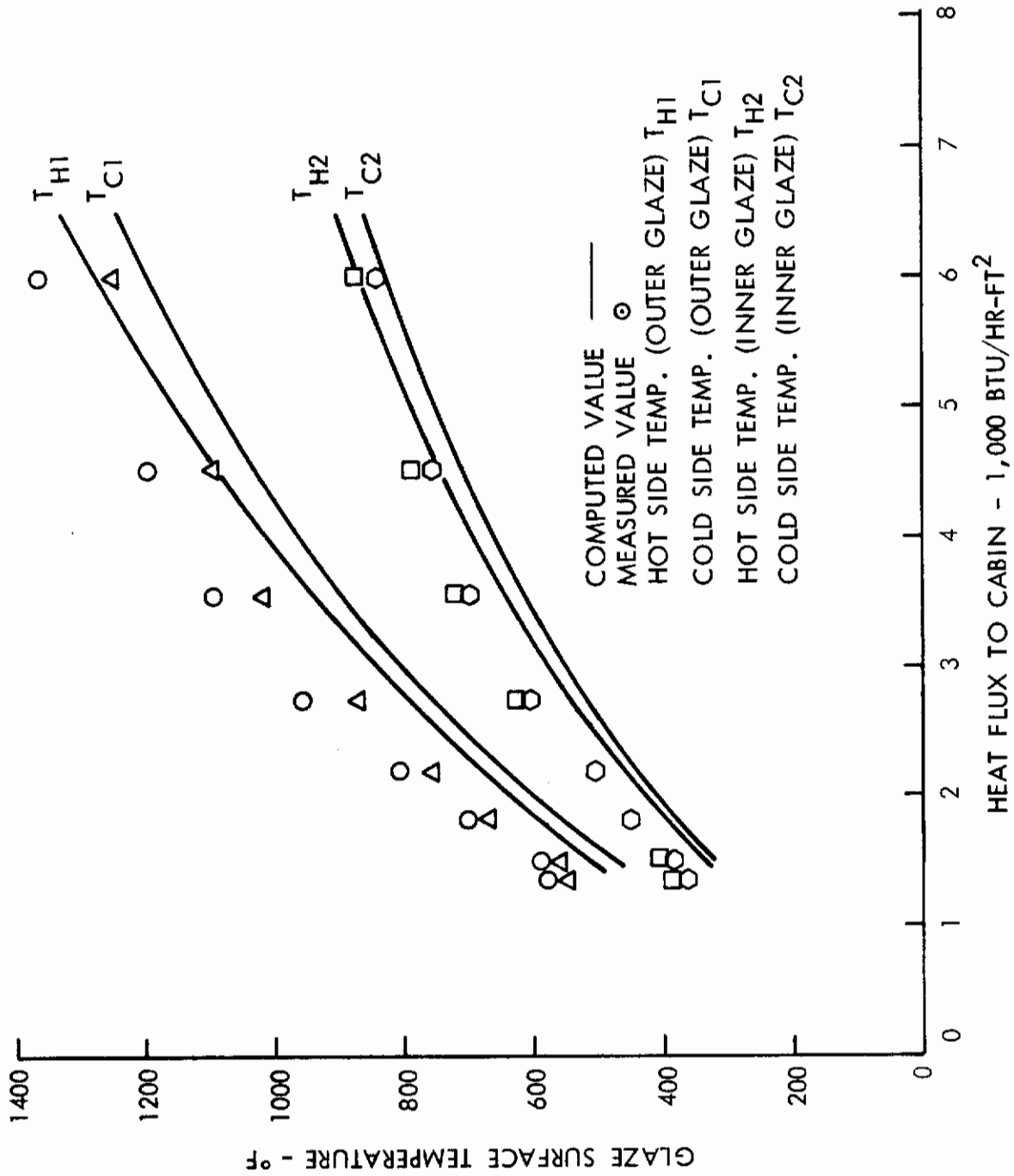


Figure 24 - 1/4-In. Fused Silica, 1/8-In. Vycor Double Pane Window Heated by Radiation and Convection in Air, Steady-State Conditions



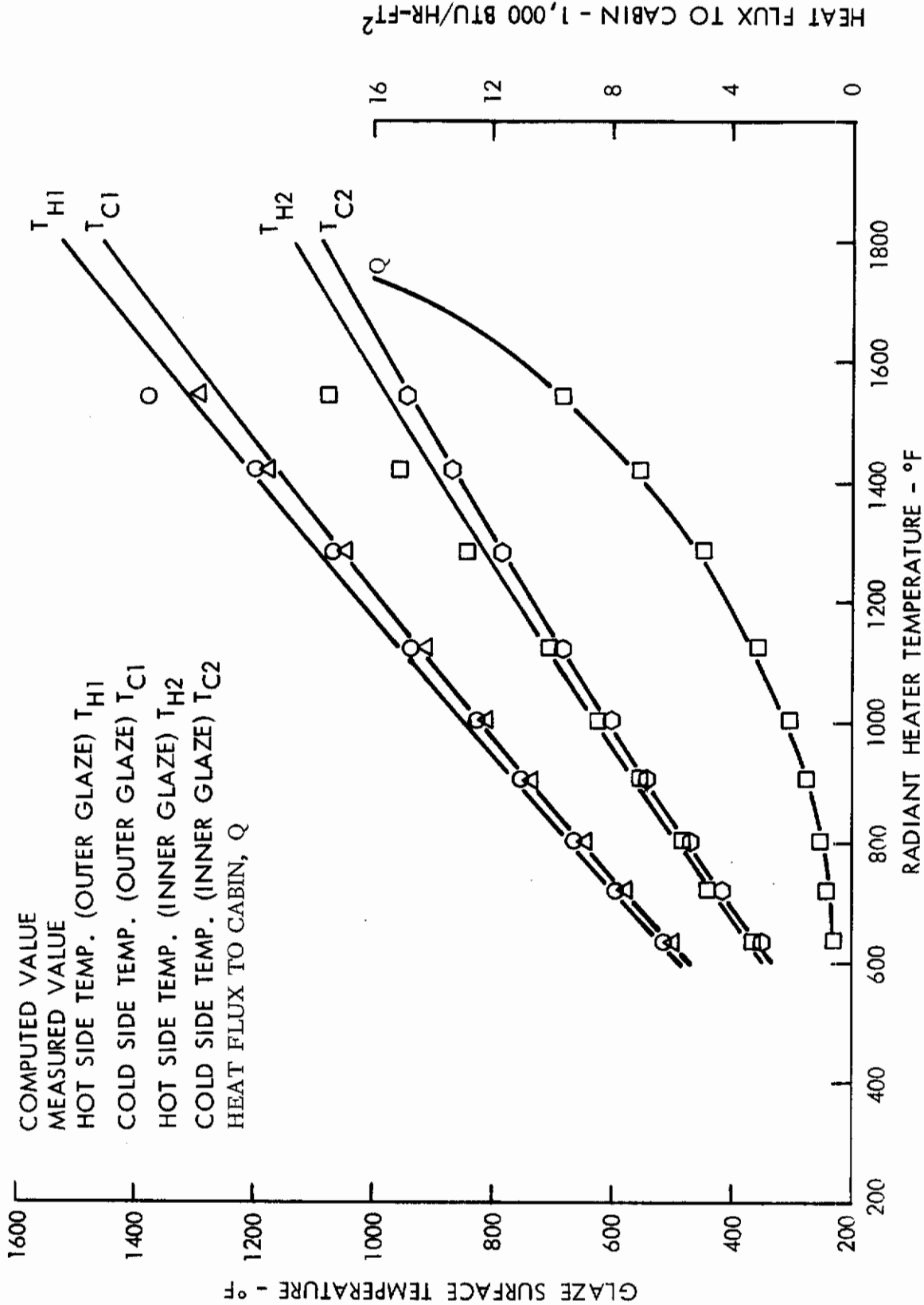


Figure 25 - 1/4-In. Fused Silica, 1/8-In. Vycor Double Pane Window Heated by Radiation in a Vacuum, Steady-State Conditions

# Contrails

TABLE IV

TEMPERATURES AND HEAT FLUXES FOR VARIOUS GLAZE CONFIGURATIONS  
AND A CONSTANT RADIATIVE INPUT

Glaze Configuration		Heat Input (Btu/hr-ft <sup>2</sup> )	Outer Glaze				Inner Glaze				Flux to Cath. (Btu/hr-ft <sup>2</sup> )	
			Hot Side		Cold Side		Hot Side		Cold Side			
Outer Glaze	Inner Glaze		Comp.	Meas.	Comp.	Meas.	Comp.	Meas.	Comp.	Meas.	Comp.	Meas.
1/4 in. Fused Silica	1/8 in. Vycor	$Q_R = 12,480$ ↓	1,033	1,025	987	977	727	732	700	707	4,800	4,800
3/8 in. Fused Silica	1/8 in. Vycor		1,044	1,028	976	958	716	720	680	695	5,220	4,800
1/4 in. Fused Silica	3/8 in. Fused Silica		1,041	1,040	997	970	756	730	680	647	5,290	5,150
3/8 in. Alumino-silicate	3/8 in. Alumino-silicate		1,072	1,039	986	957	702	732	668	643	4,170	3,860
1/4 in. Fused Silica	1/4 in. Alum.		1,056	1,037	1,015	980	795	790	724	712	4,950	4,450
3/8 in. Alum.	1/4 in. Alum.		1,065	1,032	974	945	733	703	671	648	4,280	3,600
1/4 in. Alum.	3/8 in. Alum.		1,063	1,065	1,005	981	783	770	685	678	4,400	3,850
3/8 in. Fused Silica	1/4 in. Alum.		1,065	1,042	1,004	980	784	765	715	697	4,795	4,200
1/4 in. Fused Silica	3/8 in. Alum.		1,065	1,025	1,025	980	823	795	717	690	4,750	4,200

$Q_R$  = Radiation incident on outer surface of outer glaze; radiant heater temperature,  $T_h = 1250^\circ\text{F}$ .

TABLE V

TEMPERATURES AND HEAT FLUXES FOR VARIOUS GLAZE CONFIGURATIONS  
AND A CONSTANT CONVECTIVE INPUT

Glaze Configuration		Heat Input (Btu/hr-ft <sup>2</sup> )	Outer Glaze				Inner Glaze				Flux to Cath. (Btu/hr-ft <sup>2</sup> )	
			Hot Side		Cold Side		Hot Side		Cold Side			
Outer Glaze	Inner Glaze		Comp.	Meas.	Comp.	Meas.	Comp.	Meas.	Comp.	Meas.	Comp.	Meas.
1/4 in. Fused Silica	1/8 in. vycor	$Q_C = 5724$ ↓	917	948	861	881	582	600	557	584	2,110	- - -
3/8 in. Fused Silica	1/8 in. Vycor		926	965	854	880	582	610	562	598	2,100	- - -
1/4 in. Fused Silica	3/8 in. Fused Silica		936	1,010	885	915	619	640	559	570	2,100	- - -
3/8 in. Alumino-silicate	3/8 in. Alumino-silicate		956	995	868	898	647	645	576	603	2,275	- - -
1/4 in. Fused Silica	1/4 in. Alum.		951	1,010	900	937	633	675	583	608	2,340	- - -
3/8 in. Alum.	1/4 in. Alum.		940	1,012	853	905	619	652	573	598	2,260	- - -
1/4 in. Alum.	3/8 in. Alum.		944	990	881	910	652	685	579	595	2,275	- - -
3/8 in. Fused Silica	1/4 in. Alum.		951	1,028	878	925	617	654	569	602	2,240	- - -
1/4 in. Fused Silica	3/8 in. Alum.		968	1,020	917	950	659	700	584	613	2,340	- - -

$Q_C$  = Convective input to outer surface of outer glaze.

# Contrails

TABLE VI

TEMPERATURES AND HEAT FLUXES FOR VARIOUS COATING CONFIGURATIONS ON A 1/4-IN. FUSED SILICA AND 1/8 IN. VYCOR WINDOW SYSTEM IN AN AIR ENVIRONMENT

Coatings				Heat Input (Btu/hr-ft <sup>2</sup> )	Outer Glaze				Inner Glaze				Flux to Cabin (Btu/hr-ft <sup>2</sup> )	
Outer Glaze		Inner Glaze			Hot Side		Cold Side		Hot Side		Cold Side		Comp.	Meas.
Hot Side	Cold Side	Hot Side	Cold Side		Comp.	Meas.	Comp.	Meas.	Comp.	Meas.	Comp.	Meas.		
None	None	None	None	$Q_R = 12,480$ ↓	1,033	1,025	987	977	727	732	700	707	4,800	4,840
None	UV-IR	None	None		1,035	1,000	988	963	714	720	687	694	4,800	4,710
None	UV-IR	HEA	HEA		1,035	1,000	969	969	714	730	667	691	4,550	3,990
HEA	HEA	HEA	HEA		1,035	1,002	989	980	722	715	685	681	4,950	4,180
None	UV-IR	Gold	HEA		1,112	1,095	1,084	1,058	606	670	585	585	2,460	2,170
None	None	None	None	$Q_c = 6,360$ ↓	955	993	900	920	611	645	590	620	2,350	- - -
None	UV-IR	None	None		974	923	919	888	623	679	601	602	2,450	- - -
None	UV-IR	HEA	HEA		973	1,015	918	958	623	661	601	620	2,460	- - -
HEA	HEA	HEA	HEA		972	1,040	917	959	627	660	604	628	2,500	- - -
None	UV-IR	Gold	HEA		1,003	996	966	955	512	515	480	490	1,500	- - -

TABLE VII

TEMPERATURES AND HEAT FLUXES FOR VARIOUS COATING CONFIGURATIONS ON A 1/4-IN. FUSED SILICA AND 1/8-IN. VYCOR WINDOW SYSTEM IN A VACUUM ENVIRONMENT

Coatings				Heat Input (Btu/hr-ft <sup>2</sup> )	Outer Glaze				Inner Glaze				Flux to Cabin (Btu/hr-ft <sup>2</sup> )	
Outer Glaze		Inner Glaze			Hot Side		Cold Side		Hot Side		Cold Side		Comp.	Meas.
Hot Side	Cold Side	Hot Side	Cold Side		Comp.	Meas.	Comp.	Meas.	Comp.	Meas.	Comp.	Meas.		
None	None	None	None	$Q_c = 3,800$ ↓	975	965	945	930	727	721	700	693	3,600	3,400
None	UV-IR	None	None		972	940	941	908	710	701	690	675	3,365	3,600
None	UV-IR	HEA	HEA		971	952	940	915	709	678	683	658	3,260	2,950
HEA	HEA	HEA	HEA		971	951	940	928	716	705	686	685	3,515	3,080
None	UV-IR	Gold	HEA		1,030	1,020	1,011	984	580	645	553	550	1,630	1,630

Radiant heater temperature,  $T_h = 1150^\circ\text{F}$ .

## B. Additional Experimental Results

In addition to supplying data for validation of the computer program, a second objective of the experimental testing was to provide empirical data on realistic window glaze components. Toward this end a large number of heat transfer tests were conducted, and data from 50 representative tests are presented in Appendix F of this report.

## C. Additional Analytical Results

Calculations, in addition to those made for the validation of the analysis, were accomplished for the comparison of interesting analytical results and to check out the in-flight radiative and convective heating subroutines. A comparison of window temperatures and heat flux to the cabin was made for:

1. An opaque analysis as opposed to the semitransparent analysis;
2. A window heated by radiation and by convection;
3. A window heated in air and in a vacuum; and
4. An increasing number of panes in a window system.

The in-flight cases included the calculation of window temperatures and cabin heat flux for:

1. A hypersonic re-entry;
2. A supersonic trajectory;
3. A convective heating rate versus time specified by input data; and
4. A circular orbit.

Figure 26 is a plot of the computed temperature distributions within a 1/4-in. fused silica window subjected to radiative heating assuming the glaze to be semitransparent in one case and to be opaque in a second case. The semitransparent analysis resulted in lower computed glaze temperatures and a higher heat flux to the cabin since radiant energy from the heater was not totally absorbed as it passed through the window. In the opaque analysis it was assumed that radiation is absorbed at the surface. A similar effect is seen when comparing the temperature distribution in a glaze heated by convection and by radiation (Figure 27). The convective heat is applied to the surface, whereas the radiative heat is partially absorbed

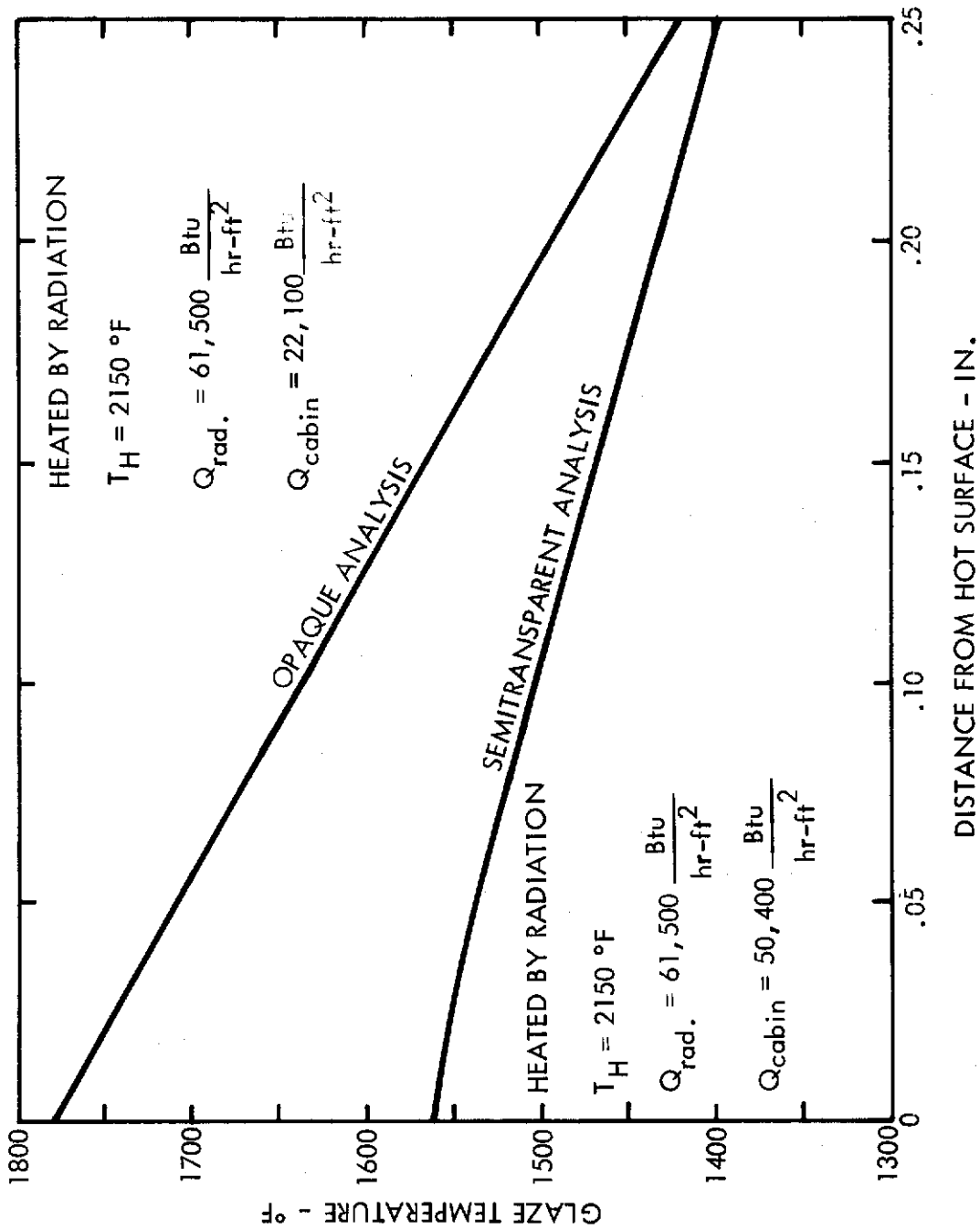


Figure 26 - Computed Temperature Distribution in 1/4-In. Fused Silica, Opaque and Semitransparent Analysis



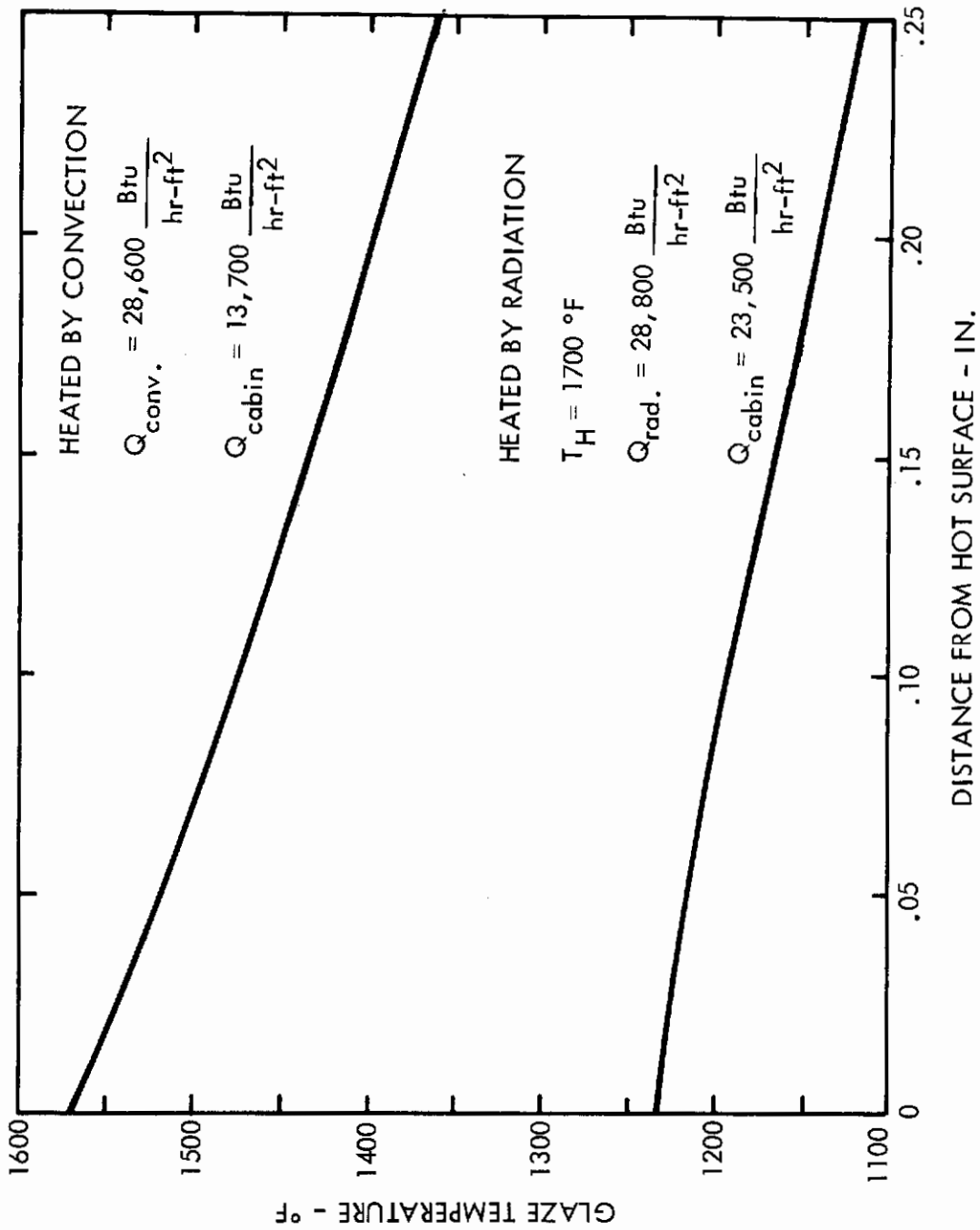


Figure 27 - Computed Temperature Distribution in 1/4-In. Fused Silica, Heated by Radiation and by Convection

# Contrails

and partially transmitted by the window. The temperature gradient computed in the semitransparent analysis is less than that in the opaque case. This is due to the internal radiation between the glaze elements, which is accounted for in the semitransparent analysis.

Figure 28 compares glaze temperatures and heat flux to the cabin for the 1/4-in. fused silica, 1/8-in. Vycor window heated by radiation in air and in a vacuum. The cabin heat flux is higher in the air environment since the heat flux to the calorimeter in the apparatus cold plate includes conduction through the air as well as radiation from the glazes. Since the heat flux from the window to the cold plate was greater for the air environment, the steady-state glaze temperatures were lower than those measured in the vacuum tests. At elevated temperatures radiation becomes the predominant mode of heat transfer resulting in smaller differences between the air and vacuum cases.

The effects of increased number of glazes on the temperatures of and heat transfer through a window system heated by radiation are presented in Table VIII. These values were calculated with the subject computer program for windows having from one to five uncoated 1/8-in. Vycor glazes. As expected, an increase in the number of glazes increases the resistance to heat transfer, resulting in a higher outermost surface temperature and lower innermost surface temperature of the window system, and a lower heat flux through the window to the cabin.

As stated above, window temperatures and heat fluxes were predicted for various types of missions in order to check out the subroutines employed in computing the flight heating conditions. Figure 29 is a plot of the thermal performance of a double-pane window during a hypersonic skip-glide re-entry. The flight path employed in this calculation is that presented in Figure 30 which is for a re-entry vehicle with a wing load of  $W/S = 25\text{PSF}$  and an initial velocity of 26,000 ft/sec at 400,000 ft. (Figure 4 of Ref. 1). The window configuration for this case consisted of a 1/4-in. fused silica outer pane and a 1/8-in. VYCOR inner pane.

Window temperatures and cabin heat flux predicted for a portion of a supersonic transport flight are presented in Figure 31. The flight path is described in Figure 32 and is typical of a New York to Paris flight plan. In this case the window configuration analyzed contained two coated panes. The outer pane was a 1/4-in. fused silica glaze with an ultraviolet-infrared (UV-IR) reflecting coating on its emergent side. A 1/8-in. VYCOR glaze with a gold infrared reflecting coating on its incident surface and a high efficiency antireflection (HEA) coating on its emergent side was employed as the inner window pane.

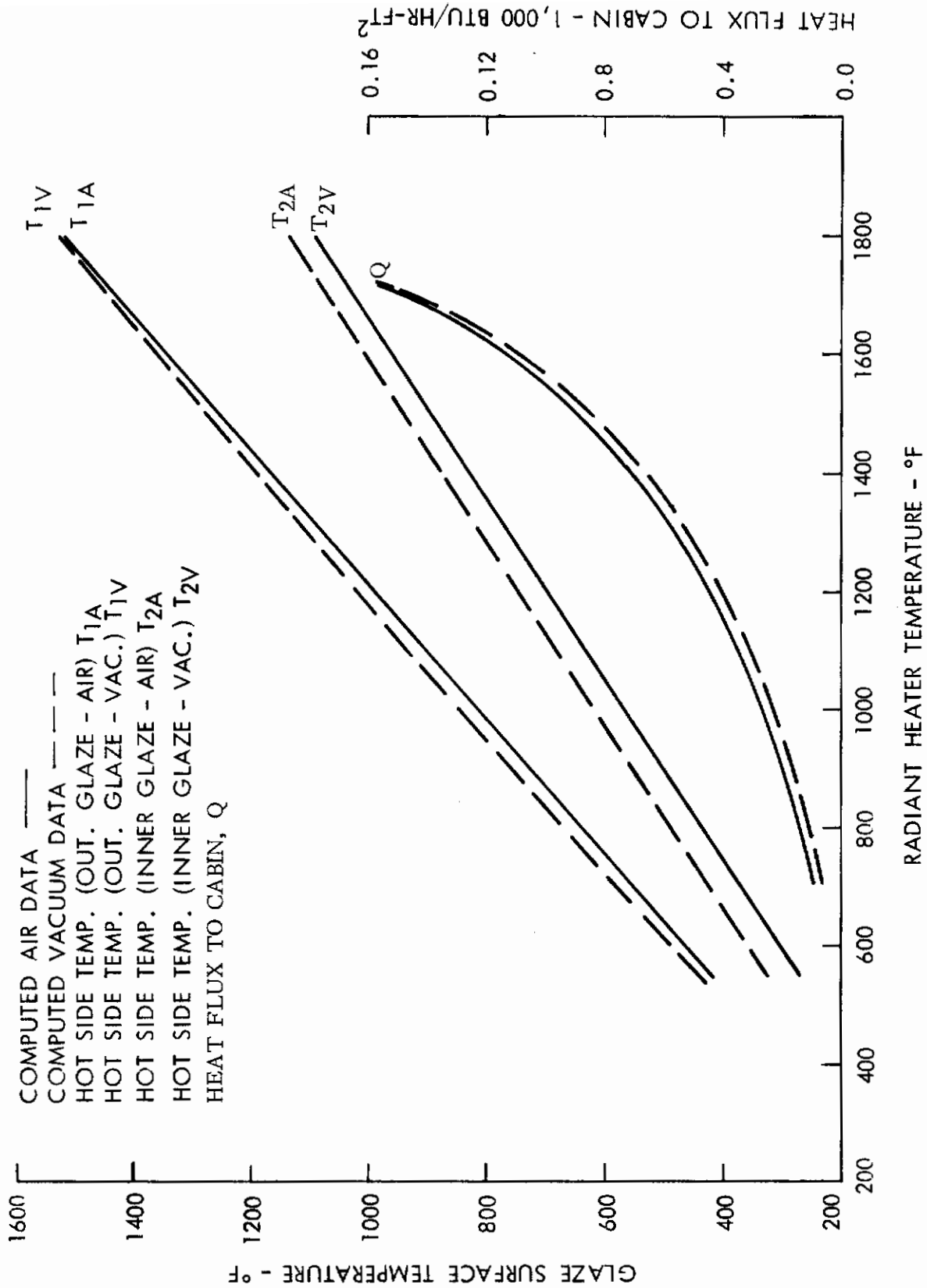



Figure 28 - Comparison of Temperatures and Cabin Heat Flux of Window System Heated by Radiation in Air and in a Vacuum

TABLE VIII  
 EFFECT OF NUMBER OF GLAZES IN A WINDOW SYSTEM  
 ON TEMPERATURES AND HEAT FLUX

Number of Glazes in Window System	Heat Input (Btu/hr-ft <sup>2</sup> )	Hot Side Temperature (Outer Most Glaze) °F	Cold Side Temperature (Inner Most Glaze) °F	Flux to Cabin (Btu/hr-ft <sup>2</sup> )
1	$Q_R = 89,000$ 	1628	1528	61,000
2		1886	1296	50,500
3		2009	1163	43,300
4		2082	1073	38,200
5		2149	1040	34,600

Radiant heater temperature,  $T_h = 2300^\circ\text{F}$ .

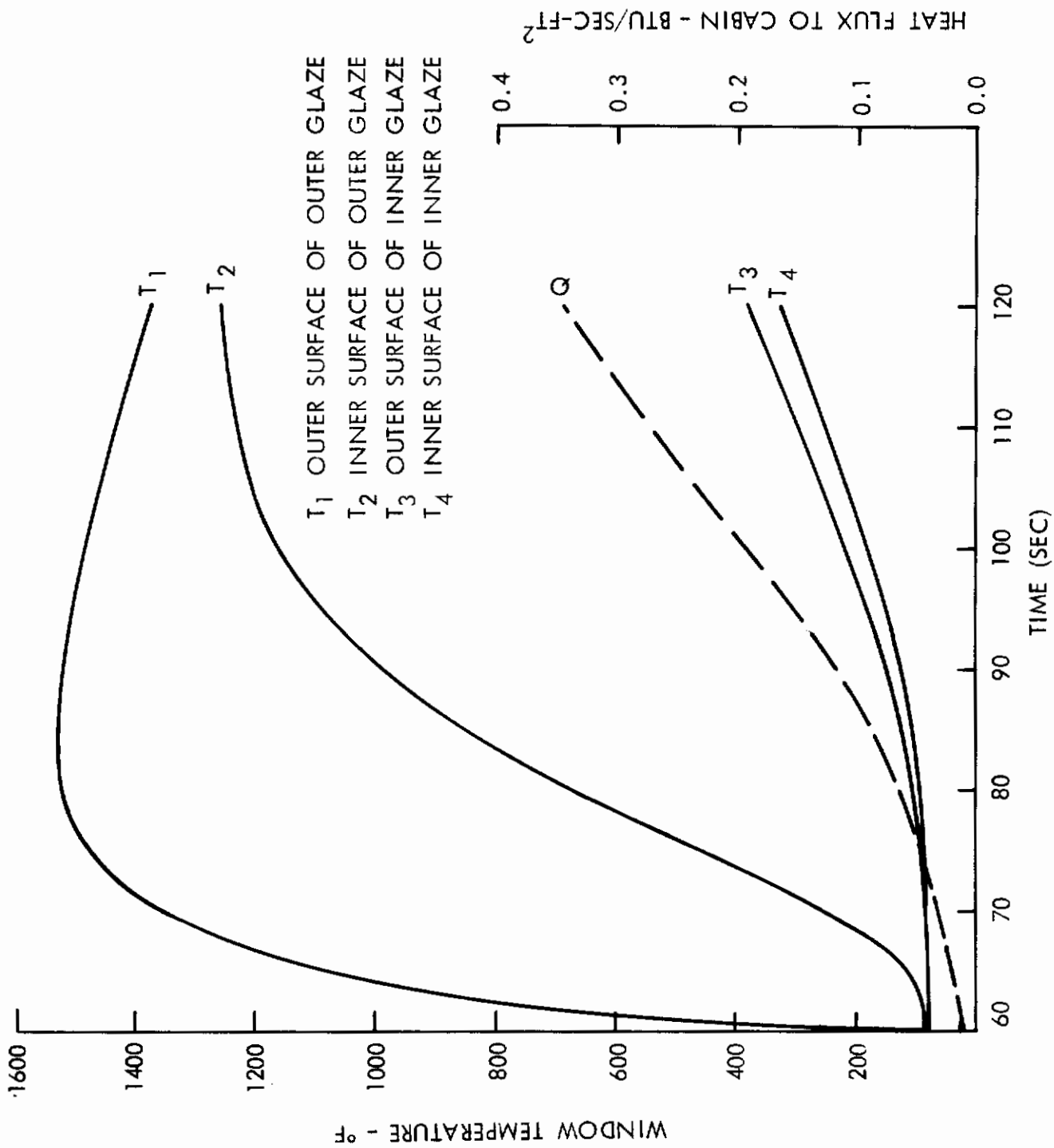


Figure 29 - Thermal Performance of a Double Pane Window During a Hypersonic Skip-Glide Re-entry



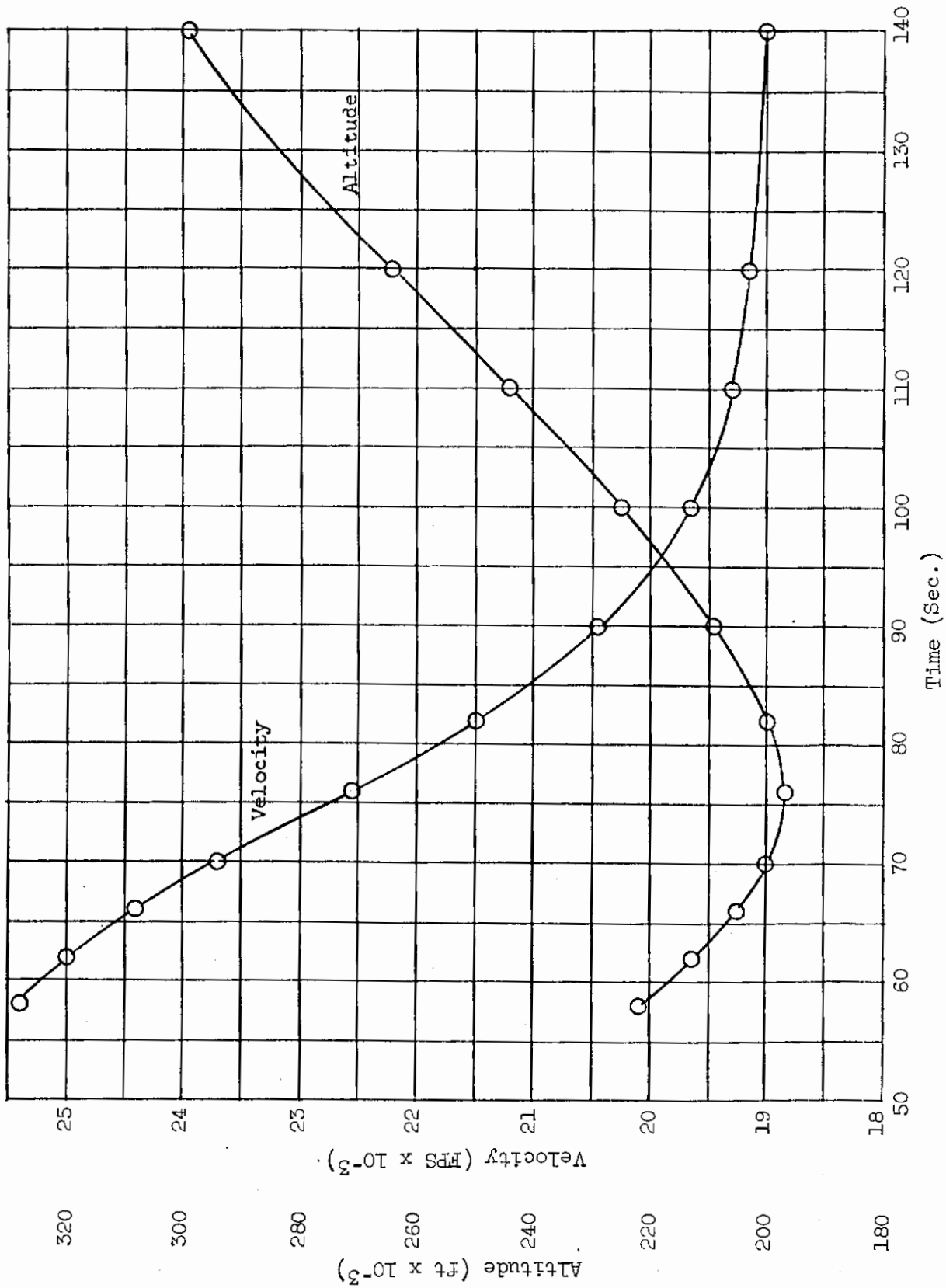


Figure 30 - Portion of Hypersonic Skip-Glide Re-Entry Trajectory

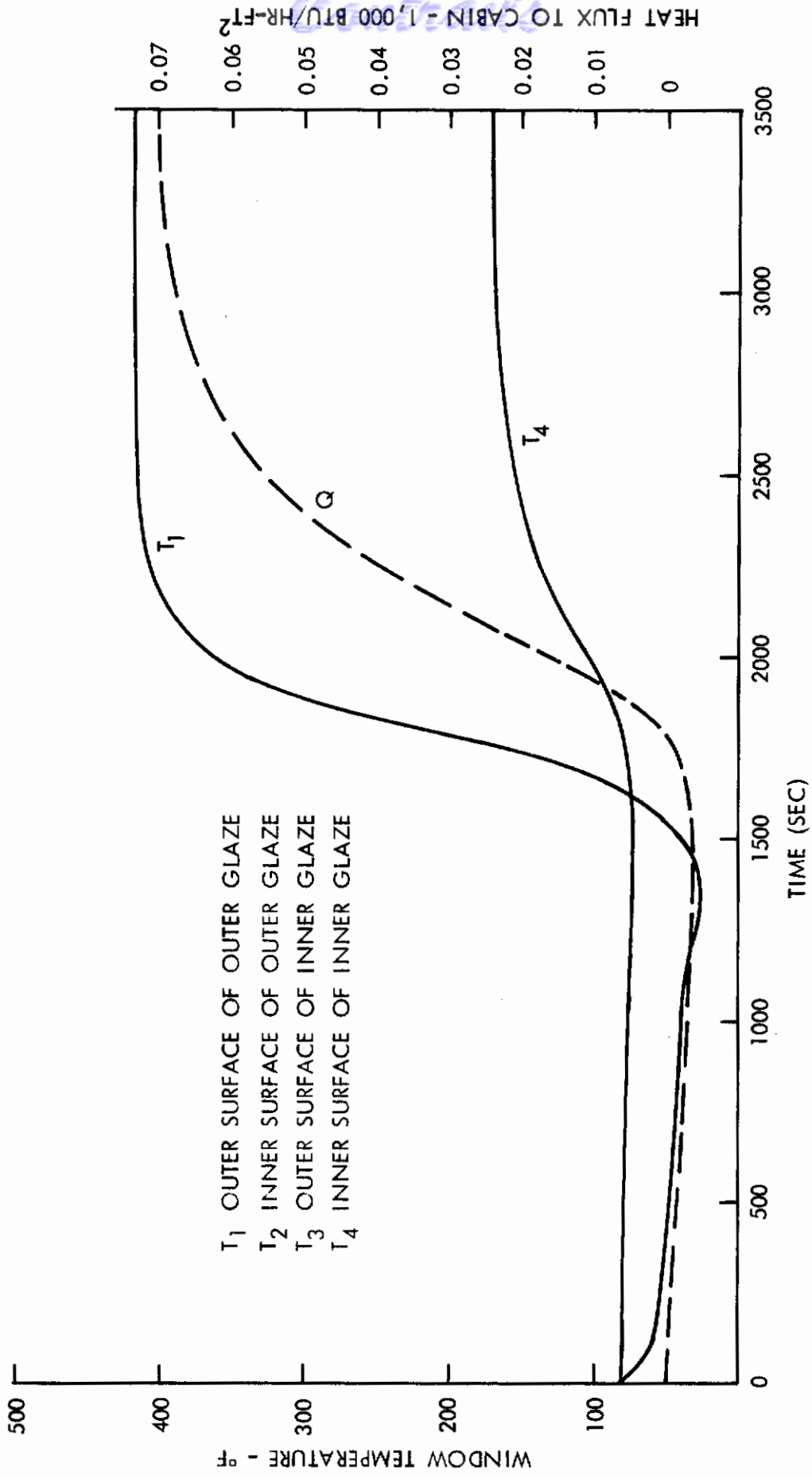


Figure 31 - Thermal Performance of a Double Pane Window During a Mach 3 Supersonic Flight

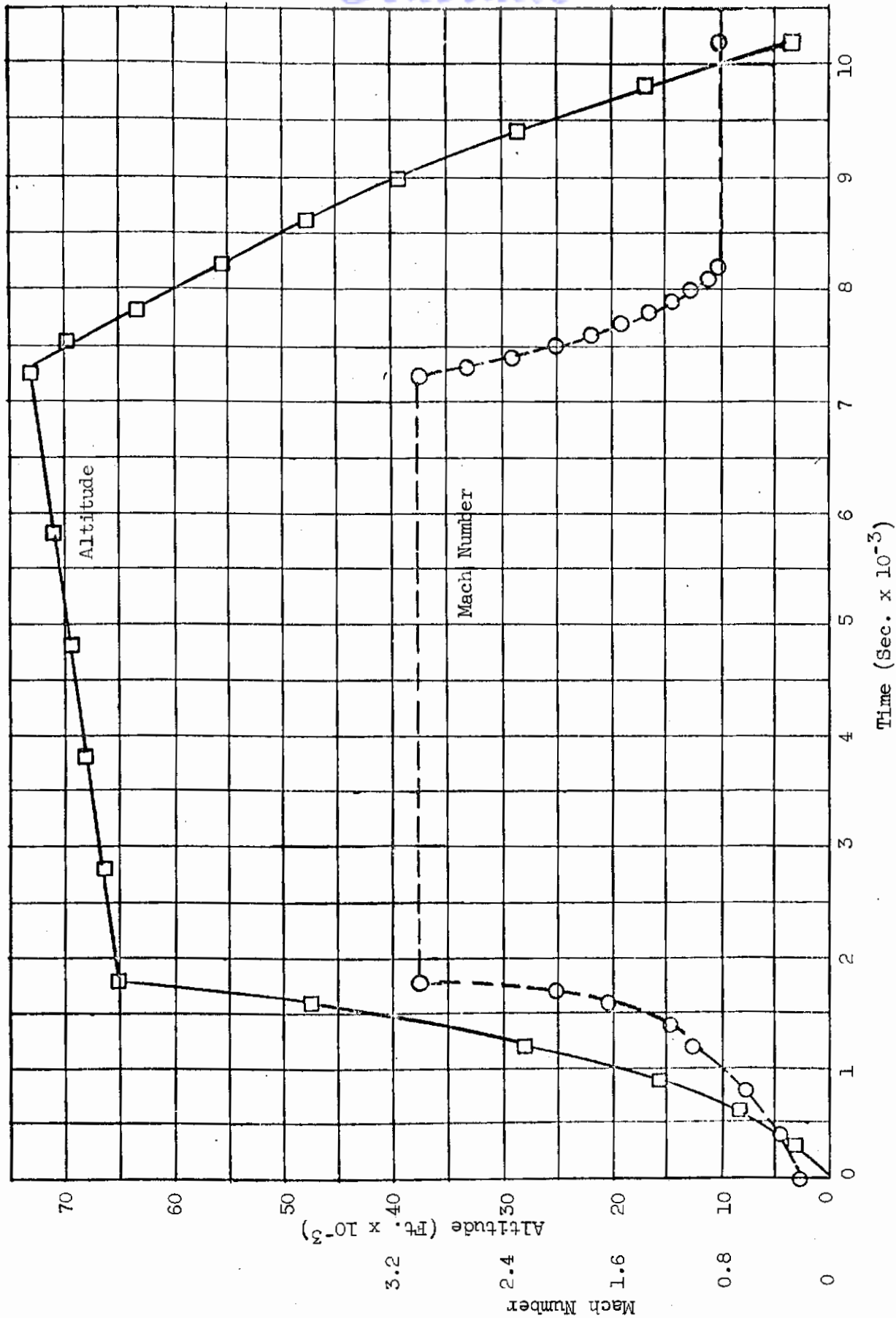


Figure 32 - Mach 3 Supersonic Transport Flight Path

# Contrails

Figure 33 presents the thermal analysis of a window of a spacecraft in a 200-nautical-mile circular orbit. The window configuration used in the orbital flight was identical to the one described above for the supersonic transport case. Techniques utilized by the computer program sub-routines to compute radiative and convective heating to the windows for the hypersonic, supersonic, and orbital flights described above are discussed in Appendix D.

In addition to the cases in which the radiative and aerodynamic heating were computed by the program, the thermal response was predicted for a window subjected to a time-dependent convective heating rate as defined by input data. The input convective heat transfer rate at the window location was assumed to be 0.02 times the stagnation point heat rate plotted in Figure 34. Figure 35 presents the window temperatures and the heat flux to the cabin for a portion of flight for which the thermal environment is defined in Figure 34. A window configuration consisting of a 1/4-in. fused silica outer glaze and a 1/8-in. VYCOR inner glaze was used in this case.

- T<sub>1</sub> OUTER SURFACE OF OUTER GLAZE
- T<sub>2</sub> INNER SURFACE OF OUTER GLAZE
- T<sub>3</sub> OUTER SURFACE OF INNER GLAZE
- T<sub>4</sub> INNER SURFACE OF INNER GLAZE

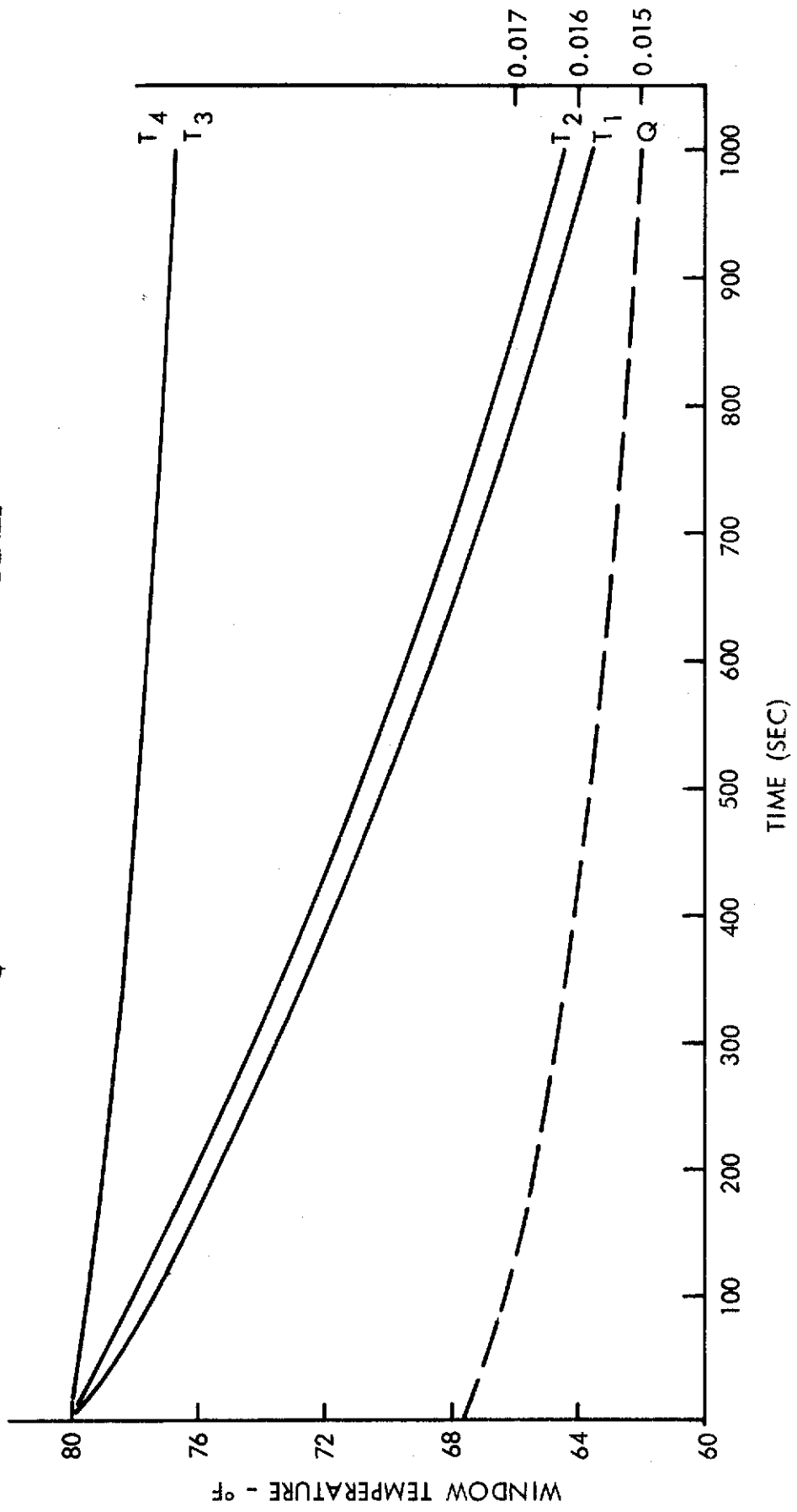


Figure 33 - Thermal Performance of a Double Pane Window in 200 NM Circular Orbit



REFERENCE LAMINAR HEAT TRANSFER RATE  
SDF TRAJECTORY CASE 380800

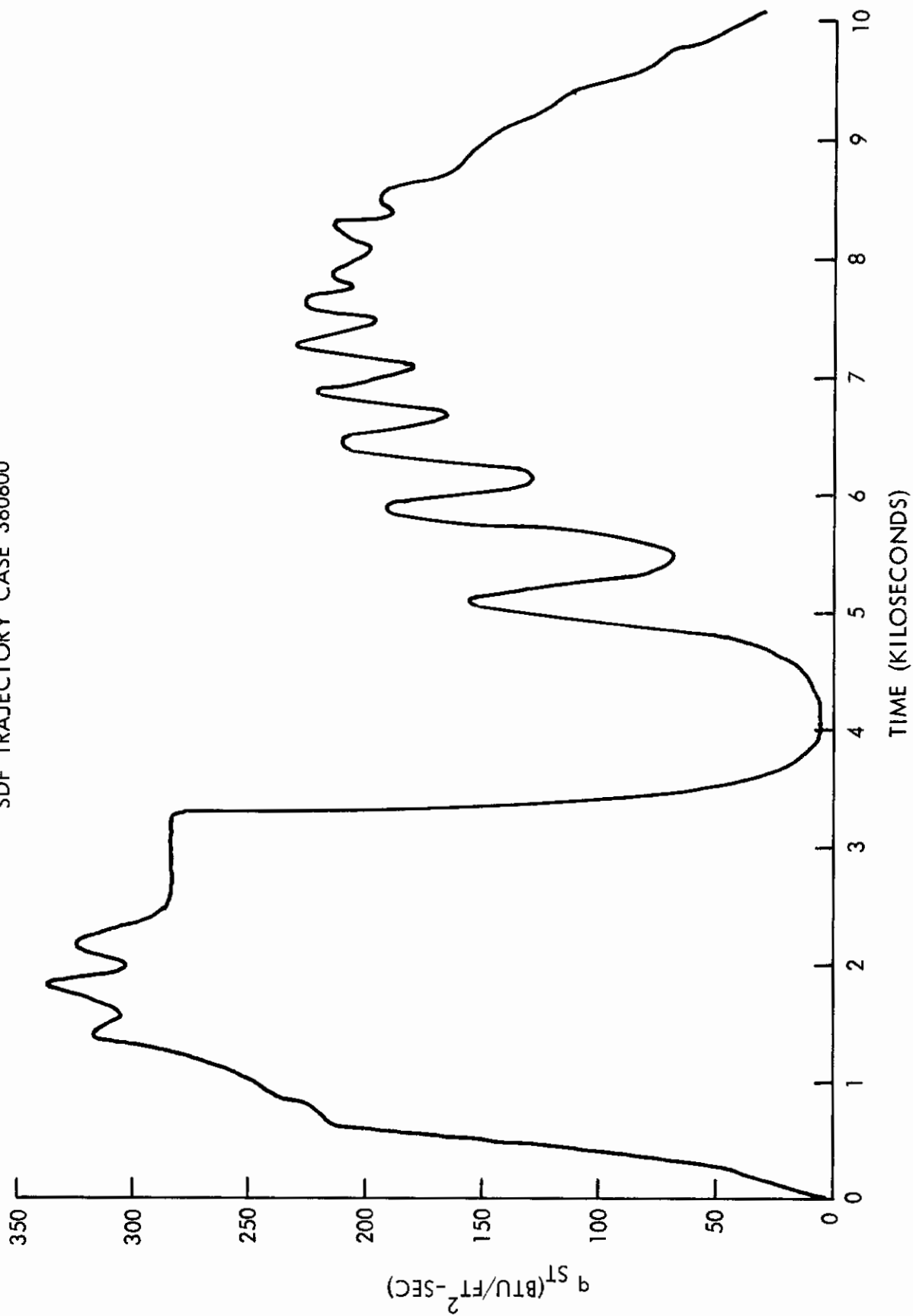
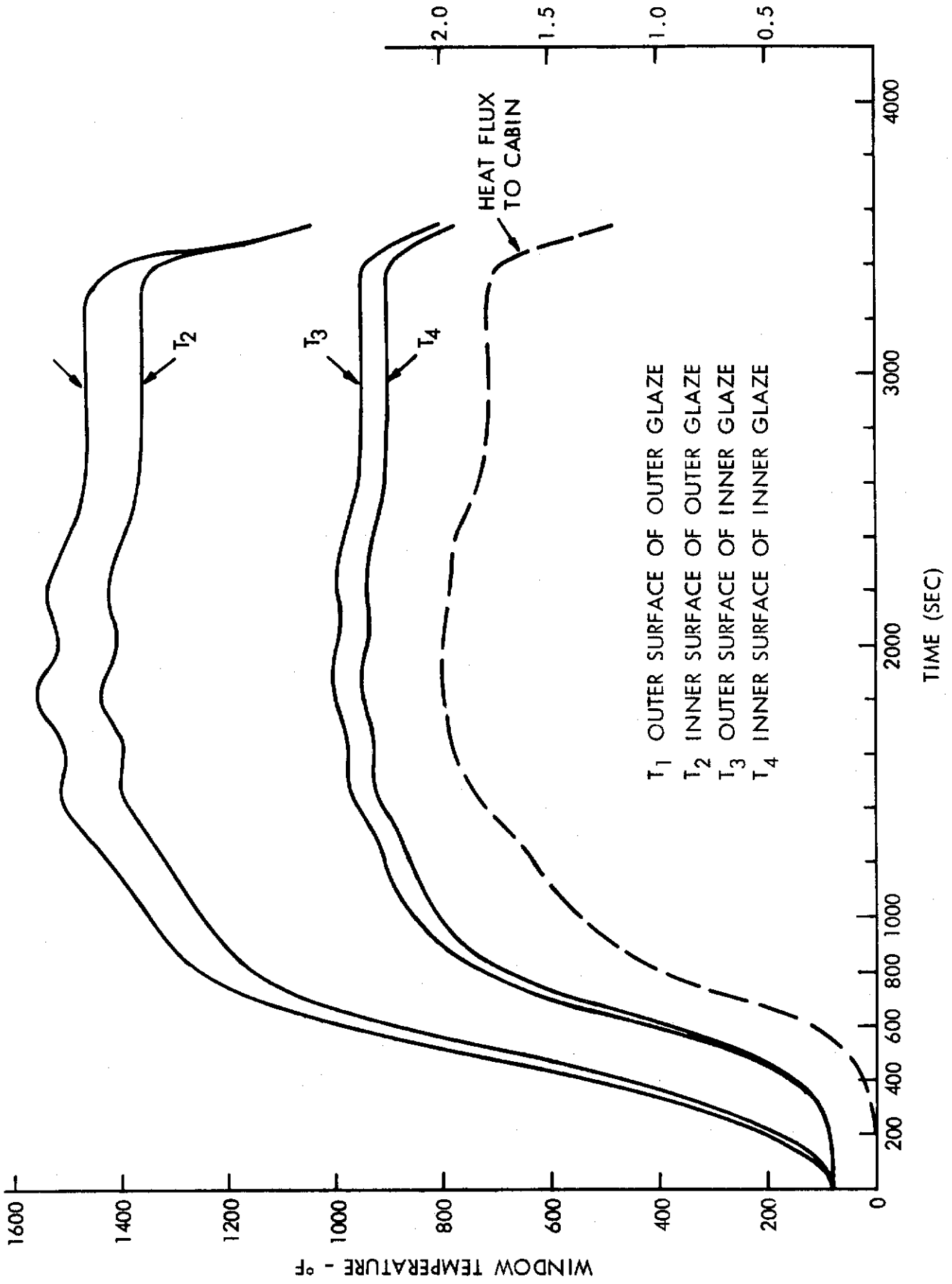


Figure 34 - Stagnation Point Heat Transfer Rate (Ref. 16)



HEAT FLUX TO CABIN - BTU/SEC-FT<sup>2</sup>

Figure 35 - Thermal Performance of a Double Pane Window Assuming Window Heating to be 0.02 Times  $q_{st}$  of Figure 33

## SECTION V

### CONCLUSIONS

A computer program was developed for predicting the temperatures distribution and heat transfer through aerospace window systems subjected to the thermal environments of hypersonic cruise, re-entry, supersonic and orbital flight. The program analysis has been experimentally validated for single and double pane windows having coated and uncoated surfaces. The subject computer program will be a valuable tool in the design of aerospace window systems when material temperature limits, thermal gradients, and cabin heating must be considered.

In addition to the experimental tests used to validate the computer program analysis, heat tests were conducted to provide empirical data on realistic window glaze components. These data can be used by the designer as a preliminary guide in selecting combinations of coated and uncoated glazes for window systems when thermal considerations are required.

A constant value of surface emittance is used by the program when computing the absorption and emission of radiation in the spectral region to which the glazes are considered opaque. When computing the temperatures of glazes coated with dielectric films (HEA and UV-IR coatings) a surface emittance equal to that of the uncoated glaze was used, resulting in good agreement with the measured temperatures. Comparison of measured and computed temperatures for the gold-coated specimens indicated that the emittance of the gold-coated surfaces is temperature-dependent. For example, to obtain good agreement between measured and computed steady-state temperatures (810°F) for the gold-coated glaze specimen of Table III, a value of 0.6 was used for the surface emittance. For the gold-coated specimen of Table VII ( $T = 553^\circ\text{F}$ ), an emittance value of 0.4 was required. To satisfactorily compute transient temperatures of gold-coated windows, the temperature-dependent emittance (and possibly reflectance and transmittance) of the coatings should be determined; and the program logic should be changed to use the temperature-dependent emittance, reflectance, and transmittance of thin-film coatings.

Computer time is relatively long for the subject program, especially for multiple glaze calculations, since each element in each glaze absorbs radiant energy from each element in each glaze. An example of the computation time is that required for the calculation of temperatures for the double glaze window configurations presented in Figures 31 and 35. The computation times for these two runs were 35 min. and 95 min., respectively. Simplification of the analysis could result in a decrease in computation time. For example, if polarization effects were neglected, the complexity of the auxiliary functions of the heat balance equations would be reduced.

# Contrails

As discussed in Section II, Subsection H of this report, truncation errors are minimized by comparing the temperature field computed for a time-step of  $\Delta t$  to that computed using two  $\Delta t/2$  time-steps. If the temperature fields do not agree, the input time-step is halved and the procedure is repeated until agreement is obtained. Even if agreement is obtained, the program is required to compute the temperature field at least three times for each time-step accepted. Computation time could be significantly reduced if a procedure were employed which required the temperature field to be computed only once each time-step. This could be accomplished by allowing the computer program to define an acceptable, upcoming time-step using some stability and/or accuracy criteria possibly based on the transient heating conditions. The present procedure employed by the program could be retained and used by option.

APPENDIX A

EQUATIONS FOR COMPUTING RADIATION WITHIN WINDOW GLAZES

# Contrails

## TABLE OF CONTENTS

	<u>Page No.</u>
Nomenclature . . . . .	71
Introduction . . . . .	75
Thermal Analysis . . . . .	75
Previously Developed Analytical Relationships . . . . .	76
Absorption of Radiation Entering a Glaze . . . . .	76
Absorption of Radiation Emitted within Glaze . . . . .	78
Transmission of Radiation at Glaze Surface . . . . .	80
Multiple-Glaze Analysis . . . . .	81
Radiation Absorbed by a Finite Glaze Element . . . . .	87
Glaze Elements as Radiation Sources . . . . .	87
Glaze Coatings as Radiation Sources . . . . .	89
Radiation Source External to Window . . . . .	91
Radiation Emitted by a Finite Glaze Element . . . . .	92
Heat Flux to the Cabin . . . . .	94
Radiation from Glaze Elements to the Cabin . . . . .	95
Radiation from Glaze Coatings to the Cabin . . . . .	96
Radiation from an External Source to the Cabin . . . . .	96



## NOMENCLATURE

<u>Symbols</u>	<u>Units</u>	
	<u>International</u>	<u>U.S. Customary</u>
a - surface absorptance		
G - number of media in window system		
h - convection coefficient	(Watt/cm <sup>2</sup> -°C)	(Btu/sec-ft <sup>2</sup> -°R)
i - number of absorbing element		
I - intensity	(Watt/cm <sup>2</sup> -ster-μ)	(Btu/sec-ft <sup>2</sup> -ster-μ)
j - number of emitting element		
j <sub>λ</sub> - volume emissive power	(Watt/cm <sup>3</sup> -ster-μ)	(Btu/sec-ft <sup>2</sup> -ster-μ)
k - thermal conductivity	(Watt/cm °C)	(Btu/sec-ft-°R)
L - thickness of glaze	(cm.)	(ft.)
M - medium number of glaze containing emitting element		
n - index of refraction		
N - medium number of glaze containing absorbing element		
$\hat{P}$ - function defined in text		
q - rate of heat flux	(Watt/cm <sup>2</sup> )	(Btu/sec-ft <sup>2</sup> )
Q - rate of energy per unit volume	(Watt/cm <sup>3</sup> )	(Btu/sec-ft <sup>3</sup> )
s - set equal to 1 for internal glaze elements and to $\frac{1}{2}$ for edge elements		

# *Contrails*

<u>Symbols</u>	<u>Units</u>	
	<u>International</u>	<u>U.S. Customary</u>
t - time	(sec.)	(sec.)
T - absolute temperature	(°K)	(°R)
W - radiant flux	(Watt/cm <sup>2</sup> )	(Btu/sec-ft <sup>2</sup> )
x - distance of the absorbing element, i, from the glaze upper surface	(cm.)	(ft.)
y - distance of the emitting element, j, from the glaze upper surface		
z - total number of thin-film coatings in window system		

## Greek Symbols

$\alpha$ - angle between the direction of the beam and the normal to the glaze slab	(radians)	(radians)
$\gamma$ - glaze absorption coefficient	(cm. <sup>-1</sup> )	(ft. <sup>-1</sup> )
$\epsilon$ - emittance		
$\lambda$ - wavelength	(microns)	(microns)
$\nu$ - function defined in text		
$\rho$ - surface reflectance		
$\sigma$ - Stefan-Boltzmann constant	(Watt/cm <sup>2</sup> -°K <sup>4</sup> )	(Btu/sec-ft <sup>2</sup> -°R <sup>4</sup> )
$\tau$ - surface transmittance		
$\phi$ - function defined in text		

# Contrails

<u>Symbols</u>	<u>Units</u>	
	<u>International</u>	<u>U.S. Customary</u>
$\chi$ - function defined in text		
$\rho c$ - volumetric specific heat	(Watt sec/cm <sup>3</sup> °C)	(Btu/ft <sup>3</sup> -°R)

## Subscripts

- $\lambda$  - denotes wavelength dependence
- A - denotes radiation absorbed by glaze finite element
- E - denotes radiation emitted by glaze finite element
- i - denotes absorbing glaze finite element
- j - denotes emitting glaze finite element
- o - denotes initial conditions
- x - denotes location at distance x from the glaze upper surface
- N - denotes medium number of glaze containing the absorbing element, i
- M - denotes medium number of glaze containing emitting element, j
- T - denotes top or upper glaze surface
- B - denotes bottom or lower glaze surface
- || - denotes parallel component of polarized beam

## Subscripts

- L - denotes perpendicular component of polarized beam
- ↑ - denotes beam striking upper surface of a glaze
- ↓ - denotes beam striking lower surface of a glaze
- c - denotes critical angle or cabin temperature
- R - denotes radiation absorbed by a given glaze finite element from the remaining elements within the window system
- F - denotes radiation absorbed by a given finite element from the emitting thin-film coatings in the window system
- H - denotes radiation absorbed by a given finite element from an external radiant source
- f - denotes emitting glaze thin-film coating
- h - denotes external heat source
- s - surface
- G - denotes innermost glaze of the window system

## INTRODUCTION

As discussed in Section II of this report, heat is transferred within semitransparent materials by the combined mechanism of conduction and radiation. Thus to predict the thermal response of heated windows, the analysis must account for the emission, absorption, attenuation, and reflection of radiant energy as well as the conduction heat transfer within the glazes. This Appendix presents and discusses the equations employed by the subject computer program in describing the radiation heat transfer within the glaze materials of a multiple glaze window system.

## THERMAL ANALYSIS

The analytical model used in the analysis was established by assuming each window glaze to be composed of eleven finite slices or elements (Figure 1). The thermal response of each element of the window glazes is defined by the heat balance equation:

$$\rho c \frac{\partial T_i}{\partial t} = \sum_{\lambda} [Q_{A\lambda}(i) + Q_{E\lambda}(i)] + k \frac{\partial^2 T_i}{\partial x^2}$$

where the radiation absorbed and emitted by the element at position  $x$  within the glaze is represented by  $Q_{A\lambda}(i)$  and  $Q_{E\lambda}(i)$ , respectively. As a result of the spectral dependence of the glaze properties that govern internal radiation,  $Q_{A\lambda}$  and  $Q_{E\lambda}$  are computed for and summed over a finite number of wavelength bands within the spectral region for which the glazes are considered to be transparent and/or semitransparent. Term  $Q_{A\lambda}(i)$  is further complicated in that it represents the absorption of radiant energy emitted from each element and surface coating of each glaze in the window system as well as that from the surroundings. Partial reflection at the glaze surfaces results in multiple reflections of radiation beams between and within the glazes of the window system (Figure 2 and A-1).

## PREVIOUSLY DEVELOPED ANALYTICAL RELATIONSHIPS

The theory employed in the thermal analysis is that developed by Gardon (References 3, 4, and 5) and as used by Lis, Barile, and Engholm (Reference 1) in developing a computer program for predicting temperatures of a single glaze window. Using the theory and analytical terms developed in References 1 through 5, the above single glaze program analysis was extensively modified and expanded to include the thermal analysis of multiple glaze windows. This theory has as its basis the Bouger-Lambert law and a volumetric emissive power derived by Gardon. The analytical terms developed by Gardon and Lis referred to in this discussion are:

1. The percent of radiant intensity of a beam entering a glaze that is absorbed by a given element within the glaze, when considering both the primary beams and its multiple reflections;

2. The percent of radiant intensity of a beam emitted by one element of a given glaze that is absorbed by another element within the same glaze, when considering both the primary beam and its multiple reflections; and

3. The percent of radiant intensity of a beam traveling within a glaze that is transmitted by a surface of the glaze, when considering both the primary beam and its multiple reflections.

### Absorption of Radiation Entering a Glaze

A beam of radiation striking a glaze surface is partially reflected and partially transmitted. As the beam enters the glaze, its angle of travel is altered according to Snell's law:

$$n_2 \sin \alpha_2 = n_1 \sin \alpha_1$$

which relates the angle of refraction,  $\alpha_2$ , to the angle of incidence,  $\alpha_1$ , the glaze index of refraction,  $n_2$ , and the index of refraction,  $n_1$ , of the incident medium. As the beam travels through the glaze, its intensity attenuation is described by the Bouger-Lambert law:

$$I_x = I_0 e^{-\gamma x \sec \alpha}$$



# Contrails

which relates the attenuation of radiation intensity to an absorption coefficient,  $\gamma$ , and to the distance,  $x \sec \alpha$ , traveled by the beam. The amount of the radiant intensity absorbed by an element at location  $x$  is equated to the attenuation of the beam as it passes through the element:

$$\Delta I_x = I_x - I_x e^{-\gamma \Delta x \sec \alpha} = I_x (1 - e^{-\gamma \Delta x \sec \alpha})$$

When the beam reaches the second glaze surface it is partially transmitted through the surface and partially reflected back into the glaze. This internally reflected radiation is treated as multiple reflections of energy which is partially reflected each time it reaches the surfaces and is partially absorbed each time it traverses the glaze. Thus, an elemental slice in the glaze absorbs energy from the multiple reflections of a beam as well as directly from a beam entering the glaze. The percent of radiant intensity absorbed from this beam and its multiple reflections is defined by the analytical expression:

$$\begin{aligned} X_{TN} = & \left( \frac{1 - e^{-\gamma s \Delta x \sec \alpha + a}}{s \Delta x} \right) \\ & \times \left\{ e^{-\gamma x \sec \alpha} + \frac{e^{-2\gamma L \sec \alpha}}{1 + \frac{\tau_{T||}}{\tau_{T\perp}}} \left[ \frac{\rho_{B\perp}}{1 - \rho_{T\perp} \rho_{B\perp} e^{-2\gamma L \sec \alpha}} \right] \right. \\ & \times \left( \rho_{T\perp} e^{-\gamma x \sec \alpha} + e^{+\gamma x \sec \alpha} \right) + \frac{\tau_{T||}}{\tau_{T\perp}} \frac{\rho_{B||}}{1 - \rho_{T||} \rho_{B||} e^{-2\gamma L \sec \alpha}} \\ & \left. \times \left( \rho_{T||} e^{-\gamma x \sec \alpha} + e^{+\gamma x \sec \alpha} \right) \right\} \end{aligned}$$

This expression is for beams entering the upper surface of the glaze. The value for  $s$  is  $\frac{1}{2}$  and the coating absorptance  $a$  is  $1 - \rho - \tau$  when the glaze finite element under consideration is a surface element, i.e., elements 1 and 11. For glaze elements 2 through 10,  $s$  is 1 and  $a$  is set to zero. When beams are entering the lower surface of the glaze, the percent of intensity absorbed by a given element at location  $x$  is defined by:

# Contrails

$$X_{BN} = \left( \frac{1 - e^{-\gamma s \sec \alpha + a}}{s \Delta x} \right)$$

$$\times \left\{ e^{-\gamma(L-x)\sec \alpha} + \frac{e^{-2\gamma L \sec \alpha}}{1 + \frac{\tau_{B||}}{\tau_{B\perp}}} \left[ \frac{\rho_{T\perp}}{1 - \rho_{T\perp} \rho_{B\perp} e^{-2\gamma L \sec \alpha}} \right] \right.$$

$$\times \left( \rho_{B\perp} e^{-\gamma(L-x)\sec \alpha} + e^{+\gamma(L-x)\sec \alpha} \right) + \frac{\tau_{B||}}{\tau_{B\perp}} \frac{\rho_{T||}}{1 - \rho_{T||} \rho_{B||} e^{-2\gamma L \sec \alpha}}$$

$$\times \left. \left( \rho_{B||} e^{-\gamma(L-x)\sec \alpha} + e^{+\gamma(L-x)\sec \alpha} \right) \right\}$$

In the development of these expressions it was assumed that the radiation is polarized parallel and perpendicularly to the plane of incidence. Both the parallel and perpendicular components are accounted for in the above analytical terms.

## Absorption of Radiation Emitted Within a Glaze

The percent of radiant intensity, of the beams emitted by one element of a given glaze, that is absorbed by another element within the same glaze is defined as:

$$\hat{P} = \left( \frac{1 - e^{-\gamma s \Delta x \sec \alpha + a}}{s \Delta x} \right)$$

$$\times \left[ e^{-\gamma|x-y|\sec \alpha} + (P_1 e^{-\gamma x \sec \alpha} + P_{12} e^{-\gamma(2L-x)\sec \alpha}) e^{-\gamma y \sec \alpha} \right. \\ \left. + (P_2 e^{-\gamma(L-x)\sec \alpha} + P_{12} e^{-\gamma(L+x)\sec \alpha}) e^{-\gamma(L-y)\sec \alpha} \right]$$

where

# Contrails

$$P_1 = \frac{1}{2} \left[ \frac{\rho_{T\perp}}{1 - \rho_{T\perp} \rho_{B\perp} e^{-2\gamma L \sec \alpha}} + \frac{\rho_{T\parallel}}{1 - \rho_{T\parallel} \rho_{B\parallel} e^{-2\gamma L \sec \alpha}} \right]$$

$$P_2 = \frac{1}{2} \left[ \frac{\rho_{B\perp}}{1 - \rho_{T\perp} \rho_{B\perp} e^{-2\gamma L \sec \alpha}} + \frac{\rho_{B\parallel}}{1 - \rho_{T\parallel} \rho_{B\parallel} e^{-2\gamma L \sec \alpha}} \right]$$

and

$$P_{12} = \frac{1}{2} \left[ \frac{\rho_{T\perp} \rho_{B\perp}}{1 - \rho_{T\perp} \rho_{B\perp} e^{-2\gamma L \sec \alpha}} + \frac{\rho_{T\parallel} \rho_{B\parallel}}{1 - \rho_{T\parallel} \rho_{B\parallel} e^{-2\gamma L \sec \alpha}} \right]$$

The percent of radiant intensity, of a beam emitted by a thin-film coating, that is absorbed by a given element within the same glaze is computed as:

$$\hat{P}_1 = \left( \frac{1 - e^{-\gamma s \Delta x \sec \alpha + a}}{s \Delta x} \right)$$

$$\times \left[ e^{-\gamma x \sec \alpha} + (P_2 e^{-\gamma(L-x) \sec \alpha} + P_{12} e^{-\gamma(L+x) \sec \alpha}) e^{-\gamma L \sec \alpha} \right]$$

when the emitting coating is on the upper surface of the glaze. If the coating is on the lower surface the percent of intensity absorbed by the given element is:

$$\hat{P}_2 = \left( \frac{1 - e^{-\gamma s \Delta x \sec \alpha + a}}{s \Delta x} \right)$$

$$\times \left[ e^{-\gamma(L-x) \sec \alpha} + (P_1 e^{-\gamma x \sec \alpha} + P_{12} e^{-\gamma(2L-x) \sec \alpha}) e^{-\gamma L \sec \alpha} \right]$$

## Transmission of Radiation at Glaze Surface

The percent of radiant intensity of a beam and its multiple reflections that is transmitted by a given glaze surface is described by the following terms depending on the direction of travel of the primary beam and the particular surface being considered. For example, the percent of the radiant intensity, of a beam striking the upper glaze surface, that is transmitted at the bottom glaze surface is expressed as:

$$v_{\uparrow B} = \frac{1}{2} \left[ \frac{\tau_{B\perp} \rho_{T\perp} e^{-\gamma L \sec \alpha}}{1 - \rho_{T\perp} \rho_{B\perp} e^{-2\gamma L \sec \alpha}} + \frac{\tau_{B\parallel} \rho_{T\parallel} e^{-\gamma L \sec \alpha}}{1 - \rho_{T\parallel} \rho_{B\parallel} e^{-2\gamma L \sec \alpha}} \right]$$

For beams striking the lower surface, the percent transmitted at the bottom surface is defined by the relationship:

$$v_{\downarrow B} = \frac{1}{2} \left[ \frac{\tau_{B\perp}}{1 - \rho_{T\perp} \rho_{B\perp} e^{-2\gamma L \sec \alpha}} + \frac{\tau_{B\parallel}}{1 - \rho_{T\parallel} \rho_{B\parallel} e^{-2\gamma L \sec \alpha}} \right]$$

The percent of intensity transmitted at the top glaze surface of a beam striking the upper surface and of a beam striking the lower surface is expressed as:

$$v_{\uparrow T} = \frac{1}{2} \left[ \frac{\tau_{T\perp}}{1 - \rho_{T\perp} \rho_{B\perp} e^{-2\gamma L \sec \alpha}} + \frac{\tau_{T\parallel}}{1 - \rho_{T\parallel} \rho_{B\parallel} e^{-2\gamma L \sec \alpha}} \right]$$

and

$$v_{\downarrow T} = \frac{1}{2} \left[ \frac{\tau_{T\perp} \rho_{B\perp} e^{-\gamma L \sec \alpha}}{1 - \rho_{T\perp} \rho_{B\perp} e^{-2\gamma L \sec \alpha}} + \frac{\tau_{T\parallel} \rho_{B\parallel} e^{-\gamma L \sec \alpha}}{1 - \rho_{T\parallel} \rho_{B\parallel} e^{-2\gamma L \sec \alpha}} \right]$$

# Contrails

## MULTIPLE GLAZE ANALYSIS

In order to demonstrate how the above analytical relationships for  $\chi$ ,  $\nu$ ,  $\hat{P}$ ,  $\hat{P}_1$ , and  $\hat{P}_2$  are utilized in the analysis, the following example is employed. For this example, the window system depicted in Figure A-1 is considered. The energy absorbed by an element in the third glaze will be determined considering the source of radiation to be an element in the first glaze.

Radiation beams of an intensity  $I_0$  are emitted at an angle  $\alpha_1$  by the element in glaze 1 of Figure A-1. The intensity of the beam striking the upper surface of glaze 1 is:

$$I_1 = I_0 e^{-\gamma y \sec \alpha_1}$$

and the intensity of this beam and its multiple reflections that are transmitted through the bottom of medium 1 is  $I_1 \nu_{\uparrow B_1}$ . Intensity,  $I_2$ , of a beam striking the lower surface of medium 1 is:

$$I_2 = I_0 e^{-\gamma(L-y)\sec \alpha}$$

and the intensity of this beam and its multiple reflections that are transmitted through the bottom of medium 1 is  $I_2 \nu_{\downarrow B_1}$ . As the beams enter medium 2, their angle of travel is altered according to Snell's law:

$$n_1 \sin \alpha_1 = n_2 \sin \alpha_2$$

which relates the angle of refraction,  $\alpha_2$ , to the angle of incidence,  $\alpha_1$ , and to the indices of refraction,  $n_1$  and  $n_2$ . Intensity,  $I_3$ , of the radiation entering medium 2 is then defined as:

$$I_3 = \left[ I_1 \nu_{\uparrow B_1} + I_2 \nu_{\downarrow B_1} \right] \frac{n_2^2 \cos \alpha_2}{n_1^2 \cos \alpha_1}$$

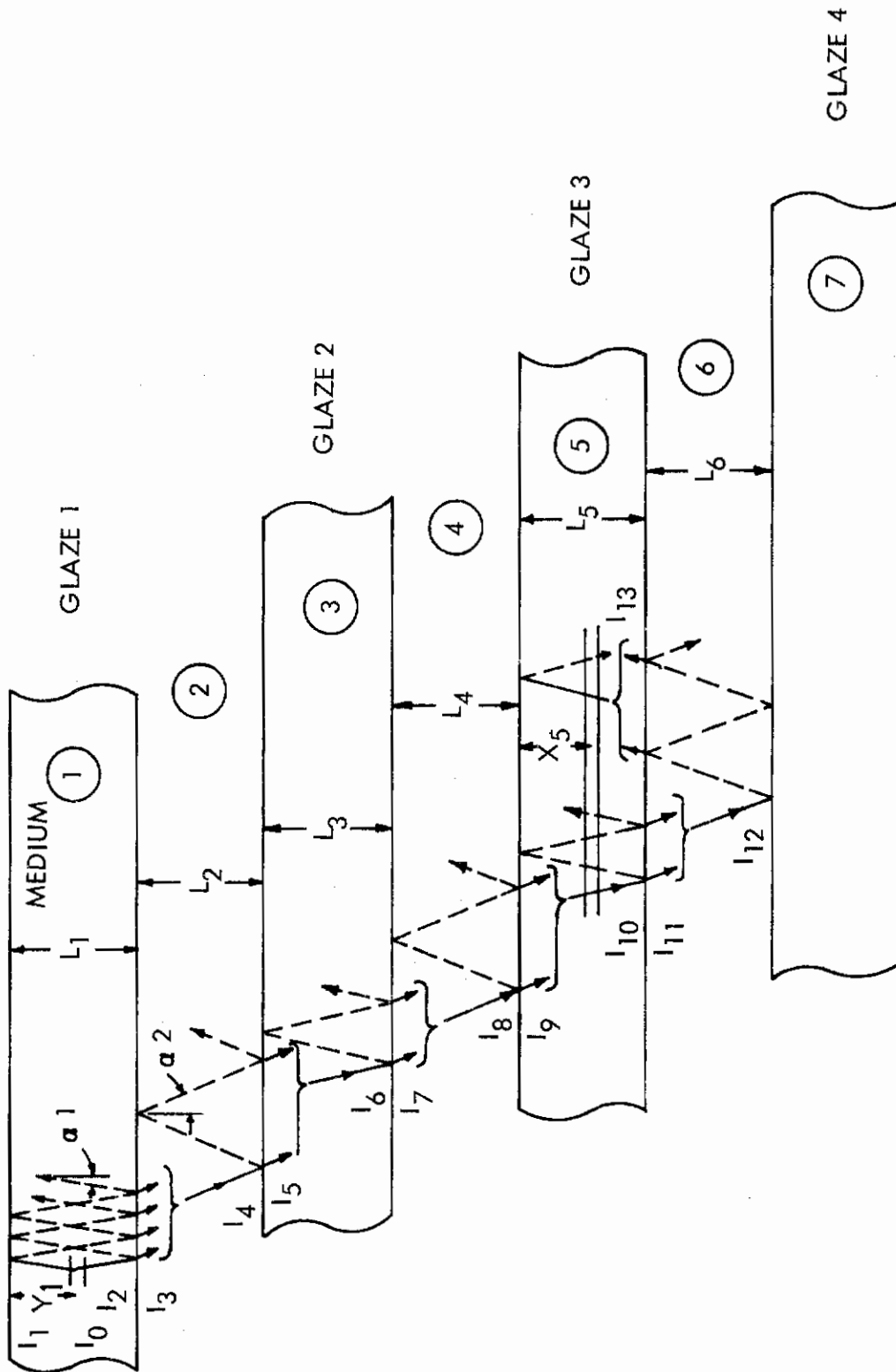


Figure A-1 - Multiple-Glaze Window System



# Contrails

If medium 2 is semitransparent, the beams of intensity,  $I_3$ , are attenuated in travel and reach the lower surface of medium 2 with an intensity of

$$I_4 = I_3 e^{-\gamma_2 L_2 \sec \alpha_2}$$

The portion of  $I_4$  that is transmitted into medium 3 (the second glaze) is expressed as:

$$I_5 = (I_4 \downarrow B_2) \frac{n_3^2 \cos \alpha_3}{n_2^2 \cos \alpha_2}$$

Continuing with the transmission of intensity at the media interfaces and the attenuation of intensity between the interfaces, the following relationships are established:

$$I_6 = I_5 e^{-\gamma_3 L_3 \sec \alpha_3}$$

$$I_7 = (I_6 \downarrow B_3) \frac{n_4^2 \cos \alpha_4}{n_3^2 \cos \alpha_3}$$

$$I_8 = I_7 e^{-\gamma_4 L_4 \sec \alpha_4}$$

$$I_9 = (I_8 \downarrow B_4) \frac{n_5^2 \cos \alpha_5}{n_4^2 \cos \alpha_4}$$

The energy absorbed by the element in glaze 3 (medium 5) from the beam of intensity,  $I_9$ , entering the glaze's upper surface is expressed as  $I_9 \chi_{T5}$ . In addition, the energy which passes through glaze 3 and is reflected back from the upper surface of glaze 4 is also considered. This energy may be significant if the lower surface of glaze 3 exhibits a high transmittance and the upper surface of glaze 4 is highly reflective to infrared radiation. Following the beam through medium 5,

# Contrails

$$I_{10} = I_9 e^{-\gamma_5 L_5 \sec \alpha_5}$$

$$I_{11} = (I_{10} \nu_{\downarrow B_5}) \frac{n_6^2 \cos \alpha_6}{n_5^2 \cos \alpha_5}$$

$$I_{12} = I_{11} e^{-\gamma_6 L_6 \sec \alpha_6}$$

$$I_{13} = (I_{12} \nu_{\downarrow T}) \frac{n_5^2 \cos \alpha_5}{n_6^2 \cos \alpha_6}$$

The energy absorbed by the element in glaze 3 from the beam entering the glaze's lower surface is expressed as  $I_{13} \chi_{B_5}$ . Adding this to the energy absorbed from the beams entering the upper surface of glaze 3 gives:

$$\Delta I_{\lambda\alpha} = I_9 \chi_{T_5} + I_{13} \chi_{B_5}$$

This, then, represents the increment of the beam intensity emitted by the element in glaze 1 that is absorbed by the element in glaze 5. Using the above relationships to define  $I_1$  through  $I_{13}$ , the equation for  $\Delta I$  in terms of  $I_0$  is derived as follows:

$$I_3 = I_0 (e^{-\gamma_1 (L_1 - y_1) \sec \alpha_1} \nu_{\downarrow B_1} + e^{-\gamma_1 y_1 \sec \alpha_1} \nu_{\uparrow B_1}) \frac{n_2^2 \cos \alpha_2}{n_1^2 \cos \alpha_1}$$

$$I_9 = I_3 e^{-\gamma_2 L_2 \sec \alpha_2} \nu_{\downarrow B_2} \frac{n_3^2 \cos \alpha_3}{n_2^2 \cos \alpha_2}$$

$$\times e^{-\gamma_3 L_3 \sec \alpha_3} \nu_{\downarrow B_3} \frac{n_4^2 \cos \alpha_4}{n_3^2 \cos \alpha_3} e^{-\gamma_4 L_4 \sec \alpha_4} \nu_{\downarrow B_4} \frac{n_5^2 \cos \alpha_5}{n_4^2 \cos \alpha_4}$$

# Contrails

$$I_9 = I_0 \left( e^{-\gamma_1(L_1 - y_1) \sec \alpha_1} \nu_{\downarrow B_1} + e^{-\gamma_1 y_1 \sec \alpha_1} \nu_{\uparrow B_1} \right) \frac{n_5^2 \cos \alpha_5}{n_1^2 \cos \alpha_1}$$

$$\times \prod_{k=2}^4 \left( e^{-\gamma_k L_k \sec \alpha_k} \nu_{\downarrow B_k} \right)$$

$$I_{13} = I_9 e^{-\gamma_5 L_5 \sec \alpha_5} \nu_{\downarrow B_5} \frac{n_6^2 \cos \alpha_6}{n_5^2 \cos \alpha_5} e^{-\gamma_6 L_6 \sec \alpha_6} \nu_{\downarrow T_6} \frac{n_5^2 \cos \alpha_5}{n_6^2 \cos \alpha_6}$$

$$= I_0 \left( e^{-\gamma_1(L_1 - y_1) \sec \alpha_1} \nu_{\downarrow B_1} + e^{-\gamma_1 y_1 \sec \alpha_1} \nu_{\uparrow B_1} \right) \frac{n_5^2 \cos \alpha_5}{n_1^2 \cos \alpha_1}$$

$$\times \prod_{k=2}^4 \left( e^{-\gamma_k L_k \sec \alpha_k} \nu_{\downarrow B_k} \right) e^{-\gamma_5 L_5 \sec \alpha_5} \nu_{\downarrow B_5} e^{-\gamma_6 L_6 \sec \alpha_6} \nu_{\downarrow T_6}$$

Substituting the above expressions for  $I_9$  and  $I_{13}$  into the equation for  $\Delta I$  and factoring out common terms gives

$$\Delta I_{\lambda\alpha} = I_0 \left\{ \left( e^{-\gamma_1(L_1 - y_1) \sec \alpha_1} \nu_{\downarrow B_1} + e^{-\gamma_1 y_1 \sec \alpha_1} \nu_{\uparrow B_1} \right) \frac{n_5^2 \cos \alpha_5}{n_1^2 \cos \alpha_1} \right.$$

$$\left. \times \prod_{k=2}^4 \left( e^{-\gamma_k L_k \sec \alpha_k} \nu_{\downarrow B_k} \right) \left[ \chi_{T_5} + e^{-\gamma_5 L_5 \sec \alpha_5} \nu_{\downarrow B_5} e^{-\gamma_6 L_6 \sec \alpha_6} \nu_{\downarrow T_6} \chi_{B_5} \right] \right\}$$

or

$$\Delta I_{\lambda\alpha} = I_0 \xi$$

where the symbol,  $\xi$ , represents the expression in the brackets,  $\{ \}$ .

# Contrails

Since the radiation from the emitting element is considered perfectly diffuse, the total radiant energy gained by the absorbing element is obtained by integrating the contribution of the incoming beams over a hemispherical surface above the absorbing element.

$$\begin{aligned} Q_{R\lambda} &= \int_0^{2\pi} \int_0^{\alpha_{c5}} I_0 \xi \sin \alpha_5 \, d\alpha_5 \, d\theta \\ &= 2\pi \int_0^{\alpha_{c5}} I_0 \xi \sin \alpha_5 \, d\alpha_5 \end{aligned}$$

Also, since the absorption coefficients of the media are wavelength dependent,  $\Delta I_\lambda$  is computed for and summed over finite wavelength bands within the spectral region for which the glazes are considered to be semi-transparent.

$$Q_R = 2\pi \sum_\lambda \int_0^{\alpha_{c5}} I_0 \xi \sin \alpha_5 \, d\alpha_5$$

The integration limit,  $\alpha_{c5}$ , represents the critical angle beyond which no energy is refracted into glaze 5.

This critical angle is computed as:

$$\alpha_{c5} = \sin^{-1} \left( \frac{n_4}{n_5} \right)$$

Using the approach described in this example, relationships were developed defining the radiant energy absorbed by a given finite element when considering the radiation from a source external to the window system, from each of the remaining elements in the window system, and from any emitting glaze coatings in the window system. These relationships are presented in the following sections.

## RADIATION ABSORBED BY A FINITE GLAZE ELEMENT

The total radiant energy, within a given spectral band to which the window is considered semitransparent, that is absorbed by a given element is represented as  $Q_{A\lambda}(i)$  in the element's heat balance equation. Sources of radiant energy include each element in each glaze, the thin-film coatings on the surfaces of the glazes, and an external radiating medium or heater. Considering these sources, the energy absorbed by a given element,  $i$ , is computed as:

$$Q_{A\lambda}(i) = Q_{R\lambda}(i) + Q_{F\lambda}(i) + Q_{H\lambda}(i)$$

The equations for  $Q_{R\lambda}(i)$ ,  $Q_{F\lambda}(i)$ , and  $Q_{H\lambda}(i)$  are presented in the following subsections.

### Glaze Elements as Radiation Sources

The radiant intensity emitted by a glaze element is defined by Gardon's volumetric emissive power as:

$$j_{\lambda} = \gamma_{\lambda} n^2 W_{B\lambda} / \pi$$

which relates the intensity emitted per unit volume to the glaze absorption coefficient, the glaze index of refraction, and the hemispherical emissive power of a blackbody radiator,  $W_{B\lambda}$ . Hemispherical emissive power is computed as:

$$W_{B\lambda} = P_{\lambda} \sigma T_j^4$$

where  $T_j$  is the temperature of the emitting element and  $P_{\lambda}$  is the percent of energy emitted within a finite wavelength band.

The energy absorbed by an element as emitted from the other elements in the window system is computed from the equation

# Contrails

$$Q_{RA}(i) = \sum_{j=1}^{11(G+1)/2} 2\pi(\gamma_{\lambda j} n_j^2 W_{B\lambda} / \pi) \phi_{\lambda ij} \Delta y$$

or

$$Q_{RA}(i) = 2 \sum_{j=1}^{11 \times G} \gamma_{\lambda j} n_j^2 W_{B\lambda} \phi_{\lambda ij} \Delta y$$

where  $i$  refers to the absorbing element,  $j$  refers to the emitting elements, and  $G$  is the number of media in the window system. The auxiliary function  $\phi_{\lambda ij}$  defines the percent of energy emitted by the beams of an emitting element,  $j$ , that is absorbed by the absorbing element,  $i$ . This auxiliary function is computed from one of three equations depending on the relative positions of elements  $i$  and  $j$ .

1. When the emitting element is in a glaze which is located above the glaze containing the absorbing element,

$$\begin{aligned} \phi_{\lambda ij} = & \int_0^{\alpha_c} \left\{ (e^{-\gamma(L-y)\sec\alpha} v_{\downarrow B} + e^{-\gamma y \sec\alpha} v_{\uparrow B})_M \right. \\ & \times \prod_{k=M+1}^{N-1} (e^{-\gamma L \sec\alpha} v_{\downarrow B})_k \left[ \chi_{TN} + (e^{-\gamma L \sec\alpha} v_{\downarrow B})_N \right. \\ & \left. \left. \times (e^{-\gamma L \sec\alpha} v_{\downarrow T})_{N+1} \chi_{BN} \right] \frac{n_N^2 \cos\alpha_N}{n_M^2 \cos\alpha_M} \sin\alpha_N \right\} d\alpha_N \end{aligned}$$

where the subscript,  $M$ , refers to the medium containing the emitting element,  $j$ , and the subscript,  $N$ , refers to the medium containing the absorbing element,  $i$ . The window glazes are represented by media 1, 3, 5, etc. (Figure A-1) with 11 elements in each glaze. Thus, the number,  $i$ , of the absorbing element ranges from:

$$i = 1 \quad \text{to} \quad i = 11(G+1)/2$$



# Contrails

Similarly the number,  $j$ , of the emitting element ranges from:

$$j = 1 \text{ to } j = 11(G+1)/2$$

2. When the glaze containing the emitting element is below the glaze containing the absorbing element, i.e., when  $M > N$

$$\begin{aligned} \phi_{\lambda ij} = & \int_0^{\alpha_c} \left\{ (e^{-\gamma y \sec \alpha} v_{\uparrow T} + e^{-\gamma(L-y) \sec \alpha} v_{\downarrow T})_M \right. \\ & \times \prod_{k=N+1}^{M-1} (e^{-\gamma L \sec \alpha} v_{\uparrow T})_k \left[ \chi_{BN} + (e^{-\gamma L \sec \alpha} v_{\uparrow T})_N \right. \\ & \left. \left. \times (e^{-\gamma L \sec \alpha} v_{\uparrow B})_{N-1} \chi_{TN} \right] \frac{n_N^2 \cos \alpha_N}{n_M^2 \cos \alpha_M} \sin \alpha_N \right\} d\alpha_N \end{aligned}$$

3. When the emitting and absorbing elements are within the same glaze, i.e., when  $M = N$

$$\begin{aligned} \phi_{\lambda ij} = & \int_0^{\alpha_{cr}} \left\{ \left[ (e^{-\gamma(L-y) \sec \alpha} v_{\downarrow B} + e^{-\gamma y \sec \alpha} v_{\uparrow B})_N (e^{-\gamma L \sec \alpha} v_{\downarrow T})_{N+1} \chi_{BN} \right. \right. \\ & + (e^{-\gamma(L-y) \sec \alpha} v_{\downarrow T} + e^{-\gamma y \sec \alpha} v_{\uparrow T})_N (e^{-\gamma L \sec \alpha} v_{\uparrow B})_{N-1} \chi_{TN} \\ & \left. \left. + \hat{P}_N \right] \sin \alpha_N \right\} d\alpha_N + \int_{\alpha_{cr}}^{\pi/2} \hat{P}_N \sin \alpha_N d\alpha_N \end{aligned}$$

## Glaze Coatings as Radiation Sources

The intensity of radiation beams from an emitting glaze thin-film coating is computed as:

# Contrails

$$I_{f\lambda} = \epsilon_f \frac{W_{B\lambda}}{\pi} \cos \alpha$$

where

$$W_{B\lambda} = P_\lambda \sigma T_f^4$$

The energy absorbed by an element as emitted from the thin-film coatings in the window system is computed as:

$$Q_{F\lambda}(i) = \sum_{f=1}^z 2\pi (W_{B\lambda}/\pi) \phi_{\lambda if}$$

where  $i$  refers to the absorbing element,  $f$  refers to the emitting thin-film coatings, and  $z$  is the number of emitting coatings in the window system. The equation employed in computing the auxiliary function,  $\phi_{\lambda if}$ , depends on the relative location of element  $i$  and coating  $f$ :

1. When  $M < N$  and the coating is on the lower surface of glaze  $M$ ,

$$\phi_{\lambda if} = \int_0^{\alpha_c} \left\{ \epsilon_f \prod_{k=M+1}^{N-1} (e^{-\gamma L \sec \alpha} \nu_{\downarrow B})_k \left[ X_{TN} + (e^{-\gamma L \sec \alpha} \nu_{\downarrow B})_N \right. \right. \\ \left. \left. \times (e^{-\gamma L \sec \alpha} \nu_{\downarrow T})_{N+1} X_{BN} \right] n_N^2 \cos \alpha_N \sin \alpha_N \right\} d\alpha_N$$

If the coating is on the upper surface of glaze  $M$ , the above integrand is multiplied by:

$$(e^{-\gamma L \sec \alpha} \nu_{\downarrow B})_M$$

# Contrails

2. When  $M > N$  and the coating is on the upper surface of glaze  $M$ ,

$$\phi_{\lambda if} = \int_0^{\alpha_c} \left\{ \epsilon_f \prod_{k=N+1}^{M-1} (e^{-\gamma L \sec \alpha \nu_{\uparrow T}})_k \left[ \chi_{BN} + (e^{-\gamma L \sec \alpha \nu_{\uparrow T}})_N \right. \right. \\ \left. \left. \times (e^{-\gamma L \sec \alpha \nu_{\uparrow B}})_{N-1} \chi_{TN} \right] n_N^2 \cos \alpha_N \sin \alpha_N \right\} d\alpha_N$$

If the coating is on the lower surface of glaze  $M$ , the above integrand is multiplied by:

$$(e^{-\gamma L \sec \alpha \nu_{\uparrow T}})_M$$

3. When  $M = N$  and the coating is on the upper surface of the glaze,

$$\phi_{\lambda if} = \int_0^{\pi/2} \left\{ \epsilon_f \left[ (e^{-\gamma L \sec \alpha \nu_{\uparrow B}})_{N-1} \chi_{TN} + \hat{P}_1 \right] \sin \alpha_N \right\} d\alpha_N$$

If the coating is on the lower surface of the glaze,

$$\phi_{\lambda if} = \int_0^{\pi/2} \left\{ \epsilon_f \left[ (e^{-\gamma L \sec \alpha \nu_{\downarrow T}})_{N+1} \chi_{BN} + \hat{P}_2 \right] \sin \alpha_N \right\} d\alpha_N$$

## Radiation Source External to Window

The intensity of radiation beams from an emitting source outside the window system is computed as:

$$I_{h\lambda} = \epsilon_h \frac{W_{B\lambda}}{\pi} \cos \alpha$$

where

$$W_{B\lambda} = P_{\lambda} \sigma T_h^4$$

Energy emitted by the external source that is absorbed by a given finite element in the window system is computed as:

$$Q_H(i) = 2\pi \left( \frac{W_{B\lambda}}{\pi} \right) \phi_{\lambda ih}$$

where  $i$  refers to the absorbing element and  $h$  refers to the external source. The auxiliary function,  $\phi_{\lambda ih}$  is calculated as follows:

$$\phi_{\lambda ih} = \int_0^{\alpha_c} \left\{ \epsilon_h \tau_{TL} \prod_{k=1}^{N-1} (e^{-\gamma L \sec \alpha} v_{\downarrow B})_k \left[ x_{TN} + (e^{-\gamma L \sec \alpha} v_{\downarrow B})_N \right. \right. \\ \left. \left. \times (e^{-\gamma L \sec \alpha} v_{\downarrow T})_{N+1} x_{BN} \right] n_N^2 \cos \alpha_N \sin \alpha_N \right\} d\alpha_N$$

## RADIATION EMITTED BY A FINITE GLAZE ELEMENT

As indicated by the heat balance equations, the thermal response of a finite glaze element,  $i$ , is partially dependent on the radiation,  $Q_{E\lambda}(i)$ , emitted by the element. Radiation intensity emitted per unit volume is defined by a volumetric emissive power derived by Gardon as:

$$j_{\lambda} = \gamma_{\lambda} n^2 W_{B\lambda} / \pi$$

which relates the intensity,  $j$ , to the glaze absorption coefficient,  $\gamma$ , the glaze index of refraction,  $n$ , and the hemispherical emissive power,  $W_{B\lambda}$ , of a blackbody radiator. The hemispherical emissive power is computed as:

# Contrails

$$W_{B\lambda} = P_{\lambda} \sigma T_i^4$$

where  $P_{\lambda}$  is the percent of energy emitted within a finite wavelength band of the spectral region in which the glaze is considered to be semitransparent.

When considering radiation emitted from the elements,  $j$ , in computing  $Q_{A\lambda}(i)$ , it was assumed that the radiation was emitted from the midpoint (nodal point) of the elements. Thus, some of the energy is attenuated (or absorbed) as it travels from the midpoint to the edge of the emitting element. As a result of this attenuation, the intensity of radiation leaving the edge of the element was defined as:

$$I = I_0 e^{-\gamma_{\lambda} \Delta x / 2 \sec \alpha}$$

In order not to violate the second law of thermodynamics, the same consideration is given to the intensity leaving an element when computing  $Q_{E\lambda}(i)$ .

The intensity leaving element,  $i$ , is defined as:

$$I_{\lambda} = j_{\lambda} e^{-\gamma_{\lambda} \Delta x / 2 \sec \alpha}$$

where  $j_{\lambda}$  is the volumetric emissive power lumped at the elements nodal point. To obtain the heat radiated from the element, the intensity,  $I_{\lambda}$ , is integrated over the surrounding spherical area as follows:

$$Q_{E\lambda}(i) = 2 \int_0^{2\pi} \int_0^{\pi/2} j_{\lambda} e^{-\gamma_{\lambda} \Delta x / 2 \sec \alpha} d\alpha d\theta$$

Substituting the analytical definition for volumetric emissive power,  $j_{\lambda}$ , into the above integrand and performing the integration over  $\theta$  gives:

$$Q_{E\lambda}(i) = 4\gamma_{\lambda} n^2 W_{B\lambda} \int_0^{\pi/2} e^{-\gamma_{\lambda} \Delta x / 2 \sec \alpha} d\alpha$$

## HEAT FLUX TO THE CABIN

The heat flux to the cabin is a result of radiation from and through the window glazes and of convection from the innermost window surface. This cabin flux is expressed analytically as:

$$q_c = h(T_s - T_c) + \left[ (1 - \rho_L)P_L + (1 - \rho_R)(1 - P_R) \right] \sigma T_s^4 - \sigma T_c^4 + \sum_{\lambda} q_{\lambda}(c)$$

Convection heat transfer from the window is computed from the term in which the difference between the window's lower surface temperature,  $T_s$ , and the cabin temperature,  $T_c$ , is multiplied by the heat transfer coefficient,  $h$ . The heat transfer coefficient is assumed to be that resulting from free convection.

The net heat transfer from the window surface to the cabin by radiation, to which the glazes are considered to be opaque, is computed by the terms:

$$\left[ (1 - \rho_L)P_L + (1 - \rho_R)(1 - P_R) \right] \sigma T_s^4 - \sigma T_c^4$$

The symbols  $P_L$  and  $P_R$  represent the percent of energy emitted at wavelengths from zero to the left cutoff point and from zero to the right cutoff point, respectively, of the spectral region in which the glaze is considered to be semitransparent. For example, fused silica is considered to be semitransparent over the wavelength region from  $\lambda = 0.4 \mu$  to  $\lambda = 4.8 \mu$ . Thus, the left and right cutoff points for fused silica are at 0.4 and 4.8  $\mu$ , respectively. Symbols  $\rho_L$  and  $\rho_R$  are the mean hemispherical reflectivities of the glaze to radiation in the spectral regions to the left and to the right of the semitransparent region.

Radiative flux through the window is represented by the term,  $q_{\lambda}(c)$ . This flux is computed for and summed over finite wavelength bands of the spectral region in which the glaze is considered to be semitransparent. Contribution of radiative flux to the cabin that is represented by  $q_{\lambda}(c)$  includes:



1. Radiation from each finite element in each window glaze;
2. Radiation from coatings on the glaze surfaces; and
3. Radiation from an external medium or heater.

Considering the above sources of radiation, the flux through the window is expressed as:

$$q_{\lambda}(c) = q_{R\lambda}(c) + q_{F\lambda}(c) + q_{H\lambda}(c)$$

The terms on the right side of the equal sign are analytically defined in the following subsections.

### Radiation from Glaze Elements to the Cabin

The radiative flux emitted by the finite elements,  $j$ , of the window glazes that travel through the window and into the cabin is computed as:

$$q_{R\lambda}(c) = \sum_{j=1}^{l(G+1)/2} 2\gamma_{\lambda j} n_j^2 W_{B\lambda j} \phi_{\lambda j c} \Delta y$$

where

$$W_{B\lambda j} = P_{\lambda} \sigma T_j^4$$

The auxiliary function,  $\phi_{\lambda j c}$ , is computed from the equation:

$$\phi_{\lambda j c} = \int_0^{\alpha_c} \left\{ (e^{-\gamma(L-y)} \sec \alpha \nu_{\downarrow B} + e^{-\gamma y} \sec \alpha \nu_{\uparrow B})_M \right. \\ \left. \times \prod_{k=M+1}^G (e^{-\gamma L} \sec \alpha \nu_{\downarrow B})_k \frac{n_G^2 \cos \alpha_G}{n_M^2 \cos \alpha_M} \sin \alpha_G \right\} d\alpha_G$$

where M refers to the medium number of the glaze containing the emitting element, and G refers to the medium number of the innermost glaze.

## Radiation from Glaze Coatings to the Cabin

Cabin heating, resulting from the radiation emitted by the glaze coatings, is computed from the equation:

$$q_{F\lambda}(c) = \sum_{f=1}^z 2W_{B\lambda f} \phi_{\lambda f c}$$

where

$$W_{B\lambda f} = P_{\lambda} \sigma T_f^4$$

If the emitting coating is on the lower surface of a glaze, the auxiliary function,  $\phi_{\lambda f c}$  is defined as:

$$\phi_{\lambda f c} = \int_0^{\alpha_{cr}} \left\{ \epsilon_f \prod_{k=M+1}^G (e^{-\gamma L \sec \alpha} v_{\downarrow B})_k n_G^2 \cos \alpha_G \sin \alpha_G \right\} d\alpha_G$$

where f refers to the emitting coating and M refers to the medium number of the glaze containing the coating. If the coating is on the upper surface of medium M, the integrand in the above equation is multiplied by:

$$(e^{-\gamma L \sec \alpha} v_{\downarrow B})_M$$

## Radiation from an External Source to the Cabin

The radiation flux emitted by an external source that travels through the glaze and into the cabin is computed from the equation:

# Contrails

$$q_{H\lambda}(c) = 2W_{B\lambda h}\phi_{\lambda hc}$$

where

$$W_{B\lambda h} = P_{\lambda}\sigma T_h^4$$

The auxiliary function,  $\phi_{\lambda hc}$ , is defined as:

$$\phi_{\lambda hc} = \int_0^{\alpha_{cr}} \tau_{T1} \left\{ \prod_{k=1}^G (e^{-\gamma L \sec \alpha} v_{\downarrow B})_k n_G^2 \cos \alpha_G \sin \alpha_G \right\} d\alpha_G$$

where  $\tau_{T1}$  is the transmittance at the upper surface of the outermost glaze.

# *Contrails*

APPENDIX B

EQUATIONS USED TO COMPUTE TRANSMITTANCE AND REFLECTANCE  
OF COATED AND UNCOATED GLAZE SURFACES

# Contrails

## NOMENCLATURE

### Symbols

- $\eta$  - Index of refraction for film layer
- $n$  - Real part of the refractive index
- $i$  - Complex or imaginary part of refractive index
- $k$  - Extinction coefficient of the film layer
- $Y$  - Admittance (ratio of electric and magnetic field intensities)
- $\phi$  - Function defined by Eq. (3)
- $\lambda$  - Vacuum wavelength
- $l$  - True geometric film thickness
- $\rho$  - Reflectance
- $a$  - Real part of admittance  $Y$
- $b$  - Imaginary part of admittance  $Y$
- $\tau$  - Transmittance
- $\psi$  - Function defined by Eq. (6a)
- $\theta_0$  - Angle of incidence in incidence medium
- $\theta_j$  - Angle of refraction in successive layers defined by Eq. (8)

### Subscripts

- $j$  - Refers to film layer under consideration
- $0$  - Refers to medium of incidence ( $j=0$ )
- $p$  - Refers to the innermost film layer ( $j=p$ )
- $p+1$  - Refers to medium of emergence
- $\parallel$  - Parallel component of polarized radiation
- $\perp$  - Perpendicular component of polarized radiation



## INTRODUCTION

The heat balance equation for the internal as well as the edge finite elements of each glaze contains auxiliary functions (see Appendix A) which include values of surface reflectance, transmittance, and absorptance. These surface optical properties can be calculated by the subject computer program for both coated and uncoated glaze surfaces. If transmittance and reflectance data are available they can be included in the input data rather than be computed by the program.

### COMPUTED UNCOATED GLAZE SURFACE OPTICAL PROPERTIES

When predicting temperatures of uncoated glazes, the reflectivity of the surfaces is computed from Fresnel's equations as follows (Ref. 2):

$$\rho_{\perp} = \left( \frac{n \cos \alpha - \sqrt{1 - n^2 \sin^2 \alpha}}{n \cos \alpha + \sqrt{1 - n^2 \sin^2 \alpha}} \right)^2$$

for radiation polarized perpendicularly to the plane of incidence, and

$$\rho_{\parallel} = \left( \frac{\frac{1}{n} \cos \alpha - \sqrt{1 - n^2 \sin^2 \alpha}}{\frac{1}{n} \cos \alpha + \sqrt{1 - n^2 \sin^2 \alpha}} \right)^2$$

The values of transmittance for uncoated glazes are computed as:

$$\tau_{\perp} = 1 - \rho_{\perp}$$

and

$$\tau_{\parallel} = 1 - \rho_{\parallel}$$

For unpolarized radiation, i.e., for radiation beams prior to the first reflection, the effective transmittance is given by:

$$\tau = \frac{1}{2} (\tau_{\perp} - \tau_{\parallel})$$

## COMPUTED COATED GLAZE SURFACE OPTICAL PROPERTIES

In many instances the windows of aerospace vehicles employ thin-film coatings designed to provide certain desirable optical features. For example, various coatings have been developed to reflect ultraviolet radiation, to reflect infrared radiation, and to reduce glaze surface reflection in the visual region of the spectrum. For coated glazes, the computer program incorporates a subroutine to compute the reflectance and transmittance of glaze surfaces having single or multiple layer, dielectric and/or metallic thin-film coatings. The technique employed in the computation is that developed by Berning (Ref. 5) in which the reflectance is determined as the final step in a recursion process which calculates the admittance of each layer of the thin-film coating beginning with the innermost layer and ending with the incident media. The computation procedure and equations are presented below.

The index of refraction for each film layer is denoted as

$$\eta_j = n_j - ik_j \quad (1)$$

which is complex when the film under consideration is absorptive. For nonabsorptive films the refractive index is equal to  $n_j$ .

The reflectance is obtained by the successive solution of the equation which calculates film admittance,  $Y_j$ :

$$Y_{j-1} = a_{j-1} + ib_{j-1} = \frac{Y_j \cos \Phi_j + i\eta_j \sin \Phi_j}{\cos \Phi_j + i \sin \Phi_j / \eta_j} \quad (2)$$

where

$$\Phi_j = (2\pi/\lambda)\eta_j l_j \quad (3)$$

# Contrails

Equation (2) is solved successively for each thin-film layer of the coating beginning with the innermost film until  $Y_0$  is evaluated. The calculations are started by using a value of admittance for the innermost film layer computed from the formula

$$Y_p = \eta_{p+1} = n_{p+1} - ik_{p+1} \quad (4)$$

The real and imaginary parts ( $a_0$  and  $b_0$ ) of the admittance  $Y_0$  are then evaluated and used in the calculation of the reflectance,  $\rho$ , as follows:

$$\rho = \left[ 1 - \left\{ 4 n_0 a_0 / \left[ (n_0 + a_0)^2 + b_0^2 \right] \right\} \right] \quad (5)$$

The transmittance is calculated from the formula

$$\tau = (1 - \rho) \prod_{j=1}^p \psi_j \quad (6)$$

where

$$\psi_j = a_j / \left[ a_{j-1} \left| \cos \phi_j + i Y_j \sin \phi_j / \eta_j \right|^2 \right] \quad (6a)$$

For a nonabsorbing coating, i.e.,  $\eta_j = n_j$ , the function  $\psi$  is unity and  $\tau = 1 - \rho$ .

The above equations are for radiant energy of normal incidence. For oblique incidence, the same equations are applicable if effective values of  $\eta_j$  and  $\phi_j$  are used. Upon reflection, radiation becomes polarized and is considered as having parallel polarized and perpendicular polarized components. For perpendicular polarization, the effective refractive index for any angle of incidence is given by

$$\eta_{j\perp}^{(\theta_0)} = \eta_j \cos \theta_j \quad (7)$$

where

$$\cos \theta_j = \left[ \frac{(\alpha_j^2 + \beta_j^2)^{1/2} + \alpha_j}{2} \right]^{1/2} - 1 \left[ \frac{(\alpha_j^2 + \beta_j^2)^{1/2} - \alpha_j}{2} \right]^{1/2} \quad (8)$$

and

$$\alpha_j = 1 + \left[ n_o \sin \theta_o / (n_j^2 + k_j^2) \right]^2 (k_j^2 - n_j^2)$$

$$\beta_j = -2 n_j k_j \left[ n_o \sin \theta_o / (n_j^2 + k_j^2) \right]^2 .$$

For parallel polarization the effective index is given by

$$\eta_{j||}^{(\theta_o)} = \eta_j / \cos \theta_j . \quad (9)$$

The effective thickness function is the same for both states of polarization and is given by

$$\Phi_j^{(\theta_o)} = \Phi_j \cos \theta_j . \quad (10)$$

The absorptance of the coating is evaluated as  $1 - \rho - \tau$  .

## INPUT GLAZE SURFACE OPTICAL PROPERTIES

A read-in subroutine was also included in the computer program so that the transmittance and reflectance of a given thin-film coating can be included in the input data rather than be computed by the thin-film subroutine if these data are available. When the transmittance and reflectance data for coated surfaces are input, the absorptance of the coating is computed as  $1 - \tau - \rho$  .

The data are input in an array or table which gives the average values of transmittance and reflectance versus incident angle for each of the

# Contrails

finite wavelength bands within the spectral region in which the glaze is considered to be semitransparent. Tables B-I through B-IX present transmittance data used in predicting the temperatures of the coated glaze specimens employed in the experimental heat transfer tests. Coatings used in the experimental tests included:

1. An ultraviolet-infrared (UV-IR) reflecting coating;
2. A high efficiency antireflection (HEA) coating; and
3. A gold coating for infrared reflection.

These coatings were deposited on the glaze test specimens by Optical Coating Laboratory, Inc. (OCLI). The transmittance of the glaze surfaces with UV-IR and with HEA coatings was obtained from data supplied by OCLI. These data were the spectral transmission of UV-IR and HEA coated microscope slides recorded for incident angles of 0, 20, 40 and 60 degrees. Zero transmission was assumed for the limiting incident angle, 90 degrees. The average coated surface transmittance, for each of the finite wavelength bands considered in the semitransparent analysis, was determined as follows:

$$\tau_m = \tau_c \tau_g e^{-\gamma \lambda L \sec \alpha}$$

or

$$\tau_c = \frac{\tau_m}{\tau_g e^{-\gamma L \sec \alpha}}$$

where  $\tau_m$  = transmission of coated microscope slide  
 $\tau_g$  = transmittance of uncoated surface  
 $\tau_c$  = transmittance of the coated surface  
 $\gamma$  = glaze absorption coefficient  
 $L$  = microscope thickness  
 $\alpha$  = angle of refraction

# Contrails

Average values of the above variables were used for each wavelength band considered. Transmittance versus incident angle for the gold coating was based on transmittance at zero angle of incidence and the shape of the HEA and UV-IR "transmittance versus incident angle" curves. It was assumed that the absorptance of these thin-film coatings was negligible. Thus, the reflectance was evaluated at  $1-\tau_c$ . When inputting surface transmittance and reflectance rather than computing these values, polarization effects are neglected. Transmittance and reflectance of the HEA, UV-IR, and gold multiple-layer, thin-film coatings were not computed with the subroutine discussed in the above section because the film data required for these calculations were considered by OCLI to be proprietary.

TABLE B-I

TRANSMITTANCE OF UV-IR COATING ON VYCOR GLAZE

Wavelength Band	Incident Angle			
	<u>0°</u>	<u>20°</u>	<u>40°</u>	<u>60°</u>
1	0.86	0.86	0.86	0.78
2	0.90	0.90	0.90	0.81
3	0.76	0.76	0.76	0.67
4	0.75	0.75	0.75	0.61
5	0.84	0.84	0.84	0.77

TABLE B-II

TRANSMITTANCE OF UV-IR COATING ON FUSED SILICA GLAZE

Wavelength Band	Incident Angle			
	<u>0°</u>	<u>20°</u>	<u>40°</u>	<u>60°</u>
1	0.55	0.50	0.55	0.47
2	0.86	0.89	0.88	0.77
3	0.72	0.72	0.73	0.665
4	0.74	0.74	0.78	0.71
5	0.84	0.85	0.88	0.78



TABLE B-III

TRANSMITTANCE OF UV-IR COATING ON ALUMINOSILICATE GLAZE

Wavelength Band	Incident Angle			
	<u>0°</u>	<u>20°</u>	<u>40°</u>	<u>60°</u>
1	0.48	0.45	0.56	0.46
2	0.86	0.89	0.90	0.75
3	0.71	0.74	0.73	0.65
4	0.74	0.74	0.77	0.66
5	0.85	0.85	0.87	0.76

TABLE B-IV

TRANSMITTANCE OF HEA COATING ON VYCOR GLAZE

Wavelength Band	Incident Angle			
	<u>0°</u>	<u>20°</u>	<u>40°</u>	<u>60°</u>
1	0.84	0.84	0.86	0.86
2	0.85	0.86	0.88	0.90
3	0.85	0.85	0.88	0.88
4	0.86	0.865	0.89	0.885
5	0.86	0.86	0.89	0.89

TABLE B-V

TRANSMITTANCE OF HEA COATING ON FUSED SILICA GLAZE

Wavelength Band	Incident Angle			
	<u>0°</u>	<u>20°</u>	<u>40°</u>	<u>60°</u>
1	0.87	0.86	0.87	0.865
2	0.85	0.85	0.88	0.865
3	0.85	0.85	0.89	0.865
4	0.85	0.84	0.90	0.87
5	0.88	0.87	0.90	0.88

TABLE B-VI

TRANSMITTANCE OF HEA COATING ON ALUMINOSILICATE GLAZE

Wavelength Band	Incident Angle			
	0°	20°	40°	60°
1	0.865	0.86	0.875	0.87
2	0.85	0.85	0.87	0.865
3	0.84	0.84	0.88	0.865
4	0.85	0.85	0.90	0.865
5	0.88	0.86	0.89	0.875

TABLE B-VII

TRANSMITTANCE OF GOLD COATING ON VYCOR GLAZE

Wavelength Band	Incident Angle			
	0°	20°	40°	60°
1	0.25	0.25	0.25	0.25
2	0.075	0.075	0.075	0.070
3	0.06	0.06	0.06	0.055
4	0.055	0.055	0.055	0.05
5	0.045	0.045	0.045	0.04

TABLE B-VIII

TRANSMITTANCE OF GOLD COATING ON FUSED SILICA GLAZE

Wavelength Band	Incident Angle			
	0°	20°	40°	60°
1	0.30	0.30	0.30	0.30
2	0.075	0.075	0.075	0.07
3	0.06	0.06	0.06	0.055
4	0.05	0.05	0.05	0.045
5	0.045	0.045	0.045	0.04

TABLE B-IX

TRANSMITTANCE OF GOLD COATING ON ALUMINOSILICATE GLAZE

Wavelength Band	Incident Angle			
	<u>0°</u>	<u>20°</u>	<u>40°</u>	<u>60°</u>
1	0.25	0.25	0.25	0.25
2	0.075	0.075	0.075	0.07
3	0.065	0.065	0.065	0.060
4	0.050	0.050	0.050	0.045
5	0.045	0.045	0.045	0.04

# *Contrails*

APPENDIX C

THERMOPHYSICAL AND OPTICAL PROPERTIES  
OF GLAZE MATERIALS

# Contrails

The material properties employed in the analysis are tabulated in Tables C-I through C-V for fused silica, Vycor (96% silica), aluminosilicate, borosilicate, and soda lime glazes. These properties are stored as block data in the computer program. This allows temperatures to be computed for a window system containing any combination of the above five glaze materials without inputting glaze material property data.

Properties which are considered as temperature-dependent are:

1. Index of refraction,  $n$  ;
2. Thermal conductivity,  $k$  ;
3. Heat capacitance,  $\rho c$  ; and
4. Absorption coefficient,  $\gamma$  .

The absorption coefficient is also spectrally dependent. Average values of  $\gamma$  are presented for five finite wavelength bands within the spectral region (from 0.4 to 4.8  $\mu$ ) in which the glazes are considered to be semi-transparent.

The values of index of refraction, thermal conductivity and heat capacitance were obtained from Ref. 6 for the glaze materials used in the calculations. Spectral values of absorption coefficient were determined by Finch (Appendix A of Ref. 7) based on transmittance of glaze specimens of known thicknesses and taking into account the reflectance of the specimen surfaces.



TABLE C-I

MATERIAL - FUSED SILICA

Temperature (°K)	Refractive Index	Conductivity (watts/cm °K)	$\rho c$ (watt sec/cm <sup>3</sup> °K)
0	1.45	0.011	1.216
200	1.45	0.011	1.216
400	1.45	0.0155	1.952
600	1.45	0.01805	2.292
800	1.45	0.02034	2.468
1,000	1.45	0.02207	2.587
1,200	1.45	0.02207	2.587
1,400	1.45	0.02207	2.587
1,700	1.45	0.02207	2.587
2,000	1.45	0.02207	2.587

Temperature (°K)	Absorption Coefficients (cm <sup>-1</sup> )				
	$\lambda$ from 0.4 to 2.2 $\mu$	$\lambda$ from 2.2 to 2.61 $\mu$	$\lambda$ from 2.61 to 2.9 $\mu$	$\lambda$ from 2.9 to 3.5 $\mu$	$\lambda$ from 3.5 to 4.8 $\mu$
0	0.06	0.50	17.0	0.15	11.5
300	0.06	0.50	17.0	0.15	11.5
600	0.06	0.50	17.0	0.15	11.5
900	0.06	0.50	17.0	0.15	11.5
1,200	0.06	0.50	17.0	0.15	11.5
1,500	0.06	0.50	17.0	0.15	11.5
1,800	0.06	0.50	17.0	0.15	11.5
2,000	0.06	0.50	17.0	0.15	11.5

Emissivity at wavelength below 0.4  $\mu$  is 0.92.

Emissivity at wavelength above 4.8  $\mu$  is 0.922.

TABLE C-II

MATERIAL - VYCOR (96 PERCENT SILICA)

<u>Temperature (°K)</u>	<u>Refractive Index</u>	<u>Conductivity (watts/cm °K)</u>	<u><math>\rho c</math> (watt sec/cm<sup>3</sup> °K)</u>
0	1.45	0.0133	1.34
200	1.45	0.0133	1.34
400	1.45	0.0162	1.946
600	1.45	0.01763	2.26
800	1.45	0.0185	2.49
1,000	1.45	0.0193	2.67
1,200	1.45	0.0193	2.67
1,400	1.45	0.0193	2.67
1,700	1.45	0.0193	2.67
2,000	1.45	0.0193	2.67

<u>Temperature (°K)</u>	<u>Absorption Coefficients (cm<sup>-1</sup>)</u>				
	<u><math>\lambda</math> from 0.4 to 2.2 <math>\mu</math></u>	<u><math>\lambda</math> from 2.2 to 2.61 <math>\mu</math></u>	<u><math>\lambda</math> from 2.61 to 2.9 <math>\mu</math></u>	<u><math>\lambda</math> from 2.9 to 3.5 <math>\mu</math></u>	<u><math>\lambda</math> from 3.5 to 4.8 <math>\mu</math></u>
0	0.03	0.43	17.0	1.35	19.8
300	0.03	0.43	17.0	1.35	19.8
600	0.03	0.43	17.0	1.35	19.8
900	0.03	0.43	17.0	1.35	19.8
1,200	0.03	0.43	17.0	1.35	19.8
1,500	0.03	0.43	17.0	1.35	19.8
1,800	0.03	0.43	17.0	1.35	19.8
2,000	0.03	0.43	17.0	1.35	19.8

Emissivity at wavelength below 0.4  $\mu$  is 0.914.

Emissivity at wavelength above 4.8  $\mu$  is 0.914.

TABLE C-III

MATERIAL - ALUMINOSILICATE

Temperature (°K)	Refractive Index	Conductivity (watts/cm °K)	$\rho c$ (watt sec/cm <sup>3</sup> °K)
0	1.54	0.01185	1.607
200	1.54	0.01185	1.607
400	1.54	0.01449	2.284
600	1.54	0.01469	2.677
800	1.54	0.01470	2.962
1,000	1.54	0.01471	3.192
1,200	1.54	0.01471	3.192
1,400	1.54	0.01471	3.192
1,700	1.54	0.01471	3.192
2,000	1.54	0.01471	3.192

Temperature (°K)	Absorption Coefficients (cm <sup>-1</sup> )				
	$\lambda$ from 0.4 to 2.2 $\mu$	$\lambda$ from 2.2 to 2.61 $\mu$	$\lambda$ from 2.61 to 2.9 $\mu$	$\lambda$ from 2.9 to 3.5 $\mu$	$\lambda$ from 3.5 to 4.8 $\mu$
0	0.107	0.3	6.0	5.0	14.0
300	0.107	0.3	6.0	5.0	14.0
600	0.107	0.3	6.0	5.0	14.0
900	0.107	0.3	6.0	5.0	14.0
1,200	0.107	0.3	6.0	5.0	14.0
1,500	0.107	0.3	6.0	5.0	14.0
1,800	0.107	0.3	6.0	5.0	14.0
2,000	0.107	0.3	6.0	5.0	14.0

Emissivity at wavelength below 0.4  $\mu$  is 0.907.

Emissivity at wavelength above 4.8  $\mu$  is 0.915.

TABLE C-IV

MATERIAL - BOROSILICATE

<u>Temperature (°K)</u>	<u>Refractive Index</u>	<u>Conductivity (watts/cm °K)</u>	<u><math>\rho_c</math> (watt sec/cm<sup>3</sup> °K)</u>
0	1.47	0.01021	1.448
200	1.47	0.01021	1.448
400	1.47	0.01269	1.989
600	1.47	0.01481	2.427
800	1.47	0.01756	2.800
1,000	1.47	0.02427	3.024
1,200	1.47	0.02427	3.024
1,400	1.47	0.02427	3.024
1,700	1.47	0.02427	3.024
2,000	1.47	0.02427	3.024

<u>Temperature (°K)</u>	<u>Absorption Coefficients (cm<sup>-1</sup>)</u>				
	<u><math>\lambda</math> from 0.4 to 2.2 <math>\mu</math></u>	<u><math>\lambda</math> from 2.2 to 2.61 <math>\mu</math></u>	<u><math>\lambda</math> from 2.61 to 2.9 <math>\mu</math></u>	<u><math>\lambda</math> from 2.9 to 3.5 <math>\mu</math></u>	<u><math>\lambda</math> from 3.5 to 4.8 <math>\mu</math></u>
0	0.03	0.03	5.0	4.0	28.0
300	0.03	0.03	5.0	4.0	28.0
600	0.03	0.03	5.0	4.0	28.0
900	0.03	0.03	5.0	4.0	28.0
1,200	0.03	0.03	5.0	4.0	28.0
1,500	0.03	0.03	5.0	4.0	28.0
1,800	0.03	0.03	5.0	4.0	28.0
2,000	0.03	0.03	5.0	4.0	28.0

Emissivity at wavelength below 0.4  $\mu$  is 0.915.

Emissivity at wavelength above 4.8  $\mu$  is 0.921.

# Contrails

TABLE C-V

MATERIAL - SODA LIME

Temperature (°K)	Refractive Index	Conductivity (watts/cm °K)	$\rho c$ (watt sec/cm <sup>3</sup> °K)
0	1.51	0.0113	2.51
200	1.51	0.0113	2.51
400	1.51	0.0113	2.51
600	1.51	0.0138	2.51
800	1.51	0.0163	2.51
1,000	1.51	0.0188	2.51
1,200	1.51	0.0188	2.51
1,400	1.51	0.0188	2.51
1,700	1.51	0.0188	2.51
2,000	1.51	0.0188	2.51

Temperature (°K)	Absorption Coefficients (cm <sup>-1</sup> )				
	$\lambda$ from 0.4 to 2.2 $\mu$	$\lambda$ from 2.2 to 2.61 $\mu$	$\lambda$ from 2.61 to 2.9 $\mu$	$\lambda$ from 2.9 to 3.5 $\mu$	$\lambda$ from 3.5 to 4.8 $\mu$
0	0.4	0.48	1.8	4.5	8.0
300	0.4	0.48	1.8	4.5	8.0
600	0.4	0.48	1.8	4.5	8.0
900	0.4	0.48	1.8	4.5	8.0
1,200	0.4	0.48	1.8	4.5	8.0
1,500	0.4	0.48	1.8	4.5	8.0
1,800	0.4	0.48	1.8	4.5	8.0
2,000	0.4	0.48	1.8	4.5	8.0

Emissivity at wavelength below 0.4  $\mu$  is 0.91.

Emissivity at wavelength above 4.8  $\mu$  is 0.91.

# *Contrails*

APPENDIX D

CORRELATIONS USED TO PREDICT IN-FLIGHT HEATING



## INTRODUCTION

Various methods of computing the heat transfer to the window are used by the program, depending on the mission under consideration. Missions for which the window heating can be computed by the program include hypersonic flight, re-entry, supersonic flight, or orbital flight. The analytical methods employed are based on accepted correlations for predicting aerodynamic (convective) heating, radiative heating from a shock layer, and radiative heating from the sun. These correlations as used by Lis, Barile, and Engholm for the single glaze window program of Reference 1 are also employed in the subject multiple glaze program. A description of equations used has been reproduced from Reference 1 for this Appendix.

A convective heating rate versus time can also be included in the input data. This allows the convective heat flux computed by any desirable method to be used in the program. A constant radiative heating rate can be described by input data if so desired by inputting a heat source temperature and emittance and an appropriate configuration factor. This option was used when computing glaze temperatures for comparison to those measured in the experimental heat transfer tests.

## HYPERSONIC FLIGHT AND RE-ENTRY

For hypersonic flight and re-entry, the convective input to the window is expressed as a percentage of the stagnation point heat transfer rate. The stagnation point convective heating is computed using the correlation of Kemp and Riddell (Ref. 8) as written below:

$$q''_{\text{Hyp}} = \frac{11.88}{\sqrt{R_N}} \sqrt{\rho} \left( \frac{V}{1,000} \right)^{3.25} \left( 1 - \frac{H_{\text{wall}}}{H_{\text{stag}}} \right) [\text{watts/cm}^2] \quad (1)$$

where

$R_N$  = nose radius (ft.)

$\rho$  = free stream density (lb/ft<sup>3</sup>)

$V$  = free stream velocity (fps)

$H$  = enthalpy

# Contrails

The percentage or ratio of convective heat transfer rate at the window to that at the stagnation point is generally determined by heat flux data obtained during wind tunnel tests using a model of the actual vehicle being designed.

Above a critical altitude (defined by input data), the convective heating rate for hypersonic flight is based upon stagnation point heat transfer in free molecular flow and may be expressed as (Ref. 8):

$$q = 2.271 \times 10^{-5} \rho V^3 \text{ (watt/cm}^2\text{)} \quad (2)$$

where the density,  $\rho$ , is taken as free stream density ( $\text{lb/ft}^3$ ) and the velocity,  $V$ , is taken as free stream velocity ( $10^3$  fps). The critical altitude above which free molecular flow is considered is based on

$$\frac{M}{Re} > 10$$

where  $M$  is the mach number and  $Re$  is the Reynolds number. In this flow regime, the air is highly rarefied and consequently intermolecular collisions are insignificant compared to molecule-surface collisions. The molecular mean free path is of the same order of magnitude or larger than the length of the aerospace vehicle (Ref. 17).

Radiative heating of the window during hypersonic flight and re-entry is considered to be from the hot air in a normal shock layer of a thickness equal to the stand-off distance at the stagnation point. For high speed flight, the shock layer thickness,  $\delta^*$ , is satisfactorily approximated by

$$\delta^* = \frac{2R_N}{3(K-1)} \quad (3)$$

where  $R_N$  is the nose radius and  $K$  is the ratio of normal shock to free stream density (Ref. 18).

Graybody emissivities for shock heated air per unit thickness at densities and temperatures behind the normal shock are obtained from curve fits of the data of Kivel and Bailey (Ref. 9). These curves have been fitted by a logarithmic polynomial expansion of the form:

# Contrails

$$\log \epsilon/\delta^* = a_0 + a_1 \log T + a_2 \log^2 T + a_3 \log^3 T + a_4 \log^4 T \quad (4)$$

where

$\epsilon/\delta^*$  = graybody emissivity per unit thickness ( $\text{cm}^{-1}$ )

$a_0 \dots a_4$  = constants determined from the polynomial fit

$\log$  = logarithm to the base 10

$T$  = absolute temperature ( $^{\circ}\text{K}$ )

A least-squares analysis was used to determine the constants  $a_0 \dots a_4$ . The resulting values for the constants are shown in Tables D-I and D-II. As may be noted, one set of constants is applicable in the range  $1,000 \leq T < 8,000^{\circ}\text{K}$ , and the second set of constants is applicable in the range  $8,000 \leq T \leq 18,000^{\circ}\text{K}$ . To determine intermediate values, double logarithmic interpolation is performed between temperature and density values on both sides of the values required.

TABLE D-I

COEFFICIENT FOR THE LEAST-SQUARES FIT  
LOW TEMPERATURE:  $1,000 \leq T < 8,000^{\circ}\text{K}$

<u>Density ratio</u> <u><math>\rho/\rho_0^*</math></u>	<u><math>a_0</math></u>	<u><math>a_1</math></u>	<u><math>a_2</math></u>	<u><math>a_3</math></u>	<u><math>a_4</math></u>
$10^{-6}$	-6.925307	2.8251600	-2.5936484	0.19645656	0.063094980
$10^{-5}$	-3.7398826	-2.4643677	-0.78233130	0.29189669	0.000000000
$10^{-4}$	-16.4635100	5.3745600	-1.8453232	0.28489560	0.000000000
$10^{-3}$	-64.254100	34.832836	-3.9048150	-1.1711824	0.22468464
$10^{-2}$	-21.239832	7.3043176	-1.3141154	0.14599265	0.000000000
$10^{-1}$	-75.888910	43.790509	-5.1229970	-1.4008835	0.27386482
$10^0$	49.092640	-42.948052	7.1221220	1.1666329	-0.26152723
$10^1$	104.74205	-79.760151	11.775116	2.3571684	-0.48591030

\*  $\rho_0$  is air density at sea level.

TABLE D-II

COEFFICIENTS FOR THE LEAST-SQUARES FIT  
HIGH TEMPERATURE: 8,000 ≤ T ≤ 18,000 °K

Density ratio $\rho/\rho_0^*$	$\underline{a_0}$	$\underline{a_1}$	$\underline{a_2}$	$\underline{a_3}$	$\underline{a_4}$
$10^{-6}$	-42.329078	3.3773731	0.38418980	1.1454587	-0.23198607
$10^{-5}$	-56.086180	-4.0042870	2.6224950	2.0830205	-0.43381861
$10^{-4}$	-60.699710	-4.5744890	2.9574360	2.3487883	-0.48580387
$10^{-3}$	-87.580695	7.8681740	0.49151000	2.9433819	-0.56388439
$10^{-2}$	-38.483046	-3.1711910	1.5607300	1.4969915	-0.28388548
$10^{-1}$	-11.1572062	-0.34727720	-0.23287300	0.32303328	-0.024583496
$10^0$	0.1892374	-1.3357925	-0.31752664	-0.05693168	0.051322102
$10^1$	4.7243840	-1.6747281	-0.14927570	-0.19923154	0.069056794

\*  $\rho_0$  is the density at sea level.

The effective emissivity,  $\epsilon_g$ , of the shock heated air is obtained by scaling the emissivity,  $\epsilon$ , according to the exponential (Ref. 19):

$$\epsilon_g = \frac{q_r}{\sigma T_H^4} = 1 - e^{-\epsilon} \quad (5)$$

where

$\epsilon_g$  = graybody hot gas emissivity

$q_r$  = radiative flux

$\sigma$  = Stefan Boltzmann's constant

$T_H$  = hot gas absolute temperature behind the normal shock

$\epsilon$  = emissivity defined by equations (3) and (4).

Equation (5) yields an effective emissivity of the shock heated air accurate to within 20% of the exact solution as presented in Reference 20. The basic assumptions leading to Eq. (5) are that the radiating layer is planar (normal shock) of thickness  $\delta^*$  which is divided into infinitesimal slabs having an absorptivity per unit thickness equal to their emissivity per unit thickness. The results given are then integrated over the width of the slab. Values of  $T_H$  and  $\epsilon_g$  are used in the element heat balance equations when determining the radiation absorbed by the elements during a hypersonic flight or re-entry.

## SUPERSONIC FLIGHT

For supersonic flight, the aerodynamic heating is computed from the heat transfer correlations of a flat plate at zero angle of attack (Ref. 10). The correlations are based on free stream conditions and are written as:

$$N_{St} = 0.016 N_{Re}^{-0.145} \quad (6)$$

and

$$\frac{h}{h_i} = 0.961 N_{Ma}^{-0.24} \left( \frac{T_s}{T_a} \right)^{-0.34} \quad (7)$$

where

$$N_{St} = \text{Stanton Number} = \frac{h_i}{\rho_a C_p V}$$

$$N_{Re} = \text{Reynolds Number} = \frac{VL}{\nu}$$

$$N_{Ma} = \text{Mach number}$$

$T_s$  &  $T_a$  = surface and ambient temperatures, respectively

$h$  &  $h_i$  = the local and incompressible heat transfer coefficients, respectively

# Contrails

$\rho_a$  = free stream density

$C_p$  = specific heat at constant free stream pressure

$V$  = free stream velocity

$L$  = distance from the leading edge

$\nu$  = kinematic viscosity at free stream conditions

Once the local heat transfer coefficient is determined, the convective heat transfer rate is computed by (Ref. 10):

$$q_{SSt}'' = h(T_{Wo} - T_s) \quad (8)$$

where

$$T_{Wo} = T_a(1 + 0.178 N_{Ma}^2)$$

= (the adiabatic wall temperature for a turbulent boundary layer)

No radiative heating is used for the supersonic case because the gaseous radiation is considered negligible. Since the emissivity of air is relatively low, gaseous radiation does not become significant until extreme air temperatures are reached such as those in the shock layer of hypersonic flight and re-entry.

## ORBITAL FLIGHT

The orbital heating conditions or thermal environment for the window is programmed specifically for a 200-nautical-mile circular orbit. Convective heating is based on the correlation for stagnation point heat transfer in free molecular flow, which is discussed above for hypersonic flight above the critical altitude. Based on this correlation, a constant convective heating rate of  $7.409 \times 10^{-4}$  watt/cm<sup>2</sup> is used for the 200-nautical-mile circular orbit.

# Contrails

The radiative heating from the sun is approximated by using a solar temperature of 6,000°K and an appropriate form factor. The form factor is evaluated as:

$$F = \frac{\text{solar constant}}{\sigma T_{\text{sun}}^4} = 1.882 \times 10^{-5} \quad (9)$$

where the solar constant is that above the earth's atmosphere (Ref. 21). Since the solar radiation is collimated and the computer program analysis assumes the external radiation to be diffuse, solar heating of a window is only approximated.



APPENDIX E

SUPERPOSITION TESTS

## Introduction

The experimental procedures that were used to verify the computer program are based in part on the so-called superposition technique. The primary advantage of this "additive" approach is that it required experimental tests to be run for only the two sets of boundary conditions shown in Figure E-1, all-air and all-vacuum, and eliminated the need for any of the other possible test combinations illustrated in Figure E-2.

## Superposition Terminology

Heat is transferred by three different mechanisms: conduction, convection, and radiation. The idea of superposition implies that the total heat transfer in a system can be determined by evaluating the heat transfer for each mode separately and then superimposing the results. This procedure is generally followed in a thermal analysis, but can equally be used in experimental work.

## Experimental Analysis of Superposition

The superposition method, when used properly, has always been found to agree with observations. The method becomes particularly simple and convenient in a system in which heat is transferred by conduction and radiation when the conducting medium is air or some other transparent gas. In order to meet contractual obligations, experiments were performed to show that superposition for this case can be used with confidence.

Two plates were placed parallel to each other. The upper plate was heated to a uniform temperature while the lower plate was maintained at a substantially lower uniform temperature. The upper plate consisted of the flat radial resistance heater that was developed, calibrated, and employed in the previous MRI research for the Air Force Flight Dynamics Laboratory under Contract No. AF 33(657)-9138. The lower plate was a water-cooled copper disk designed for use in both the superposition equipment and the current version of the transparent boundary apparatus. The copper plate was instrumented with Hy-Cal heat flux gauges.\*

---

\* A comparison of heat flux measurements taken with the Hy-Cal gauges with those previously taken under similar conditions with the precision water calorimeter developed by MRI indicated that the two types of instruments were in very close agreement for the applicable range of heat fluxes.

# Contrails

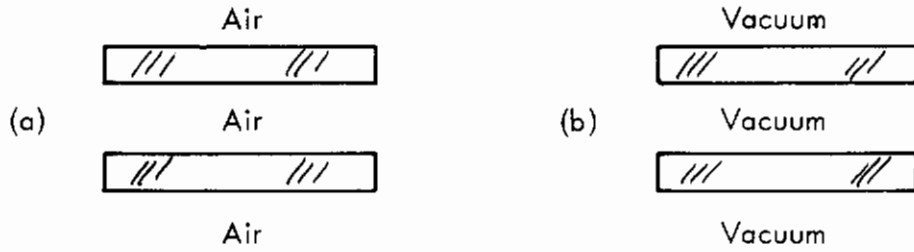


Figure E-1 - Selected Boundary Conditions

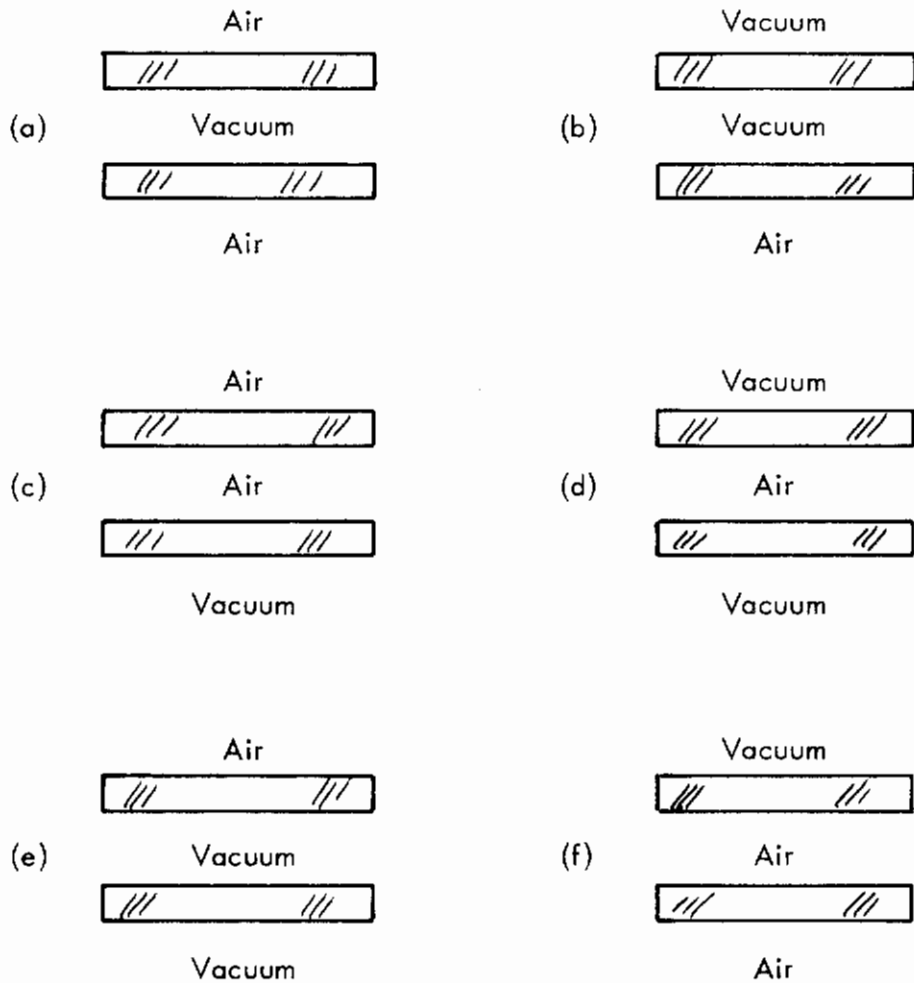


Figure E-2 - Boundary Conditions That Can Be Eliminated  
By Application of Superposition Principle

# Contrails

The apparatus was first operated in an evacuated chamber and the rate of thermal radiation was measured. Air was then introduced into the system and the resulting thermal conduction between the plates was computed from the measured temperature differences between the plates, the gap size, and the known values of thermal conductivity of air. The thermal conduction thus calculated was subtracted from the total heat flux measured by the Hy-Cal gauges and the difference, thermal radiation, was compared to the vacuum values. These tests and the subsequent conclusions are described in detail below.

The heater was first placed 9/16 in. above the copper plate. At this distance the radiation configuration factor was calculated by form factor algebra to be 0.920. The heater was then operated in a vacuum at temperatures ranging from 1500°R to 2300°R and values of impinging radiation were measured. The resulting data are plotted in Figure E-3 and based on the least mean square curve, the effective emissivity was computed to be 0.933. The heater was then similarly operated at a gap distance of 8 in. Using an effective emissivity of 0.933, the configuration factor,  $F$ , was computed from the data plotted in Figure E-4. The average value of  $F$  was calculated to be 0.151, which agrees very closely with the value determined by form factor algebra. The results of these calculations further substantiate the high accuracy of the commercial heat flux gauges which were essential not only in the superposition tests, but also in the subsequent Phases I, II, and III heat transfer tests.

Tests were next run at a 9/16 in. heater height with air present. Thus, thermal conduction was superpositioned onto the thermal radiation mechanism. Since, under these conditions, the Rayleigh Number is considerably below the critical value of 1700, no convection currents are set up. For this case, Figure E-5 illustrates the superposition method applied to heat transfer between two parallel plates. When air is present there are two transfer paths in parallel conduction and radiation. When the air is removed (vacuum conditions) heat can only be transferred by radiation.

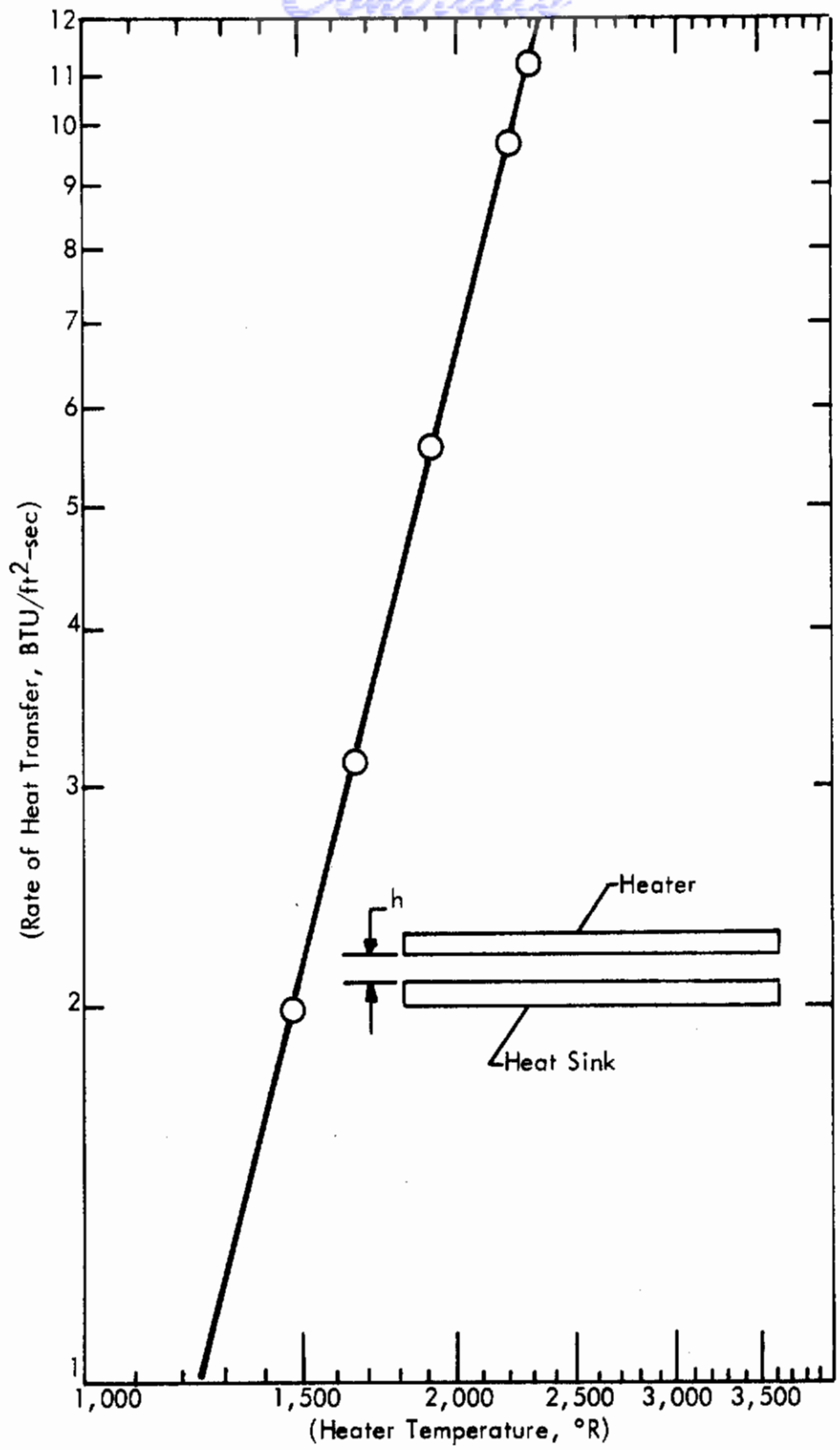


Figure E-3 - Superposition Test in Vacuum With  $h = 9/16$  In.

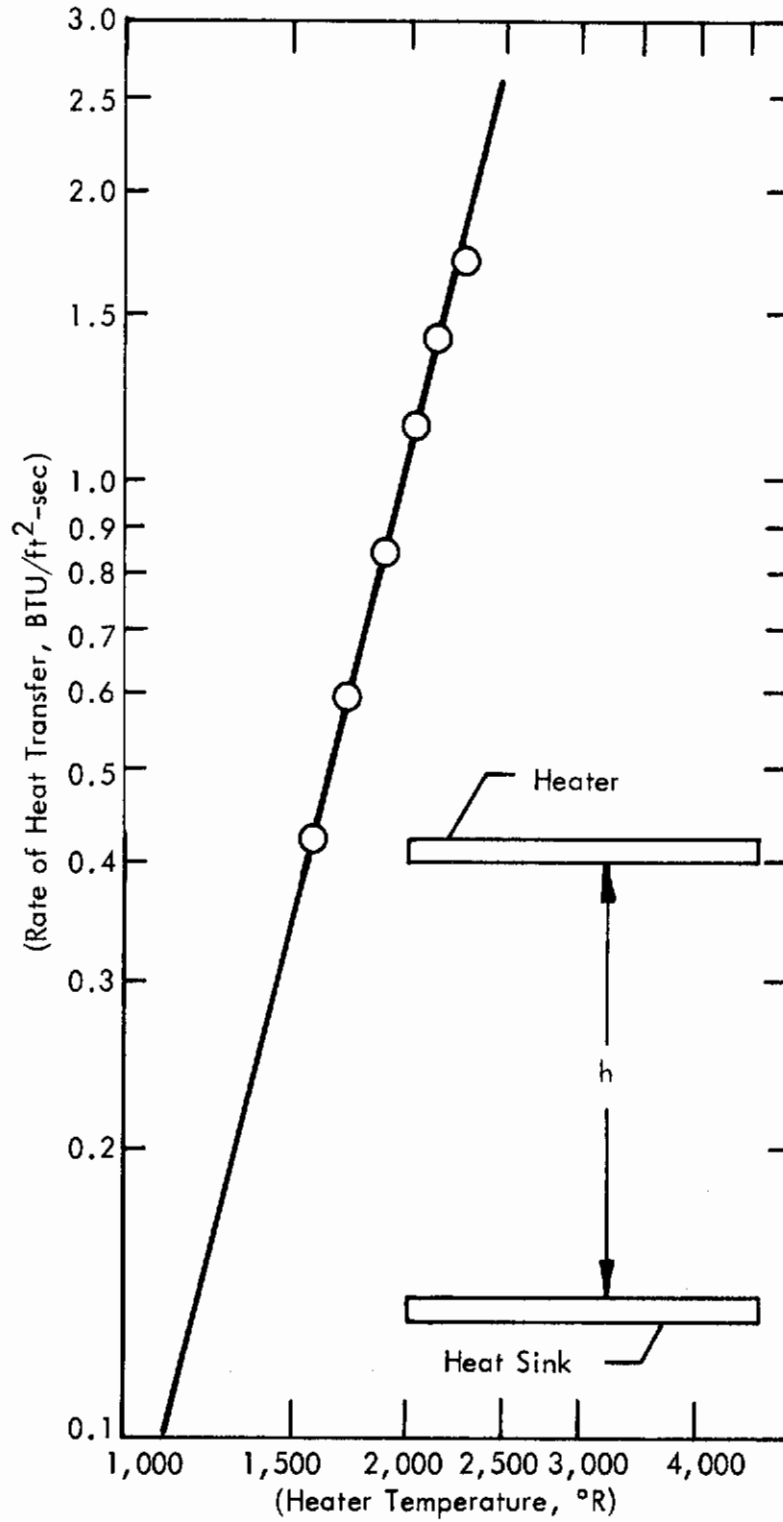


Figure E-4 - Superposition Test in Vacuum With  $h = 8.0$  In.

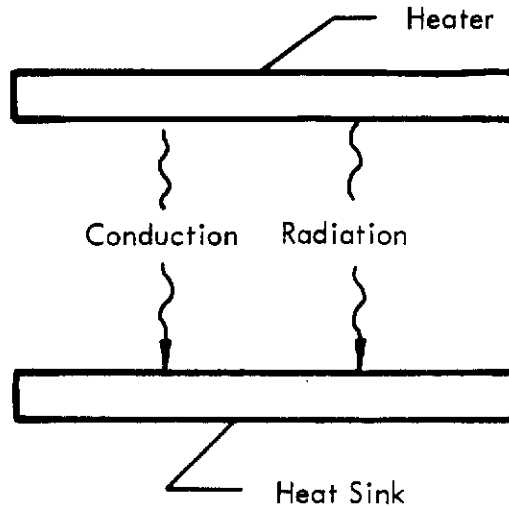


Figure E-5 - Schematic of Heat Flow Between Two Parallel Plates  
for Rayleigh Number  $\ll 1700$

The rate of heat conduction was determined from:

$$q = \frac{k}{x} (T_H - T_C)$$

where  $k$  is the thermal conductivity of air taken at the mean gap temperature,  $x$  is the gap distance, and  $T_H$  and  $T_C$  are the heater and cold plate temperature, respectively. The differences between the measured total heat and the calculated conduction were then compared (see Figure E-6) with radiation data based on the vacuum tests. It is apparent that throughout the entire range of temperatures, approximately  $1000^\circ\text{F}$  to  $1800^\circ\text{F}$ , the superposition of air had no measurable effect on the thermal radiation. In these tests the amount of thermal conduction was significant but was considerably less than the heat transfer by radiation; however, the relative magnitudes were selected so as to be similar to those that were actually encountered in the Phases I, II, and III heat transfer tests. That is, the heater was operated at temperatures which were of prime interest for glaze, and the  $9/16$  in. gap was chosen as it is a representative window spacing.

### Conclusions

The experimental tests proved conclusively that superposition is valid and is applicable to this particular project. As shown from the experimental



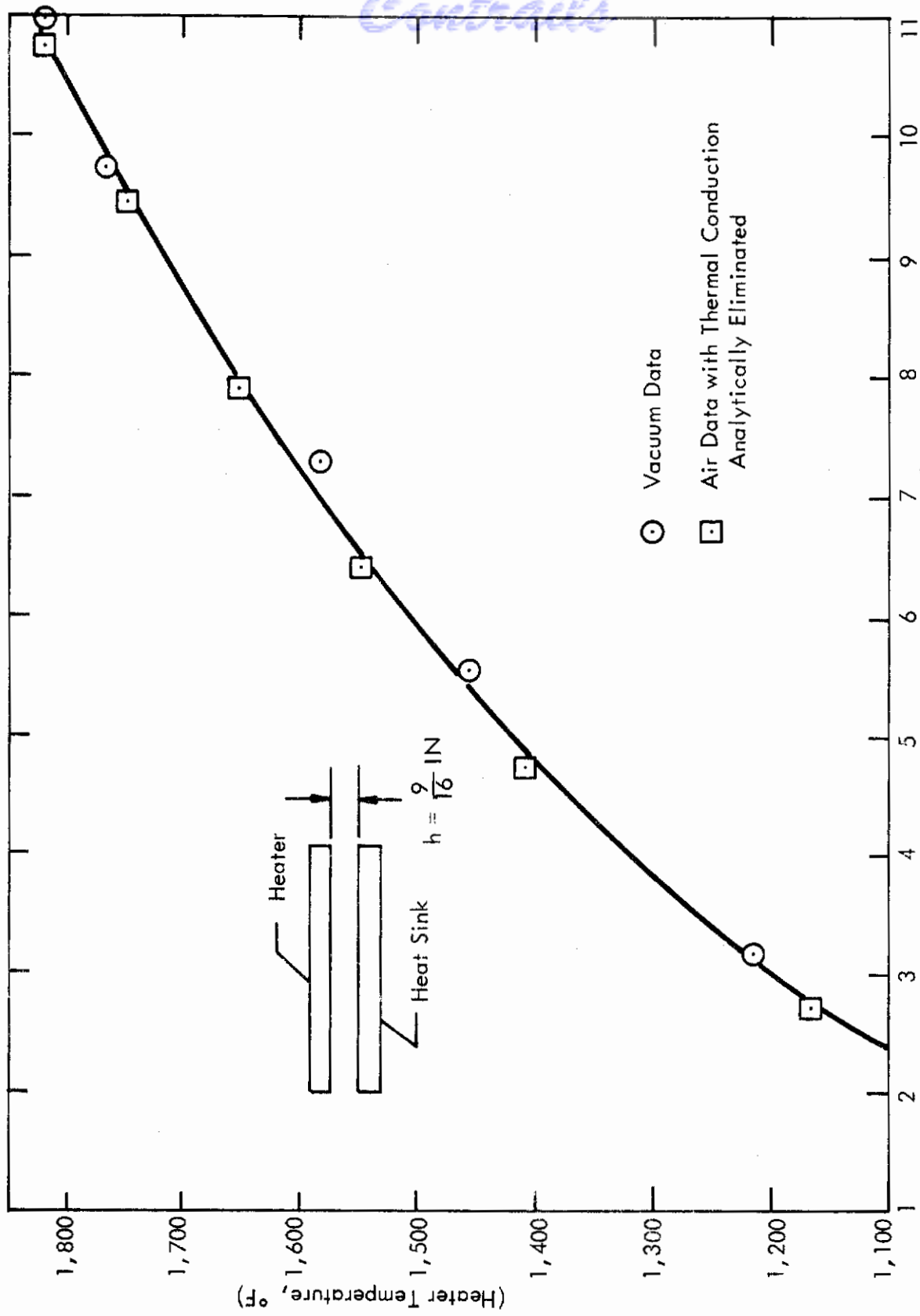


Figure E-6 - Superposition Tests

data, the difference between the total heat rate measured in air and the conduction rate calculated is equal to the radiation heat transfer through the space between two plates measured when a vacuum existed. In order to show that this agreement was independent of the rate of radiation as well as the ratio of radiation to conduction, the tests were run over a wide temperature range. In all cases, heat transfer by radiation alone could be accurately computed from the experimental data taken under conditions where radiation and conduction were occurring simultaneously. Thus, the results show that the presence or absence of a transparent medium such as air in the experimental setups which were employed in the current project is of no consequence and can be properly accounted for by straightforward and accepted heat transfer procedures.

Having shown this for one gap between two plates at various temperatures, it follows that in case there are more than two plates stacked parallel to each other as in Phase III, the absence or presence of air between any two surfaces will not introduce a new factor which could invalidate the superposition method of calculation. For example, if in the arrangement shown in Figure E-7, tests were first conducted with air between glass surfaces 3 and 4 and then without air in this space, the only change in the heat transfer through the gap below would be due to a change in  $T_5$  and the net rate of radiation. Since, as shown by the experiments, the effect on the rate of conduction due to a change in  $T_5$  can be calculated, irrespective of the amount of thermal radiation, the presence or absence of air in any other gap will not cause any problems in determining the desired radiation heat transfer.

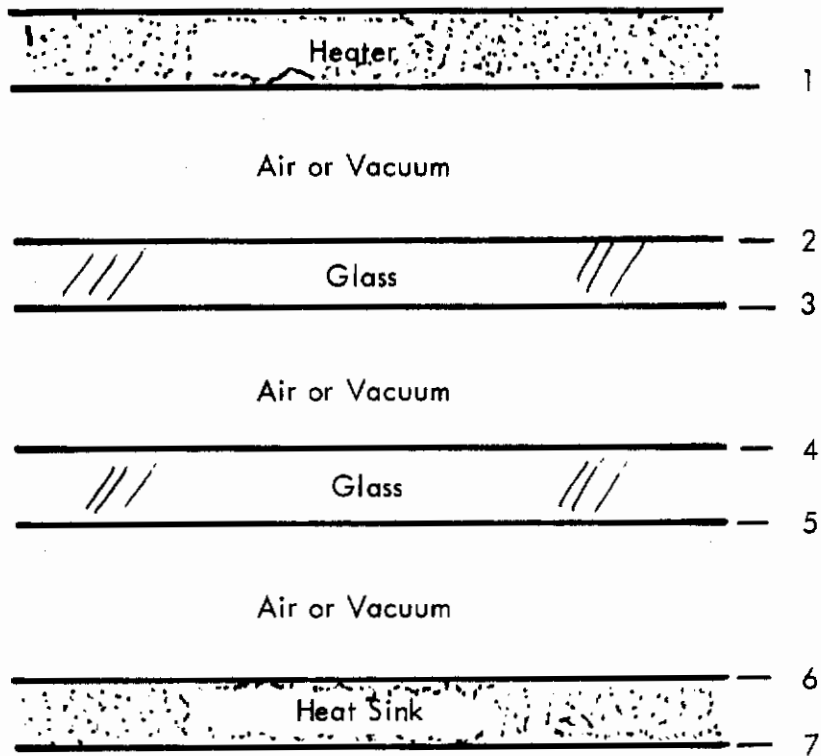


Figure E-7 - Phase III Test Setup

APPENDIX F

EXPERIMENTAL RESULTS

## Data Symbols

- Temperature of upper surface of outer glaze
- △ Temperature of lower surface of outer glaze
- Temperature of upper surface of inner glaze
- ▲ Temperature of lower surface of inner glaze
- Heat flux from and through the glazes to the calorimeter

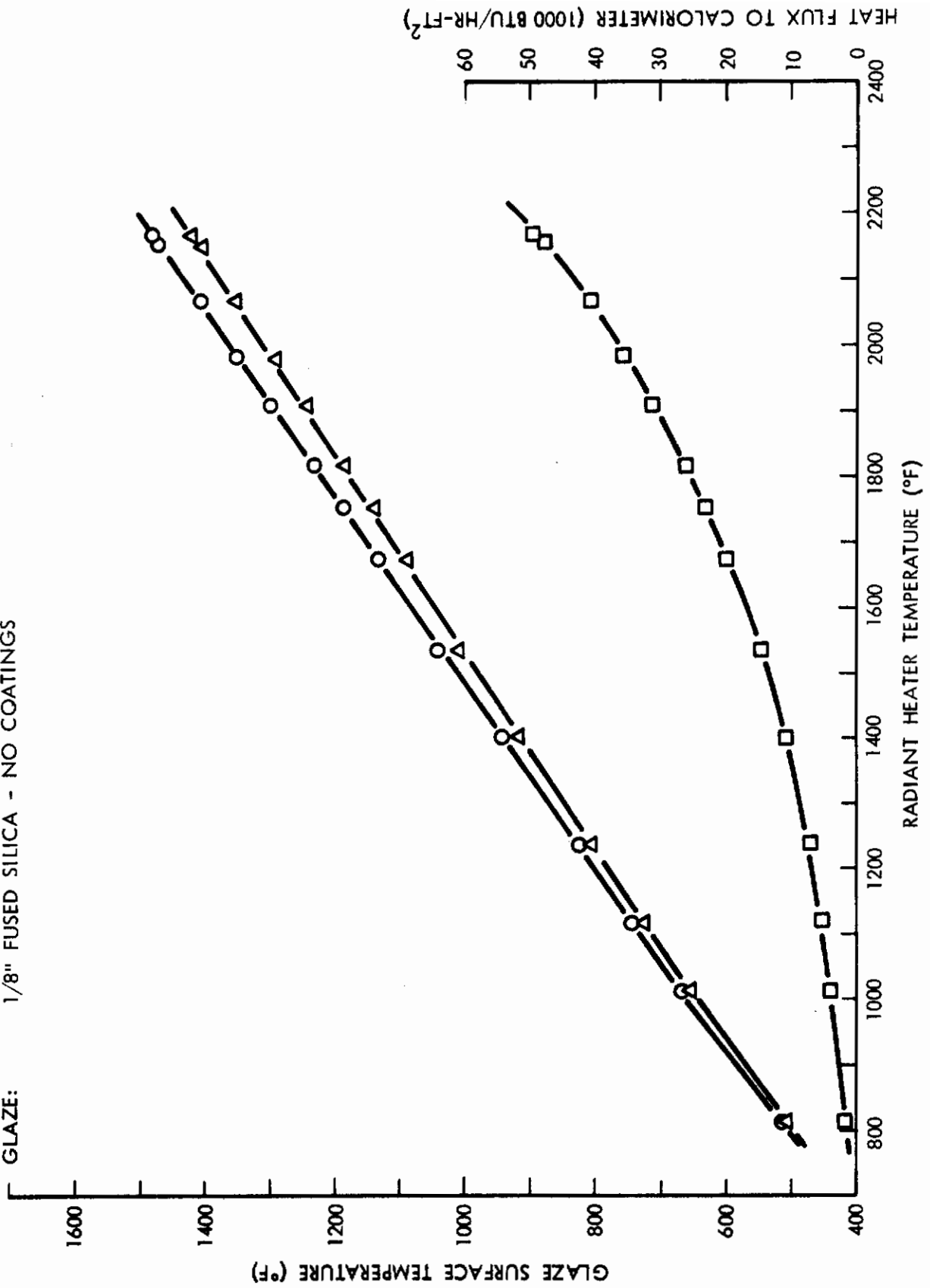
## Glaze Coating Symbols

- HEA High efficiency anti-reflection coating
- UV-IR Ultraviolet-infrared reflecting coating

Note: The HEA and UV-IR coatings are multiple-layer, thin-film coatings designed and applied to the glaze test specimens by the Optical Coating Laboratory, Inc. (OCLI). The gold coating employed in the test specimens was also applied by OCLI and consists of multiple layers of gold and dielectric materials.

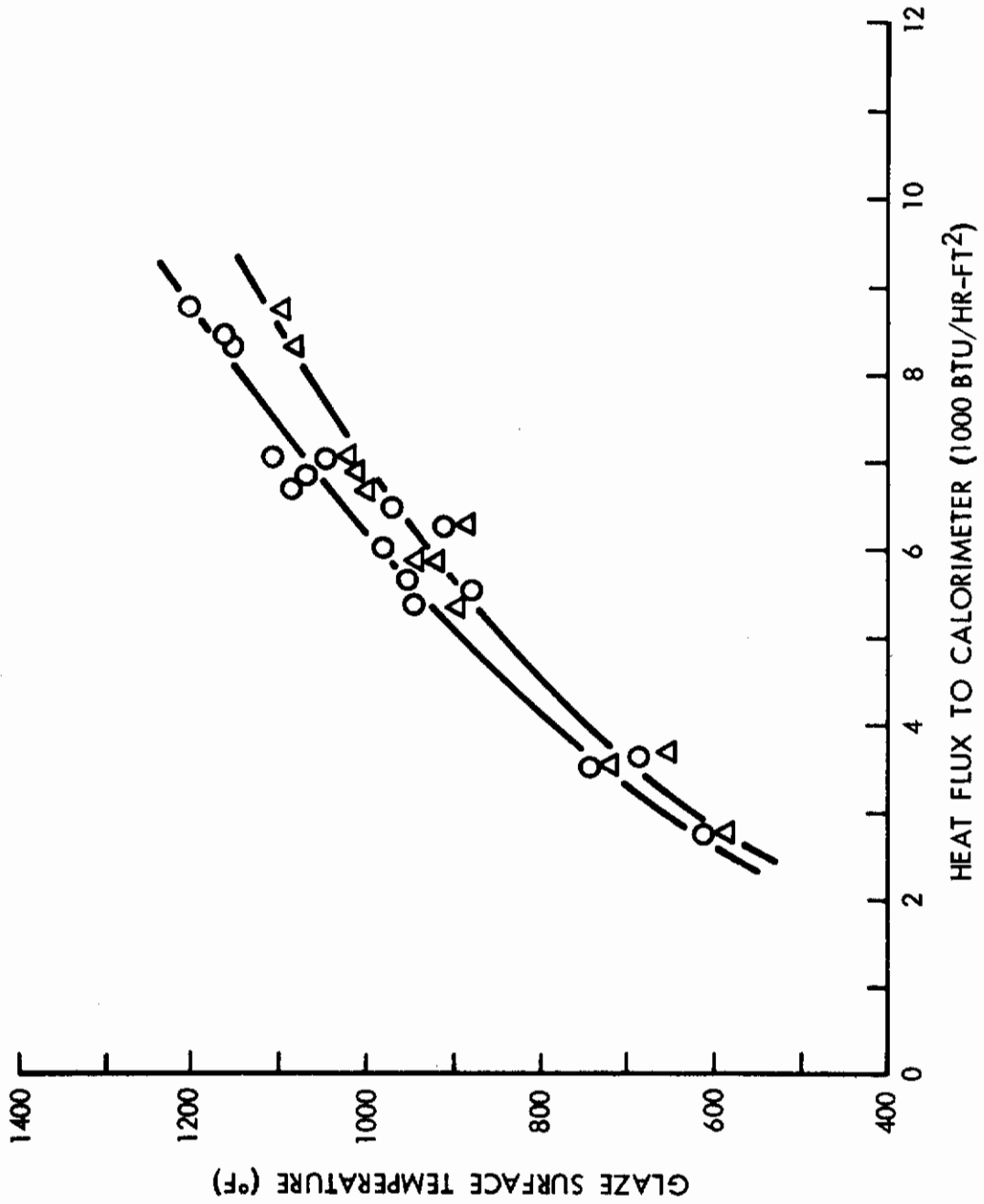
SINGLE GLAZE HEAT TRANSFER TEST

TEST NUMBER: I-20 (AIR)  
HEAT SOURCE: RADIATION  
GLAZE: 1/8" FUSED SILICA - NO COATINGS



SINGLE GLAZE HEAT TRANSFER TEST

TEST NUMBER: I-1 (AIR)  
HEAT SOURCE: CONVECTION  
GLAZE: 1/8" FUSED SILICA - NO COATINGS



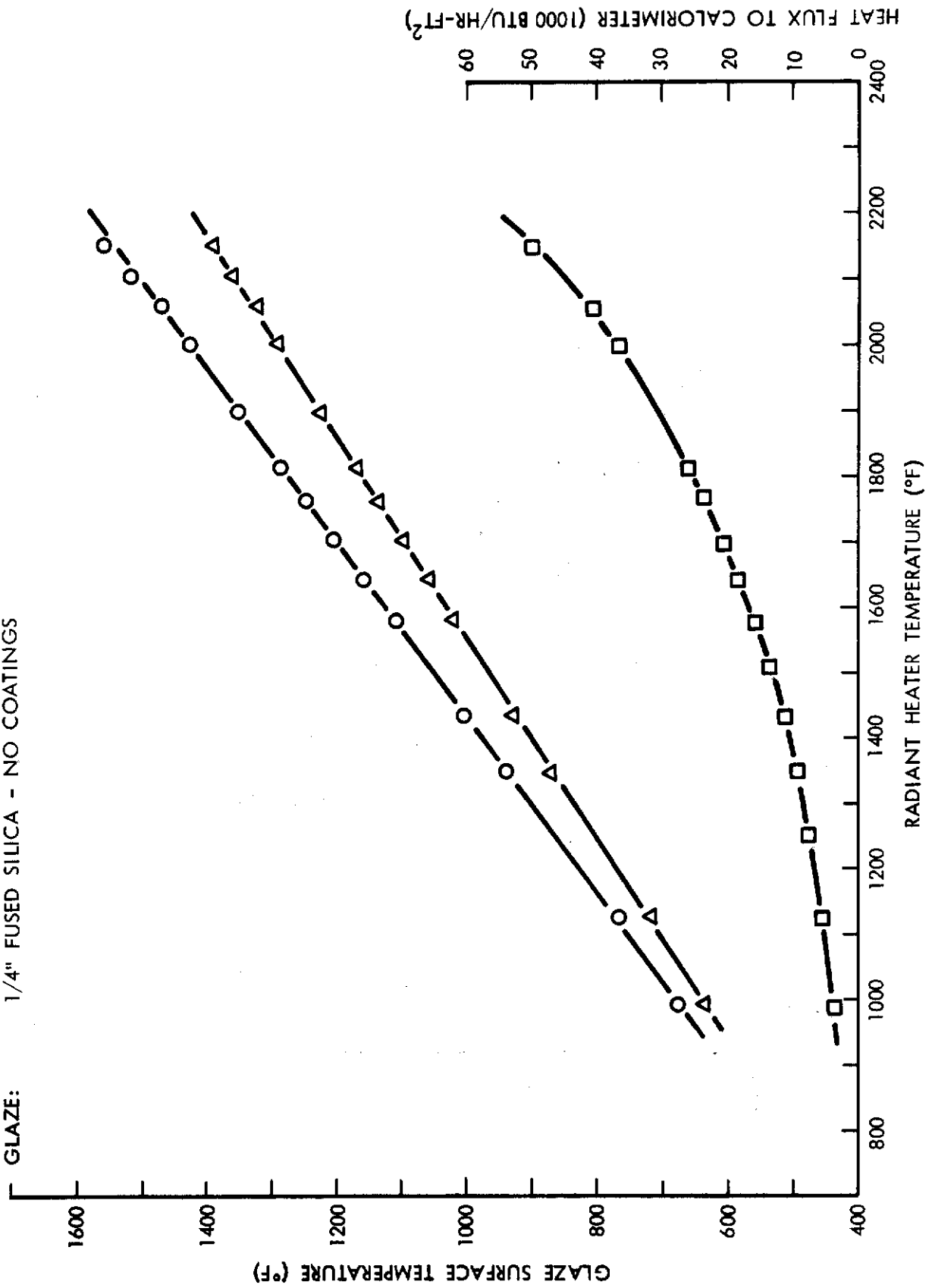


SINGLE GLAZE HEAT TRANSFER TEST

TEST NUMBER: 1-6 (AIR)

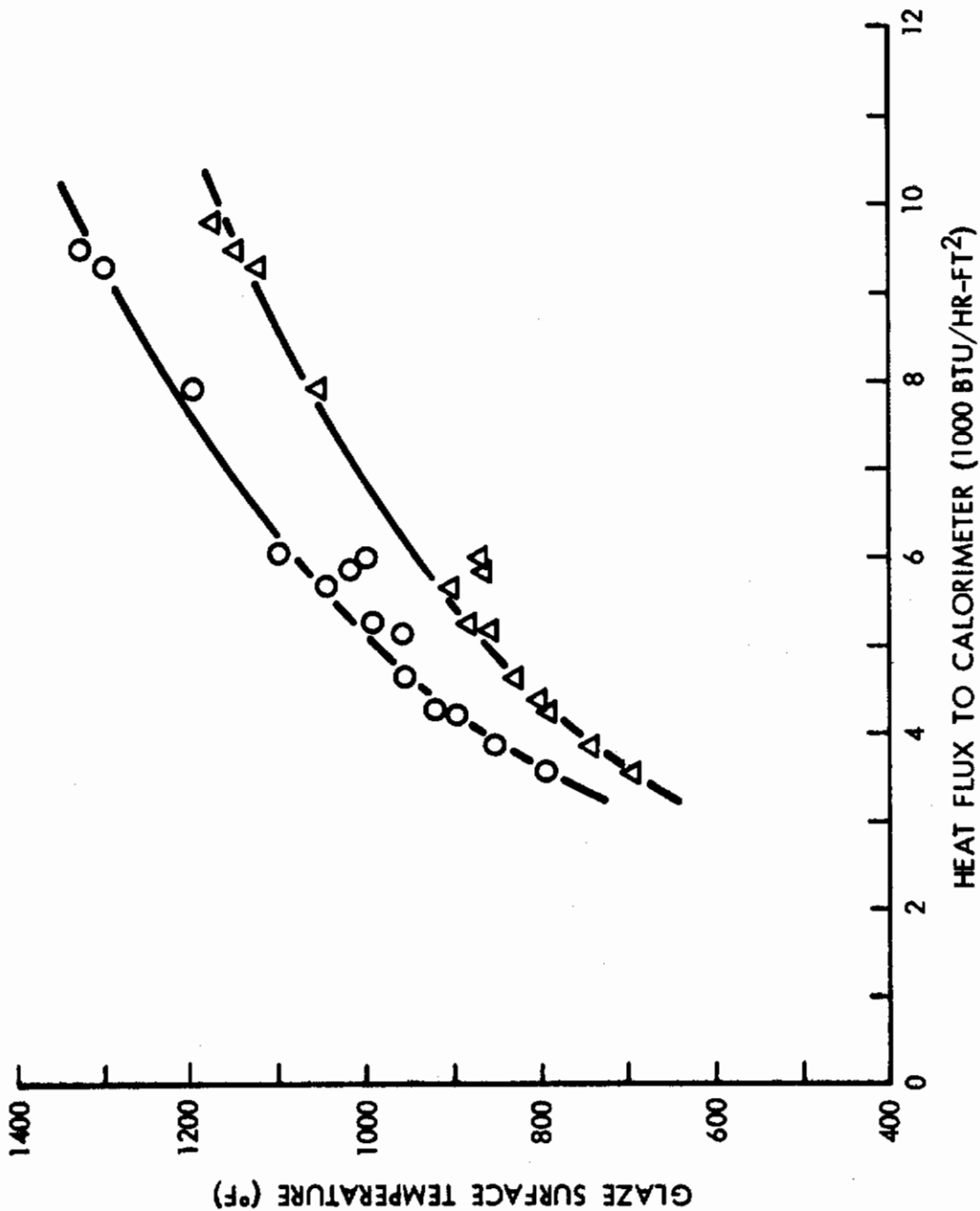
HEAT SOURCE: RADIATION

GLAZE: 1/4" FUSED SILICA - NO COATINGS



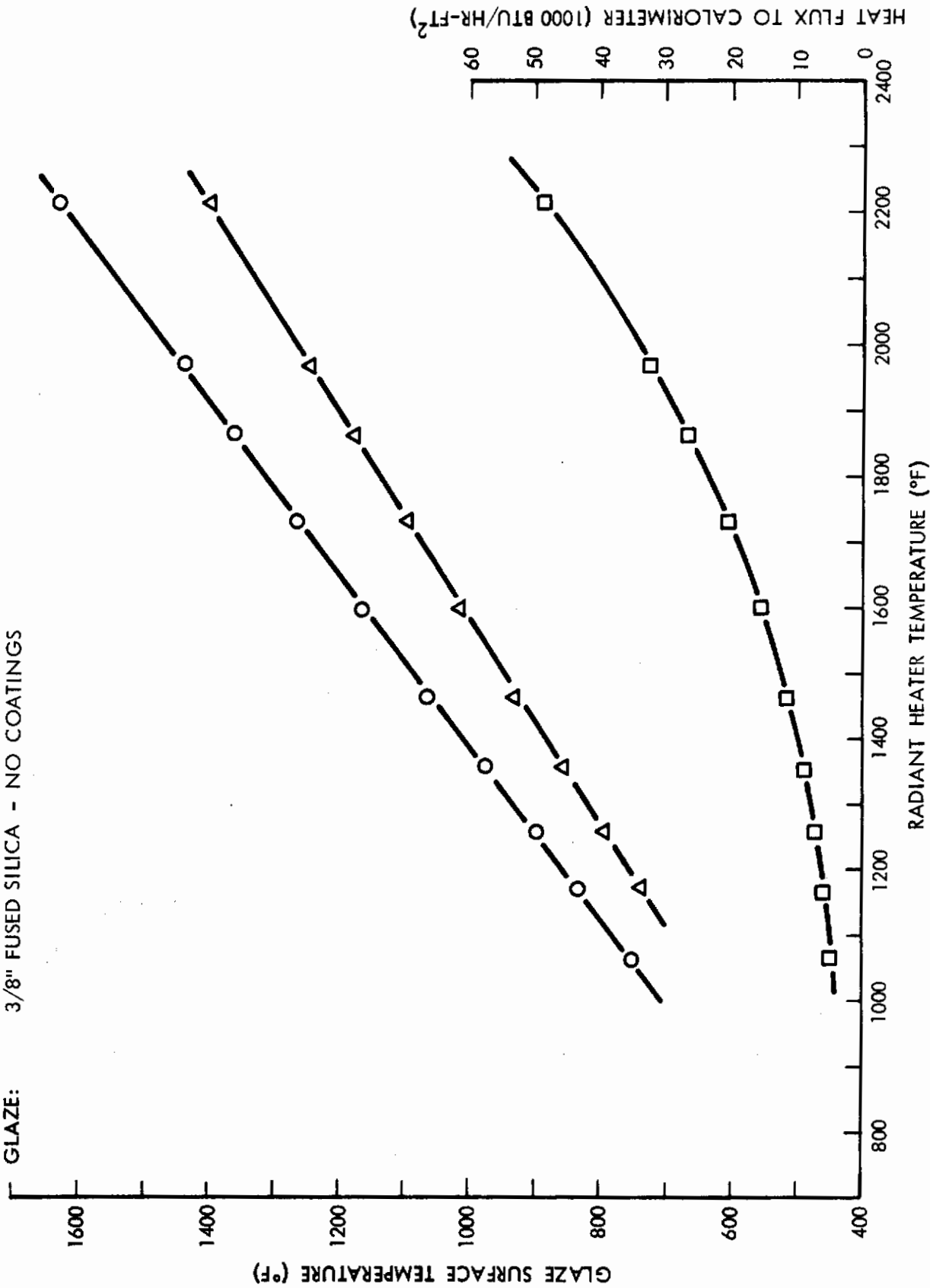
SINGLE GLAZE HEAT TRANSFER TEST

TEST NUMBER: 1-7 (AIR)  
HEAT SOURCE: CONVECTION  
GLAZE: 1/4" FUSED SILICA - NO COATINGS



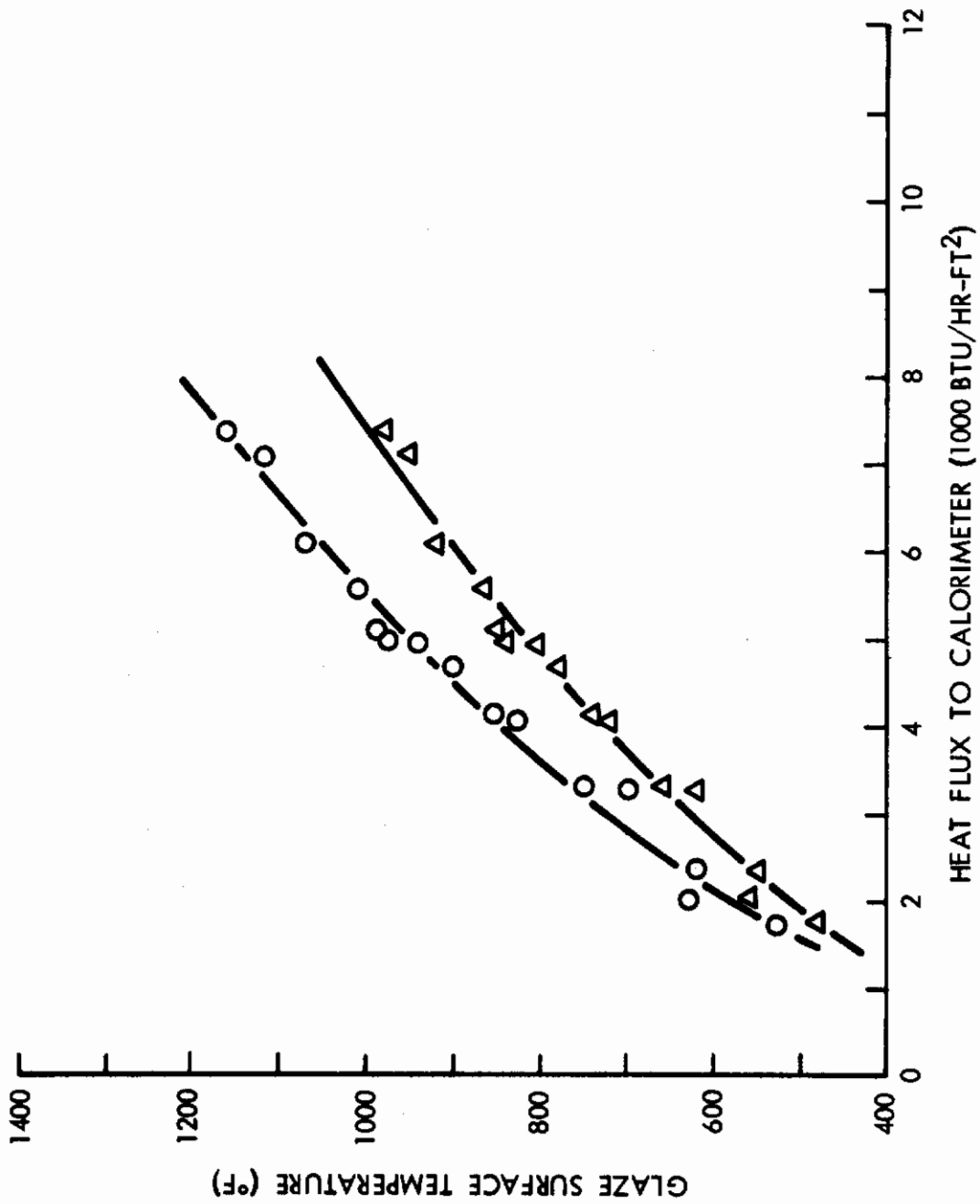
SINGLE GLAZE HEAT TRANSFER TEST

TEST NUMBER: I-23 (AIR)  
HEAT SOURCE: RADIATION  
GLAZE: 3/8" FUSED SILICA - NO COATINGS



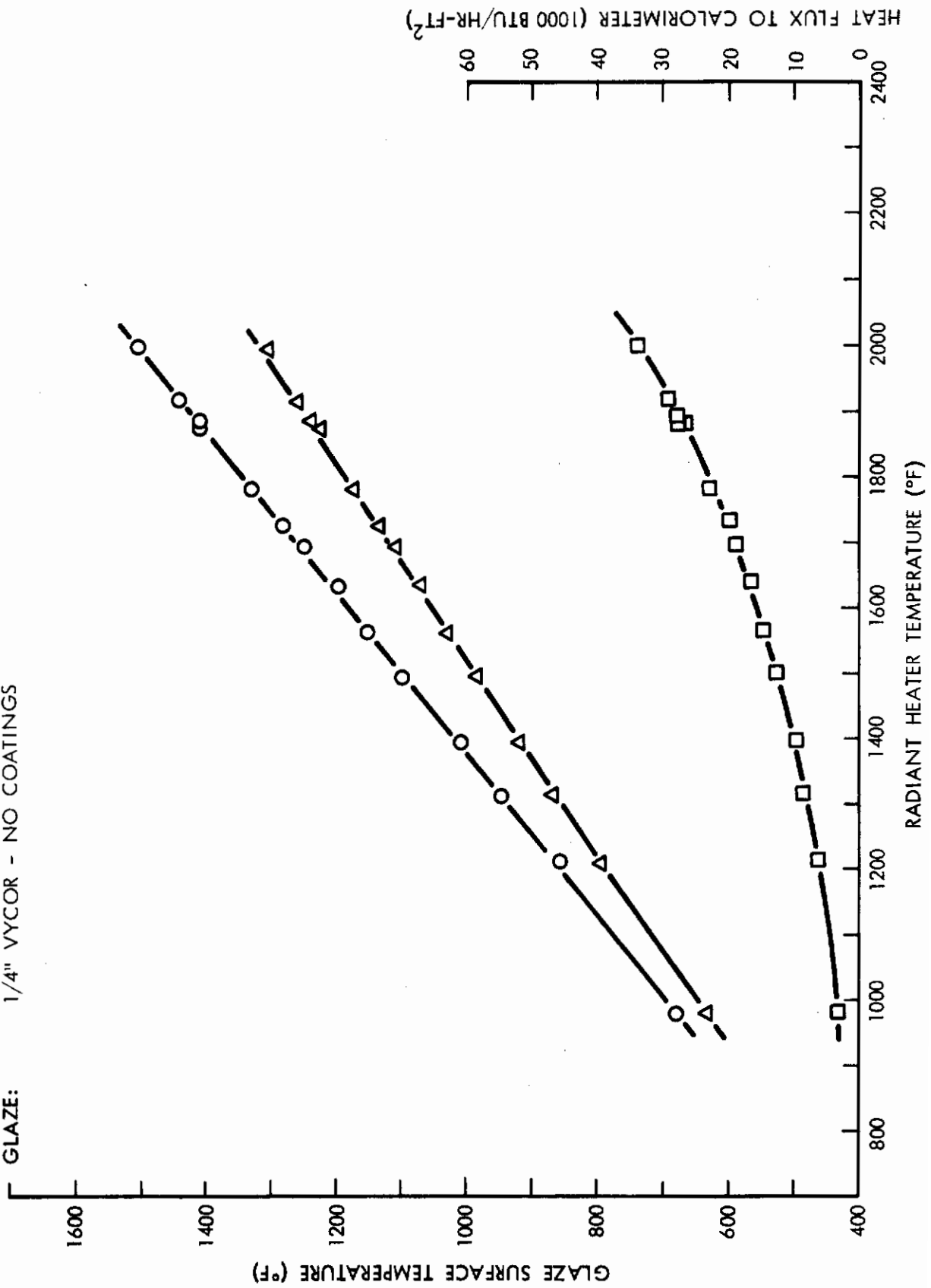
SINGLE GLAZE HEAT TRANSFER TEST

TEST NUMBER: 1-21 (AIR)  
HEAT SOURCE: CONVECTION  
GLAZE: 3/8" FUSED SILICA - NO COATINGS



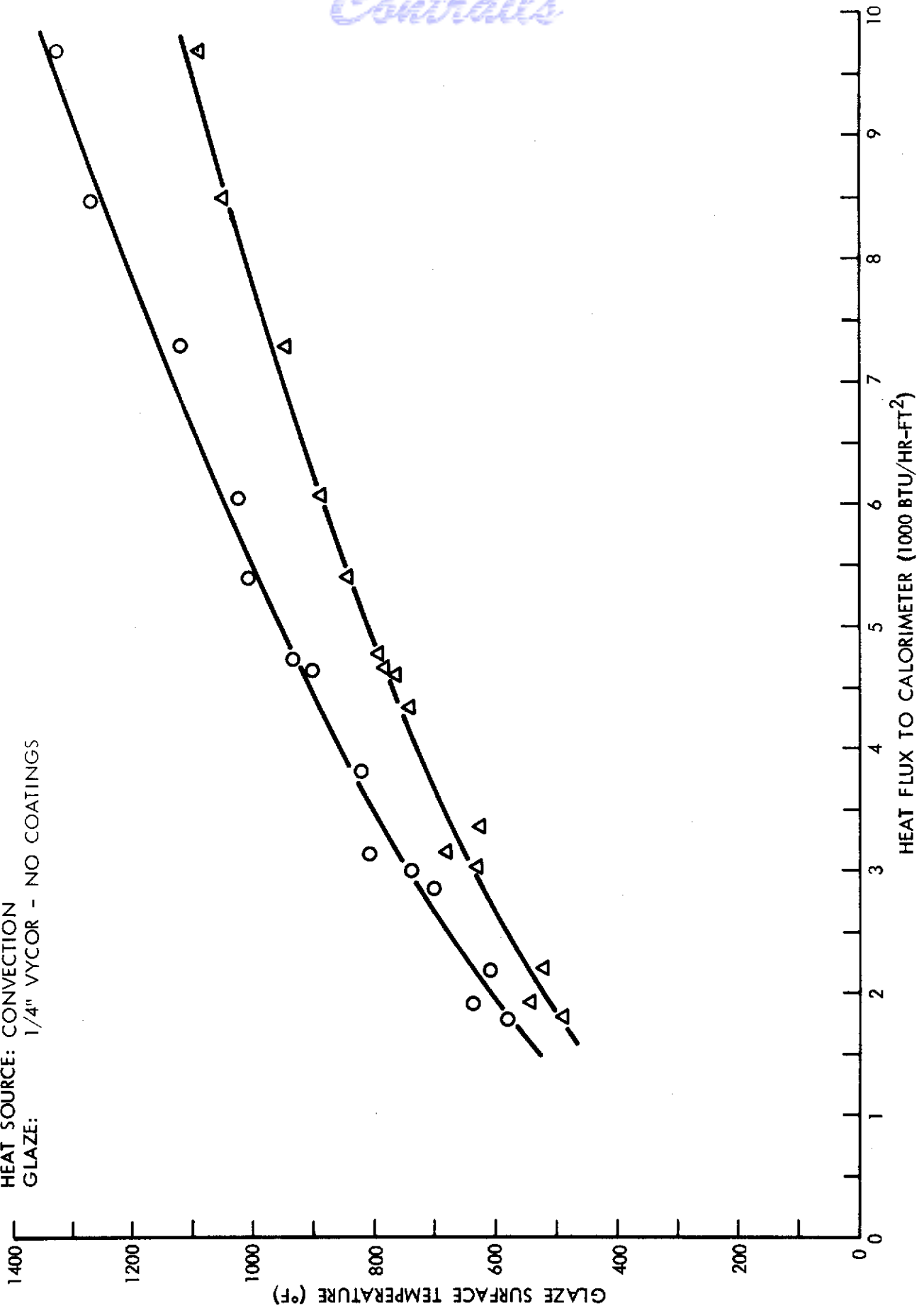
SINGLE GLAZE HEAT TRANSFER TEST

TEST NUMBER: 11-11 (AIR)  
HEAT SOURCE: RADIATION  
GLAZE: 1/4" VYCOR - NO COATINGS



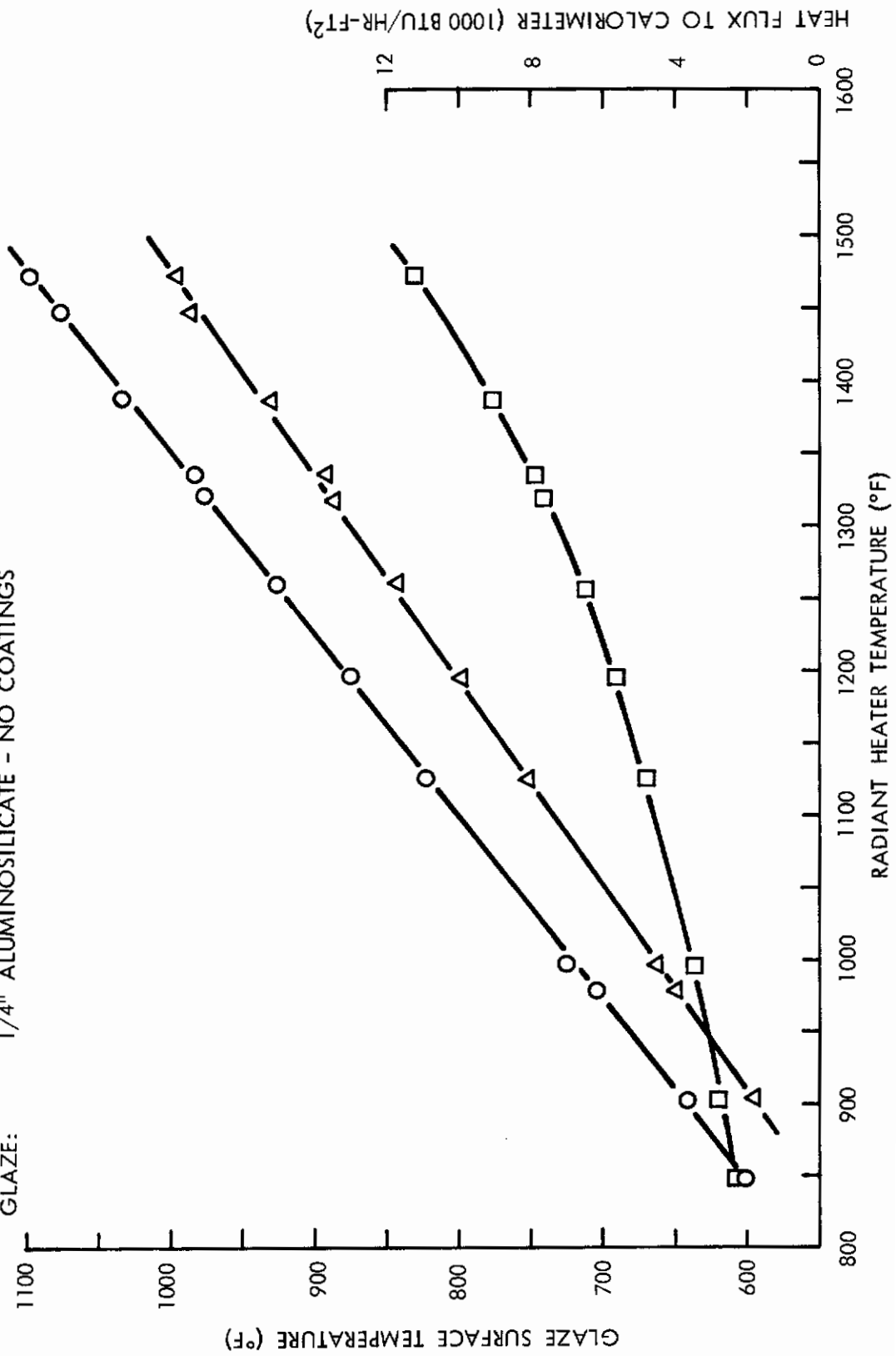
SINGLE GLAZE HEAT TRANSFER TEST

TEST NUMBER: 1-12 (AIR)  
HEAT SOURCE: CONVECTION  
GLAZE: 1/4" VYCOR - NO COATINGS



SINGLE GLAZE HEAT TRANSFER TEST

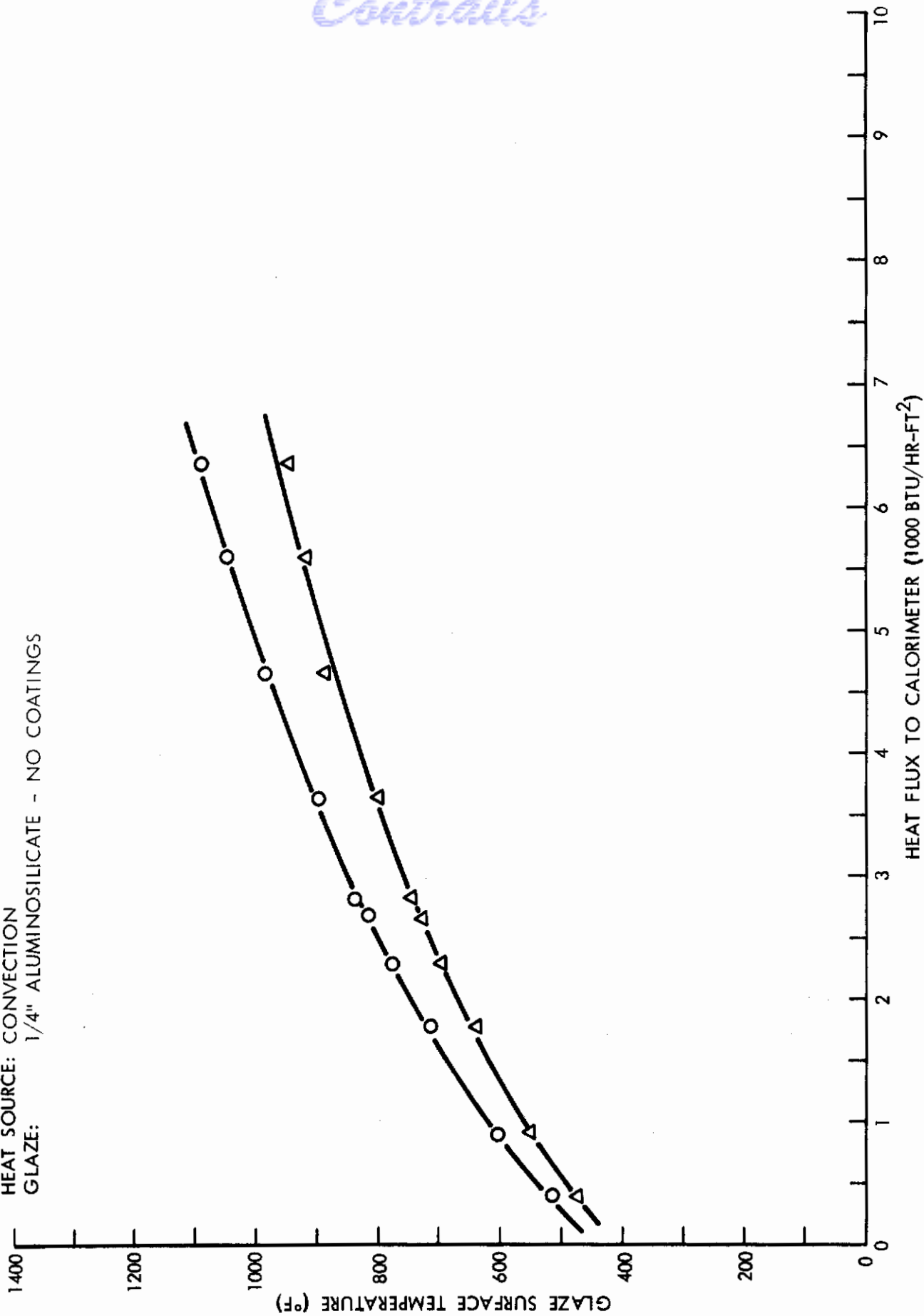
TEST NUMBER: I-14 (AIR)  
HEAT SOURCE: RADIATION  
GLAZE: 1/4" ALUMINOSILICATE - NO COATINGS





SINGLE GLAZE HEAT TRANSFER TEST

TEST NUMBER: 1-15 (AIR)  
HEAT SOURCE: CONVECTION  
GLAZE: 1/4" ALUMINOSILICATE - NO COATINGS



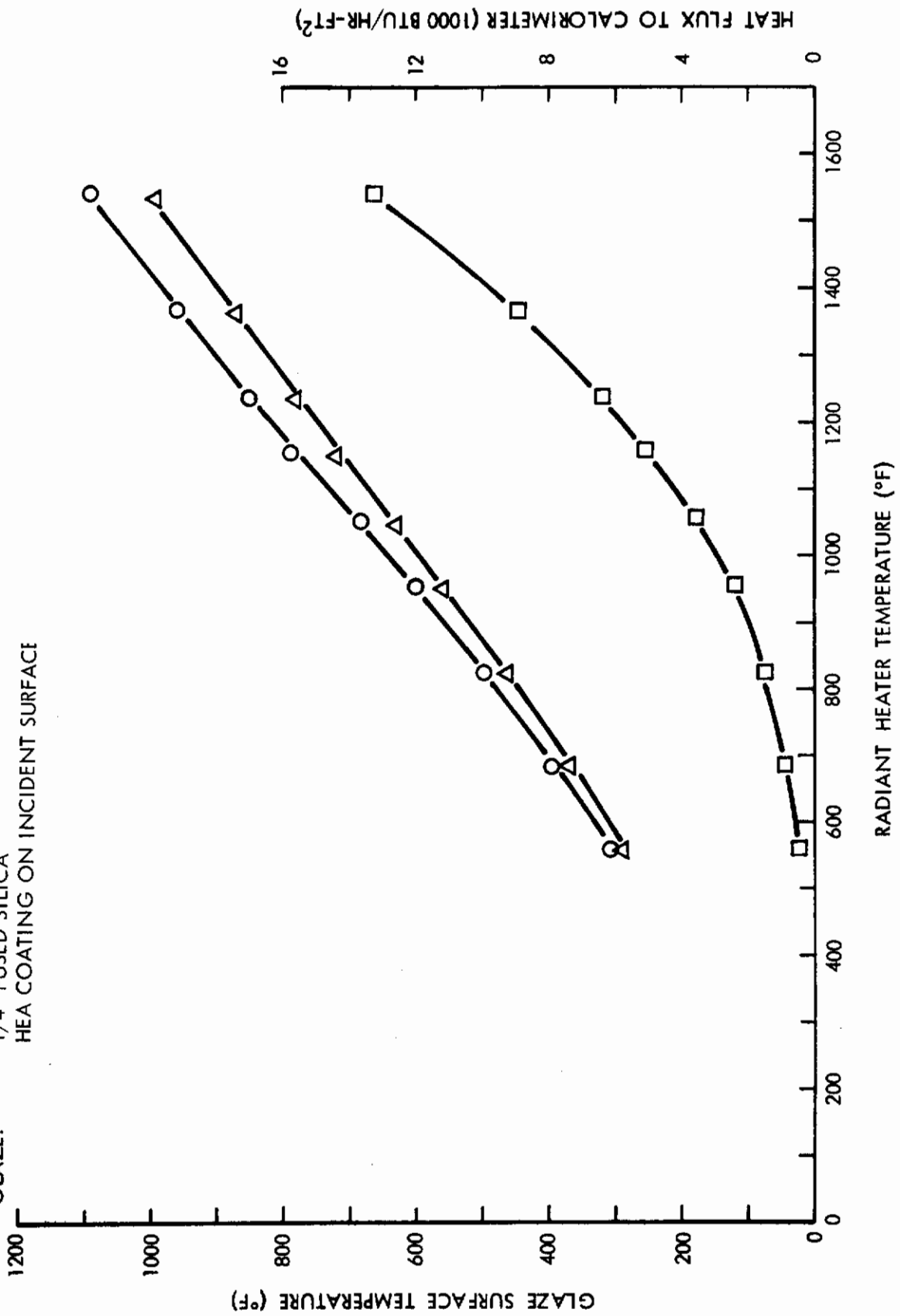
SINGLE GLAZE HEAT TRANSFER TEST

TEST NUMBER: 11-69 (AIR)

HEAT SOURCE: RADIATION

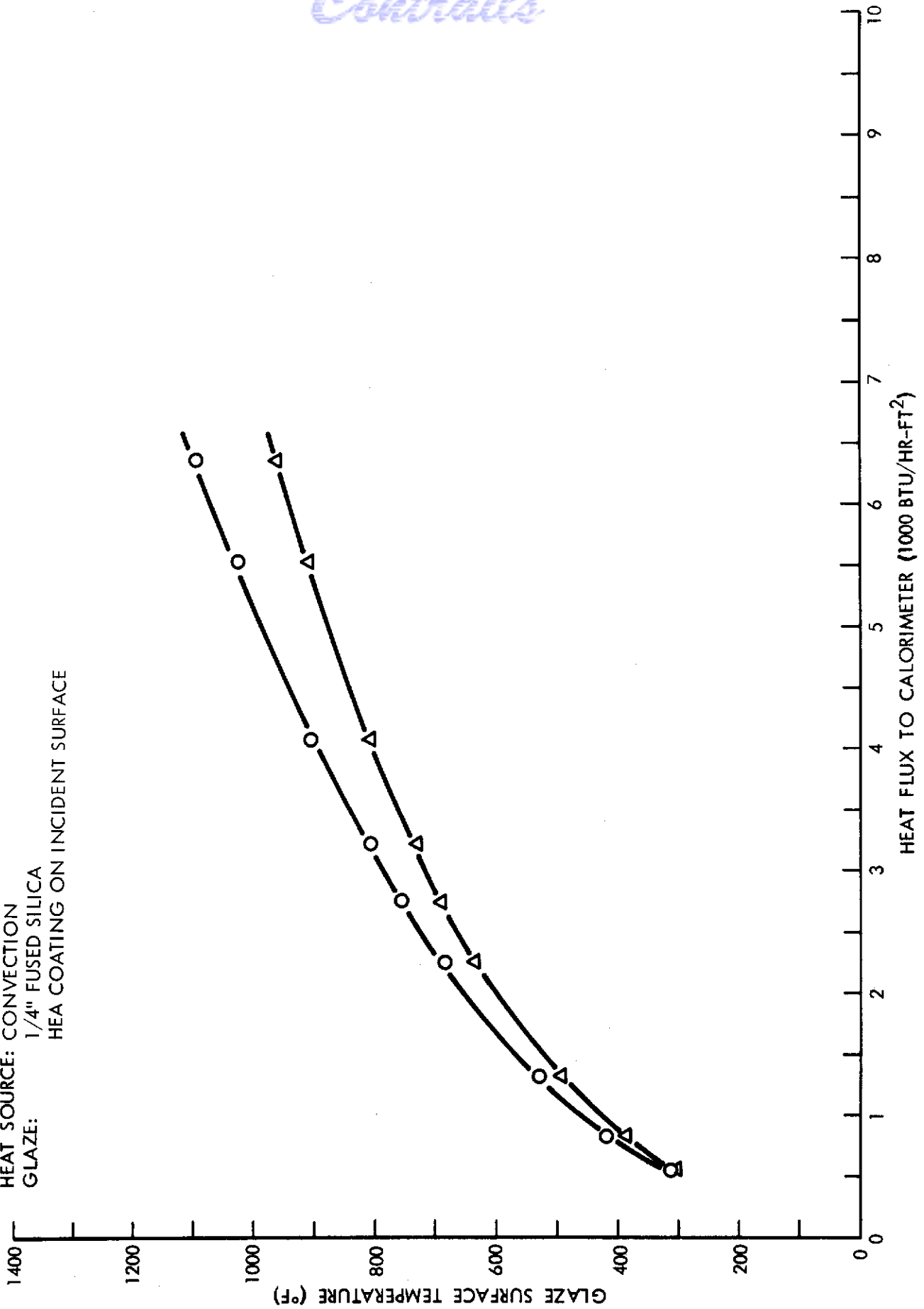
GLAZE: 1/4" FUSED SILICA

HEA COATING ON INCIDENT SURFACE



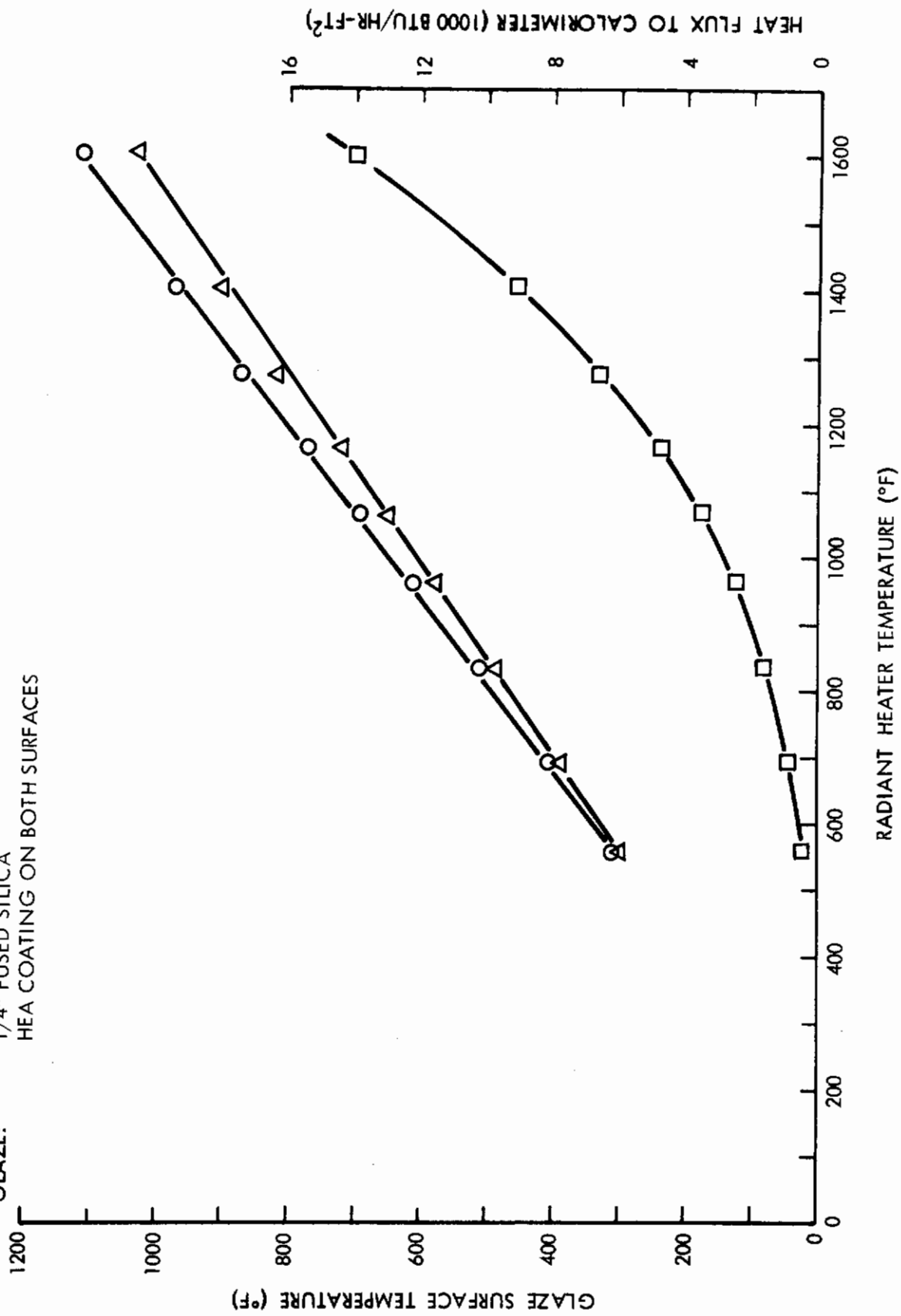
SINGLE GLAZE HEAT TRANSFER TEST

TEST NUMBER: II-68 (AIR)  
HEAT SOURCE: CONVECTION  
GLAZE: 1/4" FUSED SILICA  
HEA COATING ON INCIDENT SURFACE



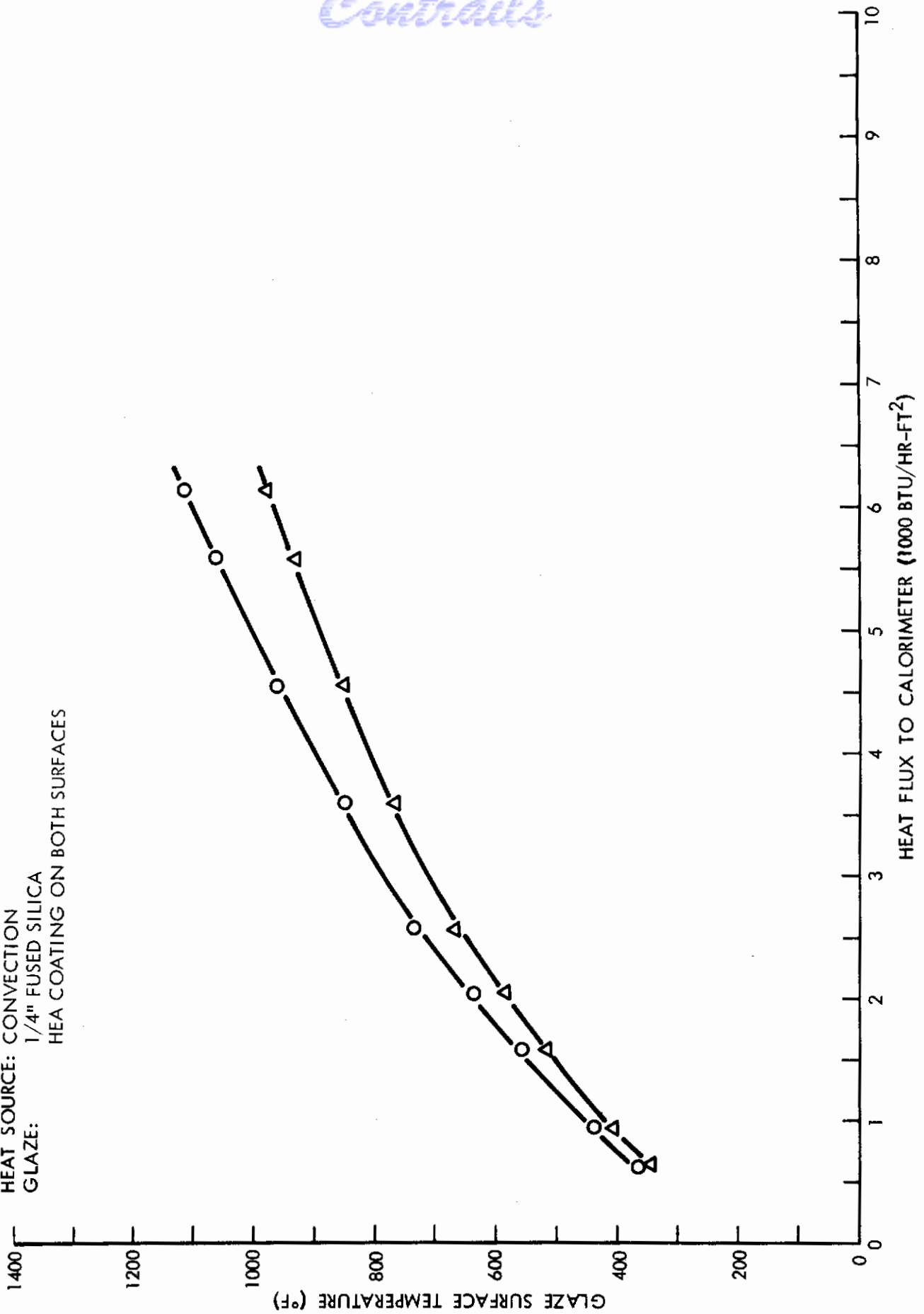
SINGLE GLAZE HEAT TRANSFER TEST

TEST NUMBER: II-81 (AIR)  
HEAT SOURCE: RADIATION  
GLAZE: 1/4" FUSED SILICA  
HEA COATING ON BOTH SURFACES



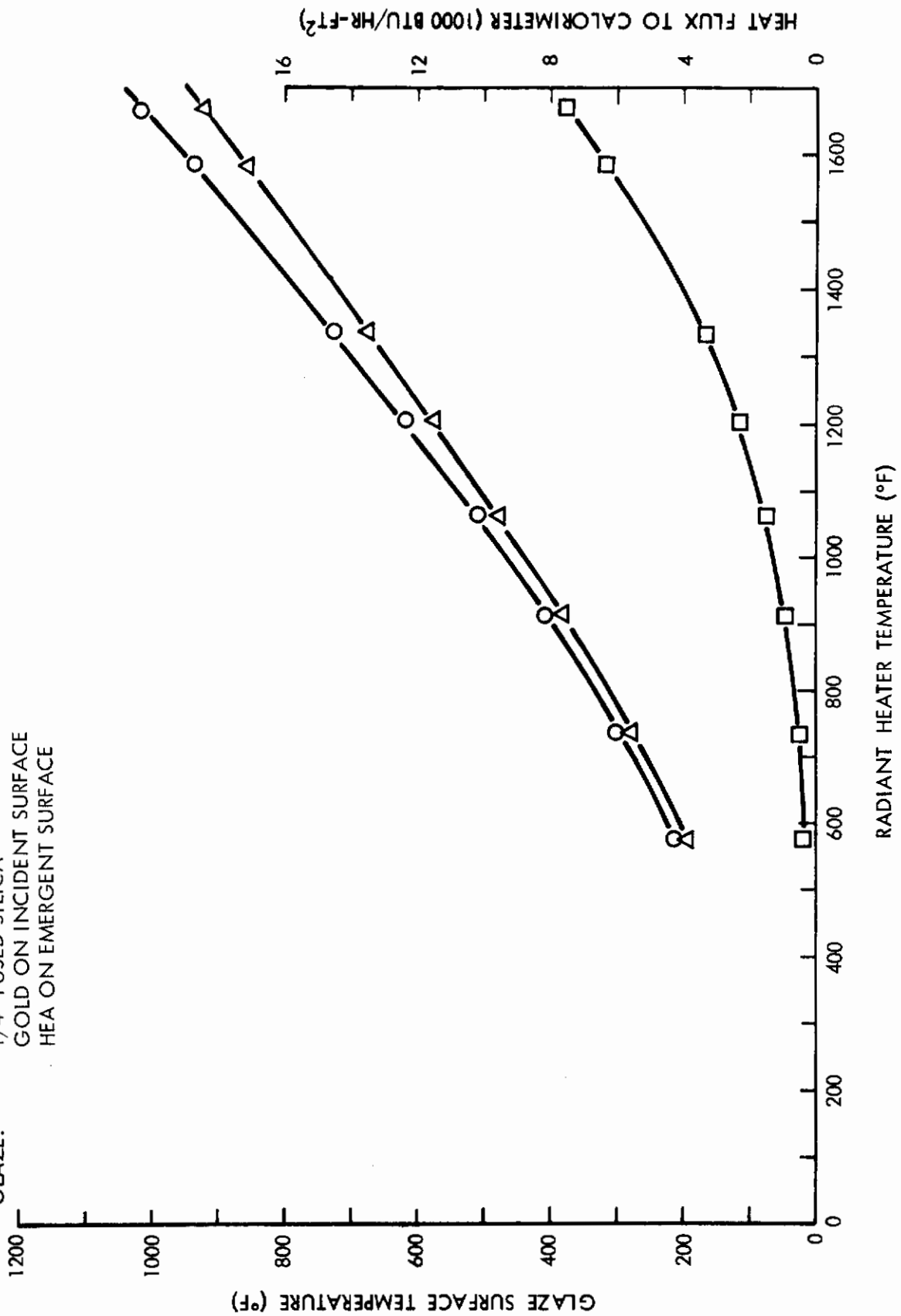
SINGLE GLAZE HEAT TRANSFER TEST

TEST NUMBER: 11-82 (AIR)  
HEAT SOURCE: CONVECTION  
GLAZE: 1/4" FUSED SILICA  
HEA COATING ON BOTH SURFACES



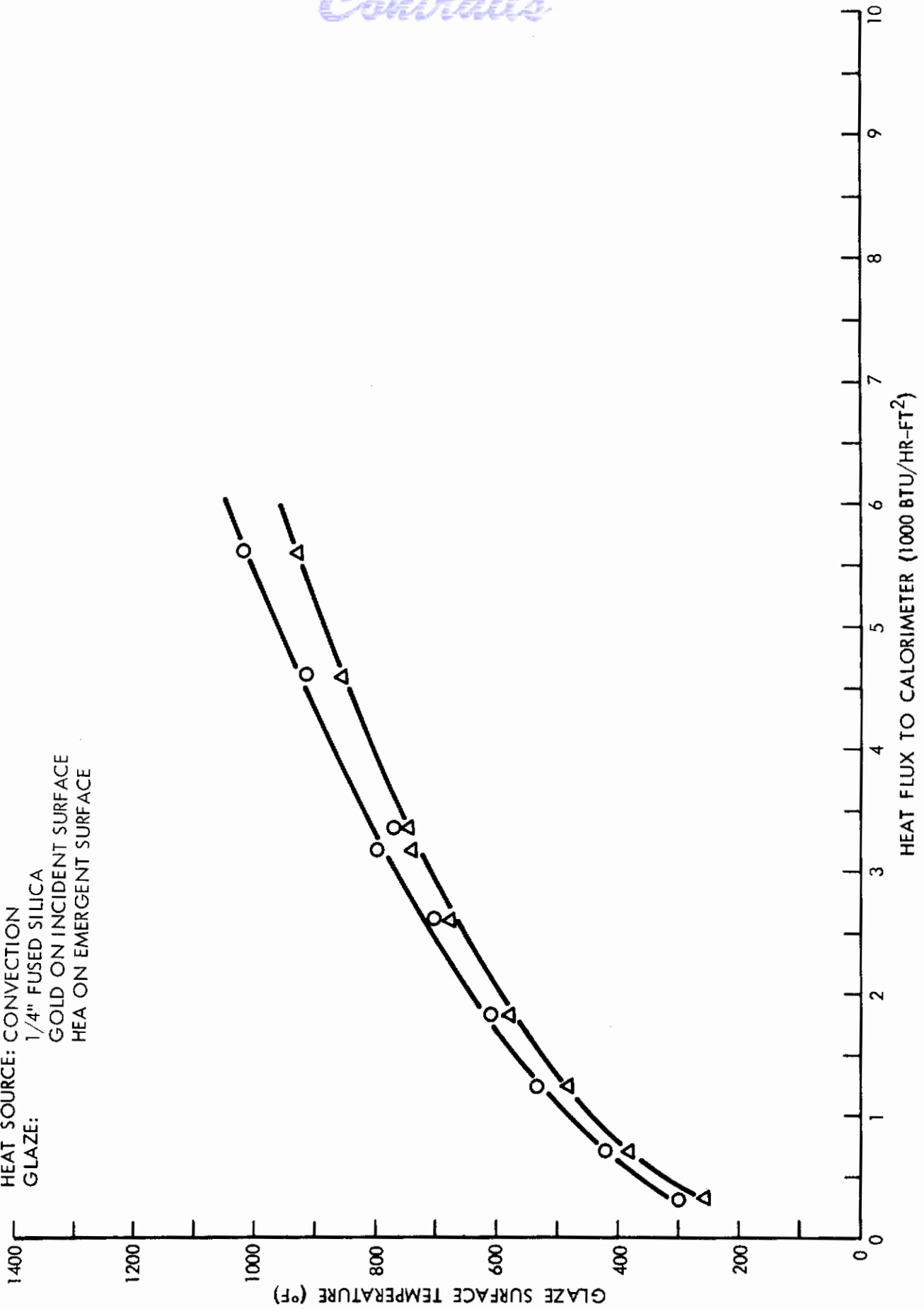
SINGLE GLAZE HEAT TRANSFER TEST

TEST NUMBER: II-76 (AIR)  
HEAT SOURCE: RADIATION  
GLAZE: 1/4" FUSED SILICA  
GOLD ON INCIDENT SURFACE  
HEA ON EMERGENT SURFACE



SINGLE GLAZE HEAT TRANSFER TEST

TEST NUMBER: II-77 (AIR)  
HEAT SOURCE: CONVECTION  
GLAZE: 1/4" FUSED SILICA  
GOLD ON INCIDENT SURFACE  
HEA ON EMERGENT SURFACE



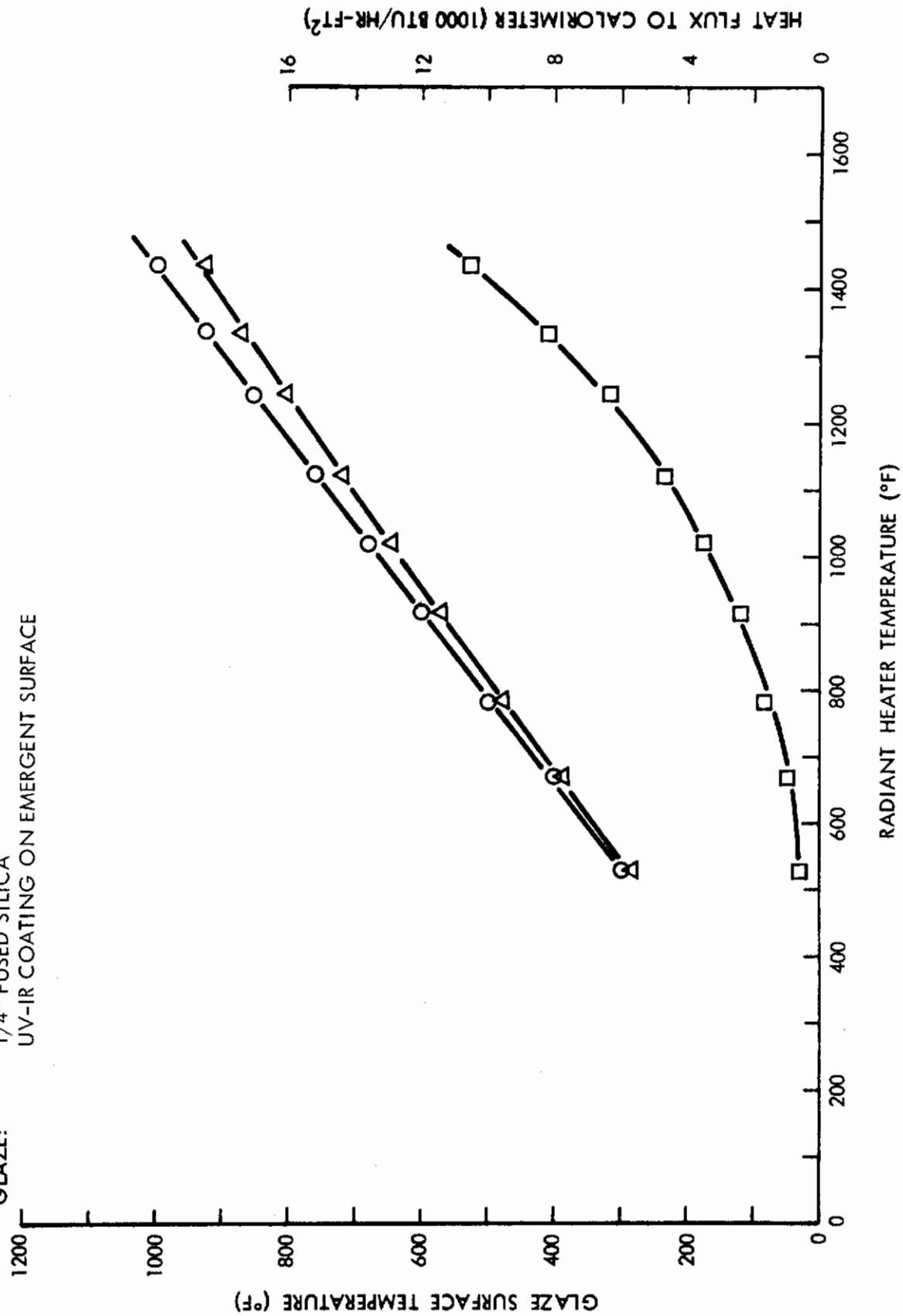
SINGLE GLAZE HEAT TRANSFER TEST

TEST NUMBER: 11-55

HEAT SOURCE: RADIATION

GLAZE: 1/4" FUSED SILICA

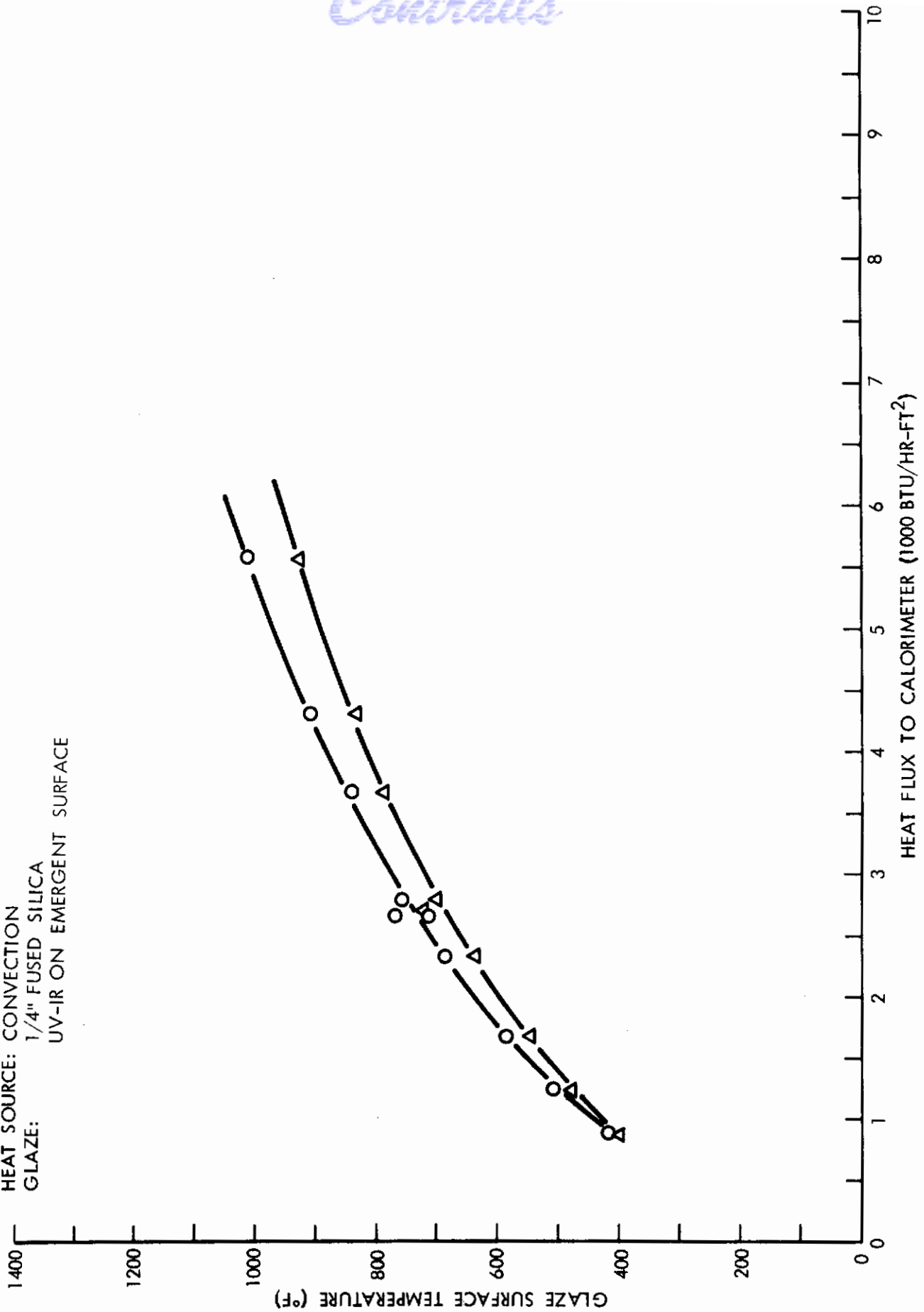
UV-IR COATING ON EMERGENT SURFACE





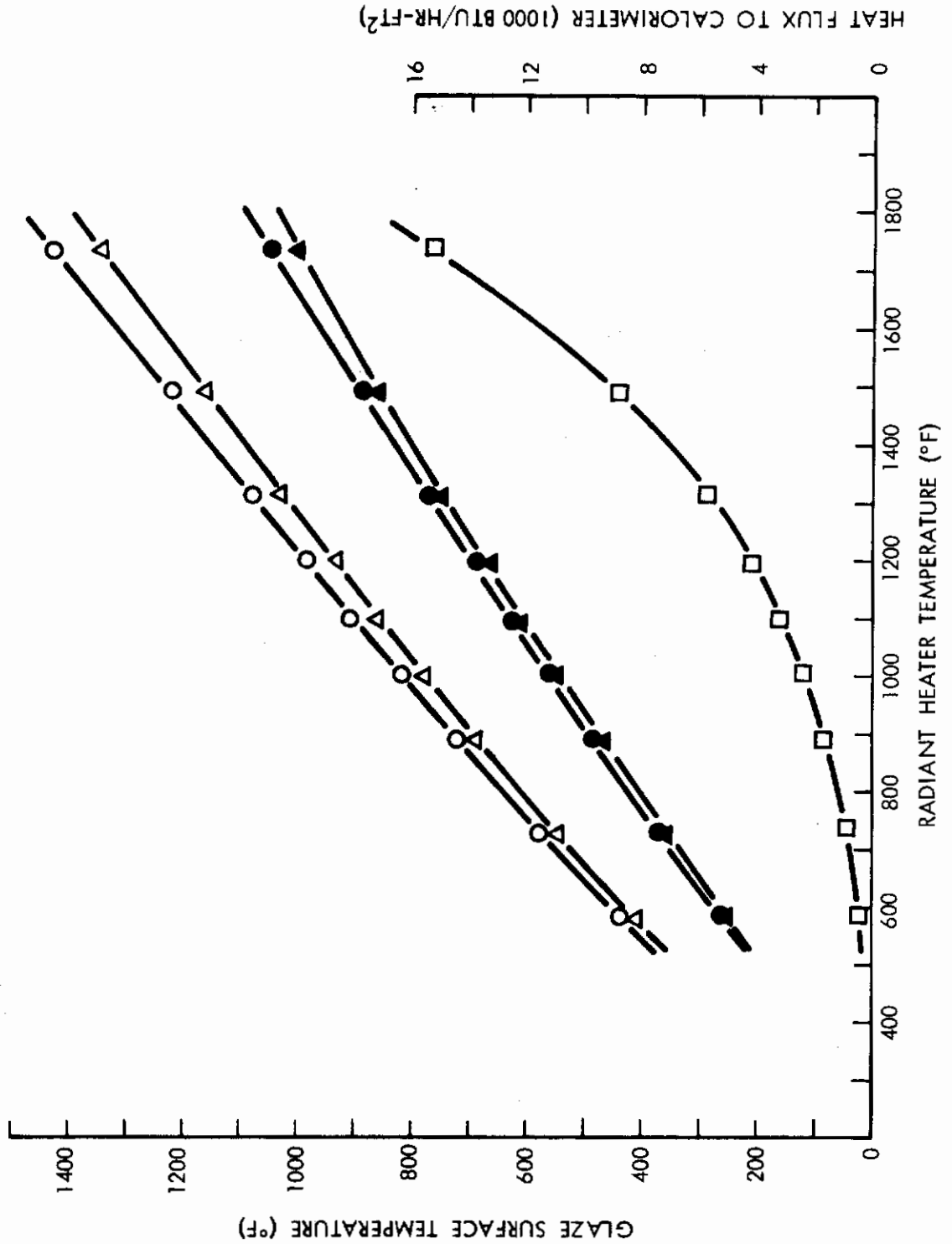
SINGLE GLAZE HEAT TRANSFER TEST

TEST NUMBER: 54  
HEAT SOURCE: CONVECTION  
GLAZE: 1/4" FUSED SILICA  
UV-IR ON EMERGENT SURFACE



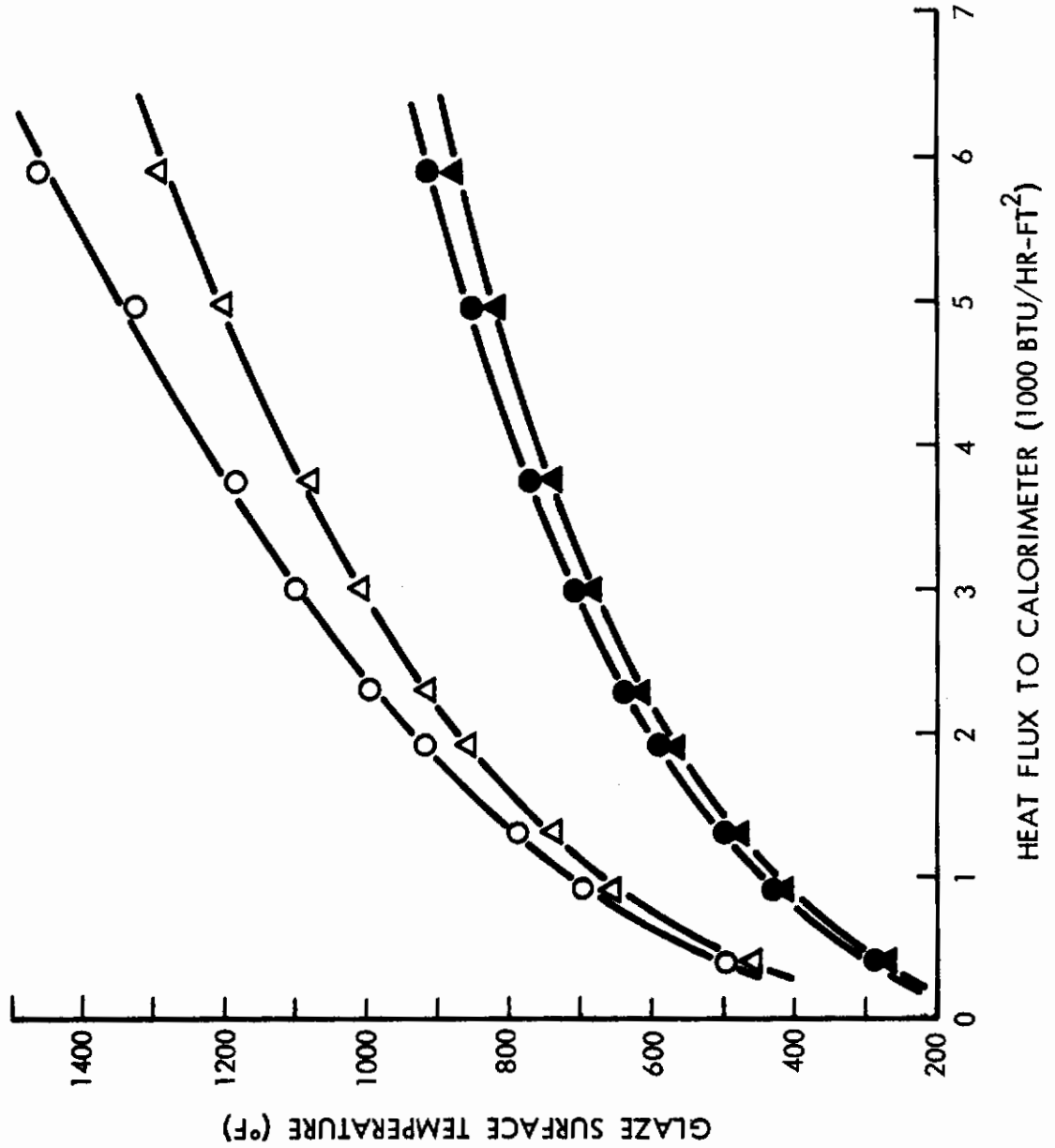
MULTIPLE GLAZE HEAT TRANSFER TEST

TEST NUMBER: III-31 (AIR)  
HEAT SOURCE: RADIATION  
OUTER GLAZE: 1/4" FUSED SILICA - NO COATING  
INNER GLAZE: 1/8" VYCOR - NO COATING



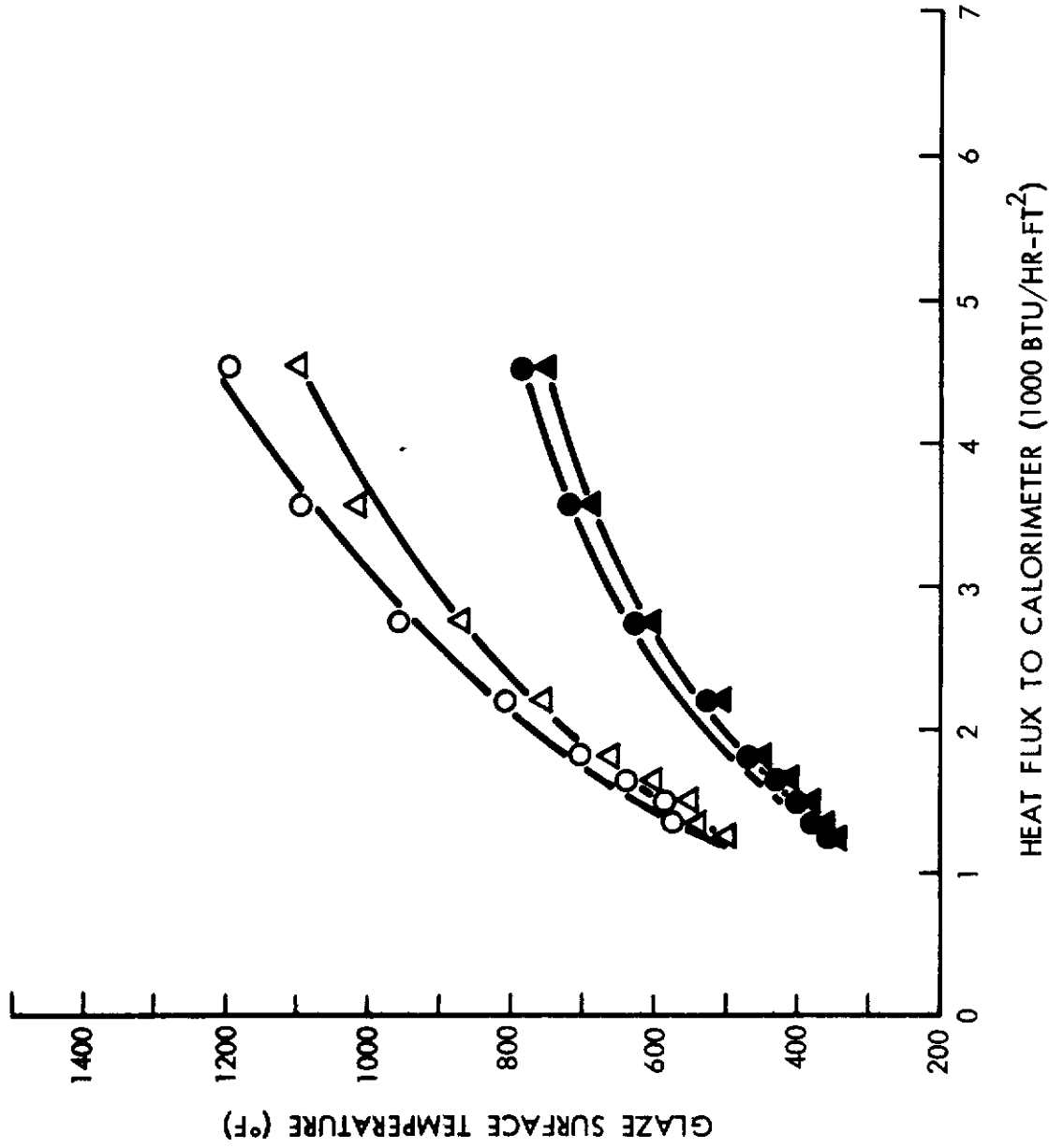
MULTIPLE GLAZE HEAT TRANSFER TEST

TEST NUMBER: III-57 (AIR)  
HEAT SOURCE: CONVECTION  
OUTER GLAZE: 1/4" FUSED SILICA - NO COATING  
INNER GLAZE: 1/8" VYCOR - NO COATING



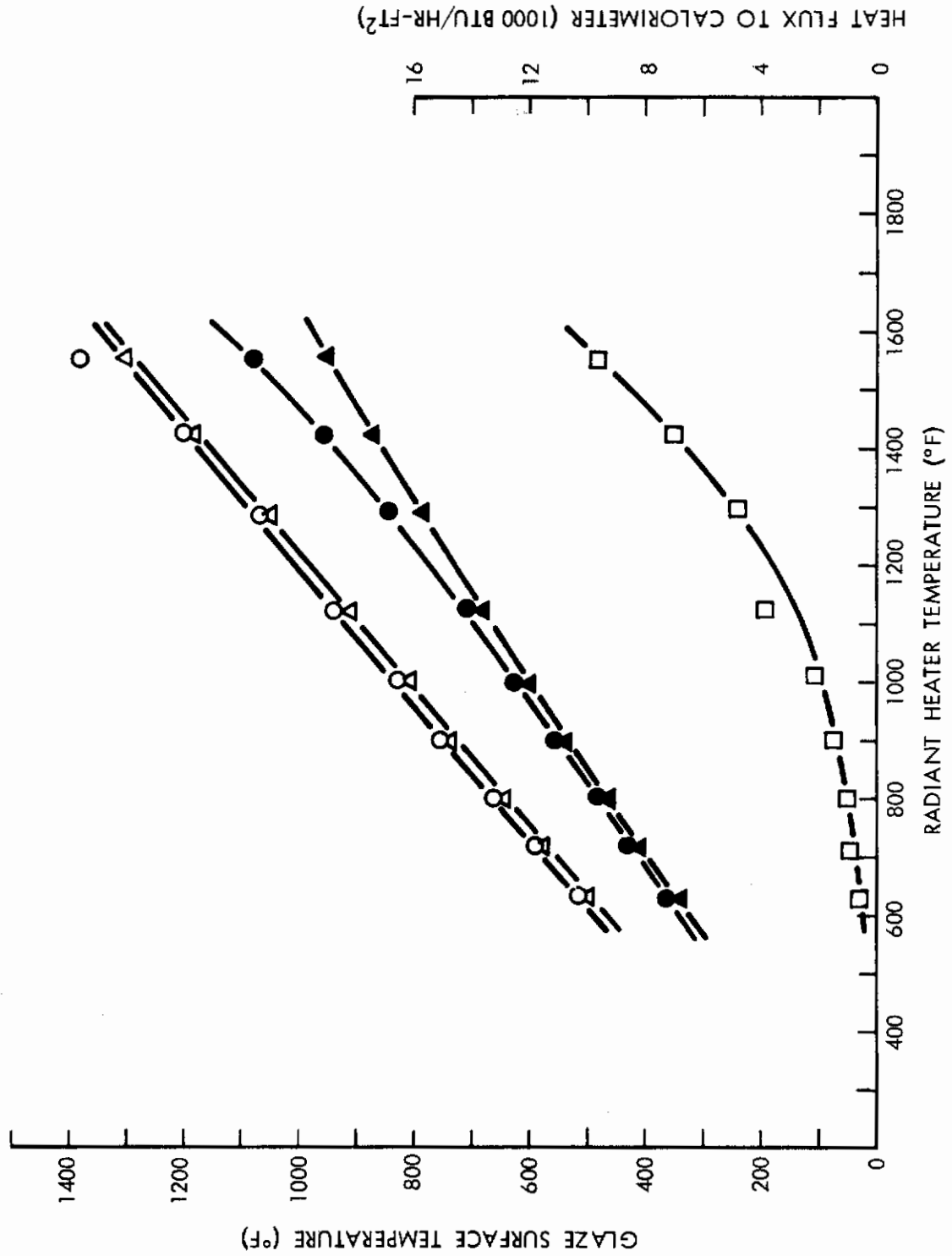
MULTIPLE GLAZE HEAT TRANSFER TEST

TEST NUMBER: III-68 (AIR)  
HEAT SOURCE: RADIATION & CONVECTION  
OUTER GLAZE: 1/4" FUSED SILICA - UNCOATED  
INNER GLAZE: 1/8" VYCOR - UNCOATED



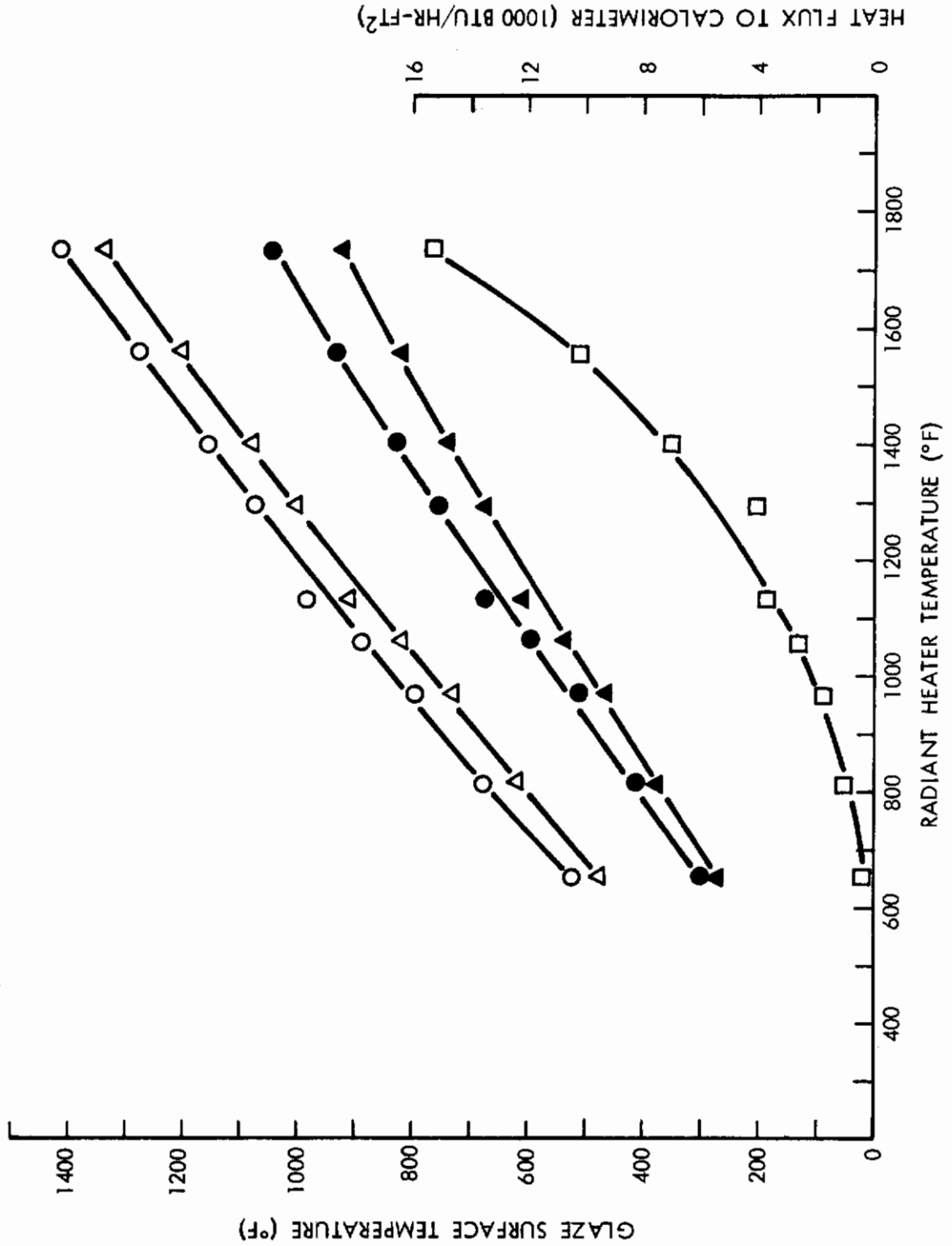
MULTIPLE GLAZE HEAT TRANSFER TEST

TEST NUMBER: III-90 (VACUUM)  
 HEAT SOURCE: RADIATION  
 OUTER GLAZE: 1/4" FUSED SILICA - NO COATING  
 INNER GLAZE: 1/8" VYCOR - NO COATING



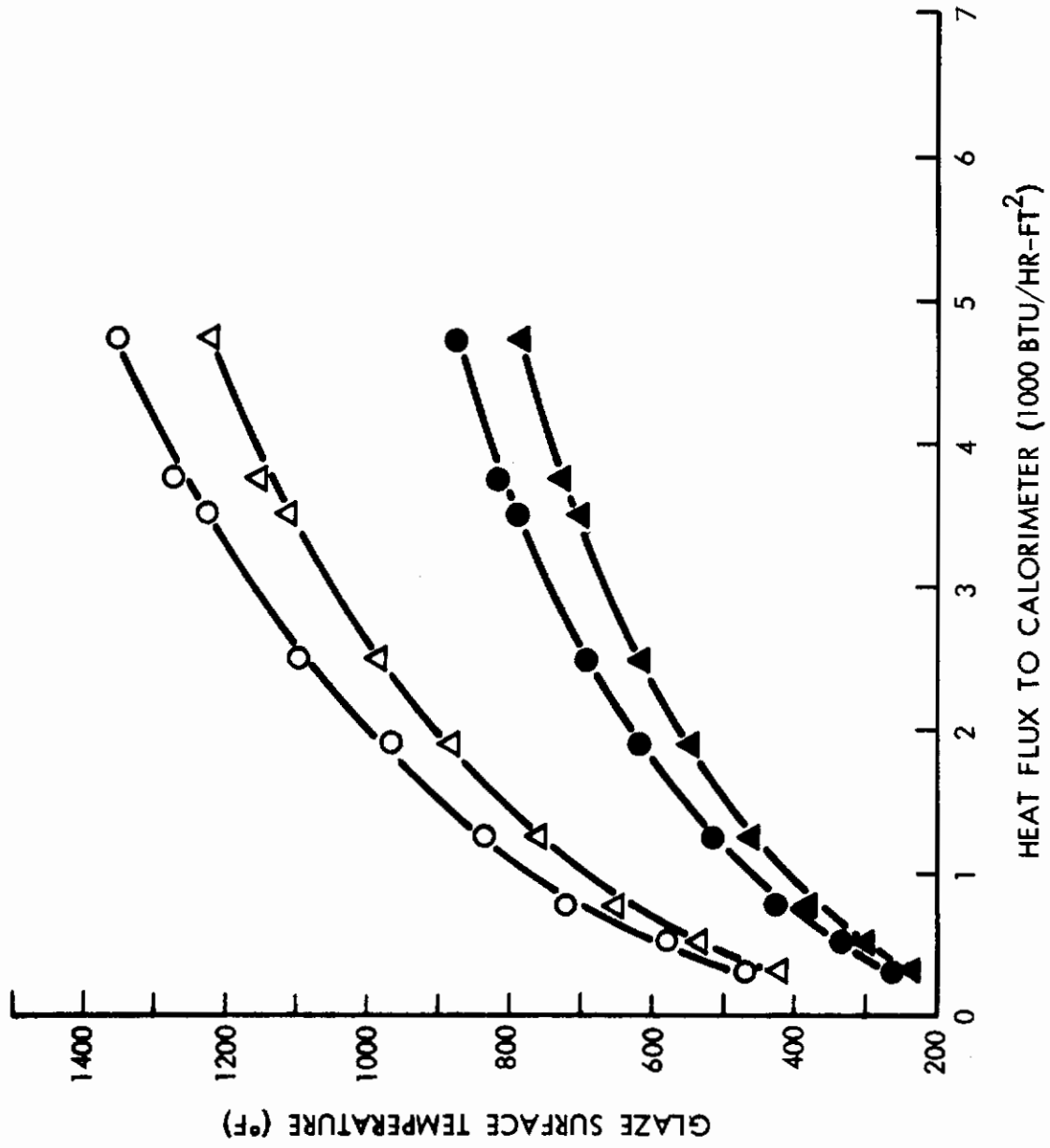
MULTIPLE GLAZE HEAT TRANSFER TEST

TEST NUMBER: III-24 (AIR)  
HEAT SOURCE: RADIATION  
OUTER GLAZE: 1/4" FUSED SILICA - NO COATING  
INNER GLAZE: 3/8" FUSED SILICA - NO COATING



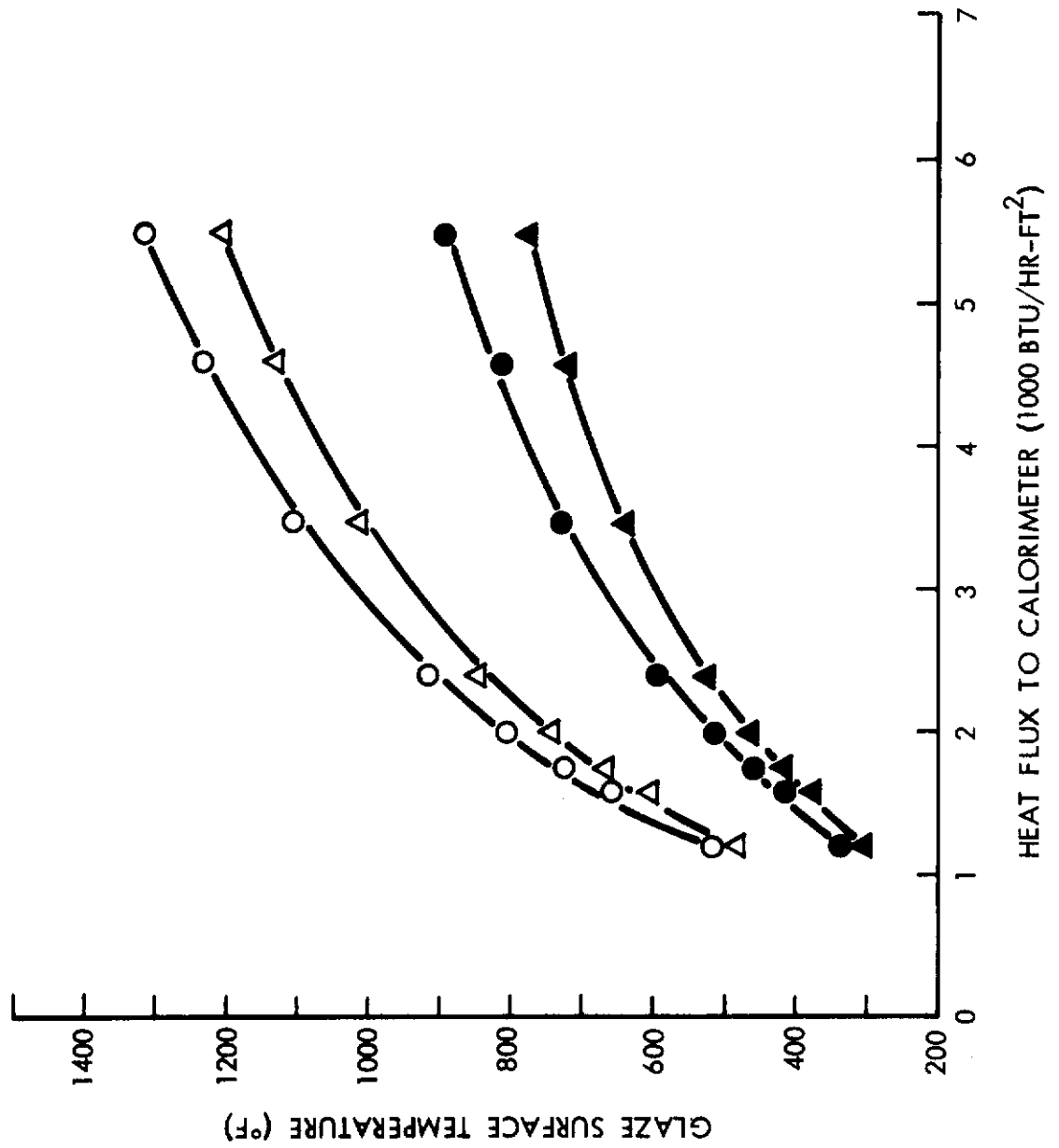
MULTIPLE GLAZE HEAT TRANSFER TEST

TEST NUMBER: III-23 (AIR)  
HEAT SOURCE: CONVECTION  
OUTER GLAZE: 1/4" FUSED SILICA - NO COATING  
INNER GLAZE: 3/8" FUSED SILICA - NO COATING



MULTIPLE GLAZE HEAT TRANSFER TEST

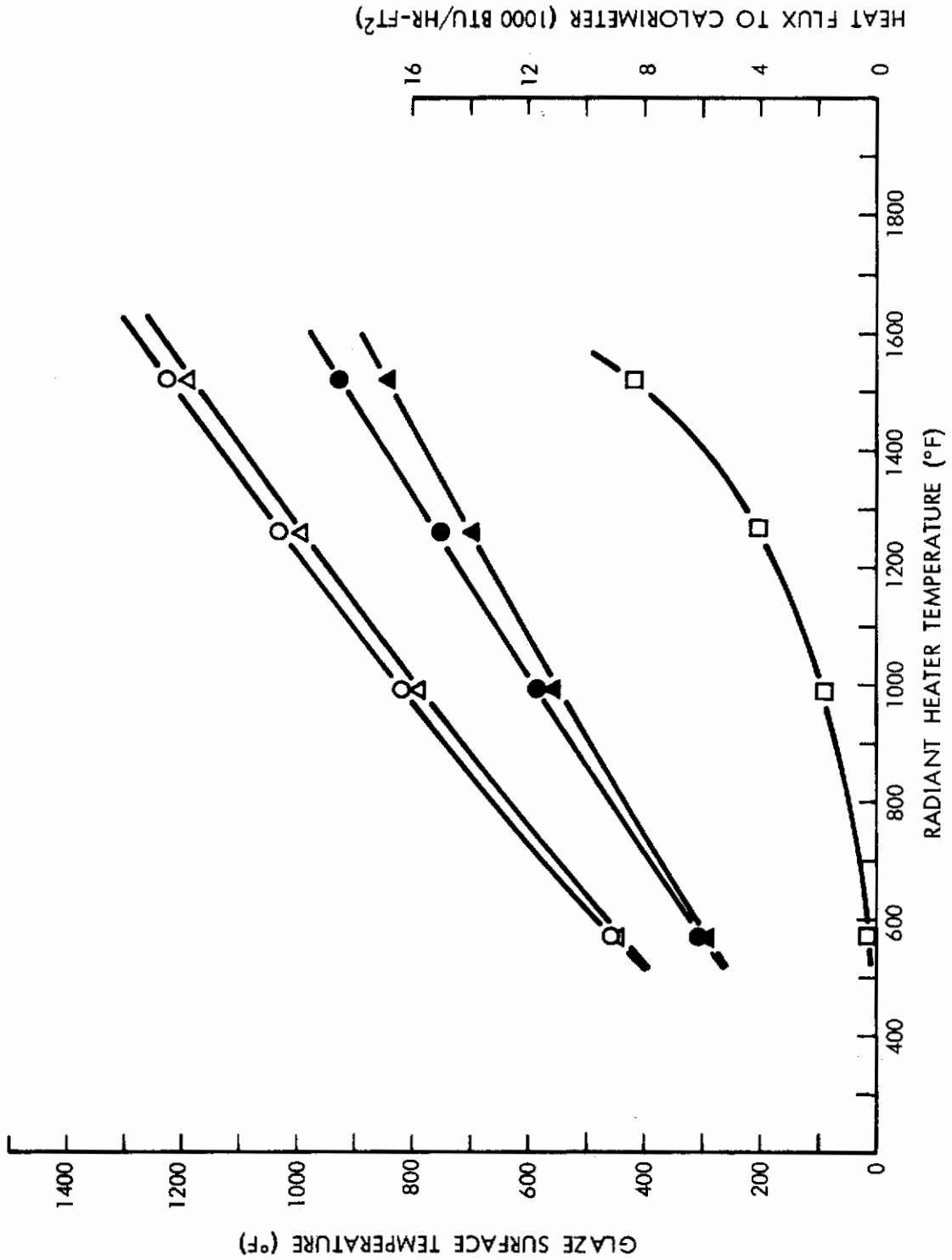
TEST NUMBER: III-22 (AIR)  
HEAT SOURCE: RADIATION & CONVECTION  
OUTER GLAZE: 1/4" FUSED SILICA - NO COATING  
INNER GLAZE: 3/8" FUSED SILICA - NO COATING





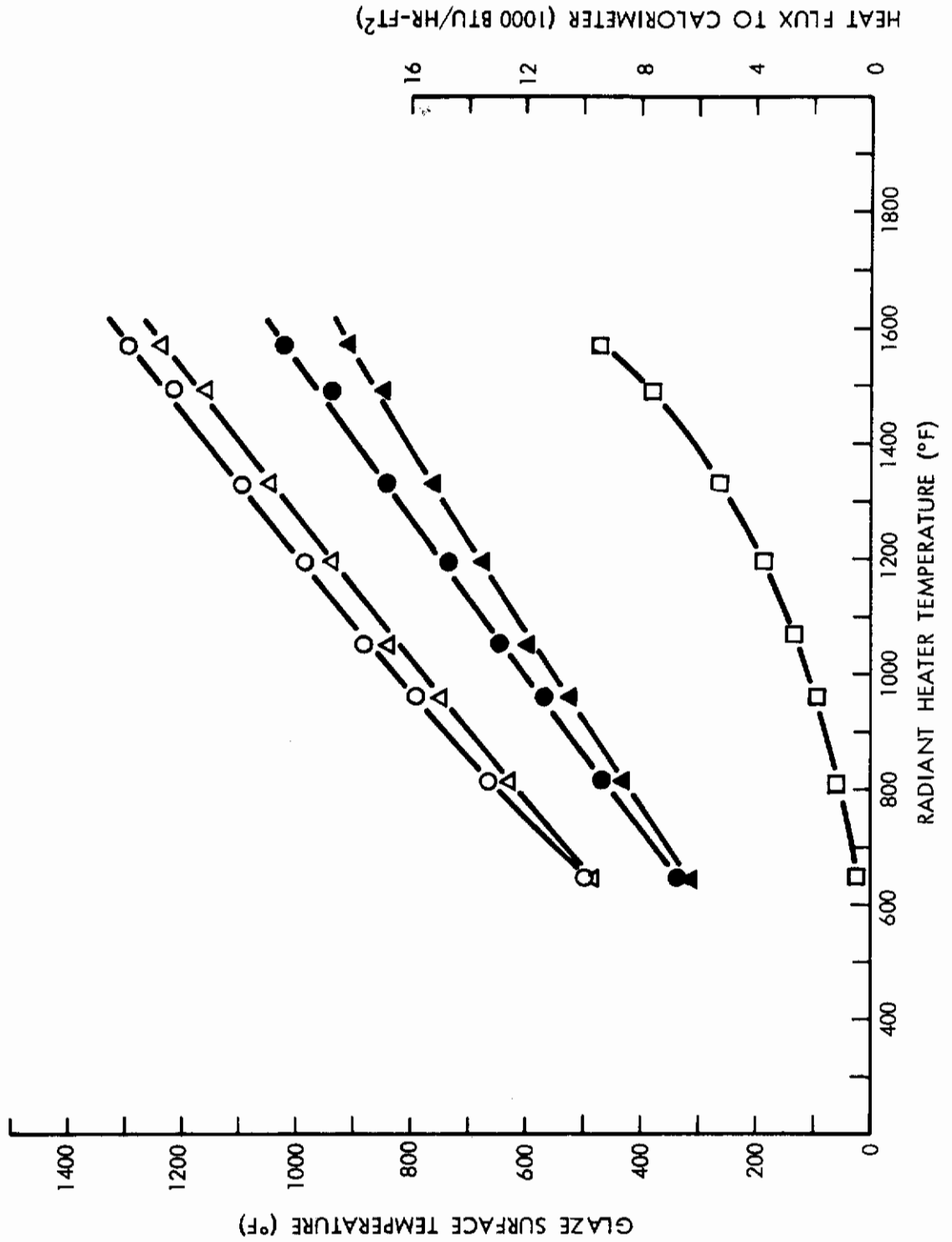
MULTIPLE GLAZE HEAT TRANSFER TEST

TEST NUMBER: III-104 (VACUUM)  
 HEAT SOURCE: RADIATION  
 OUTER GLAZE: 1/4" FUSED SILICA - NO COATING  
 INNER GLAZE: 3/8" FUSED SILICA - NO COATING



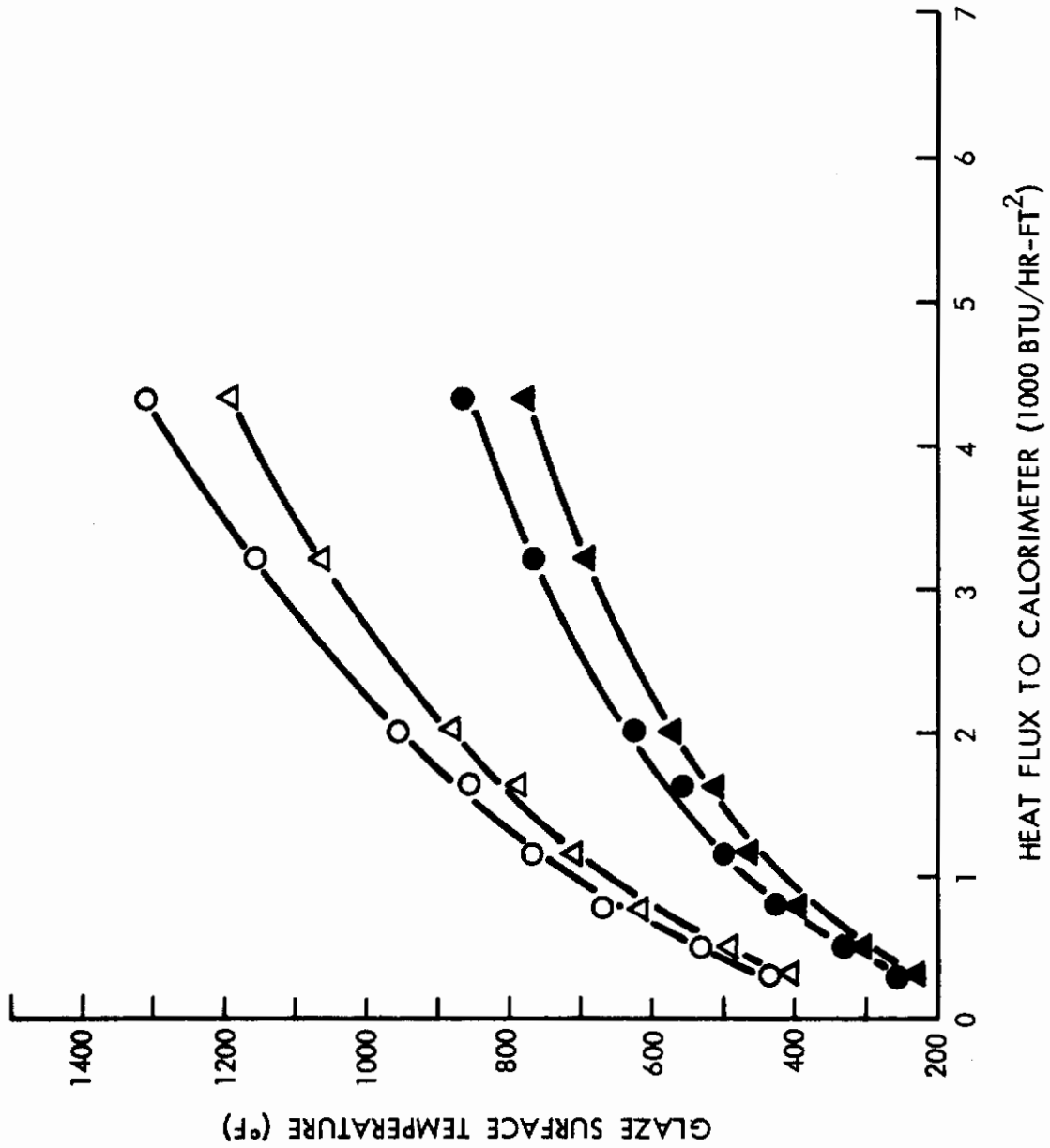
MULTIPLE GLAZE HEAT TRANSFER TEST

TEST NUMBER: III-19 (AIR)  
HEAT SOURCE: RADIATION  
OUTER GLAZE: 1/4" FUSED SILICA - NO COATING  
INNER GLAZE: 1/4" ALUM. - NO COATING



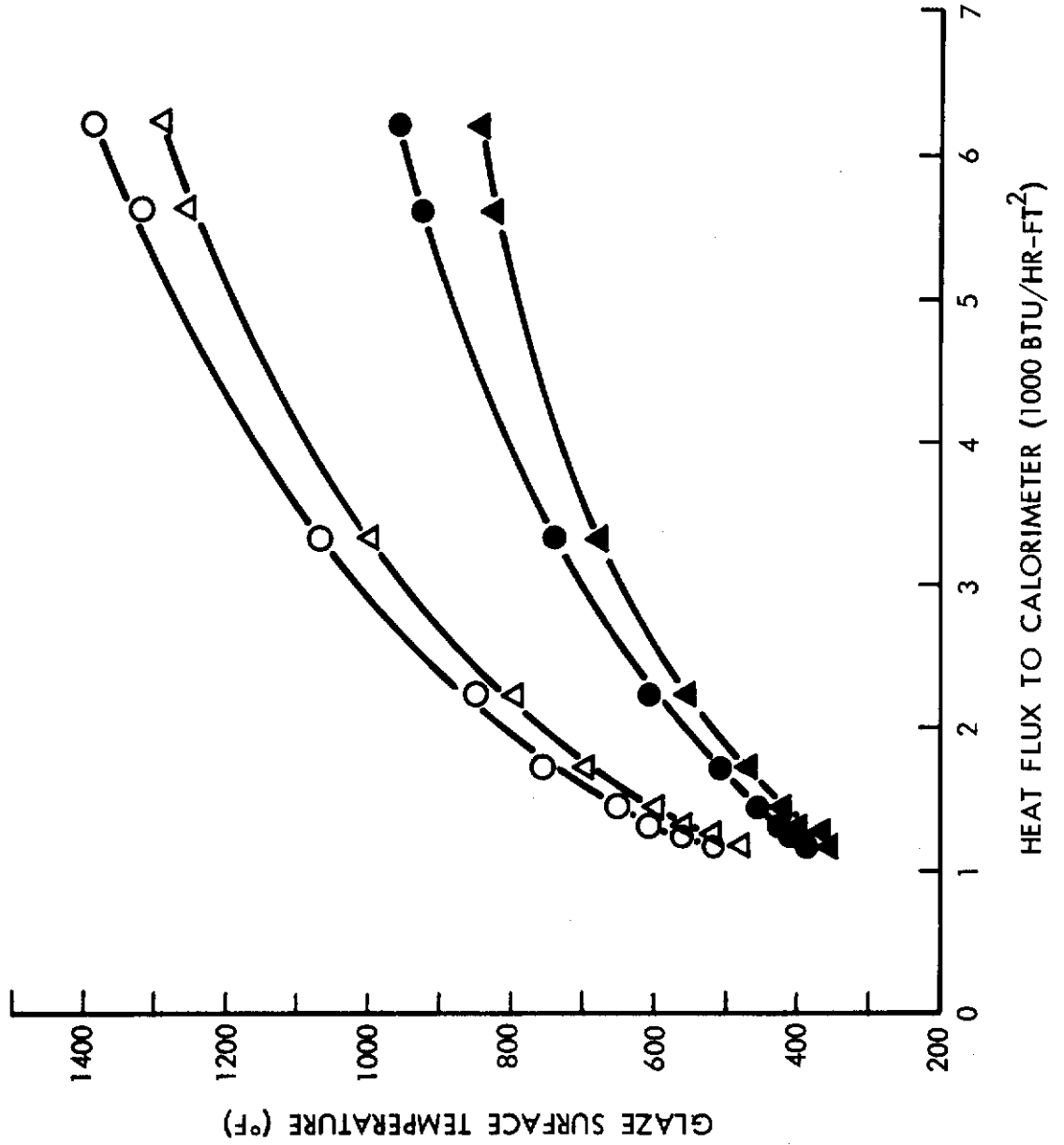
MULTIPLE GLAZE HEAT TRANSFER TEST

TEST NUMBER: III-20 (AIR)  
HEAT SOURCE: CONVECTION  
OUTER GLAZE: 1/4" FUSED SILICA - NO COATING  
INNER GLAZE: 1/4" ALUMINOSILICATE - NO COATING



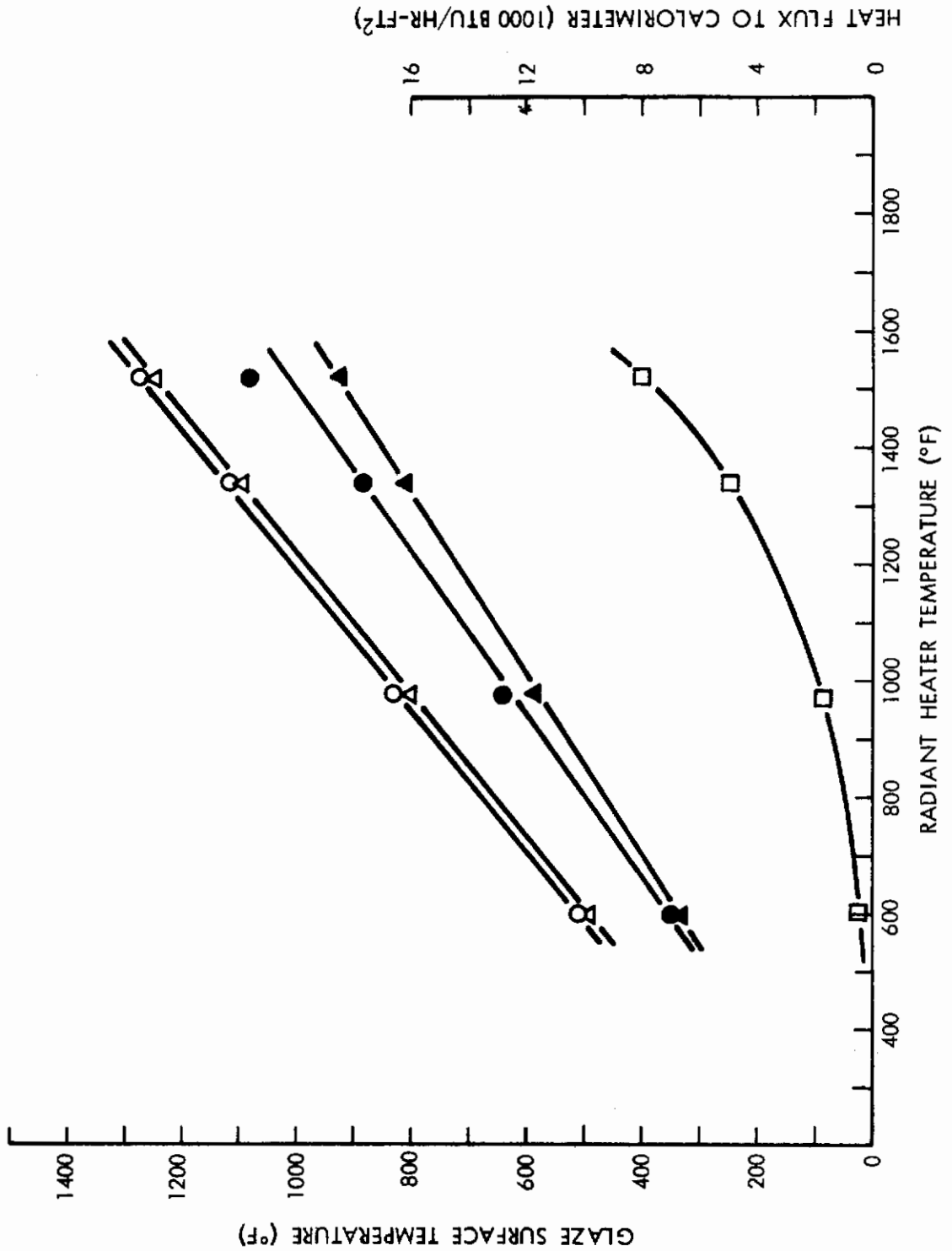
MULTIPLE GLAZE HEAT TRANSFER TEST

TEST NUMBER: III-21 (AIR)  
HEAT SOURCE: RADIATION & CONVECTION  
OUTER GLAZE: 1/4" FUSED SILICA - NO COATING  
INNER GLAZE: 1/4" ALUMINOSILICATE - NO COATING



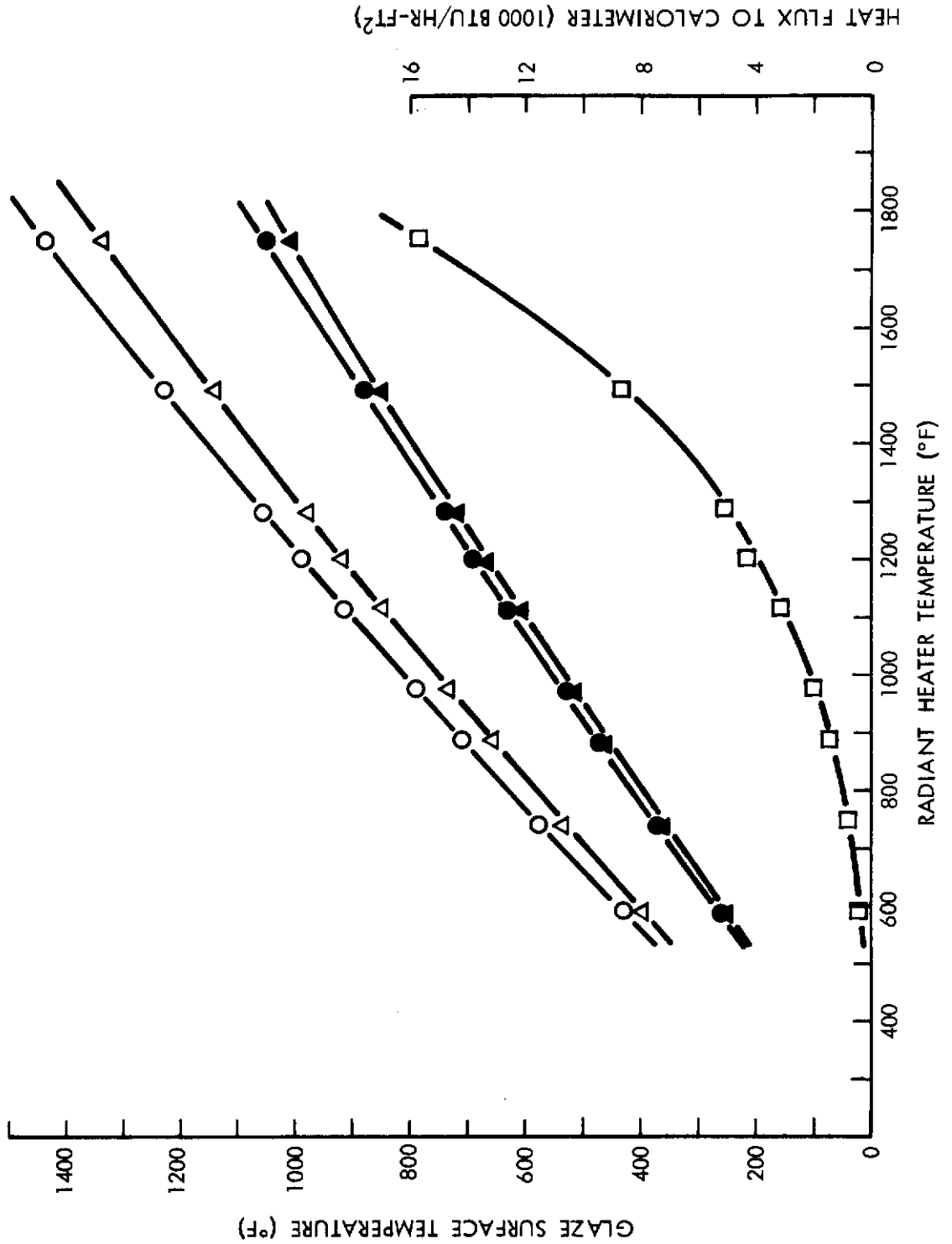
MULTIPLE GLAZE HEAT TRANSFER TEST

TEST NUMBER: III-105 (VACUUM)  
HEAT SOURCE: RADIATION  
OUTER GLAZE: 1/4" FUSED SILICA - NO COATING  
INNER GLAZE: 1/4" ALUMINOSILICATE - NO COATING



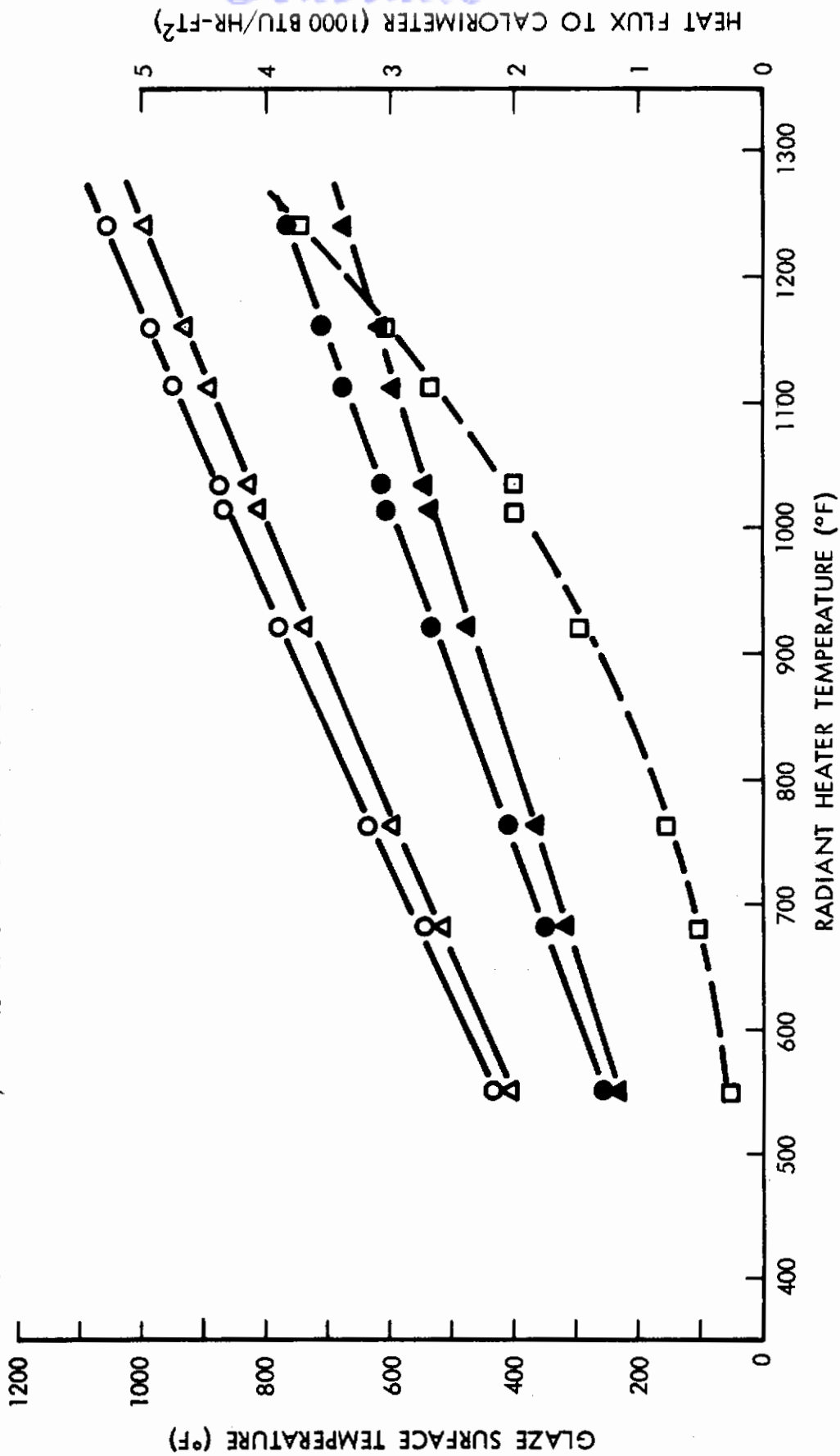
MULTIPLE GLAZE HEAT TRANSFER TEST

TEST NUMBER: III-28 (AIR)  
 HEAT SOURCE: RADIATION  
 OUTER GLAZE: 3/8" FUSED SILICA - NO COATING  
 INNER GLAZE: 1/8" VYCOR - NO COATING



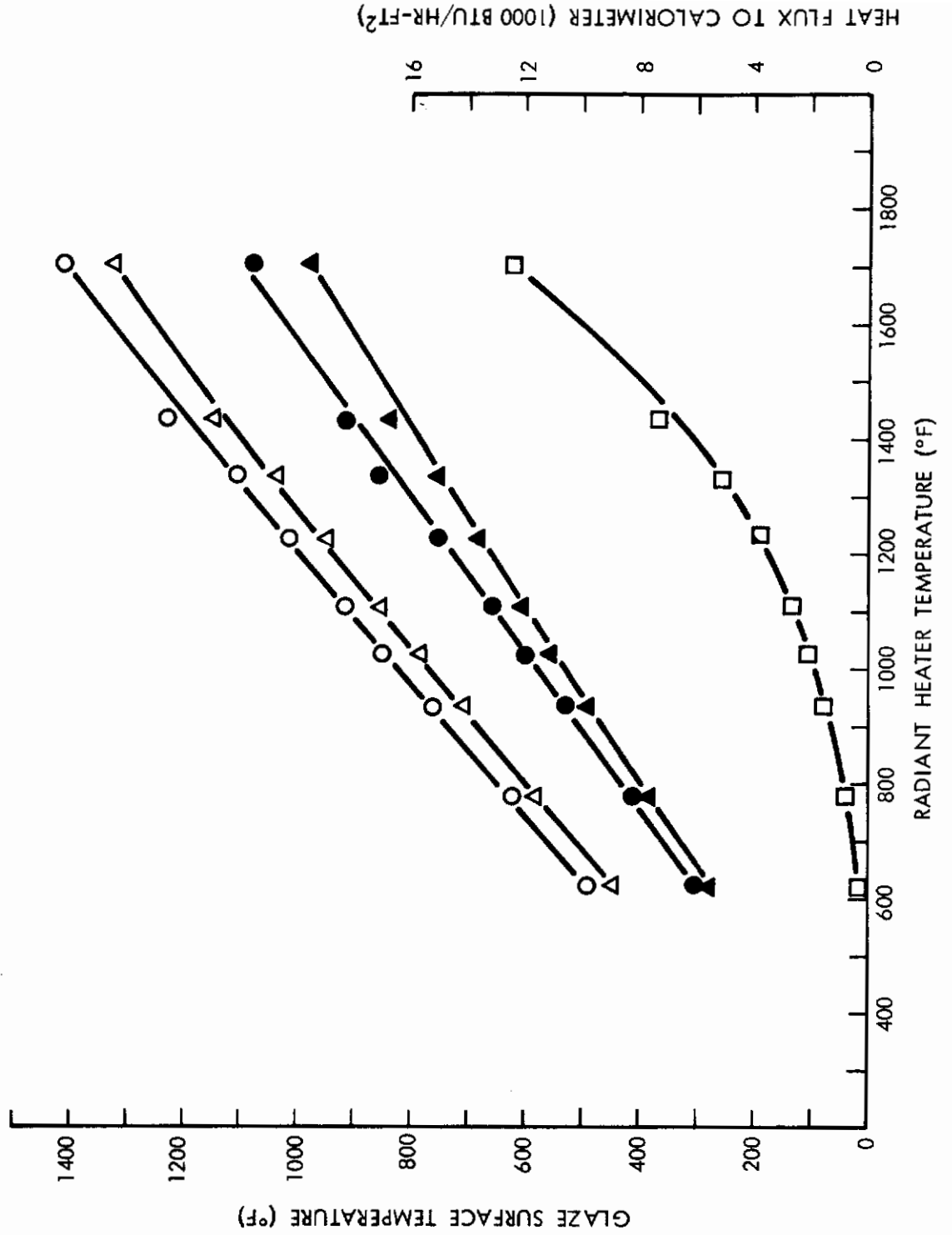
MULTIPLE GLAZE HEAT TRANSFER TEST

TEST NUMBER: III-27 (AIR)  
HEAT SOURCE: RADIATION  
OUTER GLAZE: 1/4" ALUMINOSILICATE - NO COATING  
INNER GLAZE: 3/8" ALUMINOSILICATE - NO COATING



MULTIPLE GLAZE HEAT TRANSFER TEST

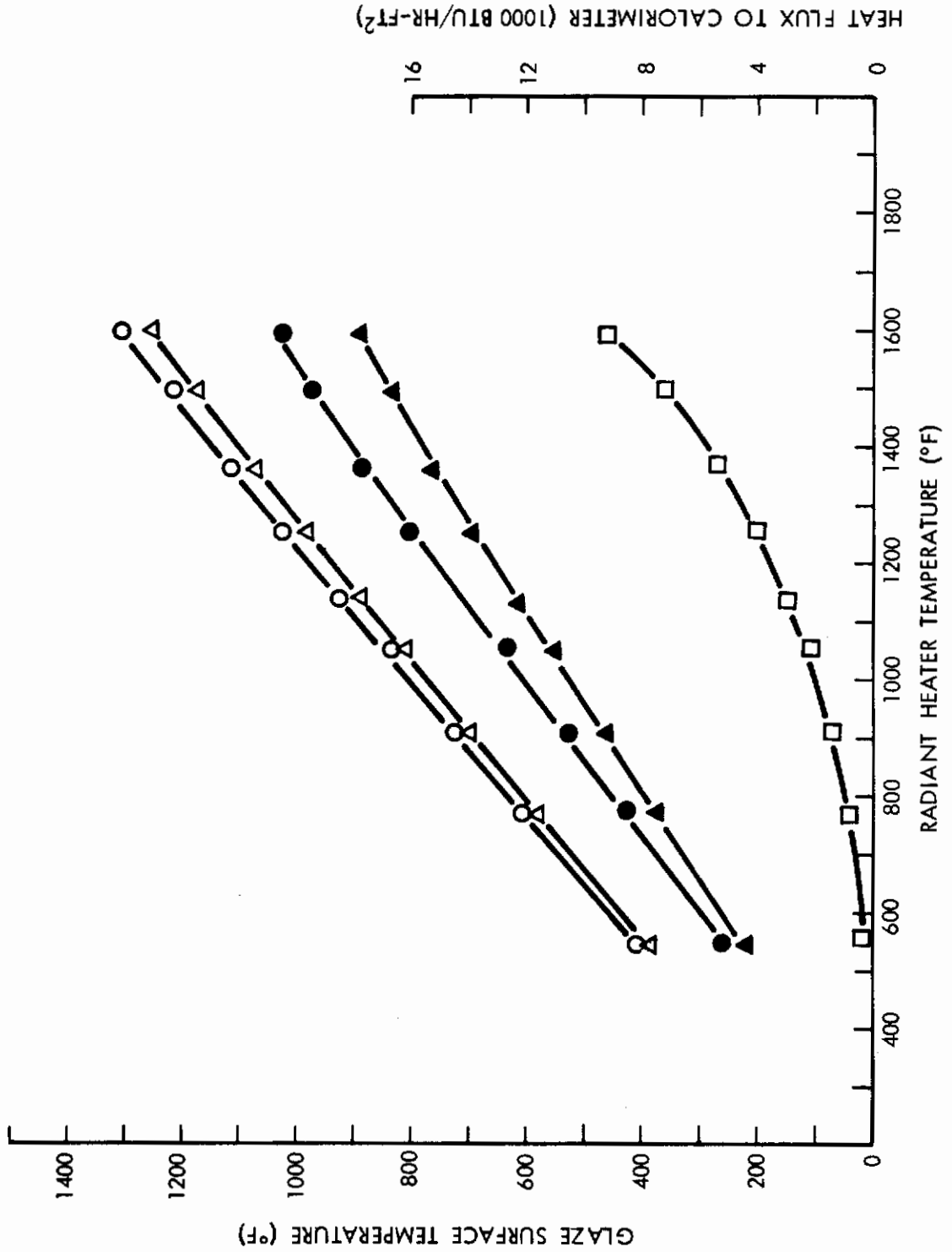
TEST NUMBER: III-18 (AIR)  
HEAT SOURCE: RADIATION  
OUTER GLAZE: 3/8" FUSED SILICA - NO COATING  
INNER GLAZE: 1/4" ALUMINOSILICATE - NO COATING





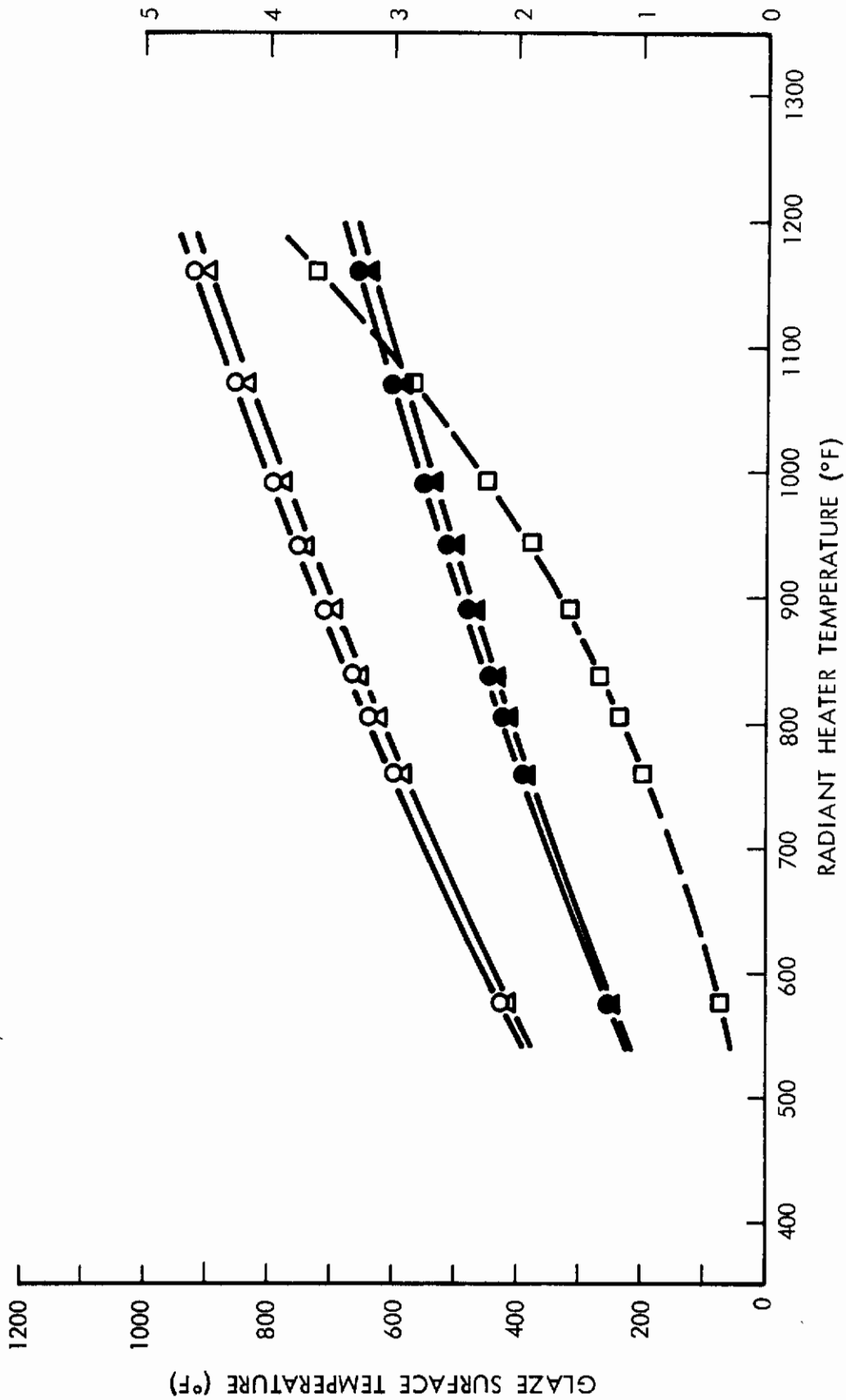
MULTIPLE GLAZE HEAT TRANSFER TEST

TEST NUMBER: III-56 (AIR)  
HEAT SOURCE: RADIATION  
OUTER GLAZE: 1/4" FUSED SILICA - UNCOATED  
INNER GLAZE: 3/8" ALUMINOSILICATE - UNCOATED



MULTIPLE GLAZE HEAT TRANSFER TEST

TEST NUMBER: III-37 (AIR)  
 HEAT SOURCE: RADIATION  
 OUTER GLAZE: 1/4" FUSED SILICA - UV-IR ON EMERGENT SURFACE  
 INNER GLAZE: 1/8" VYCOR - NO COATING

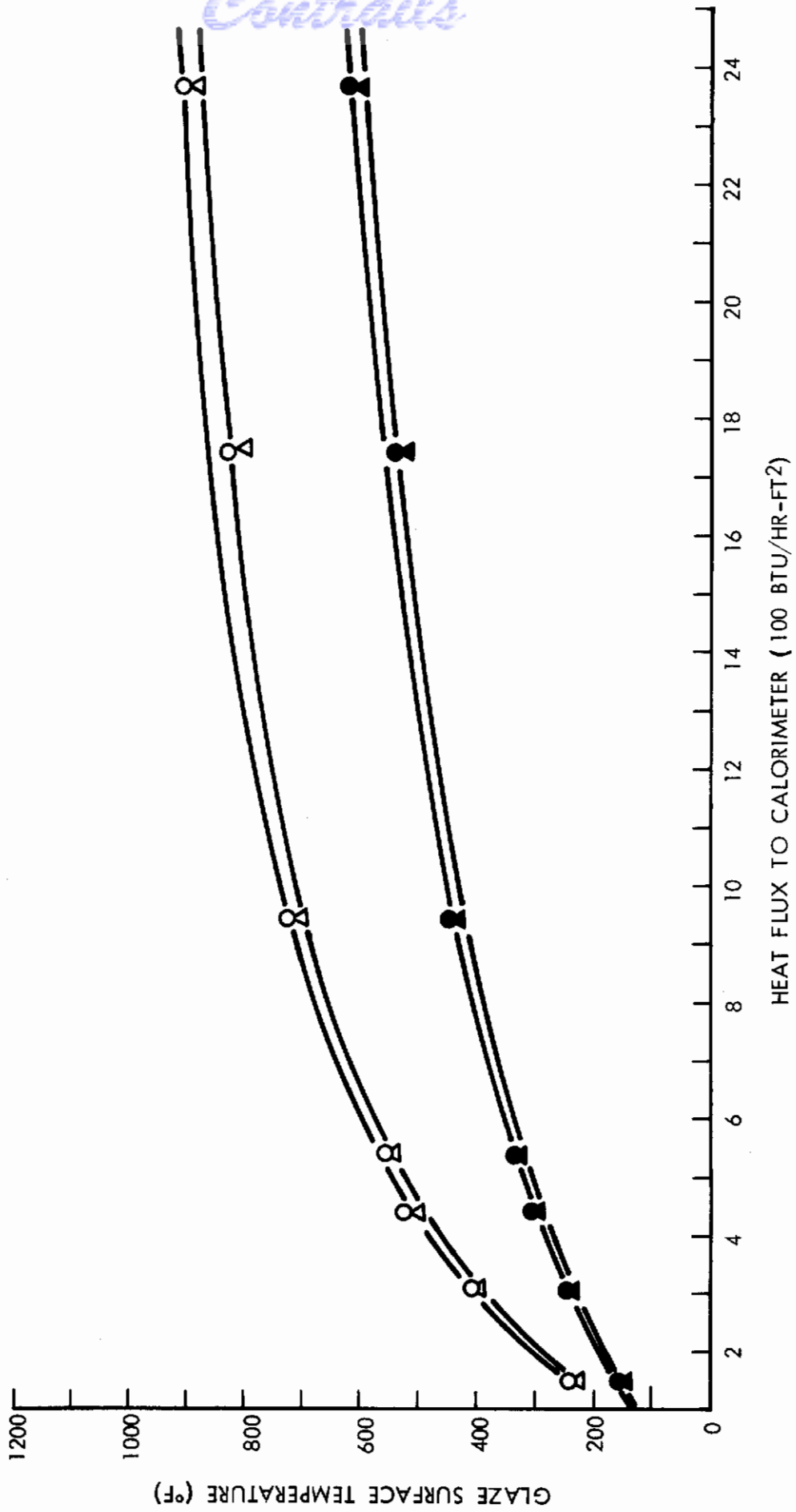


Contrails  
 HEAT FLUX TO CALORIMETER (1000 BTU/HR-FT<sup>2</sup>)

*Contrails*

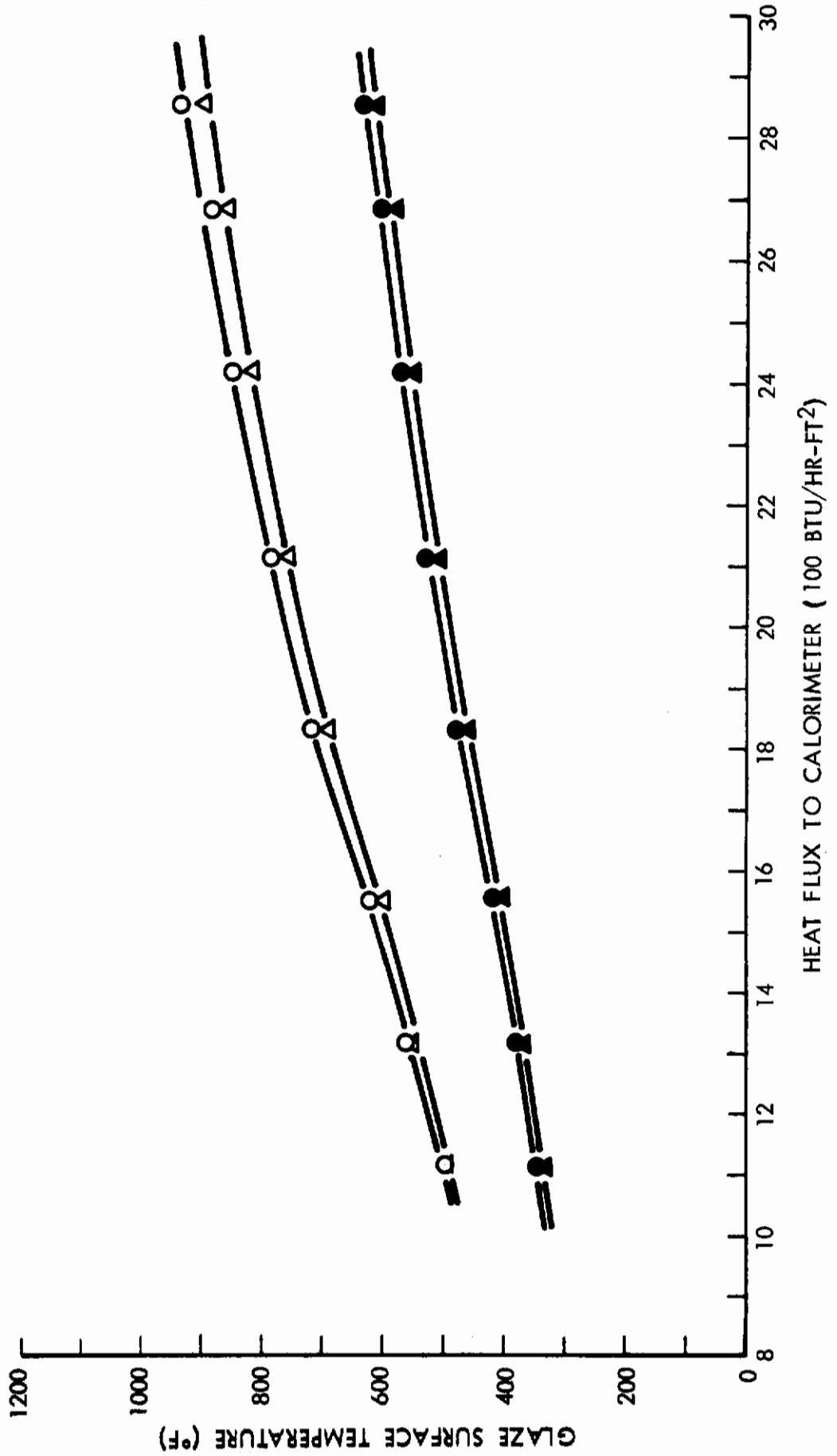
MULTIPLE GLAZE HEAT TRANSFER TEST

TEST NUMBER: III-36 (AIR)  
HEAT SOURCE: CONVECTION  
OUTER GLAZE: 1/4" FUSED SILICA - UV-IR ON EMERGENT SURFACE  
INNER GLAZE: 1/8" VYCOR - NO COATING



MULTIPLE GLAZE HEAT TRANSFER TEST

TEST NUMBER: III-35 (AIR)  
HEAT SOURCE: RADIATION & CONVECTION  
OUTER GLAZE: 1/4" FUSED SILICA - UV-IR ON EMERGENT SURFACE  
INNER GLAZE: 1/8" VYCOR - NO COATING



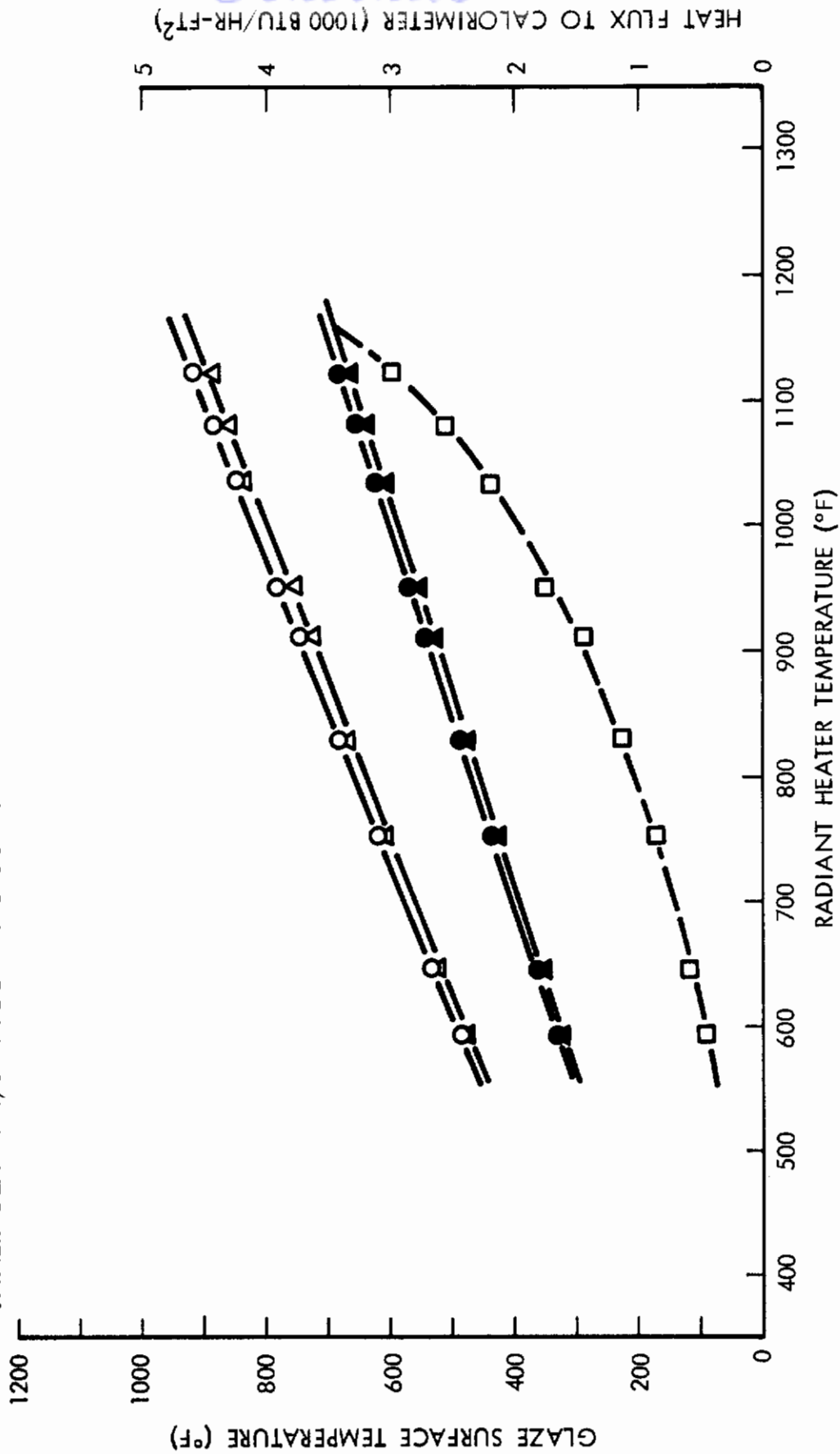
MULTIPLE GLAZE HEAT TRANSFER TEST

TEST NUMBER: III-88 (VACUUM)

HEAT SOURCE: RADIATION

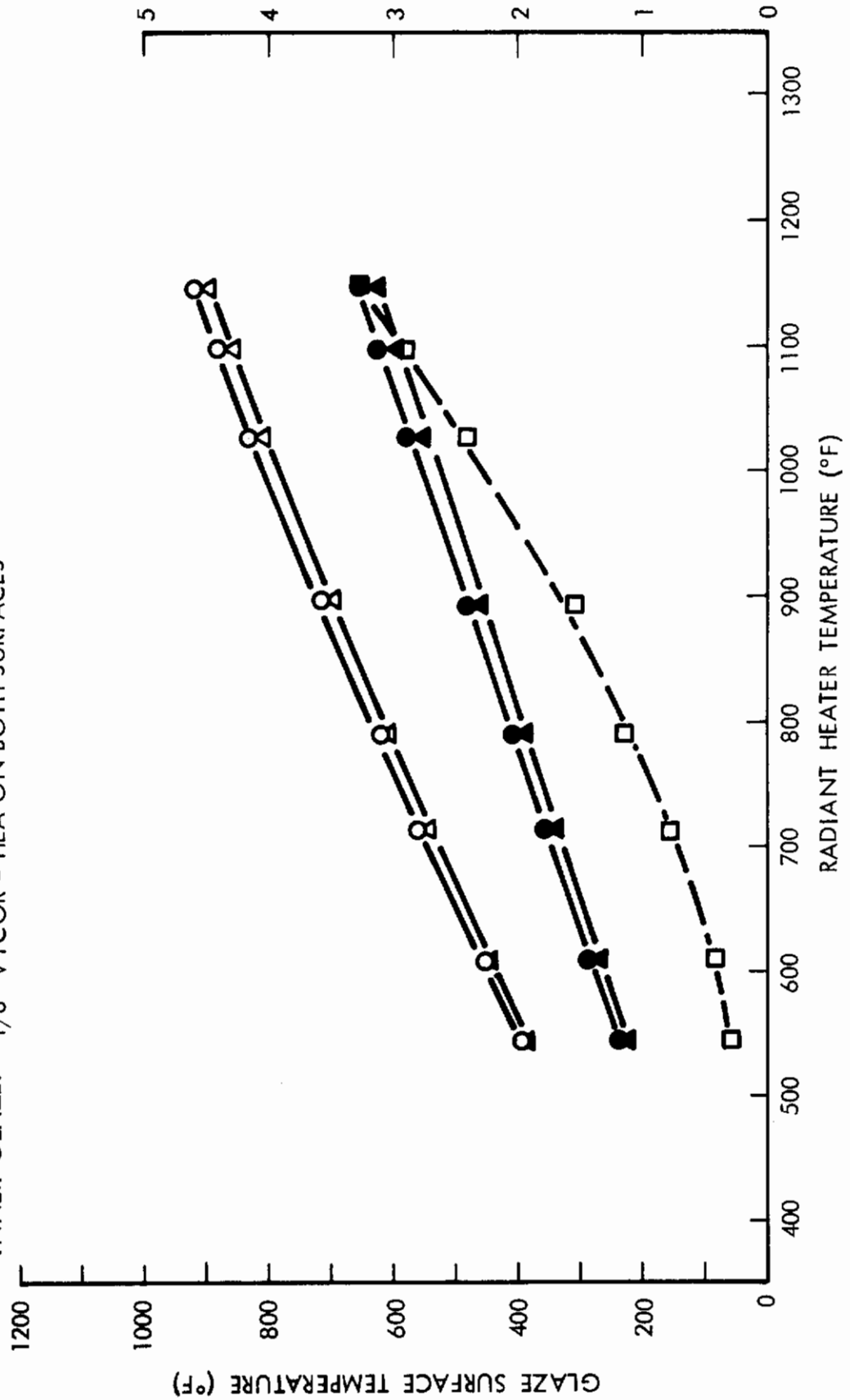
OUTER GLAZE: 1/4" FUSED SILICA - UV-IR EMERGENT SURFACE

INNER GLAZE: 1/8" VYCOR - NO COATING



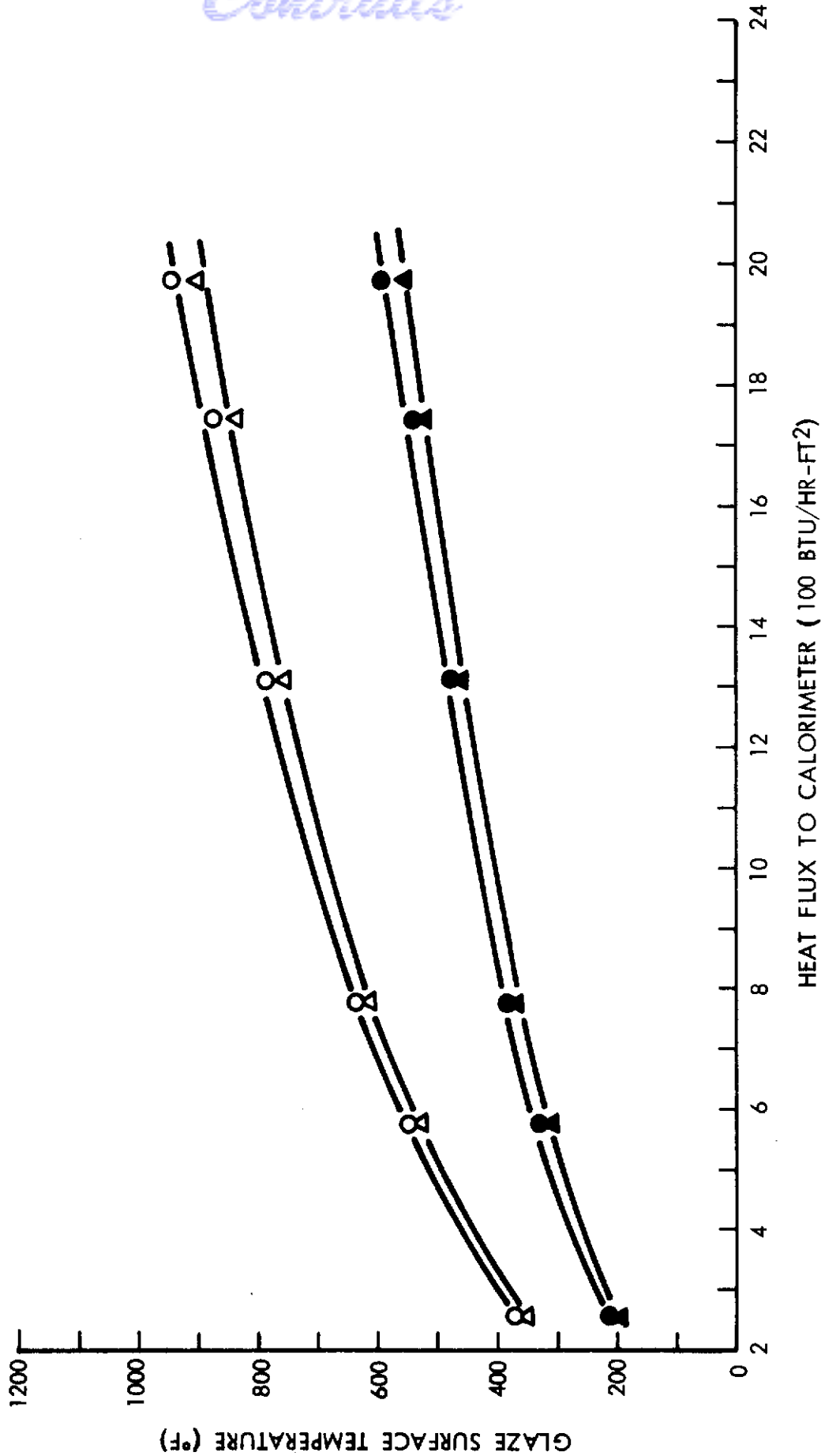
MULTIPLE GLAZE HEAT TRANSFER TEST

TEST NUMBER: III-12 (AIR)  
HEAT SOURCE: RADIATION  
OUTER GLAZE: 1/4" FUSED SILICA - UV-IR ON EMERGENT SURFACE  
INNER GLAZE: 1/8" VYCOR - HEA ON BOTH SURFACES



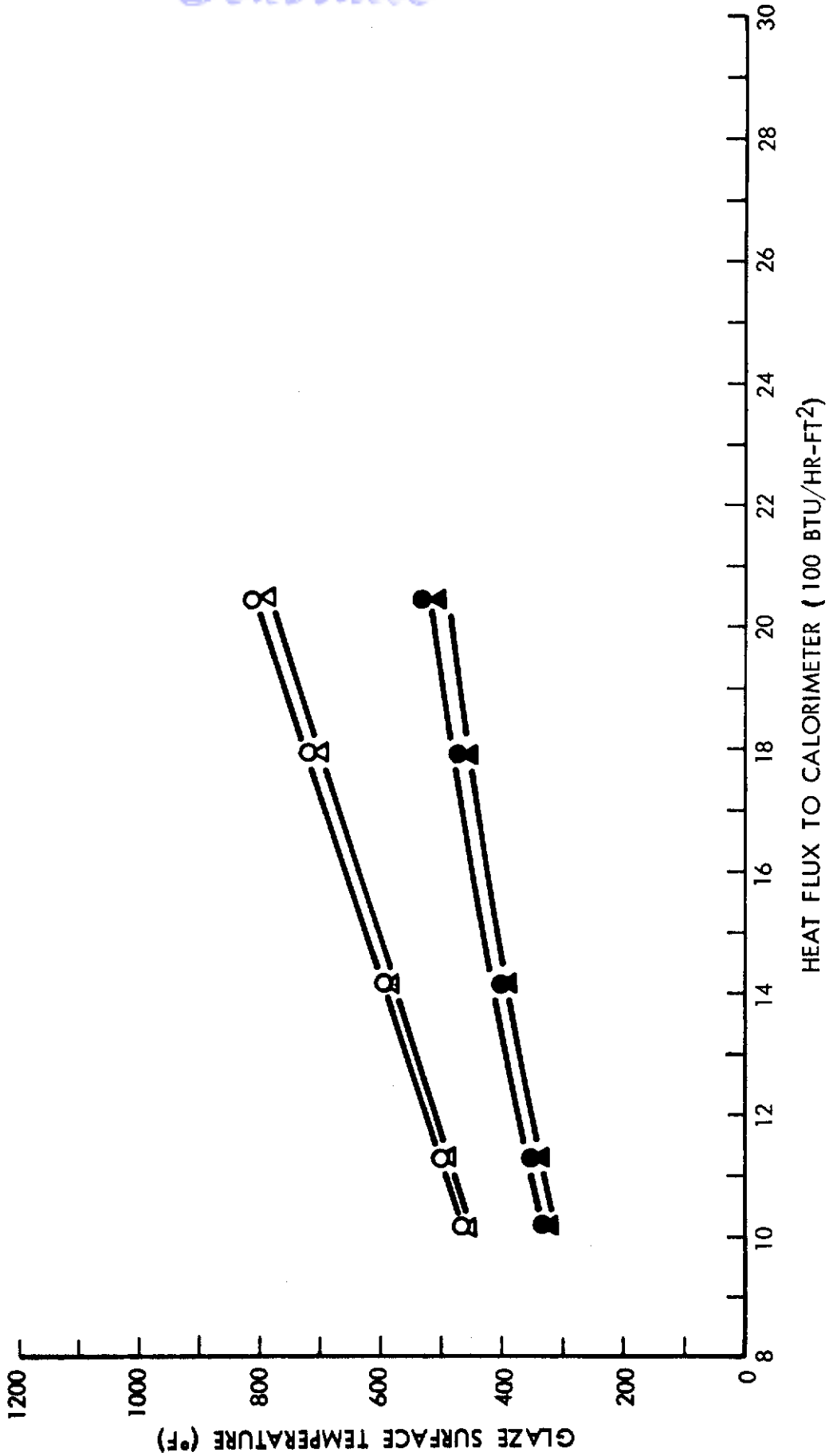
MULTIPLE GLAZE HEAT TRANSFER TEST

TEST NUMBER: III-9 (AIR)  
HEAT SOURCE: CONVECTION  
OUTER GLAZE: 1/4" FUSED SILICA - UV-IR ON EMERGENT SURFACE  
INNER GLAZE: 1/8" VYCOR - HEA ON BOTH SURFACES



MULTIPLE GLAZE HEAT TRANSFER TEST

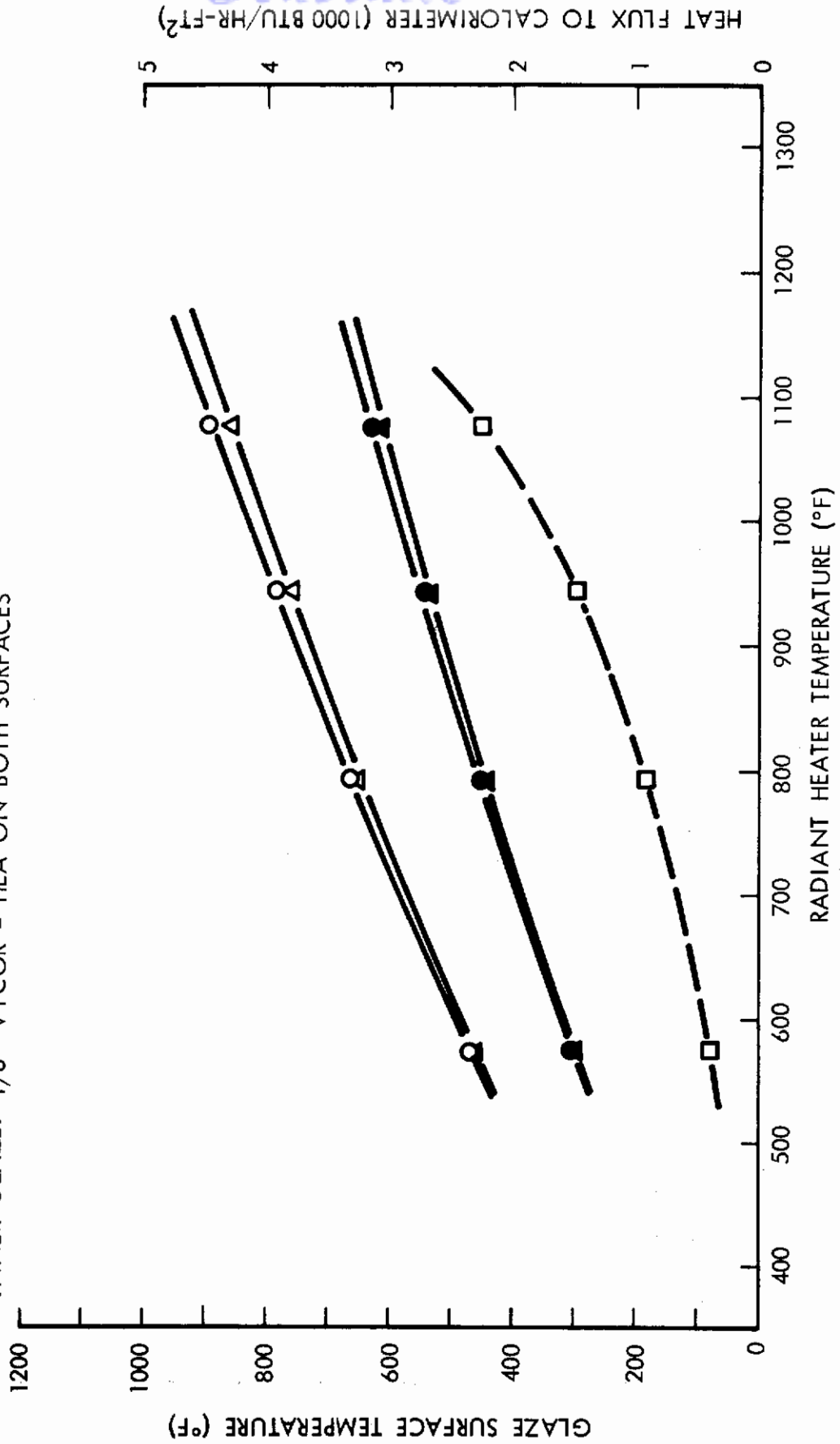
TEST NUMBER: III-10 (AIR)  
HEAT SOURCE: RADIATION & CONVECTION  
OUTER GLAZE: 1/4" FUSED SILICA - UV-IR ON EMERGENT SURFACE  
INNER GLAZE: 1/8" VYCOR - HEA ON BOTH SURFACES





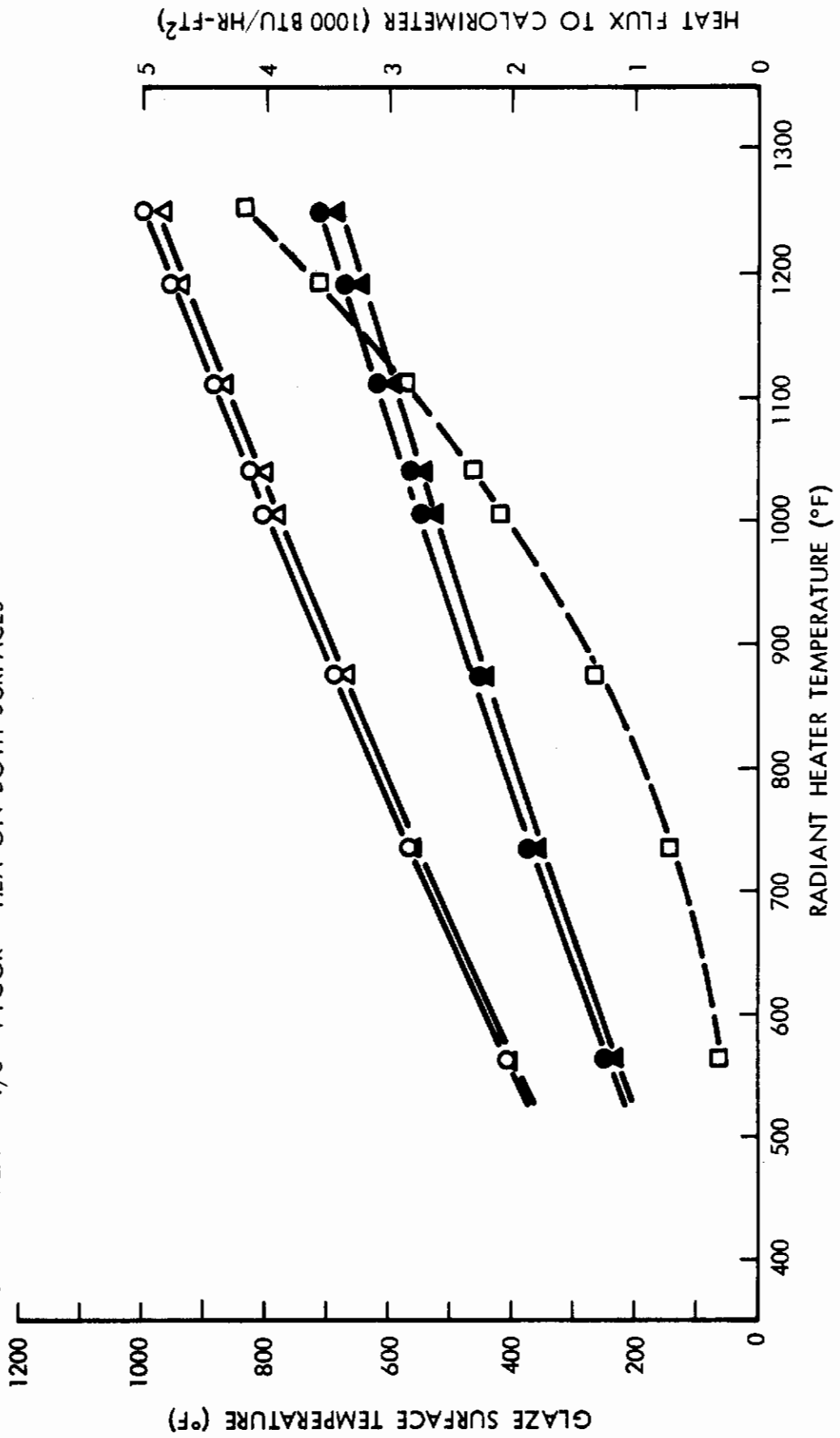
MULTIPLE GLAZE HEAT TRANSFER TEST

TEST NUMBER: III-103 (VACUUM)  
HEAT SOURCE: RADIATION  
OUTER GLAZE: 1/4" VYCOR - UV-IR ON EMERGENT SURFACE  
INNER GLAZE: 1/8" VYCOR - HEA ON BOTH SURFACES



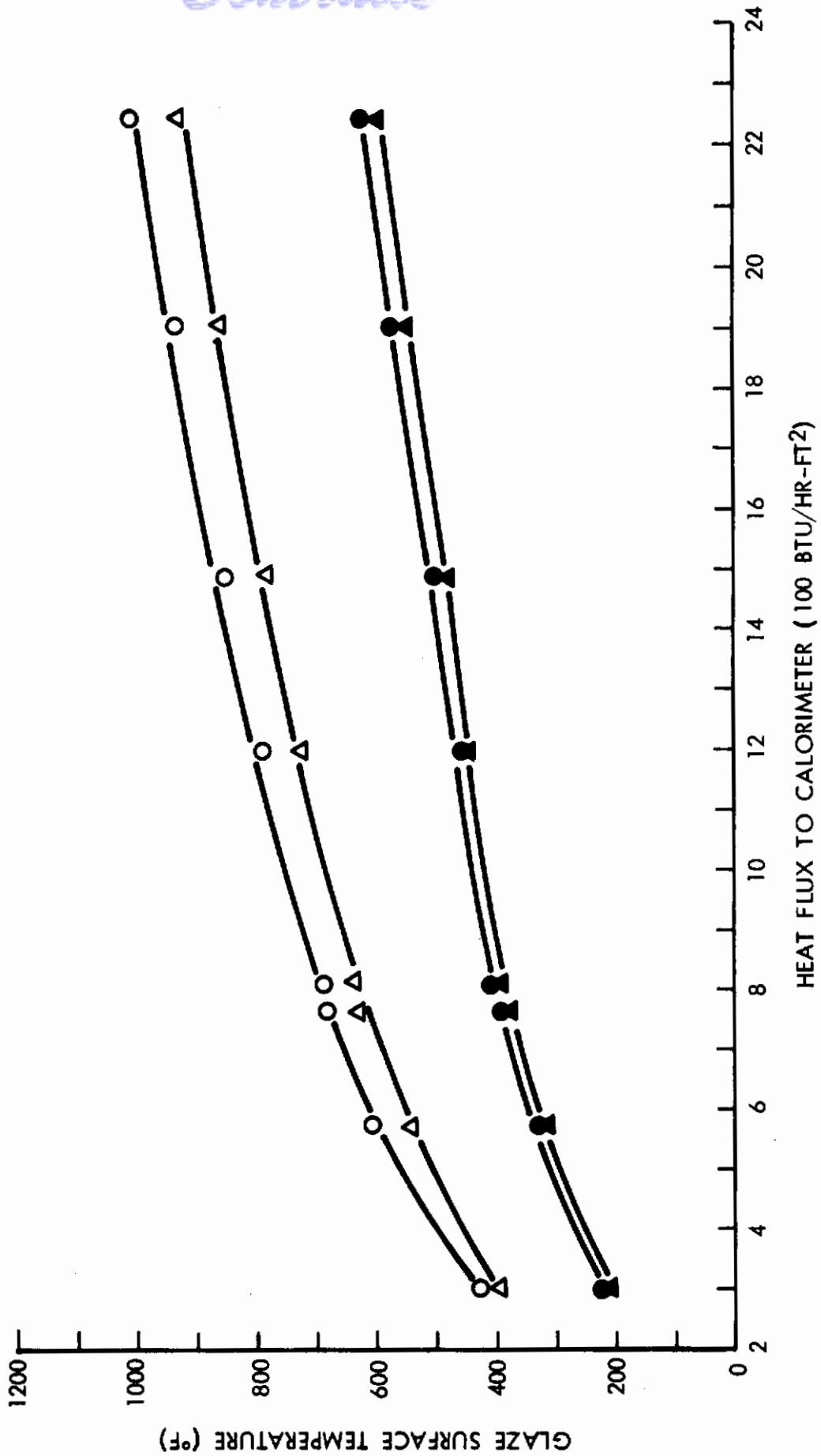
MULTIPLE GLAZE HEAT TRANSFER TEST

TEST NUMBER: III-42 (AIR)  
HEAT SOURCE: RADIATION  
OUTER GLAZE: 1/4" FUSED SILICA - HEA ON BOTH SURFACES  
INNER GLAZE: 1/8" VYCOR - HEA ON BOTH SURFACES



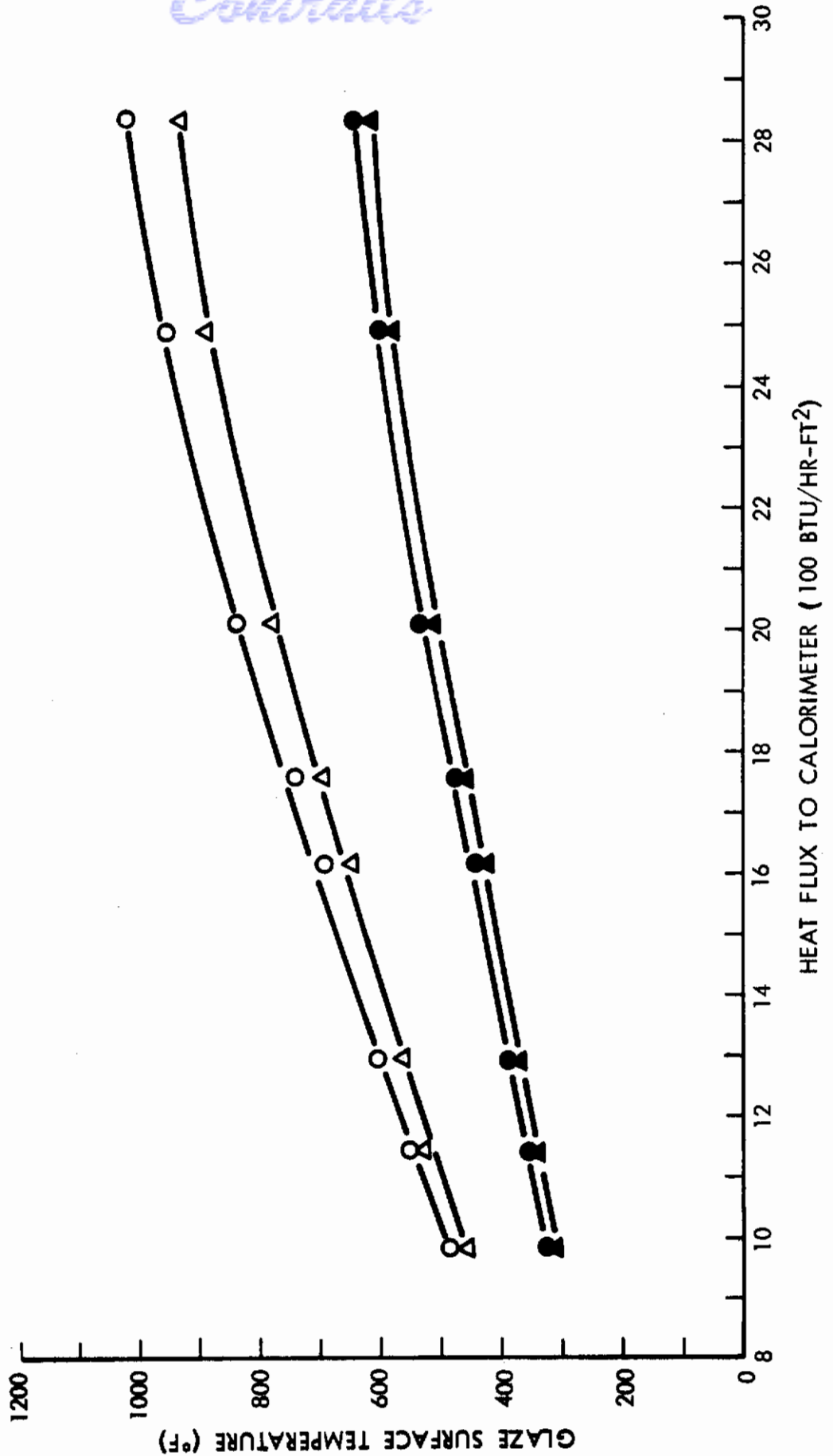
MULTIPLE GLAZE HEAT TRANSFER TEST

TEST NUMBER: III-7 (AIR)  
HEAT SOURCE: CONFECTION  
OUTER GLAZE: 1/4" FUSED SILICA - HEA ON BOTH SURFACES  
INNER GLAZE: 1/8" VYCOR - HEA ON BOTH SURFACES



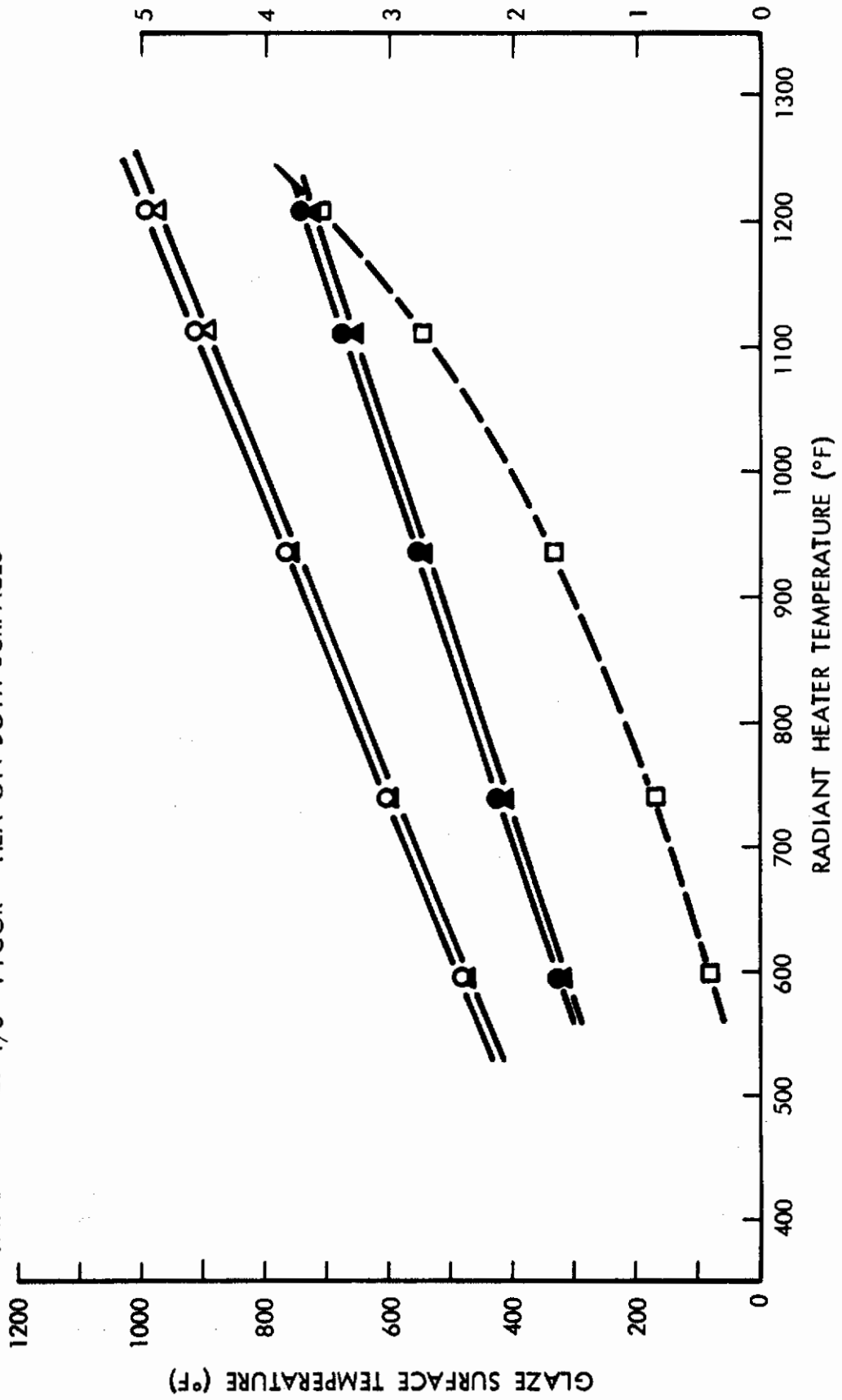
MULTIPLE GLAZE HEAT TRANSFER TEST

TEST NUMBER: III-8 (AIR)  
HEAT SOURCE: RADIATION & CONVECTION  
OUTER GLAZE: 1/4" FUSED SILICA - HEA ON BOTH SURFACES  
INNER GLAZE: 1/8" VYCOR - HEA ON BOTH SURFACES



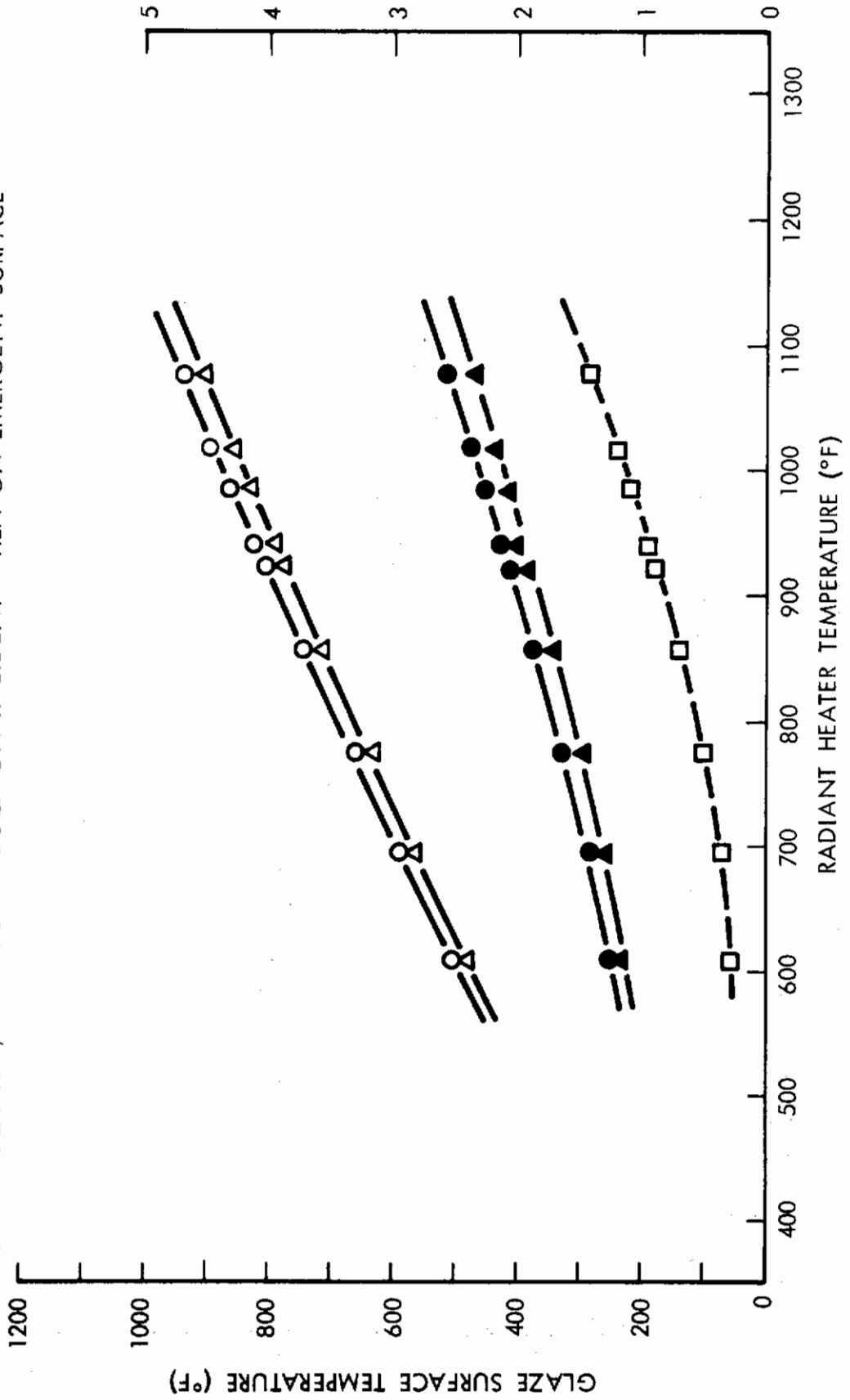
MULTIPLE GLAZE HEAT TRANSFER TEST

TEST NUMBER: III-93 (VACUUM)  
 HEAT SOURCE: RADIATION  
 OUTER GLAZE: 1/4" FUSED SILICA - HEA ON BOTH SURFACES  
 INNER GLAZE: 1/8" VYCOR - HEA ON BOTH SURFACES



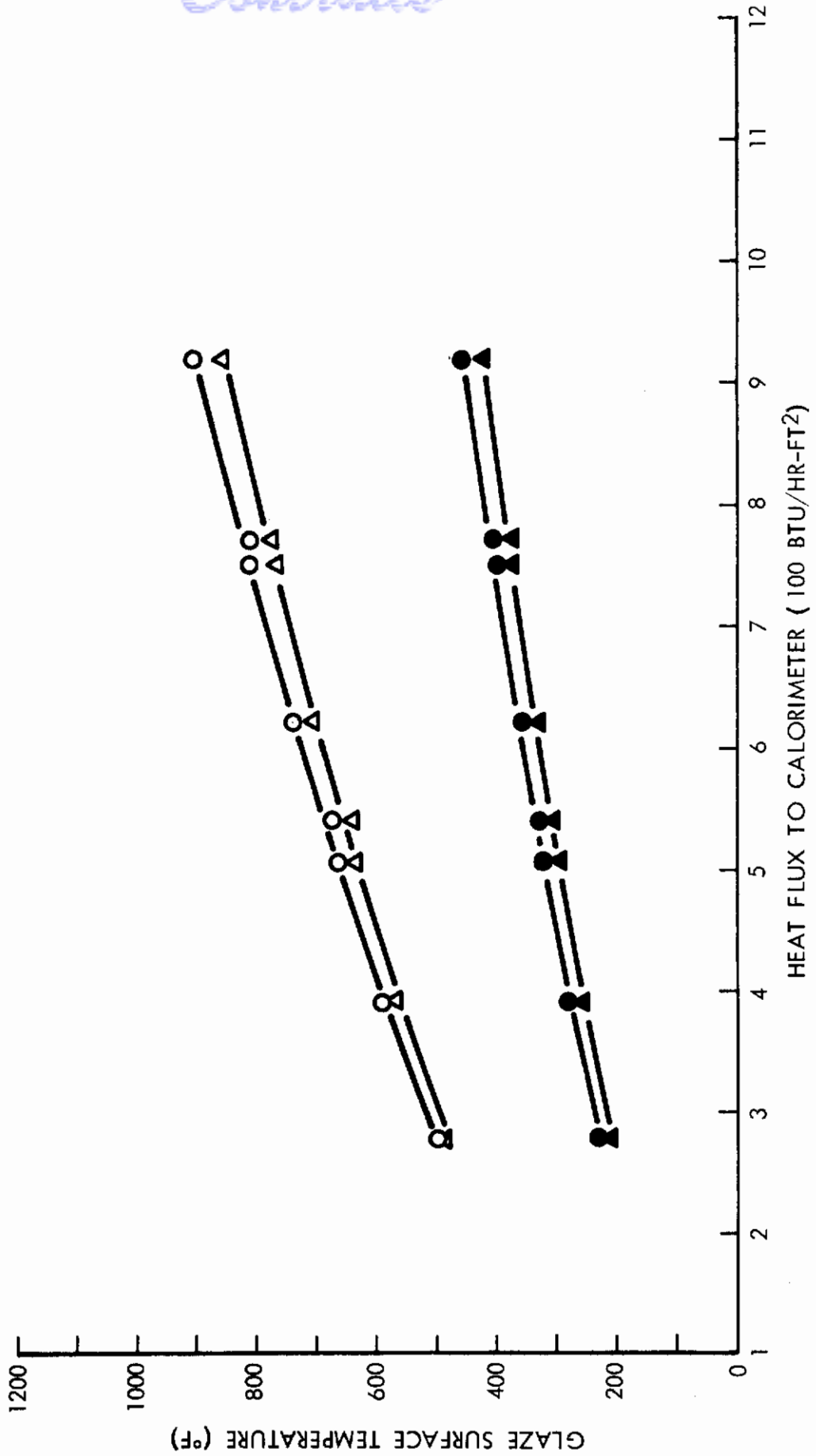
MULTIPLE GLAZE HEAT TRANSFER TEST

TEST NUMBER: III-81 (AIR)  
HEAT SOURCE: RADIATION  
OUTER GLAZE: 1/4" VYCOR - UV-IR ON EMERGENT SURFACE  
INNER GLAZE: 1/4" VYCOR - GOLD ON INCIDENT - HEA ON EMERGENT SURFACE



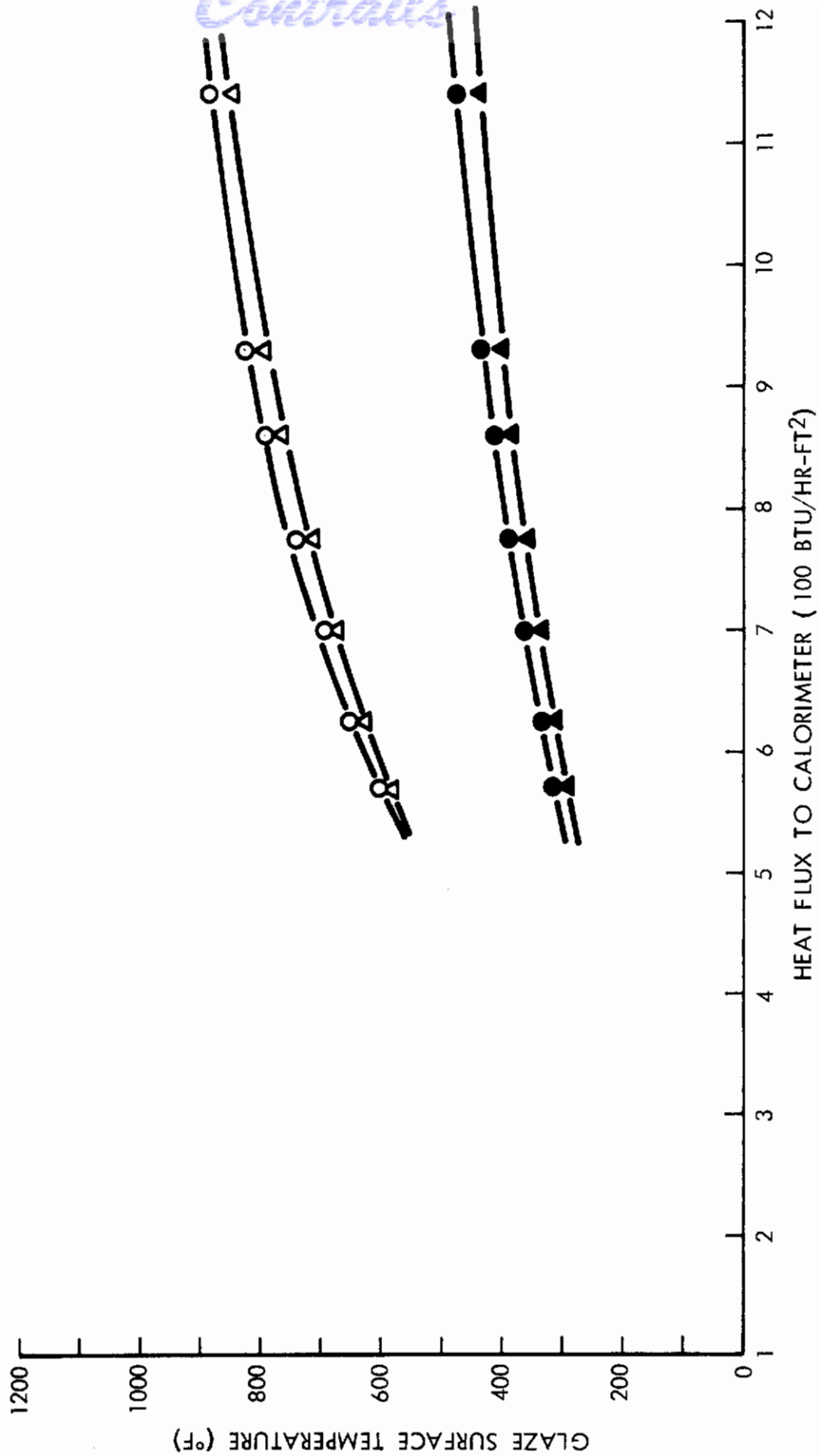
MULTIPLE GLAZE HEAT TRANSFER TEST

TEST NUMBER: III-74 (AIR)  
HEAT SOURCE: CONVECTION  
OUTER GLAZE: 1/4" VYCOR - UV-IR ON EMERGENT SURFACE  
INNER GLAZE: 1/4" VYCOR - GOLD ON INC. - HEA ON EMERGENT



MULTIPLE GLAZE HEAT TRANSFER TEST

TEST NUMBER: III-76 (AIR)  
HEAT SOURCE: RADIATION & CONVECTION  
OUTER GLAZE: 1/4" VYCOR - UV-IR ON EMERGENT SURFACE  
INNER GLAZE: 1/4" VYCOR - GOLD ON INCIDENT - HEA ON EMERGENT SURFACE





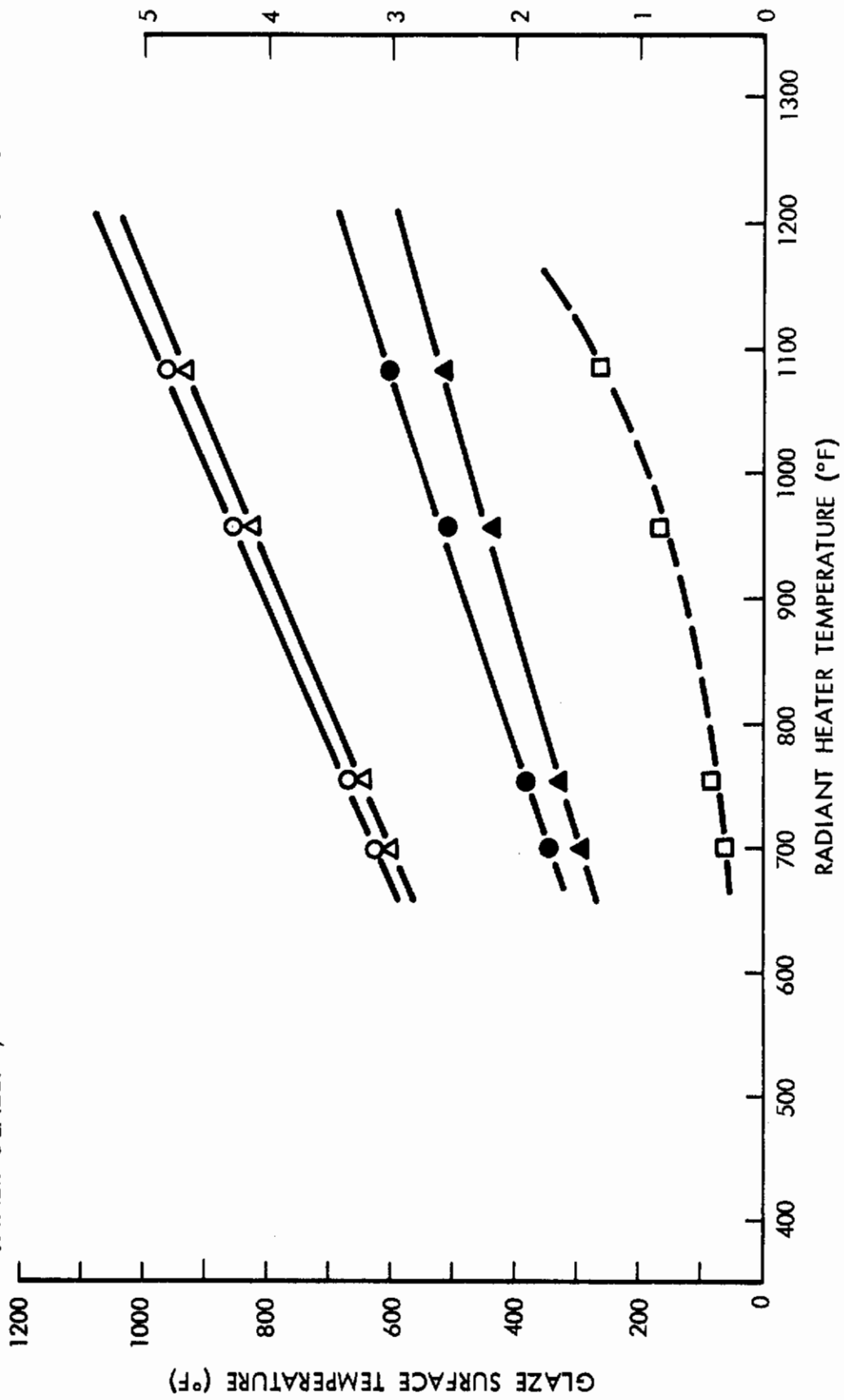
MULTIPLE GLAZE HEAT TRANSFER TEST

TEST NUMBER: III-99 (VACUUM)

HEAT SOURCE: RADIATION

OUTER GLAZE: 1/4" VYCOR - UV-IR EMERGENT SURFACE

INNER GLAZE: 1/4" VYCOR - GOLD INCIDENT SURFACE - HEA ON EMERGENT SURFACE



## REFERENCES

1. Lis, S. J., R. G. Barile, and G. Engholm, "Window Systems for Advanced Vehicles," Air Force Flight Dynamics Laboratory, FDL-TDR-64-39, December 1964.
2. Gardon, R., "Calculation of Temperature Distributions in Glass Plates Undergoing Heat Treatment," J. Am. Cer. Soc., 41, 200-209 (1958).
3. Gardon, R., Appendix to Reference 2.
4. Gardon, R., "The Emissivity of Transparent Materials," J. Am. Cer. Soc., 39 (1956).
5. Berning, Jean A., and Peter H. Berning, "Thin-Films Calculations Using the IBM 650 Electronic Calculator," J. of the Optical Society of America, 50, No. 8, 813-816, August 1960.
6. Corning Materials Handbook, Sixth Ed., Corning Glass Works, Corning, New York, April 1963.
7. Finch, H. L., M. Noland, and C. Moeller, "Experimental Verification of the Analysis and Computer Programs Concerning Heat Transfer Through Semitransparent Materials," AFFDL-TR-65-136, July 1965.
8. Kemp, N. H., and F. R. Riddell, "Heat Transfer to Satellite Vehicles Re-entering the Atmosphere," Jet Propulsion, 27, 132-137 (1957).
9. Kivel, B., and K. Bailey, Tables of Radiation from High Temperature Air, AVCO Research Laboratory, RR21, December 1957.
10. Przemieniecki, J. S., "Design of Transparencies," J. Roy. Aero. Soc., 63 620 (1959).
11. Gaumer, G. R., "Stability of Three Finite Difference Methods of Solving for Transient Temperatures," ARS Journal, 1595, October 1962.
12. Dusenberre, G. M., "Heat Transfer Calculations by Finite Differences," International Textbook Company, Scranton, Pennsylvania (1961).
13. Hamilton, D. C., and W. R. Morgan, "Radiant Interchange Configuration Factors," NACA TN 2836 (1952).
14. Moeller, C. E., and M. Noland, "Gold Resistance Thermometers for Surface-Temperature Measurements of Semitransparent Materials: A Development Study," 5th Temperature Measurements Society Conference, March 14, 1967.

## REFERENCES (Concluded)

15. Fowle, A. A., P. F. Strong, and D. F. Comstock, "Computer Program for Prediction of Heat Transfer Through Glass," Sixth Conference on Thermal Conductivity, October 1966.
16. Reuber, Lt. David B., Air Force Technical Monitor of Subject Contract AF 33(615)-5164, personal correspondence.
17. Reeves, B. L., "Aerodynamic Heating in Slip, Intermediate, and Free Molecular Flow Regimes," McDonnell Aircraft Company Report No. 6859, November 1969.
18. Serbin, H., "Supersonic Flow about Blunt Bodies," J. Aero Sci., 25, No. 1, p. 58 (1958).
19. Koh, J. C. Y., "Radiation from Non-Isothermal Gas to the Stagnation Point of a Hypersonic Blunt Body," ARS J., 32, pp. 1374-7 (1962).
20. Lighthill, M. J., "Dynamics of a Dissociating Gas, Part I, Equilibrium Flow," J. Fluid Mech., 2, pp. 1-32 (1957).
21. Handbook of Physics and Chem., 34th Ed., Chem. Rubber Publishing Company, Cleveland, p. 2875.

# Contrails

## DISTRIBUTION LIST AFFDL-TR-69-28

<u>Activities at Wright-Patterson AFB, Ohio 45433</u>	<u>Activities at Wright-Patterson AFB, Ohio 45433</u>
AFFDL (FDE/Library)	ASD (ASB)
AFFDL (FDP/Stinfo)	ASD (ASBED)
AFFDL (FDT)	ASD (ASEP)
AFFDL (FDCC/Capt. J. R. Pruner)	ASD (ASLE)
AFFDL (FDCR/R. R. Davis)	ASD (ASLE-6)
AFFDL (FDFR/E. O. Roberts)	ASD (ASM)
AFFDL (FDMS/C. J. Cosenza)	ASD (ASN)
AFAL (AVG)	ASD (ASNFS)
FAAL (AVR)	ASD (ASNKM)
AFML (MAG)	ASD (ASNMC) <u>(2 cys)</u>
AFML (MAAE/R. E. Wittman)	ASD (ASNN)
AFML (MAAM)	ASD (ASNQ) <u>(2 cys)</u>
AFML (MAEE/S. Allinikov)	ASD (ASQ)
AFML (MAN)	ASD (ASR) <u>(2 cys)</u>
AFML (MAYT)	ASD (AST)
AFIT (Tech Library)	ASD (ASW)
AMRL (MRHE) <u>(2 cys)</u>	ASD (ASZBE)
AMRL (MRT/C. A. Dempsey)	ASD (ASZM)
AMRL (MRB)	ASD (ASNPD-30)
ARL (ARIL)	EWABE (Library)

# Contracts

## AIR FORCE

Air University Library  
Maxwell AFB, Alabama 36112

BSRG/Lt. Col. Manlove  
Norton AFB, California 92409

Headquarters, USAF (AFCSAI)  
Washington, D. C. 20330

AFSC (SCAP)  
Andrews AFB  
Washington, D. C. 20331

USAF (SMKOR/Lt. Col. Loper)  
Brooks AFB, Texas 78235

Headquarters, USAF (AFRDDG)  
Washington, D. C. 20330 (2 cys)

AFSC (SCTR)  
Andrews AFB  
Washington, D. C. 20331

DOL (SCTSM)  
Bolling AFB, D. C. 20332 (2 cys)

AFOSR  
1400 Wilson Boulevard  
Arlington, Virginia 22209

SAMSO (Tech. Library)  
AF Unit Post Office  
Los Angeles, California 90045

SAMSO (Tech. Library)  
Norton AFB, California 92409

## NAVY

Commander  
Naval Air Systems Command  
Headquarters (AIR-604)  
Washington, D. C. 20360

Commander  
Naval Air Systems Command  
Headquarters (AIR-320)  
Washington, D. C. 20360

Commander  
Naval Air Systems Command  
Headquarters (AIR-5302)  
Washington, D. C. 20360

Commanding Officer  
Naval Air Engineering Center  
Philadelphia, Pennsylvania 19112

US Navy  
Attn: Code PID-23  
17th & Constitution Avenue  
Washington, D. C. 20000

## ARMY

Commanding Officer  
US Army Transportation Res. Command  
Fort Eustis, Virginia 23604

US Army R&D Laboratory  
Attn: Tech. Document Unit  
Fort Belvoir, Virginia 22060

US Army Research Office-Durham  
Attn: Scientific Synthesis Office  
Box CM, Duke Station  
Durham, North Carolina 27706

## OTHER US GOVERNMENT AGENCIES

DDC-TIAAS  
Cameron Station  
Alexandria, Virginia 22314 (20 cys)

NASA  
Scientific and Tech. Info. Facility  
P. O. Box 33  
College Park, Maryland 20740 (2 cys)

# Contracts

## OTHER US GOVERNMENT AGENCIES (Concluded)

NASA  
Attn: RV-2  
Washington, D. C. 20546

NASA  
Attn: RAL  
Washington, D. C. 20546

NASA (Tech. Library)  
Langley Research Center  
Langley Station  
Hampton, Virginia 23365

NASA  
Manned Spacecraft Center  
Attn: Tech. Library  
Houston, Texas 77058

NASA (Materials Research)  
1520 H Street, N.W.  
Washington, D. C. 20000

NASA  
Manned Spacecraft Center  
Attn: Edward Cheminti  
Head, Heat Transfer Section  
EF-55  
Houston, Texas 77058

NASA  
Manned Spacecraft Center  
Attn: G. Screwball  
R. G. Brown  
Thermo-Structures Branch  
Houston, Texas 77058

National Bureau of Standards  
US Department of Commerce  
Attn: Library  
Washington, D. C. 20000

## NON-GOVERNMENT AGENCIES

Aerojet-General Corporation  
Attn: Tech. Library  
P. O. Box 296  
Azusa, California 91703

Aerojet-General Corporation  
Attn: Tech. Library  
9100 East Flair Drive  
El Monte, California 91734

Aeronca, Incorporated  
Attn: Engineering Department  
Librarian  
1712 Germantown Road  
Middletown, Ohio 45042

Aerospace Corporation  
Reports Acquisition  
P. O. Box 95085  
Los Angeles, California 90045

American Optical Company  
Attn: Research Division  
32 Mechanic Street  
Southbridge, Massachusetts 01551

Arthur D. Little Company  
Attn: David Richardson  
Room 20-544  
Acorn Park

Cambridge, Massachusetts 02140

AVCO Research and Advanced  
Development Laboratory  
Attn: Tech. Library  
Wilmington, Massachusetts 01887

AVCO Corporation  
Attn: Tech. Library  
P. O. Box 210  
Nashville, Tennessee 37202

# Contracts

## NON-GOVERNMENT AGENCIES (Continued)

AVCO Corporation  
Research and Advanced  
Development Division  
Attn: M. E. Ihnat  
Lowell Industrial Park  
Lowell, Massachusetts 01851

Barber-Colman Company  
Attn: Don Schaeede  
Electro-Mechanical Products  
Division  
Rockford, Illinois 61100

Battelle Memorial Institute  
DMIC, Attn: Tech. Library  
505 King Avenue  
Columbus, Ohio 43201

Battelle Memorial Institute  
DMIC, Attn: J. F. Lynch  
505 King Avenue  
Columbus, Ohio 43201

Bausch and Lomb Incorporated  
84059 St. Paul Street  
Rochester, New York 14602

Beech Aircraft Corporation  
Attn: Engineering Department  
Librarian  
9709 East Central Avenue  
Wichita, Kansas 67201

Bell Aerospace Corporation  
Attn: Engineering Department  
Librarian  
P. O. Box 1  
Buffalo, New York 14240

Bendix Corporation  
Bendix Systems Division  
Ann Arbor, Michigan 48107

The Boeing Company  
Wichita Division  
Attn: Engineering Department  
Librarian  
Wichita, Kansas 67201

The Boeing Company  
Aerospace Group  
Attn: Tech. Library  
P. O. Box 3707  
Seattle, Washington 98124

The Boeing Company  
Airplane Division  
Attn: Tech. Library  
Renton, Washington 98055

The Boeing Company  
Attn: G. L. Brower/Dept. 6-2000  
Mail Stop 59-88  
Renton, Washington 98055

The Boeing Company  
Aerospace Group  
Attn: John McGinnis  
Jim Klosen  
P. O. Box 3996  
Seattle, Washington 98124 (2 cys)

The Boeing Company  
Aerospace Group  
Attn: Karl Wiedekamp  
Box 3707, Mail 28-81  
Seattle, Washington 98124

Cornell Aeronautical Laboratory, Inc.  
Attn: Tech. Library  
P. O. Box 235  
Buffalo, New York 14221

Corning Glass Works  
Attn: Dr. M. G. Britton  
Manager, Tech. Liaison  
Corning, New York 14832



## NON-GOVERNMENT AGENCIES (Continued)

Dow Corning Corporation  
Attn: Tech. Library  
592 Saginaw Road  
Midland, Michigan 48640

Emerson and Cuming, Inc.  
Attn: Robert Schaffer  
869 Washington Street  
Canton, Massachusetts 02021

Englehard Industries, Inc.  
Attn: J. B. Blandford, Jr.  
3605 N. Dixie Drive  
Dayton, Ohio 45414

Fairchild Hiller Corporation  
Aircraft Division  
Attn: Tech. Library  
Hagerstown, Maryland 21740

Fairchild Hiller Corporation  
Republic Aviation Division  
Attn: Non-Metallics Section,  
Structures  
Farmingdale, Long Island  
New York 11735

Fairchild Hiller Corporation  
Attn: Tech. Library  
Fairchild Drive  
Germantown, Maryland 20767

General American Trans Corporation  
MRD Division  
Attn: S. J. Lis  
7501 N. Natchez Avenue  
Niles, Illinois 60648

General Electric Company  
Missile and Space Division  
Re-Entry Systems Department  
Attn: Tech. Library  
3198 Chestnut Street  
Philadelphia, Pennsylvania 19101

General Electric Company  
Lamp Glass Department  
24400 N. Highland Road  
Richmond Heights, Ohio 44121

General Dynamics Corporation  
Astronautics Division  
Attn: Tech. Library  
Mail Zone 580-60X  
P. O. Box 1128  
San Diego, California 92112

General Dynamics Corporation  
Fort Worth Division  
Attn: Tech. Library  
P. O. Box 748  
Fort Worth, Texas 76101

Goodyear Aerospace Corporation  
Attn: Engineering Department  
Librarian  
1210 Massillon Road  
Akron, Ohio 44315

Goodyear Aerospace Corporation  
Attn: D. C. Culley  
1210 Massillon Road  
Akron, Ohio 44315

Grumman Aircraft Engineering Corporation  
Attn: Tech. Library  
Bethpage, Long Island  
New York 11714

Homalite Corporation  
11-13 Brookside Drive  
Wilmington, Delaware 19806

Hughes Aircraft Company  
Aerospace Group  
Attn: Tech. Library  
Centinela and Teal Streets  
Culver City, California 90230



# Contracts

## NON-GOVERNMENT AGENCIES (Continued)

IIT Research Institute  
Attn: W. J. Christian  
10 West 35th Street  
Chicago, Illinois 60616

Libbey-Owens-Ford Glass Company  
Attn: W. L. Elton  
1701 East Broadway  
Toledo, Ohio 43605

Libbey-Owens-Ford Glass Company  
Liberty Mirror Division  
851 Third Avenue  
Brackenridge, Pennsylvania 15014

Ling-Temco-Vought, Incorporated  
Attn: Engineering Department  
Librarian  
P. O. Box 5907  
Dallas, Texas 75222

Lockheed Aircraft Corporation  
Missiles and Space Division  
Attn: Engineering Department  
Librarian  
P. O. Box 504  
Sunnyvale, California 94088

Lockheed Aircraft Corporation  
Marietta Georgia Division  
Attn: Engineering Department  
Librarian  
Marietta, Georgia 30061

Lockheed Missile and Space Company  
Technical Information Center  
3251 Hanover Street  
Palo Alto, California 94304

Lockheed Aircraft Corporation  
Attn: Frank Norris  
Building 63  
Department 746 SST - Box 551  
Burbank, California 91503

Lockheed Aircraft Corporation  
Attn: Engineering Department  
Librarian  
2555 North Hollywood Way  
Burbank, California 91503

Marquardt Corporation  
Attn: Tech. Library  
16555 Staticoy Street  
Van Nuys, California 91409

The Martin Company  
Attn: Tech. Library  
Friendship International Airport  
Maryland 21240

The Martin Company  
Attn: J. H. Flesher  
Department 2560, Mail No. 6057  
Friendship International Airport  
Maryland 21240

McDonnell Douglas Corporation  
McDonnell Douglas Astronautics Company  
333 West First Street  
Attn: H. E. Pierce  
Dayton, Ohio 45402

McDonnell Douglas Corporation  
McDonnell Douglas Astronautics Company  
Space Systems Center  
Attn: A3-332 Library  
5301 Bolsa Avenue  
Huntington Beach, California 92646

McDonnell Douglas Corporation  
Douglas Aircraft Company  
Attn: H. F. Kleckner  
3855 Lakewood Boulevard  
Long Beach, California 90801

## NON-GOVERNMENT AGENCIES (Continued)

McDonnell Douglas Corporation  
Douglas Aircraft Company  
Attn: E. M. Kunreuther  
3855 Lakewood Boulevard  
Long Beach, California 90801

McDonnell Douglas Corporation  
Douglas Aircraft Company (M&SSD)  
Attn: A-260 Library  
3000 Ocean Park Boulevard  
Santa Monica, California 90406

McDonnell Douglas Corporation  
Douglas Aircraft Company (M&SSD)  
Attn: R. E. Lowe/Dept. A-260  
3000 Ocean Park Boulevard  
Santa Monica, California 90406

McDonnell Douglas Corporation  
Douglas Aircraft Company  
Attn: Tech. Library  
3855 Lakewood Boulevard  
Long Beach, California 90801

McDonnell Douglas Corporation  
McDonnell Company  
Attn: Tech. Library  
P. O. Box 516  
St. Louis, Missouri 63166

Midwest Research Institute  
Attn: Tech. Library  
425 Volker Boulevard  
Kansas City, Missouri 64110

Midwest Research Institute  
Attn: Gary Korb  
425 Volker Boulevard  
Kansas City, Missouri 64110 (2 cys)

Narmco Research and Development  
Attn: Tech. Library  
3540 Aero Court  
San Diego, California 92123

Northrop Corporation  
Norair Division  
Attn: Tech. Information  
3925-31  
1001 East Broadway  
Hawthorne, California 90250

North American-Rockwell Corporation  
Columbus Division  
Attn: Tech. Library  
4300 East Fifth Street  
Columbus, Ohio 43216

North American Aviation, Inc.  
Los Angeles Division  
Attn: Tech. Library  
International Airport  
Los Angeles, California 90009

North American Aviation, Inc.  
Space and Information Systems Division  
Attn: Tech. Information Center  
12214 Lakewood Boulevard  
Downey, California 90241

North American Aviation, Inc.  
Attn: Donald Koch  
Los Angeles International Airport  
Los Angeles, California 90009

North American Aviation, Inc.  
Attn: James Nixon  
Los Angeles International Airport  
Los Angeles, California 90009

North American Aviation, Inc.  
Attn: H. H. Crotsley  
Los Angeles International Airport  
Los Angeles, California 90009

North American Aviation, Inc.  
Attn: High Haroldson, Department 56  
Los Angeles International Airport  
Los Angeles, California 90009 (2 cys)

NON-GOVERNMENT AGENCIES (Continued)

Optical Coating Laboratory, Inc. Attn: Dennis Morelli 2789 Griffen Avenue Santa Rosa, California 95401 <u>(2 cys)</u>	Swedlow, Incorporated Attn: Ken Granger Aircraft Products 6986 Bandini Boulevard Los Angeles, California 90000
Philco-Ford Corporation Space and Re-Entry Systems Division Attn: Tech. Library Ford Road Newport Beach, California 92263	Swedlow, Incorporated Attn: William Yamaguchi 12605 Beach Boulevard Garden Grove, California 92641
Pittsburgh Plate Glass Company Glass Research Center Box 11472 Pittsburgh, Pennsylvania 15222	University of Illinois Attn: R. G. Hering Department of Mechanical and Industrial Engineering Urbana, Illinois 61801
Pittsburgh Plate Glass Company Attn: C. R. Frownfelter D. W. Ludwig J. S. Chess One Gateway Center Pittsburgh, Pennsylvania 15222 <u>(3 cys)</u>	Vidya Research and Development 2626 Hanover Street Palo Alto, California 94304
The Rand Corporation Attn: Tech. Library 1700 Main Street Santa Monica, California 90401	
Ryan Aeronautical Company Attn: Tech Library 2701 Harbor Drive San Diego, California 92112	
The Sierracin Corporation Attn: H. G. Partridge 12780 San Fernando Road San Fernando Valley Sylmar, California 91342 <u>(2 cys)</u>	
Southwest Research Institute Attn: Engineering Department Librarian 8500 Culebra Road San Antonio, Texas 78200	

DOCUMENT CONTROL DATA - R & D

(Security classification of title, body of abstract and indexing annotation must be entered when the overall report is classified)

1. ORIGINATING ACTIVITY (Corporate author) Midwest Research Institute 425 Volker Boulevard Kansas City, Missouri 64110		2a. REPORT SECURITY CLASSIFICATION Unclassified	
		2b. GROUP	
3. REPORT TITLE DEVELOPMENT AND EXPERIMENTAL VERIFICATION OF A COMPUTER PROGRAM FOR PREDICTING TEMPERATURE DISTRIBUTION AND HEAT TRANSFER THROUGH COATED AND UNCOATED, SINGLE OR MULTI-GLAZE WINDOW SYSTEMS			
4. DESCRIPTIVE NOTES (Type of report and inclusive dates) Final Technical Report (15 June 1966 - 15 February 1969)			
5. AUTHOR(S) (First name, middle initial, last name) Gary M. Korb                      Duncan Sommerville Ronald D. Dayton			
6. REPORT DATE April 1969	7a. TOTAL NO. OF PAGES 209	7b. NO. OF REFS 21	
8a. CONTRACT OR GRANT NO. AF 33(615)-5164	9a. ORIGINATOR'S REPORT NUMBER(S)		
b. PROJECT NO.    1368			
c. Task No. 136802	9b. OTHER REPORT NO(S) (Any other numbers that may be assigned this report) AFFDL-TR-69-28		
d.                      "			
10. DISTRIBUTION STATEMENT    This document is subject to special export controls and each transmittal to foreign governments or foreign nationals may be made only with prior approval of the AF Flight Dynamics Laboratory (FDTS), Wright-Patterson Air Force Base, Ohio 45433.			
11. SUPPLEMENTARY NOTES		12. SPONSORING MILITARY ACTIVITY AF Flight Dynamics Laboratory (FDTS) Air Force Systems Command Wright-Patterson AFB, Ohio 45433	
13. ABSTRACT The severe thermal environment of future hypervelocity aerospace vehicles will place rigorous demands on direct vision window systems. At the high temperatures encountered, heat will be transferred within window materials by both conduction and radiation. This report describes the development and experimental verification of a computer program for predicting the temperature distribution and heat transfer through coated and uncoated, single or multiple glaze window systems. The heat balance equations in the computer program account for emission, attenuation, and absorption of radiant energy within the glaze. Reflection and transmission of glaze surfaces having multilayer, thin-film coatings are computed. Window temperatures and heat flux can be predicted for transient conditions of individual and/or combined convective and radiative heating. The computer program was experimentally verified with heat transfer tests in which specimens of various glaze materials and thicknesses were used. Typical aerospace reflection and antireflection coatings were employed on one and/or both surfaces of the test specimens. The work was performed in three phases. In the first phase the research was applicable to single uncoated glazes. In the second phase the scope was expanded to include coated single glazes, and in the third phase coated and uncoated multiple glazes were investigated. Good agreement between the analytical and experimental results was obtained. The computer program is written in FORTRAN IV language and for the IBM 7094 digital computer. A program user's manual is available as a separate publication.			

14. KEY WORDS	LINK A		LINK B		LINK C	
	ROLE	WT	ROLE	WT	ROLE	WT
Aerospace Windows						
Heat Transfer Analysis						
Computer Program Developed						
Experimental Verification						
Semitransparent Materials						